

PYROLYSIS AND SPECTROSCOPY  
OF CYCLIC AROMATIC COMBUSTION INTERMEDIATES

by

GRANT THORNTON BUCKINGHAM

B.A. Carleton College 2010

A thesis submitted to the  
Faculty of the Graduate School of the  
University of Colorado in partial fulfillment  
of the requirement for the degree of  
Doctor of Philosophy  
Department of Chemistry and Biochemistry

2016

This thesis entitled:  
Pyrolysis and Spectroscopy of Cyclic Aromatic Combustion Intermediates  
written by Grant Thornton Buckingham  
has been approved for the Program of Chemical Physics

---

G. Barney Ellison

---

Veronica M. Bierbaum

Date\_\_\_\_\_

The final copy of this thesis has been examined by the signatories, and we find that both the content and the form meet acceptable presentation standards of scholarly work in the above mentioned discipline.



Buckingham, Grant Thornton (Ph.D., Chemical Physics)

Pyrolysis and Spectroscopy of Cyclic Aromatic Combustion Intermediates

Thesis Directed by Emeritus Professor G. Barney Ellison

We have studied the pyrolysis of aromatic combustion intermediates using an array of detection techniques. The molecules investigated include cyclic aromatic molecules with hydrocarbon substituents (ethylbenzene, n-propylbenzene, isopropylbenzene, and styrene), oxygen-containing substituents (anisole and phenol), triply substituted systems (vanillin), resonance stabilized radicals (benzyl radical and tropylium radical) and phenyl radical. At the exit of a resistively heated micro-reactor (1 mm inner diameter, 3 cm long), the pyrolysis fragments are detected using photoionization mass spectrometry (PIMS), matrix isolation vibrational spectroscopy, microwave spectroscopy, tunable VUV synchrotron-based PIMS, and table-top VUV PIMS with photoelectron photoion coincidence spectroscopy (PEPICO). This array of detection methods allows for the identification of all possible fragments including metastables, radicals, and atoms. The findings allow for detailed mechanistic information regarding which pathways are active at different pyrolysis temperatures. The findings can also be used to help identify products and individual isomers that are formed during the gas-phase thermal decomposition of aromatic systems. By providing direct experimental pyrolysis data, models for fuel decomposition and soot formation can be improved to help understand current combustion systems and eventually aid in the design of superior fuel sources in the near future.

## ACKNOWLEDGMENTS

I think that I am on the verge of concluding one of the luckiest graduate school experiences possible. The amount that I learned about chemistry, physics, and science in general is fantastic but the 6 years I had in Boulder may be some of the most important years of my life. I arrived in Colorado as a young, ignorant, insecure, and poorly defined person and I write this now as a confident self-sufficient, and driven man. For this I am deeply indebted to 1) my family, 2) to my two research advisors, David Nesbitt and Barney Ellison, and 3) to the group of friends I found in Boulder. My advisors taught me about chemical physics and life as a scientist but the other two camps helped me find who I am. To all three groups I am eternally grateful.

For the first two-and-a-half years of my degree, I worked with David Nesbitt, who may be the most careful and creative thinker and teacher I have ever met. The completeness of his understanding is truly staggering and the vigor with which he pursues knowledge is something I will always strive to emulate. For the next 3.5 years I worked with Barney Ellison learning a very different type of chemistry. Barney's ability to find and solve interesting problems, as well as amass a wonderful group of colleagues and friends to help him do it showed me how great science can really be. Working with him and learning to navigate academia has been more fun than I thought graduate school could be. The combination of these two mentors has allowed me to gain such a wealth (and breadth) of knowledge that I can't imagine a more rewarding Ph.D. experience.

It has been a pleasure working with so many fun and intelligent people during my time here. In the Nesbitt group, I benefitted from knowing Melanie Roberts, Chih-Hsuan Chang, Rob Roscioli, Kevin Early, Nick Dupuis, Mia Zutz, Andy Gisler, Mike

Ziemkiewicz, Andrej Grubisic, Monika Gruetter-Kasumaj, Dan Nelson, Eric Holmstrom, Tom Baker, and Julie Fiore and all of the JILA staff. In the Ellison group I enjoyed working with Kimberly Urness, Jessie Porterfield, Josh Baraban, Tom Ormond, Jong Kim, Fiona Deguillaume, John Stanton, John Daily, Qi Guan, Don David, the Ion Super Group, Ronnie Bierbaum, Carl Lineberger, and Mathias Weber. I also had the pleasure of collaborating with Mark Nimlos and David Robichaud at NREL; Tim Zwier and his very welcoming group at Purdue University; the ALS team at Berkeley: Musa Ahmed, Tyler Troy, and Oleg Kostko; Mike McCarthy and Marie-Aline Martin at Harvard CfA; Hans-Heinrich Carstensen from the University of Gent; Bill Peters and David Couch from the KM group; and Bryan Changala and Ben Spaun of Jun Ye's group.

I also need to acknowledge the tremendous experience I had at Carleton College, where I learned about chemistry but also learned to love learning. The education I received from the faculty there, especially Will Hollingsworth and Marion Cass, helped me to succeed in graduate school but also showed me how to be passionate about science.

The people I spend my free time with were hugely important to my time in Boulder. My housemates at Armer: Jordan "Jo'j" Mirocha, Anthony Harness, Marek Slipski, Emily Kraus, and Tristan Weber were always there for me to make me laugh. Book Club with Eric Coughlin helped keep my life in balanced and coffee with Greg Salveson helped keep me awake. Mia Zutz, Andy Gisler and Nick Dupuis were my constant ski team and dinner crew. Galen Gorski, Kevin Early, Kevin Pollock, Matt Nock, and Austin Hall were all there for me from a distance.

Finally, and most importantly, I want to acknowledge everything that my family has done for me along the way. The unwavering support from my parents Kim

Thornton and Kent Buckingham and sister Katherine Buckingham allowed me to persevere and thrive during this stage of my life, and all the stages that preceded it. There is no doubt that all of my strengths as a person came from being lucky enough to be born into the family that I was.

# CONTENTS

## Chapter 1. Introduction

I. Motivation	1
II. Understanding Current Combustion Systems	2
III. Selecting Better Future Fuels	7
IV. Outline	11
References for Chapter 1	14

## Chapter 2. Experimental Methods

I. Introductions	17
II. High Resolution Absorption Spectroscopy	18
A. Difference Frequency Infrared Production	18
B. Slit Discharge Radical and Ion Production	19
III. Pyrolysis of Gas-Phase Biofuel Intermediates Using a Heated Micro-Reactor	22
A. Pyrolysis in a heated Micro-Reactor	23
B. Photoionization Mass Spectroscopy	27
i. Photoionization Mass Spectrometry Using the 9 <sup>th</sup> harmonic of an Nd:YAG Laser and Reflectron Time-of-Flight Detection	28
ii. Photoionization Mass Spectrometry Using Synchrotron Radiation and Time-of-Flight Reflectron Detection	29
iii. Photoionization Mass Spectrometry Using Synchrotron Radiation and Imaging Photoelectron Photoion Coincidence Spectroscopy	30

iv. Photoionization Mass Spectrometry Using a Tabletop Vacuum Ultraviolet Laser and Photoelectron Photoion Coincidence Spectroscopy	32
C. Matrix Isolation Infrared Absorption Spectroscopy	35
D. Sample Preparation	36
References for Chapter 2	39

### **Chapter 3. High-Resolution Rovibrational Spectroscopy of Jet-Cooled Phenyl Radical: The $\nu_{19}$ Out-of-Phase Symmetric CH Stretch**

Abstract	43
I. Introduction	44
II. Experimental	50
III. Results and Analysis	53
IV. Discussion	
A. Nuclear Spin Weights	62
B. Planarity and In-Plane Ring Distortion	64
C. Intramolecular Vibrational Redistribution	69
V. Summary and Conclusions	75
References for Chapter 3	76

### **Chapter 4. Observation of the $a_1$ CH Stretching Modes in Phenyl Radical using Jet-Cooled Sub-Doppler Absorption Spectroscopy**

Abstract	83
I. Introduction	83
II. Experimental	88
III. Results and Discussion	
A. Spectral Observation and Analysis	89
B. Intensity Analysis	99

IV. Summary and Conclusions	103
References for Chapter 4	104
<b>Chapter 5. Hydropyrolysis of Ethylbenzene in a Heated Micro-Reactor</b>	
Abstract	107
I. Introduction	107
II. Experimental	112
III. Results and Discussion	
A. Ethylbenzene Decomposition	113
B. Hydropyrolysis of Ethylbenzene	116
IV. Conclusions	125
References for Chapter 5	127
<b>Chapter 6. The Thermal Decomposition of the Benzyl Radical in a Heated Micro-Reactor: I. Experimental Findings</b>	
Abstract	131
I. Introduction	132
II. Experimental	139
III. Results	144
A. Decomposition of Benzyl-d <sub>0</sub> Radical	145
B. Decomposition of Benzyl-d <sub>2</sub> Radical	155
C. Decomposition of Benzyl-d <sub>5</sub> Radical	160
D. Decomposition of <sup>13</sup> C-Benzyl Radical, C <sub>6</sub> H <sub>5</sub> <sup>13</sup> CH <sub>2</sub>	161
IV. Discussion and Conclusions	167
References for Chapter 6	171

## **Chapter 7. The Thermal Decomposition of the Benzyl Radical in a Heated Micro-Reactor: II. Pyrolysis of the Tropylium Radical**

Abstract	179
I. Introduction	180
II. Experimental	
A. Heated Micro-Reactor Pyrolysis Source	185
B. Photoionization Mass Spectrometry	
i. Pulsed Vacuum Ultraviolet Radiation	186
ii. Continuous Vacuum Ultraviolet Radiation	187
C. Matrix Isolation Fourier Transform Infrared Spectroscopy	187
D. Sample Preparation	188
III. Results and Discussion	
A. Photoionization Mass Spectrometry	190
B. Matrix Isolation Spectroscopy	200
C. Cycloheptatrienyl or Norbornadiene as Tropylium Precursors?	205
IV. Conclusions	213
A. Pyrolysis of Benzyl Radical without Tropylium	214
References for Chapter 7	224

## **Chapter 8. Tabletop Vacuum Ultraviolet Laser-Based Photoionization Mass Spectrometry with Photoelectron Photoion Coincidence Detection of Pyrolysis Products**

Abstract	233
I. Introduction	233
II. Experimental	237
III. Results and Discussion	



A. Isomer Identification	240
B. Disentangling Dissociative Ionization in Mass Spectra	242
IV. Conclusions	253
References for Chapter 8	254
<b>Chapter 9. Full Bibliography</b>	<b>257</b>
<b>Appendix A</b>	<b>281</b>
<b>Appendix B</b>	<b>293</b>
<b>Appendix C</b>	<b>301</b>
<b>Appendix D</b>	<b>309</b>
<b>Appendix E</b>	<b>311</b>
<b>Appendix F</b>	<b>317</b>
<b>Appendix G</b>	<b>323</b>

## TABLES

2.1	Summary of the experimental conditions for each experiment performed with heated micro-reactor.	27
3.1	<i>Ab initio</i> theoretical and experimental rovibrational constants of phenyl radical	66
4.1	The symmetry and band origin frequencies from theoretical prediction, gas-phase, and Ar-matrix studies of phenyl radical and cation in the region of C–H stretching	92
4.2	Spectroscopic parameters of the phenyl radical in the ground state and excited CH stretching modes	96
5.1	Vibrational band assignments of toluene	124
5.2	Vibrational band assignments of styrene	125
6.1	Experimental properties of benzyl and cycloheptatrienyl radicals	137
6.2	Summary of Experimental Conditions	143
7.1	Tropyl and Benzyl Radical Experimental Properties	183

## FIGURES

1.1	The formation of soot starting from simple acyclic combustion intermediates up through 1.5 nm diameter soot particles	4
1.2	Propargyl radical in the ground electronic state	5
1.3	Sample of lignin with the different linkages and their abundances	9
1.4	The three lignin monomers (monolignols)	10
1.5	Chemical structure of three isomers of $C_7H_7$ , including their common names and the symmetry of their electronic ground states	12
2.1	Cartoon diagram of pulsed slit jet discharge	21
2.2	Cut away view of the clover heater	25
2.3	Continuous flow heated micro-reactor assembly (inset) and larger cutaway diagram	34
2.4	Sample probe for heating low-vapor pressure solids and liquids	37
3.1	Phenyl radical with its body fixed principle rotation axes labeled	45
3.2	Cartoon diagram of pulsed slit jet discharge	51
3.3	Overview rovibrational spectrum of the symmetric out-of-phase C-H stretch, $\nu_{19}$ , in phenyl radical at $T_{rot}$ roughly equal 11(1)K	55
3.4	Q branch region of the phenyl radical out-of-phase CH symmetric stretch	59
3.5	Scan of phenyl radical in the R branch region of the $\nu_{19}$ CH stretch	61
3.6	Comparison of two simulated spectra, which highlight the effect of nuclear spin statistics in the spectrum of phenyl radical in the $\nu_{19}$ region	63
3.7	<i>Ab initio</i> theoretical comparison (CCSD(T)/vtz-f12) between benzene and phenyl radical, illustrating the subtle distortion of the carbon ring upon H atom abstraction and radical formation	69
3.8	Estimates of symmetry selected vibrational state density for a series of aromatic and polycyclic aromatic hydrocarbon (PAH) molecules, based on simple density functional predictions (B3LYP/6-311++g(3df,3pd)) and an efficient backtracking algorithm	74

4.1	Structure of phenyl radical with carbon atom positions labeled	84
4.2	The displacement vectors for each vibrational mode in the region of C–H stretching of phenyl radical	87
4.3	Rotationally resolved spectrum of the phenyl radical in the region of 3068–3078 cm <sup>-1</sup>	90
4.4	Spectrum of the weak band observed at 3062 cm <sup>-1</sup> with the corresponding vibrational assignment	93
4.5	A portion of the rotationally resolved rovibrational spectrum in the vicinity of 3076 cm <sup>-1</sup>	94
4.6	Boltzmann plot of the single isolated lines in the $\nu_{19}$ band leading to a rotational temperature of about 11.2 K	100
4.7	The normalized integrated band intensity for the experimental (gas-phase and Ar matrix) observation and the theoretical prediction	102
5.1	Schematic of the chemical pathways confirmed for the pyrolysis of benzaldehyde mixed with methyl nitrite	110
5.2	PIMS spectra of the thermal decomposition of dilute ethylbenzene (0.1% in He) at 900 K, 1200 K and 1300 K	114
5.3	PIMS spectra of the thermal decomposition of 0.5% methyl nitrite in a pulsed He micro-reactor	116
5.4	A mixture of 0.1% ethylbenzene and 0.5% methyl nitrite was pyrolyzed at 900 K, 1200 K, and 1300 K in a micro-reactor and the products were detected using 118.2 nm PIMS	117
5.5	Matrix isolation IR spectra of gas mixtures (benzene, ethylbenzene and methyl nitrite, ethylbenzene, and methyl nitrite) flowed through a heated micro-reactor	121
5.6	Matrix isolation IR spectra of gas mixtures (ethylene, ethylbenzene and methyl nitrite, ethylbenzene, and methyl nitrite) flowed through a heated micro-reactor	123
6.1	Proposed benzyl radical decomposition pathways	134
6.2	Dilute ethylbenzene heated in a pulsed helium tubular micro-reactor studied using PIMS at four different reactor temperatures, 350 K, 1300 K, 1400 K, and 1500 K	146

6.3	Matrix isolation IR absorbance spectra of dilute ethylbenzene in a pulsed helium reactor at 300 K and 1500 K	148
6.4	The acetylenic stretch region of the vibrational spectrum is shown for the decomposition of ethylbenzene in pulsed neon at 300 K and 1500 K	150
6.5	Photoionization efficiency curves for $m/z$ 76 and $m/z$ 65 measured during the 1500 K decomposition of 0.2% ethylbenzene in a CW helium reactor	151
6.6	PIMS spectra recorded during the decomposition of benzyl bromide at 1200 K and 1300 K in a CW reactor	153
6.7	Thermal decomposition of benzyl bromide in a CW argon reactor measured at the tunable synchrotron lights source at the SLS	154
6.8	Dilute ethylbenzene- $d_5$ ( $C_6H_5CD_2CD_3$ ) heated in a pulsed helium tubular micro-reactor studied using PIMS at three different reactor temperatures, 300 K, 1300 K, and 1500 K	156
6.9	PIMS spectra of $C_6H_5OCH_3$ decomposition at 1300 K and the outcome of mixing 0.02% $C_6H_5OCH_3$ with 0.25% $CD_3ONO$ , a known D atom source, in pulsed helium	158
6.10	Dilute ethylbenzene- $d_5$ ( $C_6D_5CH_2CH_3$ ) heated in a pulsed helium tubular micro-reactor studied using PIMS at three different reactor temperatures, 350 K, 1300 K, and 1400 K	161
6.11	Dilute ethylbenzene- $^{13}C$ ( $C_6H_5^{13}CH_2CH_3$ ) heated in a pulsed helium tubular micro-reactor studied using PIMS at three different reactor temperatures, 300 K, 1300 K, and 1500 K	163
6.12	Photoionization efficiency curves confirming the identity of $m/z$ 91 as $C_5H_4=C=CH_2$ and $m/z$ 90 as $C_5H_4-C\equiv CH$	164
6.13	Photoionization efficiency curves confirming the identity of $m/z$ 65 and 66 as cyclopentadienyl radical	165
6.14	PIMS for the decomposition of $C_6H_5CD_2Br$ at 1250 K in a CW Ar reactor at the SLS	167
7.1	The Benson Pathway for the pyrolysis of benzyl radical	181
7.2	The 9.5 eV PIMS spectra of bitropyl ( $C_7H_7-C_7H_7$ ) pyrolyzed in a continuous flow micro-reactor heated to 600 K	191

7.3	PIMS spectra of bitropyl ( $C_7H_7-C_7H_7$ ) recorded in a continuous flow micro-reactor at temperatures of: 400 K, 1100 K, 1200 K, 1300 K, 1400 K, and 1500 K	193
7.4	Photoionization efficiency curves for $m/z$ 65 recorded during the thermal decomposition of bitropyl ( $C_7H_7-C_7H_7$ ) in a continuous flow micro-reactor in He at 900 K, 1200 K, and 1500 K	195
7.5	Neon matrix absorbance IR spectrum of the 1200 K pyrolysis of bitropyl ( $C_7H_7-C_7H_7$ ) in a pulsed micro-reactor	197
7.6	PIMS spectra comparing the thermal decomposition of the benzyl radical and the tropylium radical	199
7.7	Neon matrix absorbance IR spectra of the pyrolysis of bitropyl ( $C_7H_7-C_7H_7$ ) in a pulsed micro-reactor at 400 K, 1000 K, 1100 K, and 1200 K in the region of $3030\text{ cm}^{-1}$	202
7.8	Neon matrix absorbance IR spectra of the pyrolysis of bitropyl ( $C_7H_7-C_7H_7$ ) at 400 K, 1000 K, 1100 K, and 1200 K in the region of $1450\text{ cm}^{-1}$	204
7.9	Isomerization pathways of norbornadiene, norcaradiene, cycloheptatriene, and toluene	206
7.10	The neon matrix absorbance IR spectrum of cycloheptatriene ( $C_7H_8$ ) pyrolysis in a pulsed micro-reactor at 1300 K	208
7.11	PIMS spectra from the pyrolysis of cycloheptatriene in pulsed helium at three reactor temperatures, 300 K, 1400 K, and 1600 K	210
7.12	PIMS spectra from the pyrolysis of norbornadiene in pulsed helium at three reactor temperatures, 400 K, 1300 K, and 1600 K	212
7.13	The "extended" Benson Fragmentation pathways of the benzyl radical	216
7.14	Fragmentation pathways of the benzyl radical including the norbornadienyl pathway and $\alpha$ -methyl phenyl pathway	219
8.1	Continuous flow heated micro-reactor assembly and larger cutaway diagram	239
8.2	Photoelectron spectrum of 1-butyne flowed through an unheated CW micro-reactor	241
8.3	Photoelectron spectrum of 1,3-butadiene, 1-butyne, and a mixture of the two flowed through an unheated CW micro-reactor	242

8.4	Room temperature PIMS spectra recorded using 118.2nm light of dilute (0.07%) 2-butanol in a pulsed He micro-reactor	244
8.5	Room temperature PIMS spectra of 2% 2-butanol in a CW He micro-recorded using an XUV laser and a PEPICO detector	245
8.6	PIMS of 0.07% 2-butanol in a pulsed He micro-reactor at 1200 K, recorded with a 118.2 nm ionization source	247
8.7	PIMS of 2% 2-butanol pyrolyzed in CW helium flowed through a micro-reactor heated with 3 Amps operating at 13 Volts, recorded using an XUV laser and a PEPICO detector	248
8.8	Photoelectron spectrum of the species with $m/z$ 15 observed during 2-butanol pyrolysis, assigned to be methyl radical	250
8.9	Photoelectron spectrum of the species with $m/z$ 28 observed during 2-butanol pyrolysis, assigned to be ethylene	251
8.10	Photoelectron spectrum of the species with $m/z$ 56 observed during 2-butanol pyrolysis, cautiously assigned to a mixture of 1-butene and 2-butene	252
8.11	Photoelectron spectrum of the species coincident with $m/z$ 44 observed during 2-butanol pyrolysis, potentially assigned to a mixture of acetaldehyde and vinyl alcohol	253

# Chapter 1

## Introduction

### I. Motivation

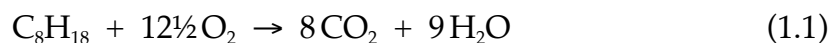
Global climate change is one of the largest and most complicated issues humanity has faced thus far. What makes this problem so challenging is that it will require the efforts of so many different fields of study. Among the more obvious ways to attack the problem is by means of scientific and engineering advancements to understand the processes involved and better plan future efforts. There exist many more subtle challenges, however, that will require the efforts of political scientists, sociologists, and even philosophers as we attempt to prioritize the health the planet and the prosperity of the people on that planet simultaneously. In the same way that many different fields all have a part to play in this challenge, there are also myriad avenues within science and engineering that contribute to an efficient and effective solution. There are currently material scientists working to push the limits of solar energy conversion, engineers trying to model the characteristics of flames and engines, and there are significant contributions yet to be made on the fundamental chemical level as we try to understand combustion on the molecular level. The latter pursuit can often feel far removed from the dramatic immediacy of climate change, but in some ways, it is the most important struggle because only from a deep understanding can a truly revolutionary solution emerge.



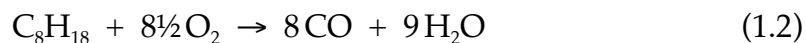
## II. Understanding Current Combustion Systems

As the power and efficiency of computational methods continues to increase, modelers are able to quantitatively characterize complex kinetic systems. Chemical and mechanical engineers are currently constructing systems of reactions to simulate the processes of combustion and pyrolysis (decomposition in the absence of oxygen) given a set of starting conditions and reactant fuel molecules. Unfortunately, even for a relatively simple system such as one with only a single fuel with no oxygen present, the number of products and intermediates detected can be quite large. In an experiment where toluene ( $C_6H_5-CH_3$ ) was heated to 1800 K in the absence of oxygen, at least 64 different species were detected.<sup>[1]</sup> In order to model the kinetics of this system one must initially allow for the reactions of all 64 molecules with each other, which leads to 2080 different potential bimolecular reactions, each with its own rate constants. Since reaction rates depend on concentration, temperature, and rate constant for each, this system is radically undetermined with only the few experimentally available parameters. A system like this can be dramatically simplified by building up complexity slowly, with dilute samples (i.e. only unimolecular reactions) and smaller precursors. This is the aim of our research program. By starting with simple systems and short reaction times, we can hope to identify all the nascent products of a unimolecular thermal decomposition. If the exact mechanism of the decomposition products can be identified, then the reaction modelers can dramatically simplify their schemes and make progress toward more complete kinetic schemes. This “bottom-up” technique requires starting with fundamental molecules but promises to provide a more complete picture of a system, however small for now.

A large problem for efficient combustion is the issue of incomplete combustion. Ideal combustion results in complete conversion of hydrocarbons and oxygen (O<sub>2</sub>) into carbon dioxide and water (see Reaction 1.1 for the combustion of octane).



If, instead, some of the carbon and hydrogen atoms in the reactant (octane) react differently to produce other products (e.g. soot) then less of the exothermicity (heat of combustion) can be utilized to do mechanical work. This incomplete combustion can also result in formation of CO (see Reaction 1.2), which is poisonous.



The processes by which fuel is incompletely combusted and converted to soot remain poorly understood. Key progress was made in 1984 to predict the exact method by which small acyclic non-aromatic molecules can react to form first monocyclic aromatic molecules (e.g. benzene) and subsequently polycyclic aromatic hydrocarbons (PAH).<sup>[2]</sup> The latter half of this mechanism, hydrogen-abstraction-C<sub>2</sub>H<sub>2</sub>-addition (HACA) is included in Fig. 1.1, which is a summary figure reproduced from a 2005 review of combustion-derived PAH involvement in environmental chemistry.<sup>[3]</sup> PAHs are important in modeling combustion because they act as a sink for hydrogen and carbon atoms. These resonance stabilized PAH molecules resist oxidation and thermal decomposition meaning that once formed, they can persist and prevent the eventual conversion to CO<sub>2</sub> and H<sub>2</sub>O, effectively sequestering potentially useful energy from further reactions.

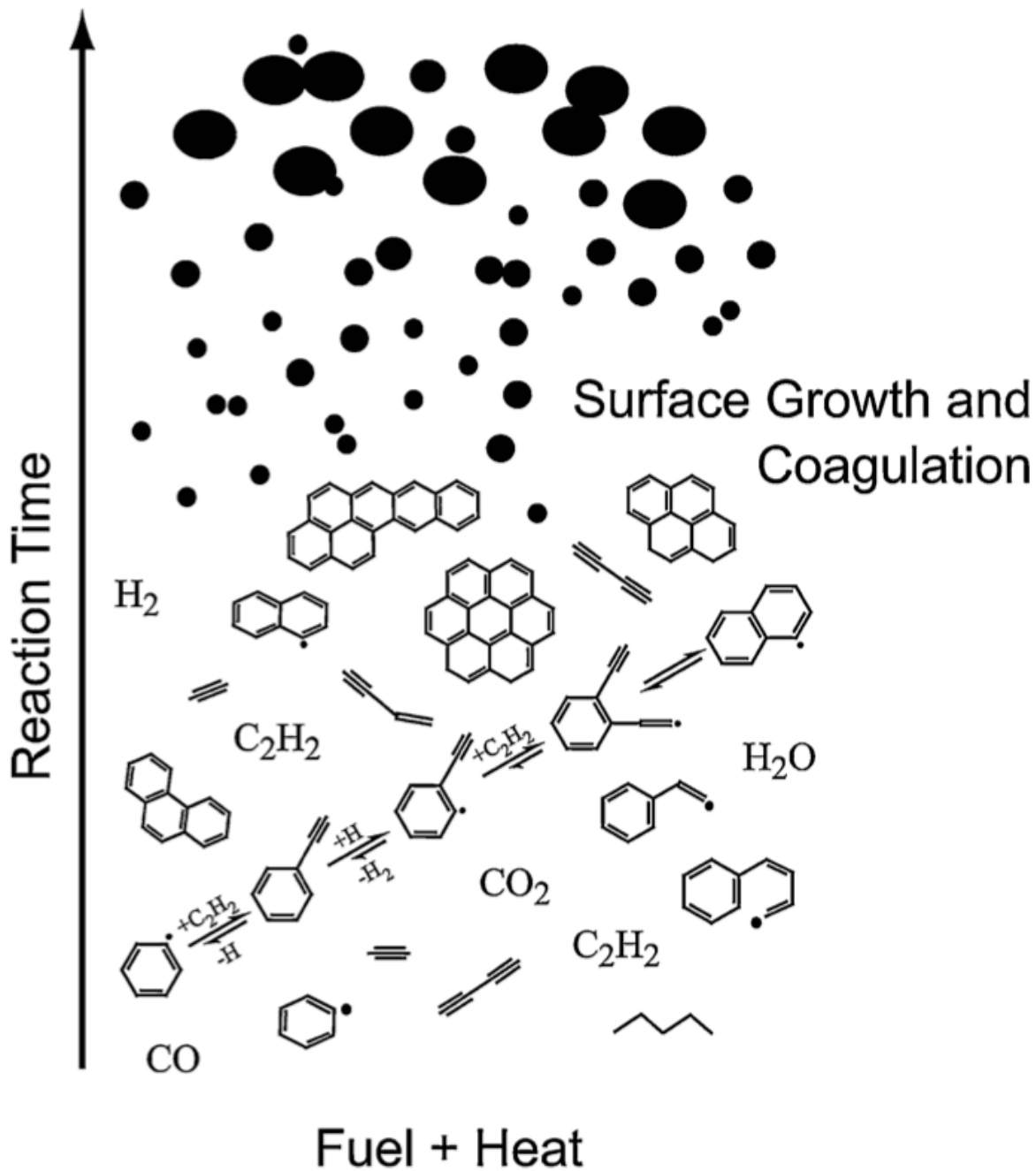


Fig. 1.1 The formation of soot starting from simple acyclic combustion intermediates up through 1.5 nm diameter soot particles. The design of the figure is based on a figure from a 2000 review paper<sup>[4]</sup> with the inclusion of the HACA reaction mechanisms to convert phenyl radical (lower left) to bicyclic naphthyl radical ( $\text{C}_{10}\text{H}_7$ ) first described by Frenklach.<sup>[2]</sup>

The stability of PAH brings to bear an important factor in combustion modeling, quantum mechanical stability via electron delocalization. One of the main reasons PAHs are significant in combustion is the marked stability that accompanies aromaticity. When organic structures allow electrons to delocalize from a single atom such that they have non-trivial probability density spread among multiple atoms, these structures are more stable than comparable molecules that lack electron delocalization. Benzene is a special example of electron delocalization that satisfies Hückel's Rule, which defines aromatic as a cyclic system with  $4n + 2 \pi$  electrons (where  $n$  is any non-negative integer). A more general example of electron delocalization is found in propargyl radical, which can be drawn in two resonance structures (see Fig. 1.2).

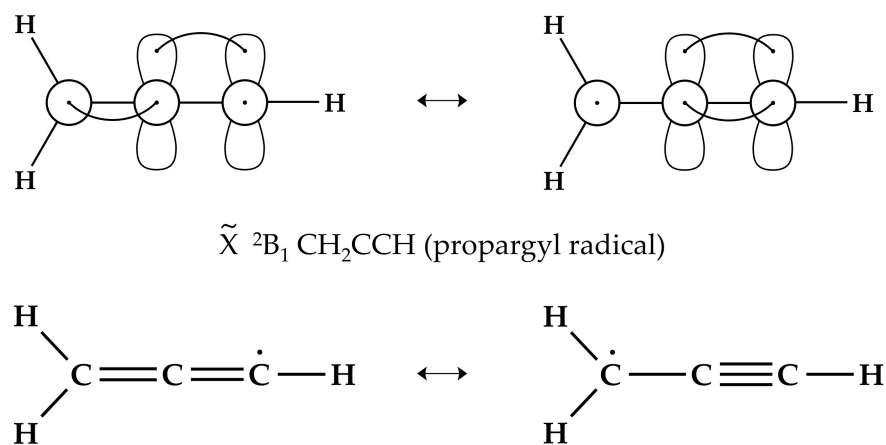


Fig. 1.2. Propargyl radical in the ground electronic state. The top two resonance structures are drawn using the generalized valence bond (GVB) description.<sup>[5]</sup> The lower two drawings are in the more standard form but represent the same electronic state structures.

Resonance stabilized radicals play an important role in combustion as they contribute to the radical pool that is evoked to describe reactivity of complex combustion systems.<sup>[6]</sup> The radical pool is a means of simplifying reaction schemes

when there are hundreds or thousands of species involved. The notion is that once some homolytic bond cleavages begin to occur, a set of radicals is formed that mediate reactions through a set of propagation reactions with neutral molecules. Resonance-stabilized radicals like propargyl radical ( $\text{CH}_2\text{CCH}$ ), allyl radical ( $\text{CH}_2\text{CHCH}_2$ ), cyclopentadienyl radical ( $\text{C}_5\text{H}_5$ ), benzyl radical ( $\text{C}_6\text{H}_5\text{CH}_2$ ), and tropyli radical ( $\text{C}_7\text{H}_7$ ) are all predicted to play important roles. Due to their relative stability, reactions between these radicals is especially important and many pathways to form PAH rely on this small set of molecules.<sup>[7-9]</sup> In these systems it is often possible to sample products after pyrolysis of fuel molecules by use of shock tubes. A limitation to these experiments is that a shock tube can only run a few times per day, meaning signal averaging on dilute molecules is limited. In most cases, reactive intermediates like radicals cannot be detected and their presence can only be inferred from the stable products detected. Given the immense number of potential mechanisms at play, inferring intermediates by the final products detected can be difficult and often leads to ambiguous conclusions even with the aid of clever isotope labeling. For this reason, short timescale pyrolysis experiments are very valuable as they allow for detection of nascent products and can often permit the direct detection of unstable intermediates like radicals.

Current gasoline contains large amounts of substituted aromatic rings. As much as  $\frac{1}{4}$  of current liquid gasoline consists of aromatic ring structures, which include benzene ( $\text{C}_6\text{H}_6$ ), toluene ( $\text{C}_6\text{H}_5\text{CH}_3$ ), ethylbenzene ( $\text{C}_6\text{H}_5\text{CH}_2\text{CH}_3$ ), xylenes (*o*, *m*, *p* -  $\text{CH}_3$ - $\text{C}_6\text{H}_4$ - $\text{CH}_3$ ) and some longer side-chain molecules. Since this class of molecules is already present in everyday systems, it is necessary to understand the decomposition mechanisms, what intermediates may exist, and what final products are formed. Although these molecules have been studied extensively in shock tubes and even

idealized flame systems, in most cases only the stable, long lived products can be detected and little is known about the radical intermediates formed. Additionally, many experiments are able to detect some subset of the products but are often incapable of detecting *all* products formed, which leaves the experimentalist vulnerable to overlooking unexpected products. In the cases where unforeseen products are formed, techniques that detect every product are very important. By gaining information about the intermediates and nascent products, much more can be learned about the chemical mechanisms responsible for the decomposition.

### **III. Selecting Better Future Fuels**

Climate change, to put it simply, is the result of anthropogenic deposition of CO<sub>2</sub> into the atmosphere that can absorb infrared (IR) light emitted from the earth's surface that would otherwise escape to space. As the concentration of CO<sub>2</sub> in the atmosphere increases, the opacity of the atmosphere increases causing heating of the planet. The long-term solution will likely be to replace all combustion-based industries with those that do not lead to release of CO<sub>2</sub>, e.g. solar, wind, or nuclear energy. Unfortunately, these methods are still being developed and will take some time before they can efficiently replace combustion. While these superior technologies are still being developed, a short-term solution is worth considering that is replacing fossil fuels with biofuels. The advantage to biofuels is that although CO<sub>2</sub> is still released during biofuel combustion, the process of making biofuels (growing plants) actively removes CO<sub>2</sub> from the atmosphere. In this way, one full cycle of growing, converting to liquid fuel, then combusting does not add new carbon to the atmospheric system. This is in stark contrast to fossil fuel burning, which converts solid-phase carbon that is sequestered in

the earth's crust into gas-phase CO<sub>2</sub>. This unidirectional deposition of CO<sub>2</sub> is problematic as the earth's energy demands continue to increase. Biofuel combustion is likely inferior to many potential replacements, but biofuel has the potential to be a short-term alternative while superior methods are being developed.

The challenges faced by biofuel designers are 1) to identify what would be a good biofuel feed stock and 2) to learn to manufacture it cheaply enough to compete with current fuels. The answer to the first question requires knowledge of what plant-matter is available (or can be made available) and if it thermally decomposes in a way that can be efficient and safe. A source of plant matter that is currently not being used for biofuels but is available in large amounts is lignin, shown in Fig. 1.3.

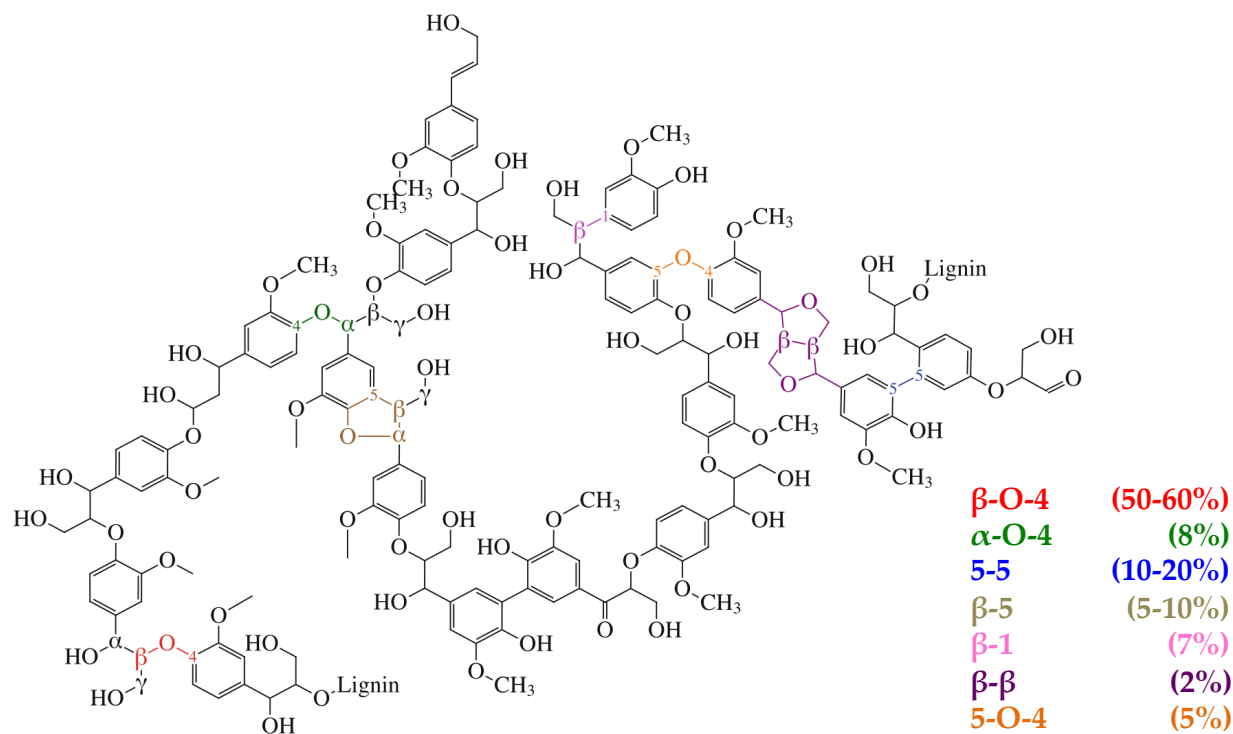


Fig. 1.3. Sample of lignin with the different linkages and their abundances shown in different colors. The percent abundance values are taken from book "Lignin and lignins: advances in chemistry".<sup>[10]</sup> The above image is taken from the book "Reaction Pathways and Mechanisms in Thermocatalytic Biomass Conversion II".<sup>[11]</sup>

Lignin is a polymer that is found in plant cell walls and is the second most abundant biopolymer on earth after cellulose. The reason that lignin is not currently used more in industry is that, although it is a polymer, it lacks the predictable and repeating linkages found in simpler polymers like cellulose. Lignin has three subunits and each has multiple potential linkage sites. The three subunits (monolignols) are shown in Fig. 1.4 along with their common names, coniferyl alcohol, coumaryl alcohol and synapyl alcohol.



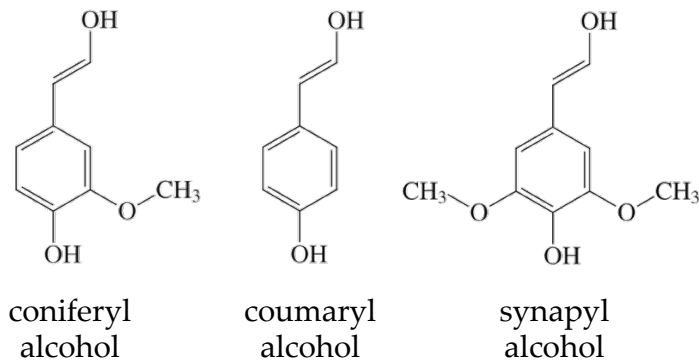


Fig. 1.4. The three lignin monomers (monolignols)

The three monomers each have an aromatic ring with vinyl alcohol groups and either one or two methyl ether or OH groups. In order to render lignocellulosic biomass viable for efficient processing, large lignin polymers must be fragmented and deoxygenated, a process that remains too costly to allow lignocellulosic fuel sources to replace fossil fuels. Recent progress in this field has used a process called integrated hydrolysis and hydroconversion (IH<sup>2</sup>),<sup>[12]</sup> whereby raw biomass is converted to liquid-phase hydrocarbons at relatively low pyrolysis temperatures, between 350°C and 480°C. Recent work at the National Renewable Energy Laboratory<sup>[13]</sup> has begun to elucidate potential chemical mechanisms active during the IH<sup>2</sup> process. This work has shown that in the gas-phase thermal decomposition of benzaldehyde, hydrogen atoms can mediate the selective removal of the aldehyde group from the ring. This hydrolysis process is likely to yield similar results for other substituted aromatic systems that can function as analogs for lignin monomers. Further exploration into these mechanisms will help to expand the understanding of and improve the future efficiency of the biomass conversion.

If and when lignin based liquid fuels become competitive with fossil fuel derived gasoline, the crucial questions to answer will be how do these fuels combust, what products are formed, and how does the combustion differ from standard gasoline combustion? These questions are a core motivation for studying cyclic aromatic molecules in pyrolysis environments, which constitutes the bulk of the present work.

#### **IV. Outline**

This thesis is organized essentially in chronological order with respect to when the research was performed. Chapter 2 provides an overview of the experimental techniques used. Chapters 3 and 4 summarize work that was done in the group of Dr. David Nesbitt. Rovibrational spectra were analyzed for the simplest aromatic radical, phenyl radical ( $C_6H_5$ ). A well-assigned IR spectrum of this radical will be crucial in identifying phenyl radical in combustion systems and the nearly 200 individually assigned rovibrational features will hopefully be used to confirm mechanisms like HACA and others in real combustion environments.

Chapters 5 – 8 summarize the work done in the group of Dr. Barney Ellison, where we worked closely with the combustion modeling community to study pyrolysis processes directly. By selecting important combustion precursors and intermediates to thermally decompose, we can establish pyrolysis pathways and help simplify radically underdetermined systems of reactions that are currently challenging for combustion modelers. Chapter 5 details the efforts made to isolate the role hydrogen atoms can play in removing substituents from aromatic molecules in the gas-phase. This work quickly motivated a detailed study of one of the most common intermediates in alkyl-substituted aromatic species decomposition, benzyl radical, summarized in Chapter 6.

Benzyl radicals are formed during the pyrolysis of any species with the formula  $C_6R_5CR_3$ , where R can be carbon or hydrogen atoms. Thermal decomposition of such molecules will form  $C_6R_5CR_2$ , which exhibits large resonance stabilization due to the radical electron delocalizing into the ring structure. The resonance stabilization of the simplest benzyl radical ( $C_6H_5CH_2$ ) has been calculated by comparing experimental heats of formation and is found to be  $11.4 \pm 1$  kcal/mol, as summarized in Chapter 7.

The study of benzyl radical proved to be much more complicated than had been anticipated and eventually spurred the study of two other  $C_7H_7$  isomers, tropyli radical and 2,5-norbornadienyl radical. The three  $C_7H_7$  radicals are shown in Fig. 1.5.

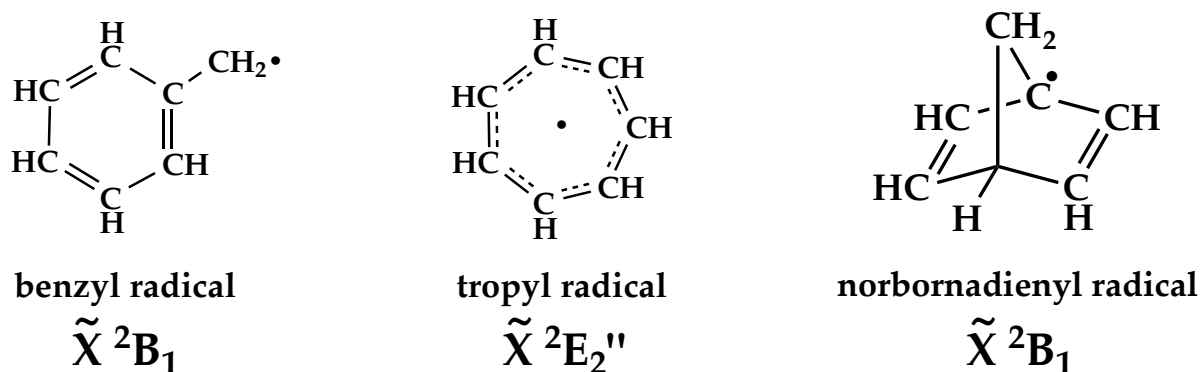


Fig. 1.5. Chemical structure of three isomers of  $C_7H_7$ , including their common names and the symmetry of their electronic ground states.

Chapter 7 provides a detailed explanation of the decomposition of tropyli radical and presents more findings related to the decomposition of benzyl radical that were discovered after the publication of our work on benzyl radical.<sup>[14]</sup>

Chapter 8 details the recent work done in collaboration with Dr. William Peters and David Couch from the research group of Dr. Margaret Murnane and Dr. Henry

Kapteyn. We have coupled our pyrolysis source to a tabletop extreme ultraviolet (XUV) laser and advanced ion imaging detector and have demonstrated a powerful new method to record PIMS spectra. Chapter 8 includes a description of this experiment along with preliminary data that demonstrate the utility of this combined experimental approach.

## References for Chapter 1

- [1] T. C. Zhang, L. D. Zhang, X. Hong, K. W. Zhang, F. Qi, C. K. Law, T. H. Ye, P. H. Zhao and Y. L. Chen. An experimental and theoretical study of toluene pyrolysis with tunable synchrotron VUV photoionization and molecular-beam mass spectrometry. *Combustion and Flame* **2009**, *156*, 2071-2083.
- [2] M. Frenklach, D. W. Clary, W. C. Gardiner and S. E. Stein. Twentieth Symposium (International) on Combustion Detailed kinetic modeling of soot formation in shock-tube pyrolysis of acetylene. *Symposium (International) on Combustion* **1984**, *20*, 887-901.
- [3] A. L. C. Lima, J. W. Farrington and C. M. Reddy. Combustion-Derived Polycyclic Aromatic Hydrocarbons in the Environment—A Review. *Environmental Forensics* **2005**, *6*, 109-131.
- [4] H. Richter and J. B. Howard. Formation of polycyclic aromatic hydrocarbons and their growth to soot - a review of chemical reaction pathways. *Progress in Energy and Combustion Science* **2000**, *26*, 565-608.
- [5] W. A. Goddard, T. H. Dunning, W. J. Hunt and P. J. Hay. Generalized valence bond description of bonding in low-lying states of molecules. *Accounts of Chemical Research* **1973**, *6*, 368-376.
- [6] K. Brezinsky. The high-temperature oxidation of aromatic hydrocarbons. *Progress in Energy and Combustion Science* **1986**, *12*, 1-24.
- [7] J. D. Savee, T. M. Selby, O. Welz, C. A. Taatjes and D. L. Osborn. Time- and Isomer-Resolved Measurements of Sequential Addition of Acetylene to the Propargyl Radical. *The Journal of Physical Chemistry Letters* **2015**, 4153-4158.
- [8] S. A. Skeen, H. A. Michelsen, K. R. Wilson, D. M. Popolan, A. Violi and N. Hansen. Near-threshold photoionization mass spectra of combustion-generated high-molecular-weight soot precursors. *Journal of Aerosol Science* **2013**, *58*, 86-102.
- [9] J. A. Miller, M. J. Pilling and J. Troe. Unravelling combustion mechanisms through a quantitative understanding of elementary reactions. *Proceedings of the Combustion Institute* **2005**, *30*, 43-88.

- [10] C. Heitner, D. Dimmel and J. Schmidt, *Lignin and lignans: advances in chemistry*, CRC press, **2010**, p. 1-10.
- [11] D. Robichaud, M. Nimlos and G. B. Ellison in *Pyrolysis Mechanisms of Lignin Model Compounds Using a Heated Micro-Reactor*, Eds.: M. Schlaf and Z. C. Zhang, Springer Singapore, **2016**, pp. 145-171.
- [12] T. L. Marker, L. G. Felix, M. B. Linck and M. J. Roberts. Integrated Hydrolysis and Hydroconversion (IH2) for the Direct Production of Gasoline and Diesel Fuels or Blending Components from Biomass, Part 1: Proof of Principle Testing. *Environmental Progress & Sustainable Energy* **2012**, *31*, 191-199.
- [13] A. K. Vasiliou, J. H. Kim, T. K. Ormond, K. M. Piech, K. N. Urness, A. M. Scheer, D. J. Robichaud, C. Mukarakate, M. R. Nimlos, J. W. Daily, Q. Guan, H.-H. Carstensen and G. B. Ellison. Biomass Pyrolysis: Thermal Decomposition Mechanisms of Furfural and Benzaldehyde *Journal of Chemical Physics* **2013**, *139*, 104310.
- [14] G. T. Buckingham, T. K. Ormond, J. P. Porterfield, P. Hemberger, O. Kostko, M. Ahmed, D. J. Robichaud, M. R. Nimlos, J. W. Daily and G. B. Ellison. The thermal decomposition of the benzyl radical in a heated micro-reactor. I. Experimental findings. *The Journal of Chemical Physics* **2015**, *142*, 044307.



## Chapter 2

### Experimental Methods

#### I. Introduction

The work of my thesis was done in two stages, first in the group of Dr. David J. Nesbitt, where I performed high-resolution absorption spectroscopy on unstable radicals and ion. The second phase of my degree took place in the labs of Dr. G. Barney Ellison, where I studied the unimolecular decomposition of combustion relevant intermediates. The work performed with Dr. Nesbitt required a specialized molecular source to produce high densities of non-interacting gas-phase radicals and ions coupled to a stable, tunable infrared (IR) light source that allowed for careful scanning of the C-H, N-H, and O-H stretching regions of the vibrational spectrum. The instrument resolution of roughly 60 MHz allowed for assignment of individual rovibrational lines and in a molecule like phenyl radical, for example, greater than 100 individual transitions can be assigned. In the Ellison lab, we were able to heat gas-phase precursors and directly detect fragments of the nascent decomposition pathways that occur within the first roughly 100 microseconds of pyrolysis. By combining multiple different precursors, unique isotopomers, and multiple complementary detection techniques, we were able to make important conclusions about how fundamental molecules and radicals decompose when heated to a range of temperatures.

Given the broad array of techniques used, it will be necessary to provide a more detailed experimental description for each project in the appropriate chapters later on.



This section will serve to describe general technical features that span many projects and familiarize the reader with the types of experiments performed.

## II. High Resolution Absorption Spectroscopy

The ability to obtain well resolved rovibrational spectra of phenyl radical ( $C_6H_5 \tilde{X}^2A_1$ ) in the gas phase relies largely on several experimental advantages: a) high radical densities per quantum state accessible with low temperature discharge expansions, b) sub-Doppler compression of velocity broadening in the slit jet, c) long absorption path geometry and d) a precisely tunable frequency stabilized IR light source. The experimental apparatus has been described in previous papers<sup>[1-2]</sup> thus only a brief summary of details relevant to the present work will be presented here.

### A. Difference Frequency Infrared Production

Infrared light is produced by spatially overlapping two visible laser beams in a temperature controlled, periodically poled lithium niobate crystal, which results in difference frequency generation of tunable light in the 2.5-4  $\mu m$  region. The two visible light sources are i) a fixed frequency argon ion ( $Ar^+$ ) laser operating at 514 nm (19429.88  $cm^{-1}$ ) and ii) a tunable ring dye laser (R6G dye) between 17500 to 16000  $cm^{-1}$ . The  $Ar^+$  laser is locked via servo-loop to the transmission fringes of an external Fabry-Perot cavity (FSR = 250 MHz), which in turn is locked to a polarization-stabilized helium-neon (HeNe) laser to achieve long-term frequency stability over multiple days. Scanning progress of the dye laser is measured with respect to fringes on the same ultrastable Fabry-Perot cavity, yielding comparable precision for frequency measurement on the difference frequency infrared (IR) light. Absolute frequencies are

determined by a reference absorption line of jet cooled methane (R(4), 3067.3000  $\text{cm}^{-1}$ ) observed under identical slit jet conditions,<sup>[3]</sup> providing a calibrated IR frequency axis with typical rms reproducibility of 8 MHz ( $< 0.0003 \text{ cm}^{-1}$ ) for the transitions reported.

The IR light is divided into two beams by a 50:50 beam splitter, with one portion measured directly on a liquid nitrogen cooled InSb reference detector. The remainder of the IR light is then directed through the slit jet discharge/Herriott cell vacuum chamber, extracted after 16 passes and re-collimated onto a matched liquid nitrogen cooled InSb signal detector. Noise between signal and reference detector is actively balanced using high bandwidth (1 MHz) home-built active subtraction electronics, with the weak absorption signals at the 50 kHz discharge modulation frequency obtained via lock-in detection to provide additional signal-to-noise enhancement. These lock-in detection signals are then further analyzed in the time domain by gated integration and differential baseline correction before, during and after the slit jet pulse, with all resulting data and frequency diagnostics stored in a computer for later analysis.

## **B. Slit Discharge Radical and Ion Production**

The spectroscopic target species are produced via C-X bond fragmentation of halogenated precursors in a slit supersonic jet expansion, yielding typical signal-to-noise on the strongest absorption peaks of roughly 50:1. The mechanism for C-X bond fission is presumed to be electron dissociative attachment to form the radical center +  $X^-$ , which, favors use of halogenated precursor species with weakest C-X bond strengths. Indeed, phenyl radical, for example, can be efficiently synthesized in the discharge with chlorobenzene ( $\text{C}_6\text{H}_5\text{Cl}$ ), bromobenzene ( $\text{C}_6\text{H}_5\text{Br}$ ), and iodobenzene ( $\text{C}_6\text{H}_5\text{I}$ ), with signal intensities greatly limited by reduced room

temperature vapor pressures of the latter. As a compromise between vapor pressure, control, and formation efficiency, the carrier gas Ne70 (70 % neon, 30 % helium) is bubbled through liquid-phase chlorobenzene cooled at 0° C, with the gas mixture further diluted with Ne70 to produce 0.5 % C<sub>6</sub>H<sub>5</sub>Cl gas samples in the stagnation region at 280 Torr total pressure. The gas is supersonically expanded through a JILA-built solenoid-driven slit valve capable of generating intense pulses with tunable duration (1000 μs, < 50 μs rise time) that exit through a 4 cm long, 300 μm wide slit into a vacuum chamber. This supersonic expansion is triggered at a repetition rate of 19 Hz, with pressure in the vacuum chamber maintained less than 50 mTorr by a 560 liter/second Roots blower (Leybold WS200). During each gas pulse, a 50 kHz modulated square wave voltage (around 500 V) is applied across an insulated 1 mm region located immediately prior to the expansion orifice, as illustrated in Fig. 2.1.<sup>[1]</sup> This voltage is sufficient to produce a glow discharge with 280 mA peak current through the sample and carrier gas mixture, which causes dissociative electron attachment and homolytic cleavage of the C-X bonds to produce the desired radicals.

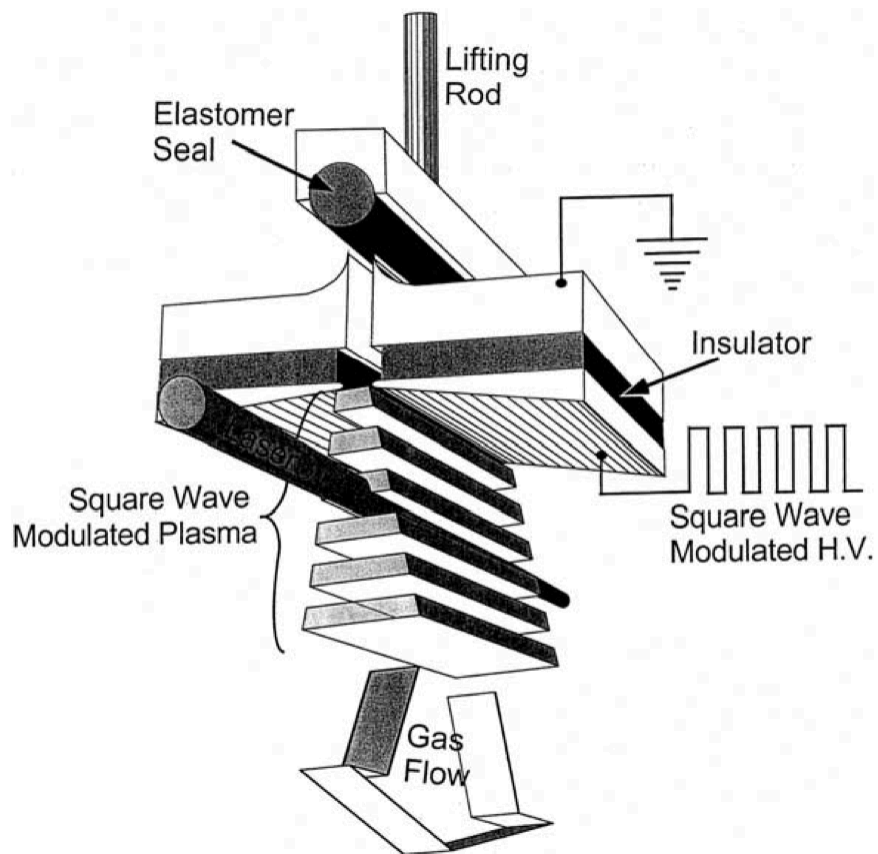


Fig. 2.1. Cartoon diagram of pulsed slit jet discharge. During the 1000  $\mu\text{s}$  gas pulse, the carrier gas and precursor flow into the discharge region where a square wave modulated voltage ( $-500\text{ V}$ ) is applied with a 50 kHz frequency. The electric field induced glow discharge results in efficient electron dissociative attachment of the weak carbon-halogen bond in the precursor. The products in the expansion are rapidly cooled to 11(1) K in the slit supersonic expansion.

The slit jet expansion rapidly cools the phenyl radical down to roughly 11(1) K, where infrared light 5 mm downstream from the nozzle orifice allows direct absorption by the newly formed radical molecules. Near shot noise limited absorption sensitivities on the order of 0.002 % ( $A = 2 \times 10^{-5}$ ) in a 10 kHz bandwidth are made possible by fast servo loop subtraction of signal and reference detector technical common mode noise on the IR laser. The signal is further augmented by increasing the absorption path length with a 16-pass Herriott cell, which is aligned directly below the slit orifice. This

alignment minimizes molecular velocity parallel to the beam path, lowers the Doppler width of the measured absorption peaks by an additional 5-10 fold (in Ne70), and thereby increases the peak absorption cross section by an equivalent 5-10 fold. In combination with the much slower ( $1/r$  vs.  $1/r^2$ ) density drop off in a slit vs. pinhole jet, this yields a net sensitivity enhancement for direct IR absorption on high reactive radicals by some 3-4 orders of magnitude. Combined with typical<sup>[4]</sup> integrated absorption strengths (5-20 km/mol) for hydrocarbon species such as phenyl radical, these absorption sensitivities translates into minimum detectable number densities of  $2 \times 10^8 \text{ cm}^{-3} \text{ quantum state}^{-1}$  in a detection region 5 mm downstream of the slit jet orifice.

### **III. Pyrolysis of Gas-Phase Biofuel Intermediates Using a Heated Micro-Reactor**

Gas-phase samples of hydrocarbons and oxygenated hydrocarbons have been pyrolyzed in a heated micro-reactor and a set of detection techniques has been employed to detect the products. By combining multiple techniques with very different detection mechanisms, we are able to identify *all* products that exit the nozzle, including radicals, metastables, and atoms. The reactor itself will be described first, including recent efforts to computationally model the flow of gasses through the reactor at elevated temperatures and with large pressure gradients. After the exit of the reactor, the detection schemes used include: i) photoionization mass spectrometry using the 9<sup>th</sup> harmonic of an Nd:YAG laser and time-of-flight (TOF) detection, ii) photoionization mass spectrometry using synchrotron radiation and TOF detection, iii) photoionization mass spectrometry using tunable synchrotron radiation and imaging photoelectron photoion coincidence spectroscopy (iPEPICO), iv) photoionization mass spectrometry

using table-top high harmonic generation and photoelectron photoion coincidence (PEPICO) spectroscopy, v) matrix-isolation IR absorption spectroscopy, and vi) laser-induced fluorescence (LIF).

### **A. Pyrolysis in a Heated Micro-Reactor**

To study pyrolysis, shock tubes have long been an attractive method as they allow for controlled conditions and myriad detection schemes. Due to their low repetition rates, however, it is challenging to study the dilute initial products and only stable products can be detected. An excellent complement to this technique is a heated micro-reactor often called a Chen Nozzle, which was developed in the lab of Dr. Peter Chen.<sup>[5-7]</sup> Initially made of silicon carbide (SiC), these reactors have 1 mm inner diameter (I.D.), 2 mm outer diameter (O.D.) and can be cut to any length but are often between 1 and 3 cm. SiC is used because its electrical resistance is such that it can be conveniently and controllably heated to temperatures of up to 2000 K with simple variable transformers and/or low cost proportional-integral-derivative (PID) servo controllers. One of the main advantages of micro-reactors is that for a given set of flow conditions, it is possible to thermally decompose samples over short times scales so that only the initial decomposition is observed.

In recent years, the micro-reactor has been used to study the thermal decomposition of fuels<sup>[8]</sup> by coupling to a matrix isolation spectroscopy scheme.<sup>[9]</sup> Initially used primarily as a source of organic radicals<sup>[10-13]</sup> for IR spectroscopic analysis, the value of the reactor as a means to study pyrolysis quickly emerged and since has been used more as a means to study thermal decomposition.<sup>[14-16]</sup> A shortcoming of the micro-reactor set-up eventually emerged that the temperature and pressure inside the

reactor are poorly characterized. Although the wall temperature can be measured directly with Type-C thermocouples and the upstream/downstream pressure can be monitored, these two variables cannot be easily solved for inside the reactor. In order to provide useful information to reaction modelers, the temperature and pressure must be known within the reactor so that the products detected can be entered into complicated kinetic schemes that are the basis of combustion researchers looking to better characterize complex chemical environments.

Collaboration with Dr. John W. Daily of the Mechanical Engineering Department has provided significant progress towards being able to directly predict the temperature and pressure at all points within the reactor. Using computational fluid dynamics (CFD) simulations of inert carrier gasses like He, Ar, or Ne, it was possible to carry out simulations of these two important variables (gas temperature and pressure) as a function of wall temperature, pressure differential, and mass flow rate. The findings are summarized in a 2014 review paper,<sup>[17]</sup> which establishes a comprehensive investigation of fluid flow through a heated micro-reactor. In order to validate the predictions of these simulations, a recent effort has been made to design new experiments that will make accessible the gas inside a heated reactor. To monitor the temperature of the gas inside the reactor, a novel heater was designed that can radiatively heat a fused silica tube (1 mm I.D., 2 mm O.D.) without obscuring optical access to the interior.<sup>[18]</sup>

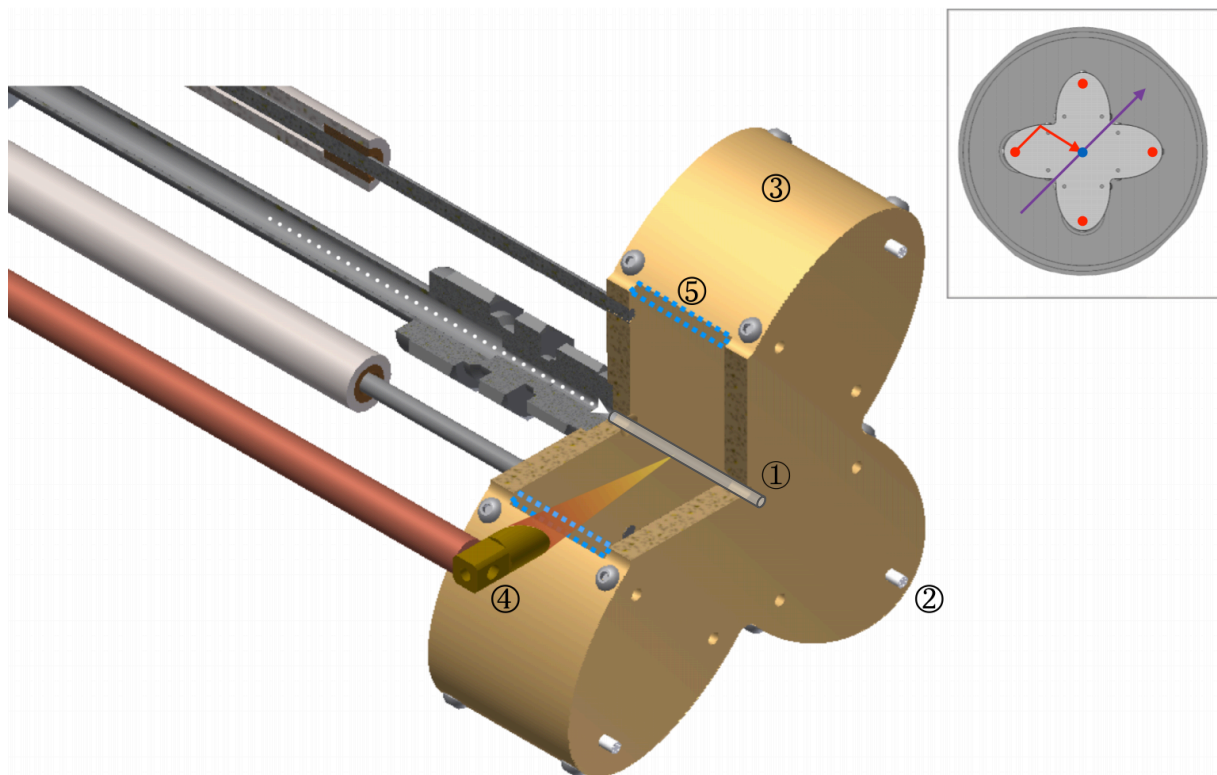


Fig. 2.2. Cut away view of the clover heater. Gas flows through the fused silica tube (1) in the center, while radiation from the four heater elements (2), of which three are shown here, is concentrated onto the micro-reactor by the elliptical mirrors (3). To the left, one parabolic mirror (4) from the custom IR thermometer illustrates how emission from the micro-reactor can be collected via slits (5) in between the elliptical mirrors. The inset schematic (upper right) depicts the simultaneous radiative heating of (red) and optical access to (purple) the micro-reactor (blue).

The heater, referred to as a “clover heater” due to its shape, is shown<sup>[18]</sup> in Fig. 2.2. Fused silica allows for ultraviolet (UV) spectroscopy to be done on the gas inside the reactor and as a proof of concept, the laser induced fluorescence (LIF) spectrum of dilute (5 %) nitric oxide (NO) in argon can be recorded on gas flowing through the heated reactor. These first experiments on NO provide a rotational temperature measurement that is in good agreement with the computational models generated by the CFD simulations.



Each experiment performed has slightly different requirements in terms of pumping speed, pumping mechanisms, and detection mechanisms. For this reason, it has been necessary to use many different configurations of carrier gas, flow condition (pulsed and continuous CW), pressures, and reactor geometries. These conditions are summarized in Table 2.1.

Experiment	Carrier Gas	Flow	Lights Source	Backing Pressure	Outlet Pressure	Reactor Geometry
Photoionization Mass Spectrometry in Colorado	Helium	Pulsed	118.2 nm (10.487 eV) Nd:YAG Laser	1500 Torr	$2 \times 10^{-6}$ Torr	I.D. 1 mm Heated Length: 15 mm
Photoionization Mass Spectrometry at the ALS <sup>a</sup>	Helium	Continuous	Tunable Synchrotron	50 Torr	$2 \times 10^{-5}$ Torr	I.D. 0.6 mm Heated Length: 10 mm
Photoionization Mass Spectrometry at the SLS <sup>b</sup>	Argon	Continuous	Tunable Synchrotron	50 Torr	$5 \times 10^{-6}$ Torr	I.D. 1 mm Heated Length: 15 mm
Photoionization Mass Spectrometry with Tabletop VUV <sup>c</sup> + PEPICO <sup>d</sup>	Helium	Continuous	Ti:sapphire High Harmonic Generation	800 – 1500 Torr	$1 \times 10^{-4}$ Torr	I.D. 1mm Heated Length: 15 mm
Matrix Isolation IR Spectroscopy in Colorado	Neon	Pulsed	none	1000 Torr	$2 \times 10^{-6}$ Torr	I.D. 1 mm Heated Length: 10 mm

Table 2.1. Summary of the conditions for each experiment performed with heated micro-reactor.

<sup>a</sup> Advanced Light Source

<sup>b</sup> Swiss Light Source

<sup>c</sup> Vacuum ultraviolet

<sup>d</sup> Photoelectron photoion coincidence

## B. Photoionization Mass Spectrometry

One of the most useful experimental techniques for identifying the pyrolysis fragments that exit a heated reactor is mass spectrometry. Within a relatively short amount of time, the mass-to-charge ratio ( $m/z$ ) of nearly all species can be identified at a wide range of temperatures. The only limit one regarding molecule detection is the energy of the ionization source employed. In Colorado, at both the University of Colorado Boulder and the National Renewable Energy Laboratory (NREL), we utilize  $\lambda = 118.2 \text{ nm}$  ( $E_{\text{photon}} = 10.487 \text{ eV}$ ) as the ionization source. This frequency of light is ideal

for ionizing pyrolysis products because it is sufficiently energetic to ionize nearly all organic species except for a short list of exceptions. The molecules with ionization energy (IE) greater than 10.487 eV cannot be observed and this set of molecules includes H<sub>2</sub>O, CO<sub>2</sub>, CO, HCC, CH<sub>4</sub>, HC≡CH, and CH<sub>2</sub>=CH<sub>2</sub>. Most other organic molecules will lose an electron upon absorbing a  $\lambda = 118.2$  nm photon and can then be detected using electrostatic ion optic techniques. The disadvantages of the 9<sup>th</sup> harmonic of an Nd:YAG in our labs in Colorado are: i) the repetition rate is low, either 10 Hz or 30 Hz; ii) fragments made that have IEs greater than 10.487 eV cannot be detected and thus mechanisms forming such fragments are challenging to confirm; iii) some molecules that have IEs lower than 10.487 eV will undergo dissociative ionization; in this process a cation is formed with enough excess energy that it can fragment to a different cation and one (or more) neutral species; and iv) many isomers may exist at a given m/z so a feature in a PIMS spectrum does not specifically identify what species is actually present. To cope with these shortcomings, our group has multiple complementary PIMS techniques using different ionization sources and different detections schemes such that all four shortcomings can be overcome. Each PIMS experimental technique will be described separately to highlight the differences between them.

### **i. Photoionization Mass Spectrometry Using the 9<sup>th</sup> Harmonic of an Nd:YAG Laser and Reflectron Time-of-Flight Detection**

PIMS with a pulsed micro-reactor<sup>[9]</sup> combines the 9<sup>th</sup> harmonic of a Nd:YAG laser (118.2 nm or 10.487 eV). The laser is synchronized to a Parker general pulsed valve backed by a helium-hydrocarbon mixture. The pulsed valve operates at 10 Hz or 30 Hz with an opening time of 1 msec. A 1 mm skimmer is placed about 1 cm from the exit of

the SiC reactor to select only the component of the expansion traveling in the longitudinal direction with respect to the reactor tube. The pressure in the chamber at the exit of the reactor is  $10^{-6}$  Torr.

The internally frequency-tripled output ( $\lambda = 355$  nm) of a Nd:YAG laser (Spectra-Physics Quanta-Ray Lab 130) is directed into a cell that is pressurized to 150 Torr with a 10:1 argon:xenon mixture. This mixture is optimized to promote sum-frequency generation that creates  $\lambda = 118.2$  nm VUV photons. Generation of 118.2 nm photons by Xe/Ar tripling cells has been studied previously.<sup>[19]</sup> Use of 30 mJ pulse<sup>-1</sup> power at 355 nm from the YAG laser and the established tripling efficiency of  $1 \times 10^{-5}$  in pure xenon<sup>[20-21]</sup> as well as the transmission efficiency of the MgF<sub>2</sub> lens at the exit of the cell indicates that we should produce roughly 30 nJ pulse<sup>-1</sup> at 118.2 nm light. This VUV laser light is directed into a vacuum chamber maintained at  $10^{-7}$  Torr by a 1200 L/s Pfeiffer TPU 1201 P turbomolecular pump and is then intersected with the skimmed output of the supersonic expansion. After ionization the molecules in the beam are accelerated into a Jordan reflectron time of flight spectrometer with an MCP detector producing PIMS spectra at 10.487 eV. The pressure in the flight tube is maintained at around  $10^{-7}$  Torr by a smaller turbomolecular pump.

## **ii. Photoionization Mass Spectrometry Using Synchrotron Radiation and Reflectron Time-of-Flight Detection**

A similar experimental setup and detection scheme is used at the Advanced Light Source (ALS) at Lawrence Berkeley National Labs (LBNL), Chemical Dynamics Beamline endstation 9.0.2. Using the synchrotron light for PIMS adds an experimental

degree of freedom: tunable VUV radiation.<sup>[22]</sup> The energy of the synchrotron photons at Beamline 9.0.2 can be tuned between 7.4 eV and 30 eV, sufficiently high to ionize all species produced in the heated reactor. The synchrotron has a repetition rate of 500 MHz and so data acquisition is much more rapid than in the laser based techniques performed in Colorado. By measuring ion current at a single mass-to-charge ratio ( $m/z$ ) while varying the photon energy it is possible to record photoionization spectra, which can be used to identify individual isomers at a given  $m/z$  by observing the ionization threshold. Signal averaging is used to increase the signal-to-noise ratio and typical spectra are the composite of between  $5 \times 10^4$  and  $2 \times 10^5$  scans. To control the flow of gas through the reactor, an MKS mass flow controller is used along with a slightly smaller (I.D. = 0.6 mm) SiC reactor. Typical flow conditions include setting the flow controller to 200 standard  $\text{cm}^3 \text{min}^{-1}$  (SCCM) backed by 5 atm of He. This yields a pressure of 100 Torr between the mass flow controller and entrance of the reactor and roughly  $10^{-4}$  Torr at the exit of the nozzle. With a 1 mm skimmer 1 to 2 cm downstream, the pressure in the ionization chamber can be maintained at roughly  $5 \times 10^{-6}$  Torr by a large turbomolecular pump.

### **iii. Photoionization Mass Spectrometry Using Synchrotron Radiation and Imaging Photoelectron Photoion Coincidence Spectroscopy**

The Swiss Light Source (SLS) at the Paul Scherrer Institute in Villigen Switzerland is able to provide photons at even lower energy than the ALS. The Coincidence Endstation at the SLS is readily able to provide photons at energies as low as 6 V, which is important when identifying isomers with small ionization energies like benzyl radical<sup>[23]</sup> (IE =  $7.2487 \pm 0.0006$  eV) and cycloheptatrienyl radical<sup>[24]</sup> (IE =  $6.221 \pm$

0.006 eV). In addition, the experiment at the SLS has the added advantage of an imaging photoelectron photoion coincidence (iPEPICO) detector, which can select only the ion counts that are detected in coincidence with electrons that are ejected with close to zero kinetic energy.

Because the pumping scheme makes use of cryogenic pumps, it is necessary for the carrier gas in these experiments to be argon. A temperature-controlled sample bubbler was used to house the liquid samples and was either heated or cooled depending on the sample vapor pressure and desired concentration in the gas flow. A backing pressure of approximately 50 Torr of argon was passed through the bubbler. The ratio of the vapor pressure at the sample temperature to the argon backing pressure was used to approximate the concentration of the target species in the argon beam. This gas mixture was then expanded through a 150  $\mu\text{m}$  pinhole directly into the SiC reactor (1 mm I.D.). A 2 mm skimmer was placed about 2-3 cm from the exit of the SiC reactor to select only the component of the beam traveling in the longitudinal direction with respect to the reactor tube. The flow rate is calculated to be less than 20 SCCM based on the backing pressure of the argon through the bubbler. This flow is slow enough that the expansion at the exit of the reactor is not choked enough to be supersonic and is instead an effusive flow.

The continuous flow enters the source chamber, which is evacuated by a 5000 L s<sup>-1</sup> Leybold COOLVAC 5000 CL cryogenic pump and a 1250 L s<sup>-1</sup> Pfeiffer TPH 1201 UP turbomolecular pump. The ionization chamber is pumped by a 1500 L s<sup>-1</sup> Leybold COOLVAC 1500 CL cryopump and a 500 L s<sup>-1</sup> Pfeiffer TMH 521 YP turbomolecular pump. The total high pumping capacity of 8250 L s<sup>-1</sup> is backed by an oil free foreline system to minimize background and contamination in the system.

At the photon energies used here, a magnesium fluoride ( $\text{MgF}_2$ ) lens is included to attenuate higher harmonics that would yield spurious ion counts on the detector. Unfortunately the  $\text{MgF}_2$  lens has decreasing transmission at lower photon energies so the photon flux below 7 eV is small compared to the higher energy portion of the spectrum. For this reason, PIMS spectra with photon energies of 7 eV yielded smaller ion counts and thus required longer collection times, which made PIEs at these energies too costly to perform.

#### **iv. Photoionization Mass Spectrometry using a Tabletop Vacuum Ultraviolet Laser and Photoelectron Photoion Coincidence Spectroscopy**

In order to combat issues of dissociative ionization, isomer ambiguity, and inability to ionize molecules with large ionization energies, we have coupled the micro-reactor to a laser system that generates harmonics of 800 nm Ti:sapphire laser light. The laser system was built in the group of Dr. Margaret Murnane and Dr. Henry Kapteyn and is modeled after the KMLabs Inc. Dragon<sup>TM</sup> system. The laser system used here is able to perform with 10 kHz repetition rate, which is important due to the low count rates required for coincidence detection. After amplifying the 30 fs output of a Ti:sapphire mode locked oscillator, the power of the IR light is on the order of 20 W. This is focused into a waveguide made of a fused silica capillary (150  $\mu\text{m}$  I.D.  $\times$  2.5 cm long) in which Xe is flowed, generating odd harmonics in the range of the 3<sup>rd</sup> harmonic (roughly 4.8 eV) up through the 11<sup>th</sup> harmonic (roughly 17.6 eV); higher harmonics up to at the 17th harmonic are possible. The molecules with the highest IE relevant to our experiments<sup>[25]</sup> is  $\text{H}_2$  (IE = 15.4 eV) so only the 9<sup>th</sup> harmonic and lower are necessary here. By filtering of higher harmonics with different rare gas filter schemes, harmonics

can be selected by making only minor alterations to the system. The laser system was not modified for these experiments and a more detailed description can be found in a previous publication and citations therein.<sup>[26]</sup>

The micro-reactor assembly in this experiment can be used without a pulse valve since the source chamber is pumped by a large turbomolecular pump (1650 L s<sup>-1</sup> Leybold MAG W 2010 C). Roughly 1 cm downstream of the reactor exit is a 300 μm skimmer that separates the source chamber from the ionization chamber and insures that a narrow molecular beam reaches the laser interaction region. In order to keep the pressure low enough for the detector, a 50 μm orifice was brazed into the stainless steel tubing just upstream of the reactor. This allows for a backing pressure of 1 to 2 atm, downstream pressures in the source chamber of 10<sup>-4</sup> Torr, and ionization chamber pressures of 10<sup>-7</sup> Torr during continuous flow of He. The reactor assembly, shown in Fig. 2.3, has a few new design features. A small stainless steel disc is included that has electrical feedthroughs installed to help stabilize the delicate (0.005") wires leading to the Type-C thermocouple. To limit the flow and maintain sufficiently low pressure for the PEPICO detector, a 50 μm orifice was brazed onto the metal just upstream of the reactor.



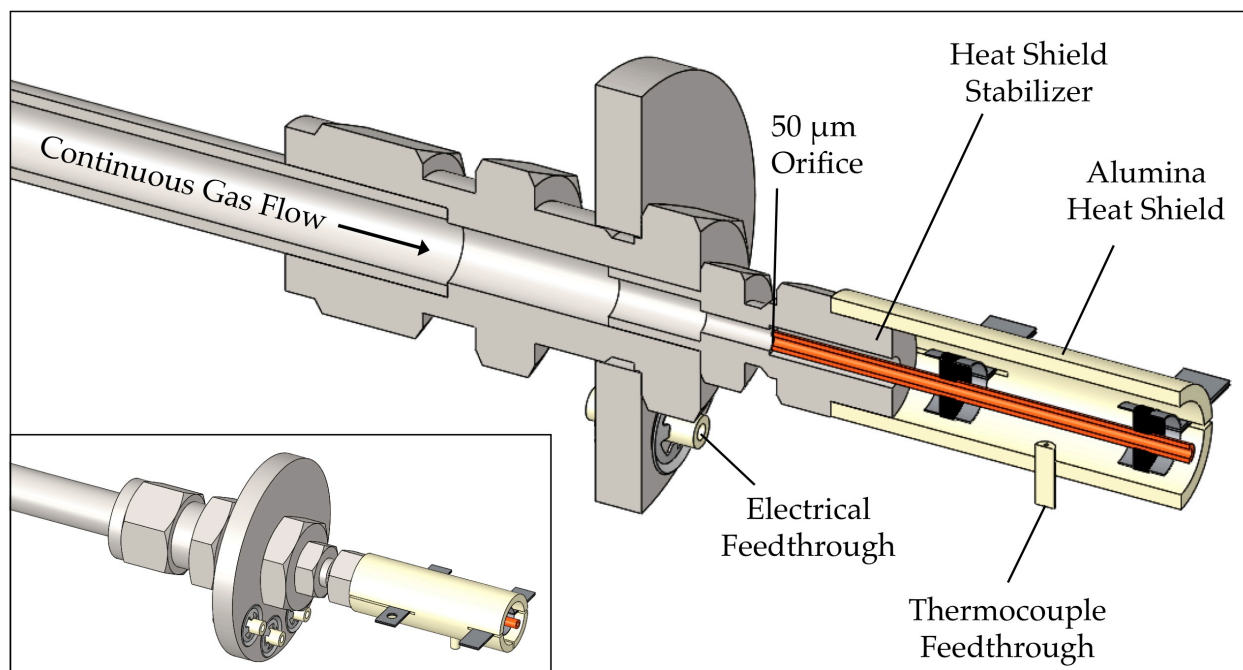


Fig. 2.3. Continuous flow heated micro-reactor assembly (inset) and larger cutaway diagram. The 50  $\mu\text{m}$  orifice limits the gas flow so that a pulsed valve is not needed to maintain appropriate upstream and downstream pressures. New design features are highlighted that help stabilize the assembly to prevent misalignment and increase thermocouple lifetime.

The detection mechanism in this experiment also adds important experimental information. Rather than a standard TOF configuration, the design of the ion optics in the interaction chamber allows us to detect both the cations and electrons formed from a single laser pulse. The count rate is intentionally attenuated so that only 1 in 10 laser pulses leads to a photoionization event, which would be challenging to maintain without the high repetition rate of the laser system (10 kHz). For a given ionization event, it is possible to correlate individual cations and their corresponding photoelectrons. The detectors for both the cations and the electrons are position sensitive so given a sufficiently small ionization volume, the distance traveled in the directions transverse to the flight axis can be used to calculate the kinetic energy of the charged particles. By plotting only the electrons detected in coincidence with a given

cation  $m/z$ , a photoelectron spectrum (PE) can be recorded. Although the instrument resolution is limited to about 0.75 eV, features in these photoelectron spectra can be identified and used as a diagnostic of given isomers. As long as two isomers have IEs that differ by more than roughly 1 eV, this detection scheme can be used to identify which isomers are present in a given  $m/z$ . Additionally, if a molecule in the molecular beam dissociatively ionizes, this detector can be used to identify the fragment mass as a product of dissociative ionization. The photoelectrons detected in coincidence with the dissociative ionization fragment will correspond to the PE spectrum of the parent molecule and not the fragment. As long as the PE spectra (or simply the IE) of the parent and the fragment are both known, peaks resulting from dissociative ionization can be removed from the recorded PIMS spectra during post-processing. These are major advantages over the Nd:YAG based TOF PIMS that has been the workhorse of this experimental technique in the past.

### **C. Matrix Isolation Infrared Absorption Spectroscopy**

Since all polyatomic molecules possess diagnostic vibrational spectra, IR spectroscopy is an excellent technique for identifying molecular species and serves as a valuable complement to PIMS experiments. The matrix IR spectrometer has been described before.<sup>[27-28]</sup> Briefly, a 1 mm I.D. SiC reactor is coupled to a pulsed valve assembly very similar to the PIMS system described above. The upstream pressure is between 800 and 1000 Torr and with the pulsed valve operating with 400  $\mu$ s opening time at 15 Hz, the pressure at the reactor exit is typically  $10^{-6}$  Torr. The pressure in this chamber is maintained with a small turbomolecular pump. The output of the reactor is aimed at a cryogenically cooled CsI window 4 cm downstream that is maintained at 5 K

by a helium compressor. The carrier gas for this experiment is neon, which condenses into a solid matrix upon colliding with the 5 K window. A standard matrix is formed by flowing 200 Torr of the sample mixture from a 3 L gas manifold with about one hour deposition time. After dosing is complete, the reactor assembly is rotated 90° out of the way and the CsI window is lowered into the beam path of a commercial Fourier transform IR (FTIR) spectrometer (Nicolet 6700). The MCT-A detector has a spectral range of 4000 to 600  $\text{cm}^{-1}$  and is operated with 0.25  $\text{cm}^{-1}$  resolution with typical spectra constructed by averaging 500 scans. Although the neon matrix is chemically inert, it does affect the vibrational spectra of entrained molecules. Average matrix shifts are on the order of 1 to 10  $\text{cm}^{-1}$  from the unperturbed gas-phase values.

#### **D. Sample Preparation**

In all experiments using the micro-reactor, sample preparation is done in one of two ways. If the sample is volatile enough, a tank of pre-mixed gasses is made and filled to between 1 and 5 atm. If the sample does not have sufficient vapor pressure at room temperature, the solid or liquid sample is held immediately upstream of the reactor in a temperature-controlled vial and pure carrier gas is flowed over it. This method assumes the vapor pressure (at the elevated temperature) is continuously reached while the gas is flowing. Whether the target molecule is a stable precursor or an unstable intermediate, a dilute mixture of gas is entrained in an inert carrier gas, either He, Ne, or Ar. Bimolecular chemistry can usually be avoided if the precursor pressure is less than or equal to 0.1 % of the total pressure. Prepared mixtures range from 800 Torr to 2000 Torr so sample pressures of 0.8 Torr to 2 Torr are often sufficiently dilute. If a more dilute sample is required (e.g. 10 times more dilute), a pre-

made sample tank (pressure =  $P_0$ ) can be evacuated to pressure =  $0.1 \cdot P_0$  and then refilled to  $P_0$  with carrier gas. This method can be repeated as long as sufficient mixing time is allotted. By introducing carrier gas in quick bursts, this diffusion time can be shortened.

When the desired precursor does not have sufficient vapor pressure for a pre-made tank, the sample must be heated to raise the vapor pressure into the range of 0.1 %. To prevent condensation of the sample on gas-manifold surfaces, a custom-designed sample probe was built that allows the solid/liquid to be placed directly behind the pulse valve and/or reactor. The sample probe, shown in Fig. 2.4, is small enough to be inserted into the 3/8" or 1/4" I.D. stainless steel tubing that leads to the pulse valve.

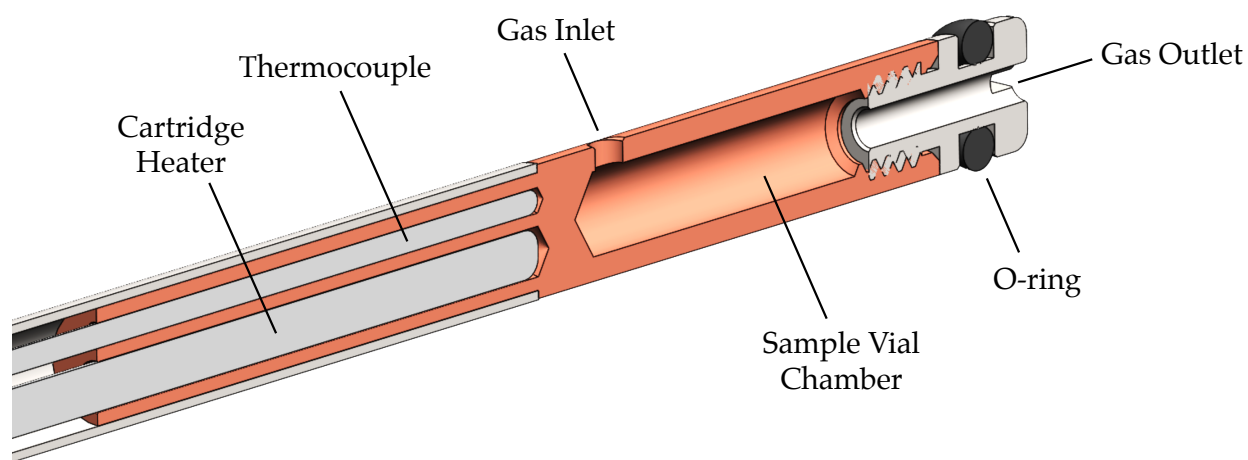


Fig. 2.4. Sample probe for heating low-vapor pressure solids and liquids. Gray colored material is stainless steel and the bronze color is copper, which provides good heat transfer. The O-ring near the end makes a seal with the tubing so that gas must flow into the inlet, around the sample vial, and then through the gas outlet, which ensures good sample pickup into the carrier gas flow.

The sample probe has a type-K thermocouple and heating element installed in the metal that jackets the sample vial, which allows for careful temperature control of

the sample using PID temperature controllers. To prevent condensation in the pulse valve and neighboring metal surfaces, temperature controlled water (or other solvents) can be circulated through custom-designed water jackets that are inside the vacuum chamber. For difficult samples with small vapor pressures (e.g. vanillin), the entire assembly inside the vacuum chamber including the pulse valve, reactor, and gas lines was maintained at roughly 98° C, while the solid sample of vanillin was held at between 90° and 120° C. A more robust heating system would make use of a circulating fluid with a higher boiling point than water to allow even higher metal wall temperatures.

## References for Chapter 2

- [1] S. Davis, M. Farnik, D. Uy and D. J. Nesbitt. Concentration modulation spectroscopy with a pulsed slit supersonic discharge expansion source. *Chemical Physics Letters* **2001**, 344, 23-30.
- [2] F. Dong, S. Davis and D. J. Nesbitt. Slit discharge IR spectroscopy of a jet-cooled cyclopropyl radical: Structure and intramolecular tunneling dynamics. *Journal of Physical Chemistry A* **2006**, 110, 3059-3070.
- [3] A. S. Pine. High-resolution methane nu-3-band spectra using a stabilized tunable difference-frequency laser system. *Journal of the Optical Society of America* **1976**, 66, 97-108.
- [4] M. Frisch, G. Trucks, H. Schlegel, G. Scuseria, M. Robb, J. Cheeseman, V. Zakrzewski, J. Montgomery Jr, R. E. Stratmann and J. Burant in *Gaussian 98, revision a. 7; gaussian, Vol. 12* Inc., Pittsburgh, PA, **1998**.
- [5] P. Chen, S. D. Colson, W. A. Chupka and J. A. Berson. Flash Pyrolytic Production of Rotationally Cold Free-Radicals in a Supersonic Jet - Resonant Multiphoton Spectrum of the  $3P^2A_2$  Origin Band of  $CH_3$ . *Journal of Physical Chemistry* **1986**, 90, 2319-2321.
- [6] P. Chen, J. B. Pallix, W. A. Chupka and S. D. Colson. Resonant multiphoton ionization spectrum and electronic-structure of CH radical - new states and assignments above  $50,000\text{ cm}^{-1}$ . *Journal of Chemical Physics* **1987**, 86, 516-521.
- [7] D. W. Kohn, H. Clauberg and P. Chen. Flash Pyrolysis Nozzle for Generation of Radicals in a Supersonic Jet Expansion. *Review of Scientific Instruments* **1992**, 63, 4003-4005.
- [8] A. L. Brown, D. C. Dayton, M. R. Nimlos and J. W. Daily. Design and characterization of an entrained flow reactor for the study of biomass pyrolysis chemistry at high heating rates. *Energy and Fuels* **2001**, 15, 1276-1285.
- [9] X. Zhang, A. V. Friderichsen, S. Nandi, G. B. Ellison, D. E. David, J. T. McKinnon, T. G. Lindeman, D. C. Dayton and M. R. Nimlos. Intense, hyperthermal source of organic radicals for matrix-isolation spectroscopy. *Review of Scientific Instruments* **2003**, 74, 3077-3086.

- [10] A. V. Friderichsen, J. G. Radziszewski, M. R. Nimlos, P. R. Winter, D. C. Dayton, D. E. David and G. B. Ellison. The Infrared Spectrum of the Matrix-Isolated Phenyl Radical. *Journal of the American Chemical Society* **2001**, *123*, 1977-1988.
- [11] S. Nandi, P. A. Arnold, B. K. Carpenter, M. R. Nimlos, D. C. Dayton and G. B. Ellison. Polarized infrared absorption spectra of matrix-isolated allyl radicals. *Journal of Physical Chemistry A* **2001**, *105*, 7514-7524.
- [12] S. Nandi, S. J. Blanksby, X. Zhang, M. R. Nimlos, D. C. Dayton and G. B. Ellison. Polarized infrared absorption spectrum of matrix-isolated methylperoxy radicals,  $\text{CH}_3\text{OO} \cdot$ . *Journal of Physical Chemistry A* **2002**, *106*, 7547-7556.
- [13] E. B. Jochowitz, X. Zhang, M. R. Nimlos, M. E. Varner, J. F. Stanton and G. B. Ellison. Propargyl Radical: *ab initio* Anharmonic Modes and the Polarized Infrared Absorption Spectra of Matrix-Isolated  $\text{HCCCH}_2$ . *Journal of Physical Chemistry A* **2005**, *109*, 3812-3821.
- [14] X. Zhang, A. T. Maccarone, M. R. Nimlos, S. Kato, V. M. Bierbaum, G. B. Ellison, B. Ruscic, A. C. Simmonett, W. D. Allen and H. F. Schaefer. Unimolecular thermal fragmentation of *ortho*-benzyne. *Journal of Chemical Physics* **2007**, *126*, -.
- [15] A. M. Scheer, C. Mukarakate, D. J. Robichaud, G. B. Ellison and M. R. Nimlos. Radical Chemistry in the Thermal Decomposition of Anisole and Deuterated Anisoles: An Investigation of Aromatic Growth. *Journal of Physical Chemistry A* **2010**, *114*, 9043-9056.
- [16] A. Vasiliou, K. M. Piech, X. Zhang, M. R. Nimlos, M. Ahmed, O. Kostko, A. Golan, D. L. Osborn, J. W. Daily, J. F. Stanton and G. B. Ellison. The products of the thermal decomposition of  $\text{CH}_3\text{CHO}$ . *Journal of Chemical Physics* **2011**, *135*, 14306-14311.
- [17] Q. Guan, K. N. Urness, T. K. Ormond, D. E. David, G. B. Ellison and J. W. Daily. The Properties of a Micro-Reactor for the Study of the Unimolecular Decomposition of Large Molecules. *International Reviews in Physical Chemistry* **2014**, *33*, 447-487.
- [18] J. H. Baraban, D. E. David, G. B. Ellison and J. W. Daily. An optically accessible pyrolysis microreactor. *Review of Scientific Instruments* **2016**, *87*, 014101.

- [19] N. P. Lockyer and J. C. Vickerman. Single photon ionisation mass spectrometry using laser-generated vacuum ultraviolet photons. *Laser Chemistry* **1997**, *17*, 139-159.
- [20] J. Boyle and L. Pfefferle. Study of higher hydrocarbon production during ethylacetylene pyrolysis using laser-generated vacuum-ultraviolet photoionization detection. *Journal of Physical Chemistry* **1990**, *94*, 3336-3340.
- [21] R. E. Bandy, C. Lakshminarayan, R. K. Frost and T. S. Zwier. The Ultraviolet Photochemistry of Diacetylene - Direct Detection of Primary Products of the Metastable  $C_4H_2^* + C_4H_2$  Reaction. *Journal of Chemical Physics* **1993**, *98*, 5362-5374.
- [22] P. A. Heimann, M. Koike, C. W. Hsu, D. Blank, X. M. Yang, A. G. Suits, Y. T. Lee, M. Evans, C. Y. Ng, C. Flaim and H. A. Padmore. Performance of the vacuum ultraviolet high-resolution and high-flux beamline for chemical dynamics studies at the Advanced Light Source. *Review of Scientific Instruments* **1997**, *68*, 1945-1951.
- [23] G. C. Eiden, F. Weinhold and J. C. Weisshaar. Photoelectron-spectroscopy of free-radicals with  $cm^{-1}$  resolution - the benzyl cation. *Journal of Chemical Physics* **1991**, *95*, 8665-8668.
- [24] K. H. Fischer, P. Hemberger, A. Bodi and I. Fischer. Photoionisation of the tropyli radical. *Beilstein Journal of Organic Chemistry* **2013**, *9*, 681-688.
- [25] D. Shiner, J. M. Gilligan, B. M. Cook and W. Lichten.  $H_2$ ,  $D_2$ , and HD ionization-potentials by accurate calibration of several iodine lines. *Physical Review A* **1993**, *47*, 4042-4045.
- [26] E. Gagnon, A. S. Sandhu, A. Paul, K. Hagen, A. Czasch, T. Jahnke, P. Ranitovic, C. Lewis Cocke, B. Walker, M. M. Murnane and H. C. Kapteyn. Time-resolved momentum imaging system for molecular dynamics studies using a tabletop ultrafast extreme-ultraviolet light source. *Review of Scientific Instruments* **2008**, *79*, 063102.
- [27] A. Vasiliou, K. M. Piech, X. Zhang, M. R. Nimlos, M. Ahmed, A. Golan, O. Kostko, D. L. Osborn, J. W. Daily, J. F. Stanton and G. B. Ellison. The products of the thermal decomposition of  $CH_3CHO$ . *Journal of Chemical Physics* **2011**, *135*, 14306-14311.
- [28] T. K. Ormond, A. M. Scheer, M. R. Nimlos, D. J. Robichaud, J. W. Daily, J. F. Stanton and G. B. Ellison. Polarized Matrix Infrared Spectra of Cyclopentadienone:



Observations, Calculations, and Assignment for an Important Intermediate in Combustion and Biomass Pyrolysis. *Journal of Physical Chemistry A* **2014**, *118*, 708-718.

## Chapter 3

### High-Resolution Rovibrational Spectroscopy of Jet-Cooled Phenyl Radical: The $\nu_{19}$ Out-of-Phase Symmetric CH Stretch

#### Abstract

Phenyl radical has been studied via sub-Doppler infrared spectroscopy in a slit supersonic discharge expansion source, with assignments for the highest frequency  $b_2$  out-of-phase C-H symmetric stretch vibration ( $\nu_{19}$ ) unambiguously confirmed by  $\leq 6$  MHz ( $0.0002 \text{ cm}^{-1}$ ) agreement with microwave ground state combination differences of McMahon *et al.* [Astrophys. J. 590, L61-64 (2003)]. Least squares analysis of over 100 resolved rovibrational peaks in the sub-Doppler spectrum to a Watson Hamiltonian yields precision excited-state rotational constants and a vibrational band origin ( $\nu_0 = 3071.8915(4) \text{ cm}^{-1}$ ) consistent with a surprisingly small red-shift ( $0.9 \text{ cm}^{-1}$ ) with respect to Ar matrix isolation studies by Friderichsen *et al.* [J. Am. Chem. Soc. 123, 1977 (2001)]. Nuclear spin weights and inertial defects confirm the vibrationally averaged planarity and  ${}^2A_1$  rovibronic symmetry of phenyl radical, with analysis of the rotational constants consistent with a modest  $C_{2v}$  distortion of the carbon backbone frame due to partial sp rehybridization of the s C radical-center. Most importantly, despite the number of atoms ( $N = 11$ ) and vibrational modes ( $3N-6 = 27$ ), phenyl radical exhibits a remarkably clean jet cooled high-resolution IR spectrum that shows no evidence of intramolecular vibrational relaxation (IVR) phenomena such as *local* or *non-local* perturbations due to strongly coupled nearby dark states. This provides strong support

for the feasibility of high-resolution infrared spectroscopy in other cyclic aromatic hydrocarbon radical systems.

## I. Introduction

Phenyl radical ( $C_6H_5$ , Fig. 3.1) is the product of homolytic CH bond cleavage in benzene and is arguably one of the most fundamental aromatic hydrocarbon radical species in all of chemistry. By virtue of its aromatic character and unpaired electron, phenyl constitutes a highly reactive radical species known to play an important role in chemistry ranging from geologic formation of hydrocarbon fuels to industrial synthesis.<sup>[1-2]</sup> Of particular interest, this radical is also strongly implicated as a crucial chemical intermediate in soot formation, combustion and polycyclic aromatic hydrocarbon (PAH) chemistry in the interstellar medium.<sup>[3-9]</sup> In multiple areas of chemistry, reaction schemes detailing the production and depletion of ring hydrocarbon species often invoke phenyl radical as a proposed intermediate,<sup>[6, 10-12]</sup> which continues to provide strong motivation for detailed first principles understanding of its fundamental properties.

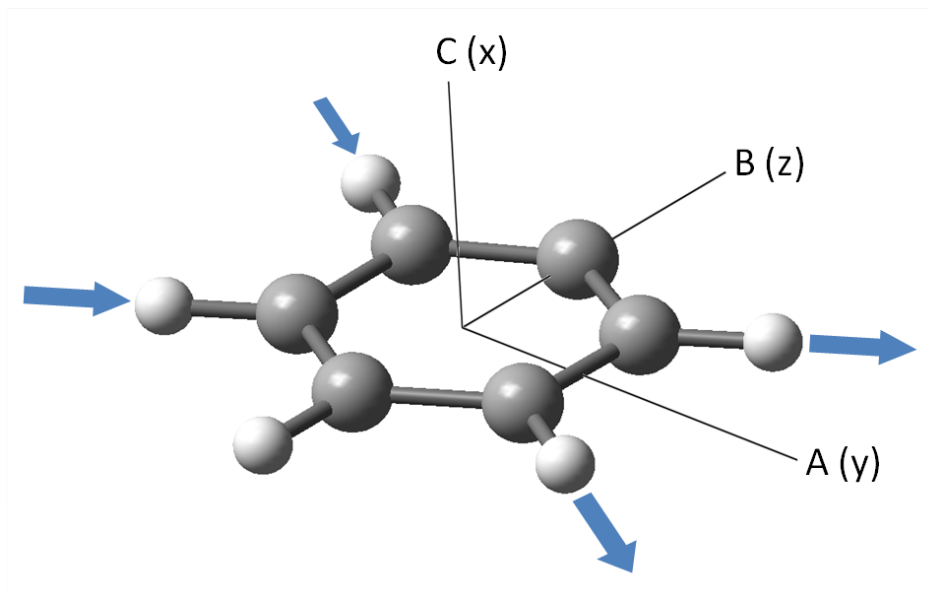


Fig. 3.1. Phenyl radical with its body fixed principal rotation axes labeled. For  $C_{2v}$  point group symmetry analysis, the  $x,y,z$  axes are taken as a right hand coordinate system pointing along the C, A, B principal axes, respectively. The arrows indicate the displacement vectors for the  $b_2$  symmetry out-of-phase symmetric CH stretch ( $\nu_{19}$ ) reported herein.

In contrast to its widespread chemical impact and importance, there is a remarkable lack of detailed spectroscopic information on phenyl radical, in particular high-resolution infrared spectroscopy in the gas phase. Indeed, a deeper understanding of the structural properties, reaction kinetics and dynamics of radicals in general can be obtained via high-resolution infrared spectroscopy of highly reactive intermediates, both in ground and vibrationally excited states. In particular, such experiments offer benchmark tests under ideal laboratory conditions with which to confirm high level theoretical predictions, as well as provide insight into complicated reactions pathways under more challenging and exotic chemical conditions. One of the reasons for this is clearly high chemical reactivity, which makes it challenging to prepare phenyl radical in sufficiently high densities per quantum state to allow such detailed characterization to be feasible. This is particularly true for relatively large polyatomic radical species with

small rotational constants such as phenyl radical, for which rotational partition functions under conventional temperature conditions can be quite large and thus yield correspondingly low populations per quantum state.

In combustion chemistry, phenyl radical is a proposed intermediate in both synthetic and destructive pathways of PAH systems.<sup>[3]</sup> The importance of phenyl radical is especially relevant for heavy oil and tar sand deposits, which greatly exceed the existing reserves of conventional oil, but require additional chemical processing due to their significant PAH content<sup>[13]</sup>. In order to convert such reserves into cleaner and more efficient fuel sources, the hydrogen-to-carbon ratio can be increased by catalytic hydrocracking, which uses homolytic bond cleavage of large aromatic molecules to yield lower molecular weight combustible reagents.<sup>[14]</sup> Indeed, for conjugated hydrocarbon systems such as those present in heavy fuel sources, phenyl radical is directly produced through breaking the biaryl C-C bonds, a process known as hydrogenolysis.<sup>[15]</sup> In addition, mechanisms for combustion of even simple aliphatic fuels also highlight phenyl radical as a critical species in the net production of aromatics and therefore a key intermediate on the path to formation of macroscopic soot.<sup>[5]</sup>

Although much less determined at present, phenyl radical is thought to play an equally central role in astrochemistry. In particular, it has been definitively established that PAHs are indeed present in the interstellar medium (ISM)<sup>[16-17]</sup> with phenyl radical a likely key player in the underlying chemistry. For example, reaction schemes such as those presented by Wang and Frenklach<sup>[3]</sup> highlight phenyl radical as a critical reactive intermediate in the conversion from the simplest aromatics (e.g. benzene) to larger PAH species. This so called hydrogen-abstraction-C<sub>2</sub>H<sub>2</sub>-addition (HACA) is initiated by activation of benzene via removal of a hydrogen atom to yield phenyl radical, which

then reacts with acetylene to form H + phenylacetylene. Subsequent hydrogen abstraction from the  $\alpha$ -carbon followed by a second C<sub>2</sub>H<sub>2</sub> addition produces a diacetylenic radical. This species can rapidly undergo electron rearrangement to produce a bicyclic aromatic radical, which in turn may either proceed with further C<sub>2</sub>H<sub>2</sub> additions or terminate via hydrogen atom addition to yield naphthalene. Indeed, such HACA pathways have been adapted from combustion chemistry and applied to PAH formation in carbon rich stars<sup>[3, 5, 17-18]</sup> where the high temperatures (roughly 1000 K) can provide sufficient energy to overcome the significant activation barriers for such a reaction scheme.

Interestingly, such combustion motivated HACA mechanisms are challenging to invoke in explaining the formation of PAHs in the ISM, where the much lower temperatures (roughly 10 K) would strongly limit such activated processes. Of particular relevance, therefore, crossed molecular beam experiments by Tielens *et al.*<sup>[19]</sup> have recently discovered a barrierless reaction between phenyl radical and vinylacetylene, whereby naphthalene can be produced in a single collision event, even at low temperatures similar to those found in the ISM. Clearly, definitive confirmation of such mechanisms for PAH synthesis in astrochemical environments will require considerable additional work, for which observational spectroscopy of relevant reaction intermediates such as phenyl radical may offer critical support. Indeed, phenyl radical is indicated as an intermediate for both low and high temperature reaction pathways, for which advanced knowledge about phenyl radical is needed to facilitate accurate predictions of its concentration and chemical activity. By way of example, the precursor molecule benzene has recently been observed spectroscopically in the proto-planetary nebula CRL 618.<sup>[20]</sup> Infrared, mm and/or microwave detection of phenyl radical spectra

in collocated regions of space could provide critical supporting evidence for such reaction mechanisms as well as information on kinetics of PAH formation.<sup>[21]</sup> This, in turn, could significantly advance future prospects for successful search for these species in the interstellar medium with new far-IR/sub-mm telescope capabilities coming on line.<sup>[22-24]</sup> Such detection and confirmation efforts would greatly profit from accurate spectroscopic characterization by laboratory studies of gas phase phenyl radical, toward which the present work is directed.

The infrared C-H stretch region of phenyl radical has been studied previously in the condensed phase via matrix isolation spectroscopy,<sup>[25]</sup> but of the 5 normal mode stretches predicted in the infrared CH stretch energy region, there has been remarkably little success at obtaining further information by high-resolution gas phase efforts.<sup>[26]</sup> Indeed, there are only two sources of high-resolution spectroscopic data on phenyl radical to date, i) pioneering microwave studies by McMahon *et al.*<sup>[27]</sup> and ii) a recent communication from our group<sup>[26]</sup> on high-resolution infrared studies of phenyl in a slit jet discharge. We have since then considerably improved our experimental conditions for phenyl radical production, and recently exploited this experimental capability for high-resolution spectral search throughout the 3000-3200  $\text{cm}^{-1}$  near-infrared region. Such efforts have yielded detailed gas phase spectra for 3 of the 5 fundamental CH stretch spectral bands in this near-IR region. The focus of this work is a more complete description and analysis of the  $b_2$  out-of-phase symmetric CH stretch mode,  $\nu_{19}$ , with spectral results for two weaker  $a_1$  symmetry CH stretching modes ( $\nu_1$  and  $\nu_2$ ) currently under analysis and to be presented elsewhere.

What is particularly noteworthy about this observation is that, despite the relatively large number of atoms in phenyl radical, the CH stretch spectra can be clearly

rovibrationally resolved, unambiguously assigned, and successfully analyzed. This is far from an obvious result, since large polyatomic hydrocarbon molecules with correspondingly many vibrational modes can exhibit extensive coupling between excited zero order vibrational “bright states” and the dense bath of near resonant “dark states” that are energetically accessible at C-H stretch frequencies.<sup>[28-31]</sup> The lack of strong rovibrational state coupling evident in the high-resolution phenyl radical spectra indicates surprisingly small complications due to intramolecular vibrational redistribution (IVR) of energy, which bodes promisingly for high-resolution spectroscopy of other cyclic aromatic radical species, as well as potentially even more complicated PAH radical systems.

The outline of this chapter is as follows. The experimental setup is described briefly in Sec. II, including a description of the pulsed slit jet discharge and present methods of producing frequency stabilized tunable IR light. Sec. III presents results and analysis of the spectroscopic data, with discussion of the relevant experimental findings in Sec. IV. In particular, the rotational constants and nuclear spin statistics offer insight into the structural planarity, in-plane distortion and rovibronic symmetry of the molecule, while the simplicity of the gas phase rovibrational spectrum at the fundamental vibrational level indicates a remarkable lack of unimolecular dynamics due to intramolecular vibrational coupling effects. Sec. V summarizes the main results and conclusions.



## II. Experimental

The ability to obtain well resolved rovibrational spectra of phenyl radical in the gas phase relies largely on several experimental advantages: i) high radical densities per quantum state accessible with low temperature discharge expansions, ii) sub-Doppler compression of velocity broadening in the slit jet, iii) long absorption path geometry and iv) precisely tunable frequency stabilized IR light source. The experimental setup has been described in previous papers<sup>[29, 32]</sup> thus only a brief summary of details relevant to the present work will be presented here.

The spectroscopic target phenyl radical species is produced via CX bond fragmentation of monohalobenzenes ( $C_6H_5X$ ) in a slit supersonic jet expansion, yielding typical signal-to-noise on the strongest absorption peaks of roughly 50:1. The mechanism for CX bond fission is presumably electron dissociative attachment to form the radical center +  $X^-$ , which would clearly favor use of halogenated precursor species with weakest CX bond strengths. Indeed, phenyl radical can be efficiently synthesized in the discharge with bromobenzene and iodobenzene, but with signal intensities greatly limited by reduced vapor pressures at room temperature. As a compromise between vapor pressure, control and formation efficiency, the carrier gas Ne70 (70 % neon, 30 % helium) is therefore bubbled through liquid-phase chlorobenzene cooled at 0° C, with the gas mixture further diluted with Ne70 to produce 0.5 %  $C_6H_5Cl$  gas samples in the stagnation region at 280 Torr total pressure. The gas is supersonically expanded through a JILA-built solenoid-driven slit valve capable of generating intense pulses with tunable duration (1000  $\mu s$ , < 50  $\mu s$  rise time) that exit through a 4 cm long, 300  $\mu m$  wide slit into a vacuum chamber. This supersonic expansion is triggered at repetition rate of 19 Hz, with pressure in the vacuum chamber maintained < 50 mTorr

by a 560 liter/second Roots blower (Leybold WS200). During each gas pulse, a 50 kHz modulated square wave voltage (around 500 V) is applied across an insulated 1 mm region located immediately prior to the expansion orifice, as illustrated in Fig. 3.2. This voltage is sufficient to produce a glow discharge with 280 mA peak current through the sample and carrier gas mixture, which causes dissociative electron attachment and homolytic cleavage of the CCl bond to produce the desired phenyl radical.

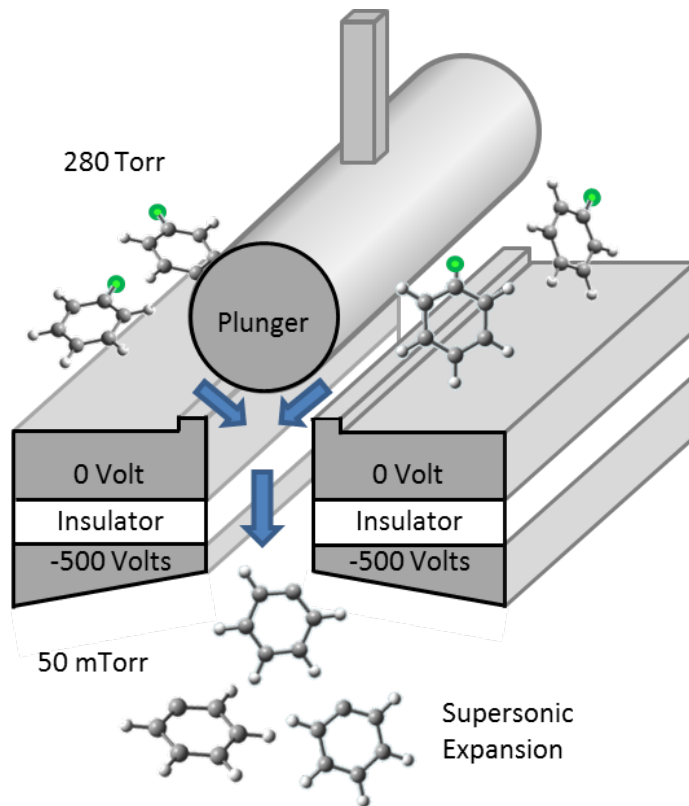


Figure 3.2. Diagram of pulsed slit jet discharge. During the 1000 ms gas pulse, the carrier gas and precursor flow into the discharge region where a square wave modulated voltage (-500 V) is applied with a 50 kHz frequency. The electric field induced glow discharge results in efficient electron dissociative attachment of the weak carbon-halogen bond. This high concentration of phenyl radicals is then rapidly cooled to roughly 11(1) K in the slit supersonic expansion.

The slit jet expansion rapidly cools the phenyl radical down to roughly 11(1) K, where infrared light 5 mm downstream from the nozzle orifice permits direct absorption by the newly formed radical molecules. Near shot-noise-limited absorption sensitivities on the order of 0.002 % ( $A = 2 \times 10^{-5}$ ) in a 10 kHz bandwidth are made possible by fast servo loop subtraction of signal and reference detector technical common mode noise on the IR laser. The signal is further augmented by increasing the absorption path length using a 16-pass Herriott cell, which is aligned directly below the slit orifice. This alignment minimizes molecular velocity parallel to the beam path, lowers the Doppler width of the measured absorption peaks by an additional 5-10 fold (in Ne70), and thereby increases the peak absorption cross section by an equivalent 5-10 fold. In combination with the much slower ( $1/r$  vs.  $1/r^2$ ) density drop off in a slit vs. pinhole jet, this yields a net sensitivity enhancement for direct IR absorption on highly reactive radicals by some 3-4 orders of magnitude. Combined with typical integrated absorption strengths<sup>[33]</sup> (5-20 km/mol) for hydrocarbon species such as phenyl radical, these absorption sensitivities translates into minimum detectable number densities of  $2$  to  $8 \times 10^8$  cm<sup>-3</sup> quantum state<sup>-1</sup> in a detection region 5 mm downstream of the slit jet orifice.

Infrared light is produced by spatially overlapping two visible laser beams in a temperature controlled, periodically poled lithium niobate crystal, which results in difference frequency generation of tunable light in the 2.5-4  $\mu$ m region. The two visible light sources are i) a fixed frequency argon ion ( $\text{Ar}^+$ ) laser operating at 514 nm ( $19429.88$  cm<sup>-1</sup>) and ii) a tunable ring dye laser (R6G dye) between 17500 to 16000 cm<sup>-1</sup>. The  $\text{Ar}^+$  laser is locked via servo-loop to the transmission fringes of an external Fabry-Perot cavity (FSR = 250 MHz), which in turn is locked to a polarization-stabilized

helium-neon (HeNe) laser to achieve long-term frequency stability over multiple days. Scanning progress of the dye laser is measured with respect to fringes on the same ultrastable Fabry-Perot cavity, yielding comparable precision for frequency measurement on the difference frequency IR light. Absolute frequencies are determined by a reference absorption line of jet cooled methane (R(4),  $3067.3000\text{ cm}^{-1}$ ) observed under identical slit jet conditions,<sup>[34]</sup> providing a calibrated IR frequency axis with typical rms reproducibility of 8 MHz ( $< 0.0003\text{ cm}^{-1}$ ) for the transitions reported.

The IR light is divided into two beams by a 50:50 beam splitter, with one portion measured directly on a liquid nitrogen cooled InSb reference detector. The remainder of the IR light is then directed through the slit jet discharge/Herriott cell vacuum chamber, extracted after 16 passes and recollimated onto a matched liquid nitrogen cooled InSb signal detector. Noise between signal and reference detector is actively balanced using high bandwidth (1 MHz) home-built active subtraction electronics, with the weak absorption signals at the 50 kHz discharge modulation frequency obtained via lock-in detection to provide additional signal-to-noise enhancement. These lock-in detection signals are then further analyzed in the time domain by gated integration and differential baseline correction before, during and after the slit jet pulse. All resulting data and frequency diagnostics are stored in a computer for later analysis.

### III. Results and Analysis

Phenyl radical is predicted to be a planar, near-oblate asymmetric top with a rigid structure described by  $C_{2v}$  point group symmetry with x, y, z axes pointing along the C, A and B principal axis directions (see Fig. 3.1). Normal mode analysis predicts

five infrared active fundamental modes in the 3000-3200  $\text{cm}^{-1}$  region consisting of predominantly CH stretching character. There are 3 CH stretch vibrations of  $a_1$  symmetry, which in order of decreasing frequency can be predominantly characterized as: i) *in-phase*, symmetric stretch of all 5 CH bonds ( $a_1$ ,  $\nu_1$ , 3192  $\text{cm}^{-1}$ ), ii) *out-of-phase*, symmetric stretch between the *ortho* (i.e., carbon atoms 2,6) and *para* (i.e., carbon atom 4) CH bond positions ( $a_1$ ,  $\nu_2$ , 3180  $\text{cm}^{-1}$ ), and iii) *in-phase*, antisymmetric stretch of the corresponding *ortho/meta* CH bonds ( $a_1$ ,  $\nu_3$ , 3160  $\text{cm}^{-1}$ ). In addition, there are 2 CH stretch vibrations of  $b_2$  symmetry: i) *out-of-phase*, *symmetric* stretch ( $b_2$ ,  $\nu_{19}$ , 3182  $\text{cm}^{-1}$ ) and ii) *out-of-phase*, *antisymmetric* stretch ( $b_2$ ,  $\nu_{20}$ , 3166  $\text{cm}^{-1}$ ) of the *ortho/meta* CH bonds. The predicted frequencies for these 5 vibrations are based on anharmonic scaling (0.9637(31)) B3LYP/6-31++g(3pd,3df) predictions of Dong *et al.*,<sup>[32-33]</sup> which in turn have been benchmarked against a comprehensive set of high-resolution CH stretch spectra for hydrocarbon radicals. Of the five IR active CH stretching modes, the  $b_2$  symmetric out-of-phase CH stretch ( $\nu_{19}$ ) is predicted from simple density functional calculations [B3LYP/6-311++g(3df,3pd)] to have the largest integrated infrared intensity ( $S_0 = 17.3 \text{ km/mol}$ ).<sup>[33]</sup> A sample overview spectral region for the phenyl radical in the slit jet discharge absorption spectrometer is shown in Fig. 3.3, revealing extensive rotationally resolved P, R branch progressions and a clear Q branch feature near 3071.9  $\text{cm}^{-1}$ . Typical isolated line absorbances are roughly 0.04 %, which for the above integrated absorption cross section translates into a typical number density per quantum state of about  $3 \times 10^9 \text{ radicals cm}^{-3}$  in the slit jet probe region and roughly  $5 \times 10^{10} \text{ radicals cm}^{-3}$  extrapolated up toward the discharge slit orifice. Although this represents greater than 10-fold lower formation efficiency than observed for other hydrocarbon radicals in the slit jet discharge geometry, this nevertheless translates into a

respectable S/N of roughly 20 for typical absorbance sensitivities of 0.002 % in our detection bandwidth.

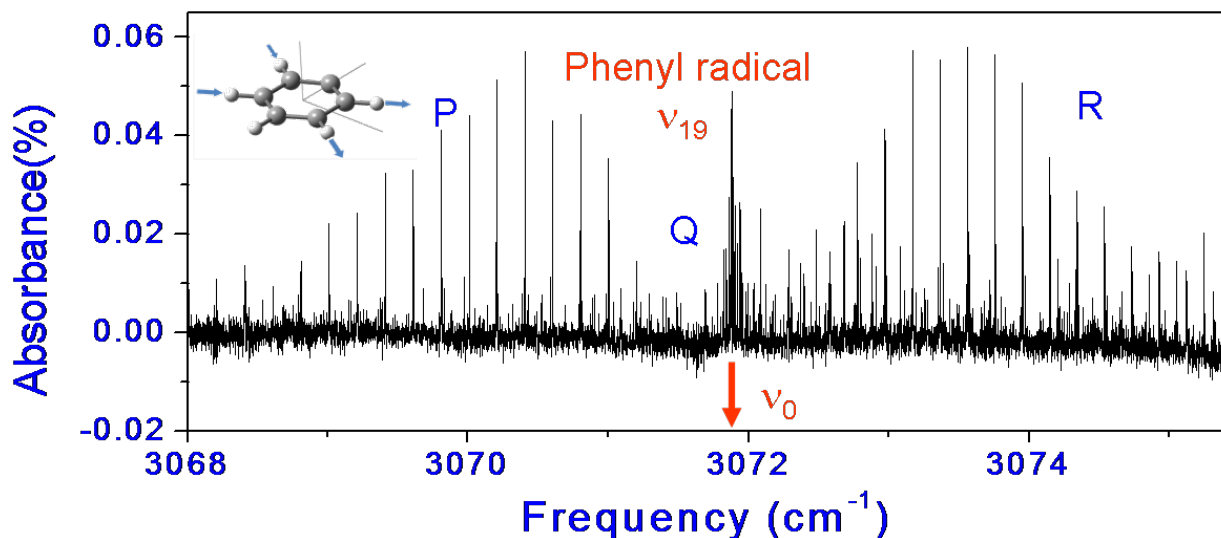


Fig. 3.3. Overview rovibrational spectrum of the symmetric out-of-phase C-H stretch,  $\nu_{19}$ , in phenyl radical at  $T_{\text{rot}}$  roughly equal 11(1)K. The band origin is at  $3071.8915 \text{ cm}^{-1}$ , with extensive P, Q, and R branch structure clearly evident. In spite of spectral overlap due to the near oblate top nature of phenyl radical, the combination of supersonic jet cooling and sub-Doppler transverse velocity compression allows for assignment and analysis of over 100 fully resolved rovibrational transitions.

As discussed in detail below, this rotational structure is indeed predominantly due to the symmetric out-of-phase CH stretch ( $\nu_{19}$ ) band, with a dipole derivative moment along the A principal axis and thus an A-type band dominated by  $DK_a = 0$  and  $DK_c = \pm 1$  transitions. Closer inspection also reveals additional B-type band transitions from the much weaker  $a_1$  totally symmetric  $n_1$  CH stretch vibration fortuitously occurring in the same spectral region, which is not considered herein. The  $\nu_{19}$  Q-branch feature near  $3071.9 \text{ cm}^{-1}$  is in good agreement with the Ar matrix isolation studies ( $\nu_{19} = 3072 \text{ cm}^{-1}$ ) performed by Friderichsen *et al.*<sup>[25]</sup> The high-resolution capabilities of

the slit jet expansion are often sufficient for resolving spin-rotation fine structure and sometimes even nuclear spin-electron spin hyperfine structure in these open shell systems. In the case of phenyl radical, however, these fine structure contributions are known from microwave studies to be quite small ( $\epsilon_{cc} = 4.8$  MHz) and in fact are seen only as unresolved additional broadening beyond the sub-Doppler limit.<sup>[27]</sup> To be consistent with our other studies, however, we will nevertheless refer to total angular momentum simply by the end-over-end rotational quantum number  $N$ , although at even higher-resolution these levels would be split into doublets by coupling with electron spin ( $S = \frac{1}{2}$ ).

Due to H atom loss and ring distortion of the C radical center, the degeneracy of the in-plane principal rotation axes is broken ( $A \geq B > C$ ), which makes phenyl radical a near-oblate asymmetric top. Although the total angular momentum  $N$  remains a conserved quantum number, the unsigned body fixed projections of  $N$  along the A and C principal axes,  $K_a$  and  $K_c$  offer a further useful designation of energy levels by  $N_{K_a K_c}$ . Although these projection quantum numbers are only approximate for an asymmetric top, the even (e) or odd (o) nature of  $K_a$  and  $K_c$  is rigorous, since these correspond to  $\pm 1$  eigenvalues for body fixed  $C_2(y)$  and  $C_2(x)$  rotation operators that commute with the total Hamiltonian. As a result, the rotational energy levels of phenyl radical can be readily solved by expanding the total asymmetric top Hamiltonian in a Wang basis set comprised of symmetric/antisymmetric linear combinations of oblate symmetric top functions (e.g.  $\frac{1}{\sqrt{2}} \{|NK\rangle \pm |N-K\rangle\}$  for  $K = \text{even/odd}$ ), where  $K$  is the signed projection along the C axis. Rotational constants for phenyl radical are then obtained by iterative assignment of absorption peak frequencies to rovibrational transitions

( $N'_{K_a'K_c'} \leftarrow N''_{K_a''K_c''}$ ) in a least squares fitting program based on a Watson asymmetric top Hamiltonian. Due to the low rotational temperatures (roughly 11(1) K) in the jet expansion, these fits are sufficient to reproduce the transition frequencies to within experimental precision without need for higher order centrifugal distortion terms, and thus the choice of reduction and representation is arbitrary.

For a near oblate asymmetric top, the eigenenergies for a given  $N$  *decrease* with increasing  $K_c$ , which implies most favorable Boltzmann factors for low  $K_a$  values with  $K_c$  roughly =  $N$ . Furthermore, for a *planar* near-oblate top (i. e.,  $A \cong B \cong 2C$ ), the structure of each  $K_c$  subband is shifted by  $\cong 2(C - \bar{B})K_c \cong -\bar{B}K_c$ , which for alternate  $K_c$  values approximately matches the  $\cong 2\bar{B}$  spacing in the P and R branch progressions. The net result is a closely spaced progression of transitions with a natural propensity for spectral overlap. We therefore begin the assignment using only spectrally fully resolved and isolated features in the P and R branch region. The advantage of this approach is that it permits immediate confirmation from 2-line combination differences based upon microwave spectroscopy of Thaddeus *et al.*,<sup>[27]</sup> to which the present assignments match within 6 MHz ( $0.0002 \text{ cm}^{-1}$ ). Therefore, the ground state constants are held fixed at the microwave values, with the excited vibrational state rotational constants ( $A'$ ,  $B'$ , and  $C'$ ) and vibrational band origin  $\nu_0$  subject to refinement in this first round of least squares fit.

This initial P/R branch analysis provides a sufficiently good fit to the Watson Hamiltonian to enable confident spectral prediction of fully resolved albeit weaker spectral structure within the central Q branch. With the inclusion of these additional Q branch lines in the fit, the spectral predictions are now sufficiently accurate to



confidently identify the weaker individual P and R branch lines ( $N \neq K_c$  and/or  $\Delta N \neq \Delta K_c$ ) that do not satisfy requirements for both high Boltzmann population and Hönl-London factor line strength. This iterative process results in more than 100 spectrally isolated transitions that can be unambiguously assigned and least squares fit to extract high-resolution rotational constants (see Table 3.1) and a band origin. Even without centrifugal distortion terms, the random errors in such a least squares analysis yield a residual standard deviation of  $0.00037 \text{ cm}^{-1}$  (11 MHz), i.e., roughly comparable to rms experimental error in our frequency measurements.

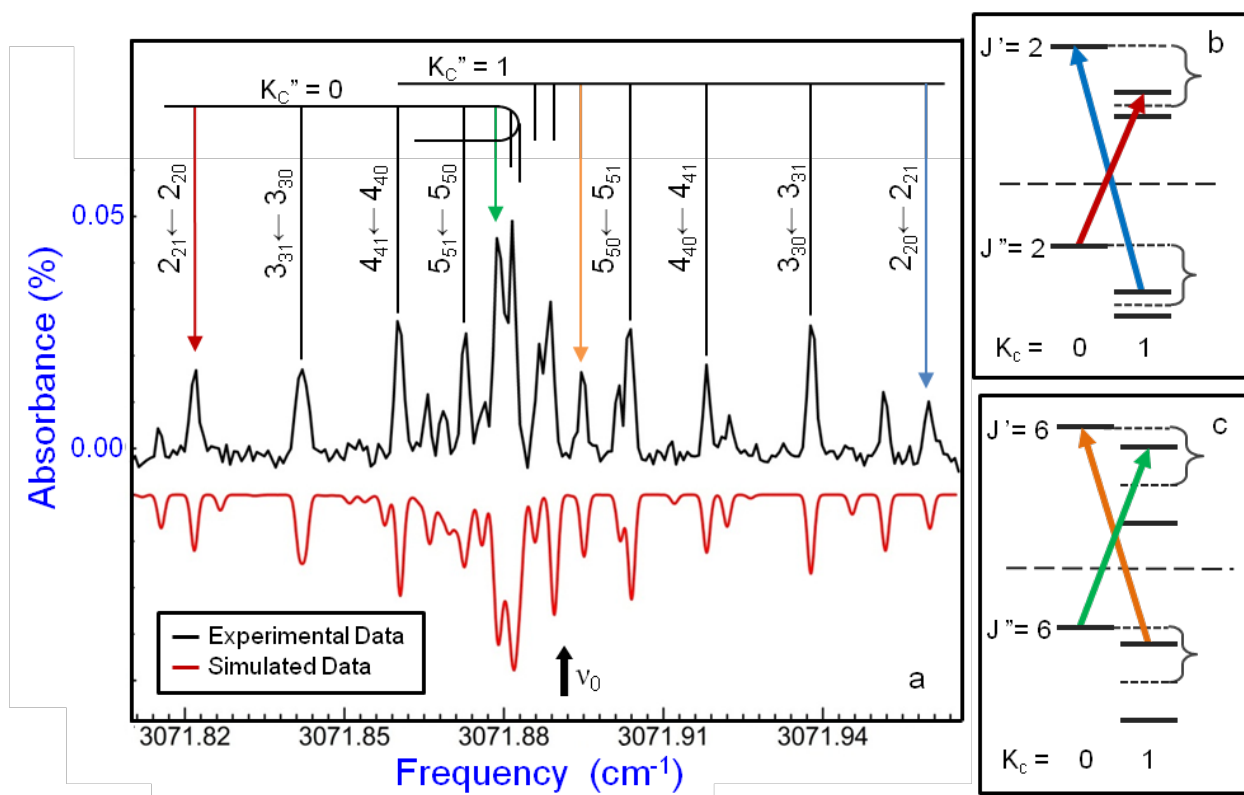


Fig. 3.4. Panel (a) shows the Q branch region of the phenyl radical out-of-phase CH symmetric stretch, band origin ( $3071.8915 \text{ cm}^{-1}$ ) labeled with a black arrow. The simulated spectrum using experimental fits is shown below in red. Panels (b) and (c) show rovibrational energy level diagrams highlighting the  $N = 2 \leftarrow 2$  and  $6 \leftarrow 6$  Q-branch manifold transitions. Color coded arrows in panel (a) correspond to transitions in panels (b) and (c).

At closer inspection, a small Q branch region for  $\nu_{19}$  phenyl radical is expanded in Fig. 3.4, with the band origin designated with a black arrow. The predicted spectrum (downward, red line) is generated using experimental least squares fit constants and recapitulates the high-resolution experimental spectrum (upward, black line) of phenyl radical quite well. As seen in Fig. 3.4, due to compensating Hönl-London factors, the strongest peaks in the Q-branch occur near the band origin and correspond to transitions that originate from higher energy states where  $K_a''$  is roughly equal  $N''$  and  $K_c''$  is small, with corresponding Q-branch transitions out of the lower energy states

(i.e., where  $K''_a$  is small and  $K''_c$  is roughly equal  $N''$ ) shifted significantly to higher ( $\Delta K_c = -1$ ) and lower ( $\Delta K_c = +1$ ) transition frequencies from  $\nu_0$ . If we focus on the Q branch transitions with small frequency shifts, these form clear blue ( $\Delta K_c = +1$ ) and red ( $\Delta K_c = -1$ ) shaded progressions out of  $K''_c = 0$  and  $K''_c = 1$ , respectively, converging upon one another near the band origin. This behavior can be rationalized by the right hand panels in Fig. 3.4, which illustrate the approximate energy level dependence on  $N$ ,  $K_a$  and  $K_c$  for pairs of Q-branch transitions. For low  $N$  values, the energy difference between  $K_c = 0$  and the mean of the split  $K_c = 1$  levels is approximately independent of  $N$  (i.e.,  $\Delta E \cong (C - B) K_c^2$ ), while the  $K_c = 1$  asymmetry splitting for low  $N$  ( $\Delta E \cong \frac{1}{2} (A - B)N(N + 1)$ ) grows quadratically with  $N$ . With increasing  $N$ , therefore, the  $N'_{N1} \leftarrow N''_{N'0}$  and  $N'_{N'0} \leftarrow N''_{N''1}$  progressions necessarily shift to the blue and red, respectively. For sufficiently high  $N$ , however, the asymmetric top energy level pattern approaches a more prolate top behavior, with the  $N_{N0}$  and  $N_{N1}$  states converging to form pairs of  $K_c$  asymmetry split levels for  $K_a = N$ . The net result is that the  $N'_{N1} \leftarrow N''_{N'0}$  and  $N'_{N'0} \leftarrow N''_{N''1}$  Q-branch progressions converge to the same transition frequency. Indeed, for negligible changes in upper and lower state rotational constants, this would predict a perfect convergence of transitions at the band origin, as is the qualitative trend evident in Fig. 3.4. With a reliable spectral assignment in hand, we can similarly look at a sample data region in the P and R branches (see Fig. 3.5). As expected for a near oblate planar asymmetric top ( $A \cong B \cong 2C$ ), the spectral structure is dominated by nearly overlapping progressions in  $\Delta N = \Delta K_c = \pm 1$ , where the congestion arises from the near commensurate match between P/R branch spacing and the shift in alternate  $K_c$  sub-band origins for an A-type band ( $\Delta K_c = \pm 1$ ). Nevertheless, agreement between

experimental data and the partially overlapping asymmetric top predictions is clearly extremely good.

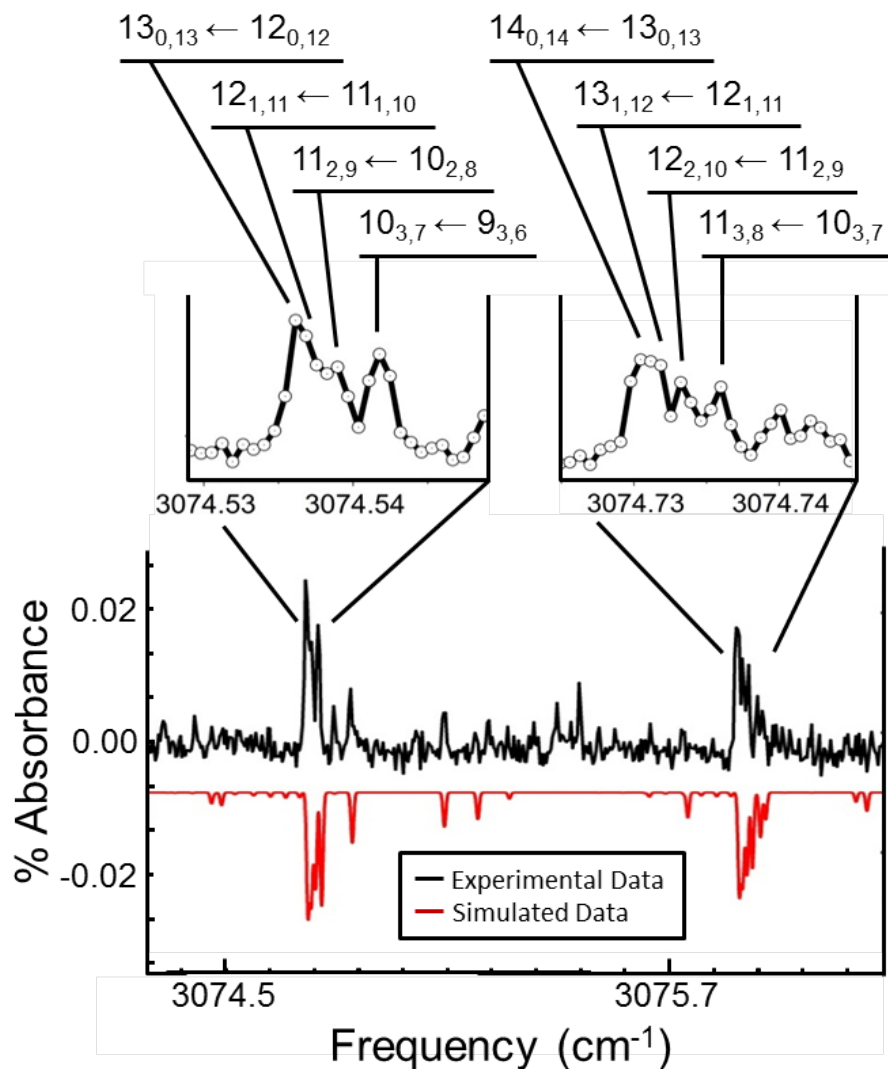


Fig. 3.5. Scan of phenyl radical in the R branch region of the  $\nu_{19}$  CH stretch. The simulated spectrum based on experimentally fit rotational and vibrational constants is shown below in red. The spectral congestion observed in these rotational structures arises naturally for a perpendicular band in a planar, near oblate asymmetric top ( $A \approx B \approx 2C$ ), for which the P/R branch spacings are near commensurate with sub-band spacings as a function of  $K_c$ .

## IV. Discussion

### A. Nuclear spin weights

As a first point of discussion, relative intensities in the rotationally resolved rovibrational spectrum can be used to provide additional confirmation on the underlying nuclear spin statistics and thus rovibronic symmetry of the phenyl radical ground state. Although the most complete treatment of nuclear spin statistics in “floppy” molecules is provided by molecular permutation group theory, this is not essential in phenyl radical, for which results are readily obtained simply by assuming a rigid structure with  $C_{2v}$  point group symmetry.<sup>[35]</sup> From a point group perspective, phenyl radical has two sets of equivalent hydrogen nuclei, each of which undergo feasible exchange by low barrier rotation of the molecule around the  $C_2$  axis. The four hydrogen atoms ( $I = 1/2$ ) have either spin up or spin down, which translates into  $2^4 = 16$  total spin states for the molecule. This forms a reducible representation of the  $C_{2v}$  point group, which can be reduced with the  $C_{2v}$  character table to yield  $\Gamma_{\text{nuc spin}} = 10A_1 \oplus 6B_2$ . To obtain nuclear spin weights, we note that Fermi-Dirac statistics requires the total wavefunction ( $\Psi_{\text{tot}}$ ) to be antisymmetric with respect to exchange of equivalent hydrogen atoms and thus *two* equivalent pairs of fermions must transform symmetrically with respect to  $C_2$  rotation. Furthermore, the eigenvalues for  $C_2$  rotation around the B axis are +1 and -1 for asymmetric top eigenfunctions with  $K_a + K_c = \text{even}$  and odd, respectively. In conjunction with a totally symmetric  $A_1$  ground vibronic state, this corresponds to a 10:6 ratio of nuclear spin statistical weights for  $K_a + K_c = \text{even/odd}$  states, respectively.

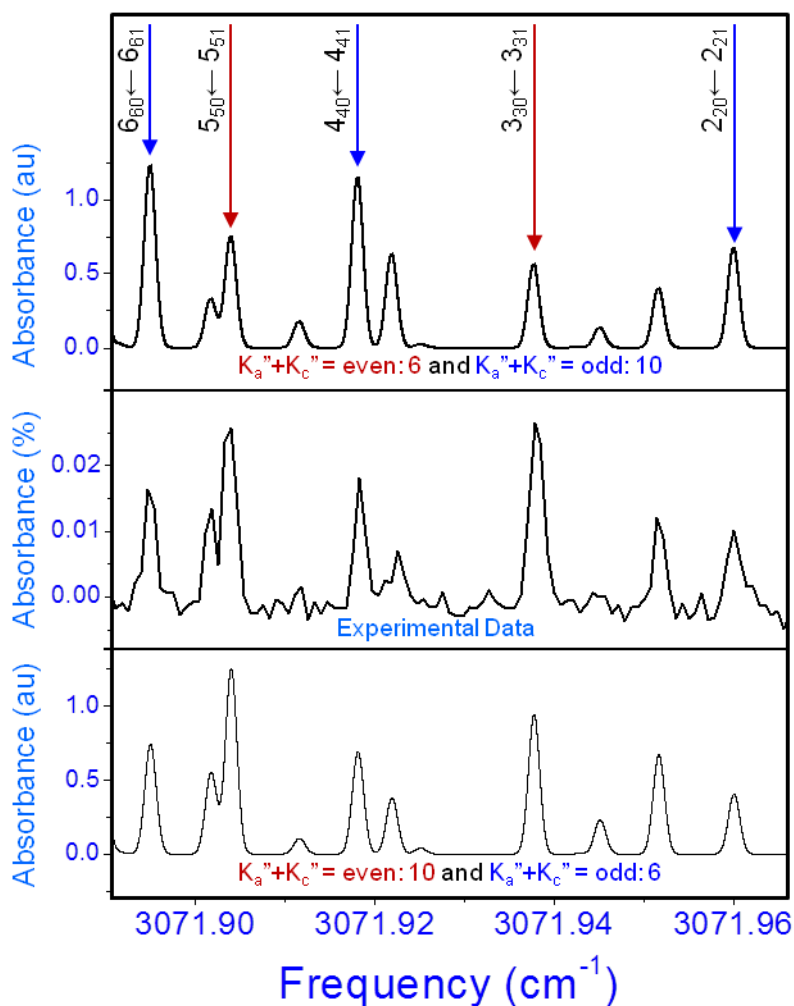


Fig. 3.6. Comparison of two simulated spectra, which highlight the effect of nuclear spin statistics in the spectrum of phenyl radical in the  $\nu_{19}$  region. The middle panel shows experimental absorption spectra, whereas the lower and upper panels present intensity predictions for correct (10:6) vs. inverted (6:10) nuclear spin statistical weights anticipated for  $K_a''+K_c'' = \text{even:odd}$  levels in the ground state. These nuclear spin weights confirm the  ${}^2A_1$  electronic symmetry of the ground state and thus the  $\sigma$  nature of the C radical center.

Spectroscopic confirmation of the correct nuclear spin weighting can be found in Fig. 3.6, which shows a small segment of the Q branch for the  $\nu_{19}$  stretch of phenyl radical. The top panel shows stick plot predictions calculated with the correct nuclear

spin ratio of 10:6 for  $K_a + K_c = \text{even}:\text{odd}$ . Conversely, the stick plot in the bottom panel is the same prediction but with nuclear spin statistics reversed, i.e., 6:10 for  $K_a + K_c = \text{even}:\text{odd}$ . Comparison of the two simulated stick plots with the high-resolution results clearly confirms a 10:6 ratio for  $K_a + K_c = \text{even}:\text{odd}$  to correctly reproduce the spectral data. It is worth noting that overall wavefunction symmetry with respect to rotation around the B axis is directly influenced by and therefore reports on the electronic symmetry of the ground state. Specifically, for a putative p radical ground state with  $B_1$  electronic symmetry,  $C_2$  rotation around the B principal axis would invoke an additional sign change, and thus the nuclear spin weights would shift from 10:6 to 6:10 for  $K_a + K_c = \text{even}:\text{odd}$  states. In conjunction with the above discussion of electronic symmetry, these 10:6 nuclear spin weights can be taken as independent spectral confirmation of a ground state  $A_1$  rather than  $B_1$  electronic symmetry, which in turn requires a  $\sigma$  vs  $\pi$  electronic structure for the radical center on the C atom. This is also consistent with aromatic stabilization of phenyl radical, which significantly lowers the energy of the  $\pi$  electron cloud and makes homolytic bond cleavage to form the  $\sigma$  radical center the energetically preferred pathway.

## B. Planarity and In-plane Ring Distortion

The rovibrationally analyzed spectra also provide additional information on the vibrationally averaged planarity of phenyl radical, as well as evidence for a static in-plane distortion of the 6-membered ring. Specifically we consider the inertial defect ( $\Delta$ ), i.e.,  $\Delta = I_c - I_a - I_b$ , where  $I_i$  is obtained from a sum over all masses times the distance squared from the corresponding principal; rotation axis. For a perfectly rigid, classical molecule with all mass constrained to a plane, the inertial defect should vanish

identically, although systematic shifts in  $D$  arise due to higher order quantum effects such as finite electron mass, zero point motion of the nuclei, as well as in-plane vs. out-of-plane vibrational motion.<sup>[36-38]</sup> Table 3.1 summarizes the experimental inertial defects for phenyl radical in ground and vibrationally excited states. The ground state value for phenyl is small ( $\Delta = + 0.046 \text{ amu \AA}^2$ ) and in fact remarkably close to benzene<sup>[39-41]</sup> in its ground vibrational state ( $\Delta = + 0.044 \text{ amu \AA}^2$ ). This is consistent with a planar aromatic molecular structure for phenyl radical, with the slight positive contribution to  $D$  arising from in-plane vibrational zero point effects. It is worth noting that this inertial defect increases by nearly 2-fold in the  $\nu_{19}$  excited state ( $\Delta = +0.089 \text{ amu \AA}^2$ ), which is also consistent with additional CH stretch motion in one of the in-plane vibrational degrees of freedom.



	theory <sup>b</sup> (CCSD(T)/vtz-f12)			experiment		
	benzene	"sp <sup>2</sup> phenyl"	phenyl	benzene (gnd state)	phenyl (gnd state)	phenyl ( $\nu_{19}$ )
A (cm <sup>-1</sup> )	0.19024	0.20472 (+7.6%)	0.20980 (+10.2%)	0.189751(25)	0.209472(10) (+10.3%)	0.209380(4) (+10.3%)
B (cm <sup>-1</sup> )	0.19024	0.19024 (0.0%)	0.18720 (-1.6%)	0.189751(25)	0.186793(7) (-1.6%)	0.186578(4) (-1.7%)
C (cm <sup>-1</sup> )	0.09512	0.09861 (+3.6%)	0.09893 (+4.0%)	0.094876(13)	0.098714988(2) (+4.0%)	0.0986098(8) (+4.0%)
$\Delta$	0	0	0		0.046	0.089

Table 3.1. *Ab initio* theoretical and experimental rovibrational constants. High level *ab initio* predictions<sup>[42]</sup> (left three columns), obtained at a fixed CCSD(T)/vtz-f12 level to facilitate quantitative comparison, reflect i) benzene, ii) sp<sup>2</sup> phenyl<sup>27</sup> (i.e., equilibrium benzene geometry with one hydrogen removed), and iii) phenyl radical. The three rightmost columns represent experimentally determined values for i) benzene,<sup>[41]</sup> ii) ground state phenyl radical<sup>[27]</sup>, and iii)  $\nu_{19}$  phenyl radical excited in the out-of-phase symmetric CH stretching mode. To aid quantitative comparison, fractional changes in each quantity with respect to theoretical and experimental values for benzene are indicated in %.

Although benzene and phenyl radical have the same number of carbon atoms and  $\pi$ -electrons, homolytic cleavage of a CH bond results in a less saturated radical carbon that is no longer purely  $sp^2$  hybridized, now mixing in partial  $sp$  character in order to generate a  $\sigma$  radical. To investigate distortion of the phenyl backbone away from 6-fold symmetry, we compare both theoretical and experimental rotational constants for a progression of  $C_6$  ring molecules in the absence or presence of such rehybridization effects due to radical formation. As summarized in Table 3.1, the leftmost three columns reflect theoretical rotational constant values calculated at a high but uniform *ab initio* level<sup>[42]</sup> (MOLPRO, CCSD(T)/vtz-f12) for i) benzene, ii) a fictitious fully “ $sp^2$  phenyl” species clamped at the  $D_{6h}$  benzene geometry but one hydrogen atom removed along the B axis, and iii) phenyl radical itself with complete relaxation of the carbon backbone allowed. Percent changes in each of these theoretical values with respect to benzene are indicated in parentheses. Similarly, the next three columns represent the experimental rotational constant values for i) ground state benzene, and phenyl radical in the ii) ground state and iii) with one quanta of excitation in the  $\nu_{19}$  stretch, again with fractional changes in the quantities shown in parentheses.

In the theoretically predicted values, there is clearly a substantial increase (10.2 %) in the A rotational constant between benzene and phenyl radical. However, the “ $sp^2$  phenyl” limit (i.e., H atom removal with no change in nuclear coordinates of the  $C_6$  frame) accounts for only roughly 75 % of the observed difference. This indicates that H atom loss cannot be the only source of increase in A and that indeed the phenyl radical ring is more compressed with respect to the A-axis. The shifts in B provide further evidence for such compression of the carbon ring. Specifically, since the H atom removed originates on the B-axis, there must be identically zero change in B between

benzene and “sp<sup>2</sup> phenyl” resulting purely from H atom removal. Experimentally, however, the B constant for phenyl radical *decreases* by an additional 1.6 % as a result of rehybridization, providing confirmation that the two pairs of *meta/ortho* C atoms must be on average stretched *further away* from the B axis than in benzene.

In the absence of a full isotope substitution study, such changes in rotational constants are insufficient to determine the nuclear coordinates of phenyl radical. However, a simple rehybridization picture consistent with these changes is illustrated in Fig. 3.7, with coordinates taken from theoretical calculations. The unique carbon atom in phenyl radical has two filled bonding molecular orbitals with a third orbital only half occupied, thus resulting in an admixture of sp and sp<sup>2</sup> character. Partial sp character yields a greater propensity toward linear vs. trigonal planar geometry that causes the C-C-C bond angle to be substantially larger (roughly + 6°) than the conventional 120° value for sp<sup>2</sup> bonding. Simply summarized, rehybridization of the C radical center results in i) *decreased* distance of the unique carbon atom to the A axis and ii) *increased* distance of the two adjacent (*para*) carbon atoms from the B axis. Such in-plane distortion is consistent with experimental results in Table 3.1, which reveal an anomalously large fractional increase in A and decrease in B from phenyl radical to benzene. Alternately stated, despite having the same number of carbon atoms and π-electrons as benzene, the one half filled bonding orbital in phenyl radical clearly has measurable effects on the ring backbone geometry of the molecule. Finally, the phenyl radical data in Table 3.1 indicate very good agreement between experiment and theory (< 1 %). Moreover, since these predictions ignore zero point quantum averaging over the vibrational wavefunction, the remaining discrepancies are largely systematic, for which one can empirically compensate by scaling to the ratio of

experimental/theoretical values for a related molecule such as benzene. The result of such scaling improves the rotational constant agreement between theory and experiment by an additional order of magnitude (roughly 0.1 %).

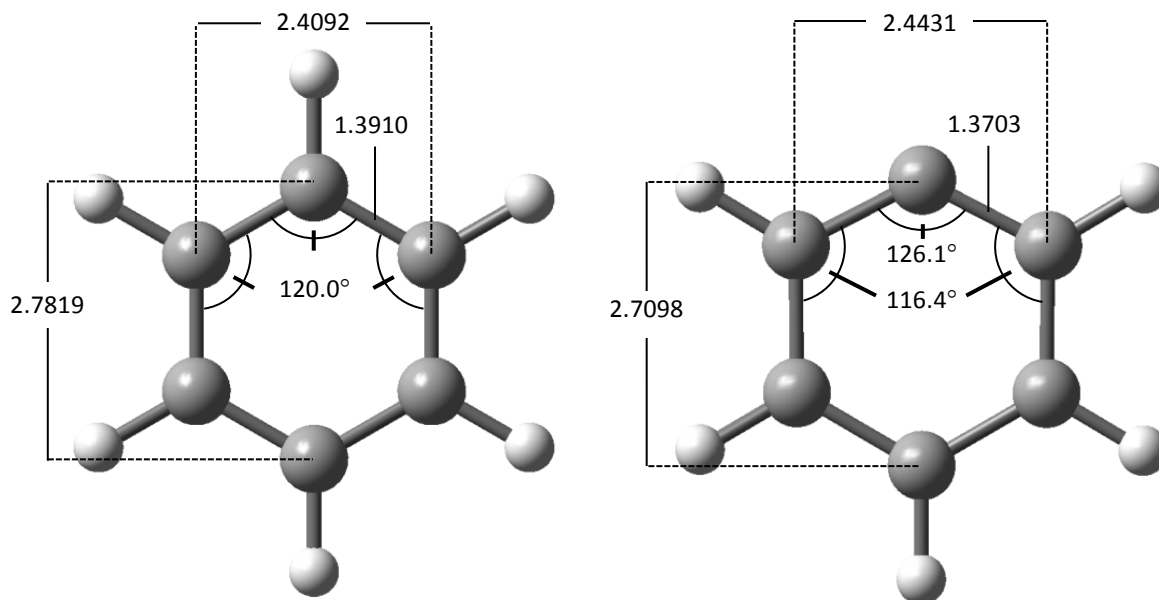


Fig. 3.7. *Ab initio* theoretical comparison (CCSD(T)/vtz-f12) between benzene (left) and phenyl radical (right), illustrating the subtle distortion of the carbon ring upon H atom abstraction and radical formation.<sup>[42]</sup> The greater  $sp$  hybridization character of the unique radical carbon atom center both i) increases the  $\text{C-C-C}$  bond angle as well as ii) decreases the adjacent C-C bond lengths.

### C. Intramolecular Vibrational Dynamics

As a final topic of discussion, we consider the role of intramolecular vibrational coupling in the phenyl spectra. In high-resolution IR spectra of sufficiently large gas phase molecules, isolated transitions which carry the oscillator strength to so called zero order “bright states” can be broadened or split into multiplets by unimolecular vibrational coupling to a typically much denser manifold of zero order “dark

states.”<sup>[28, 30, 43-44]</sup> When two or more zero order states have similar energies, residual coupling in the Hamiltonian can mix the zero order states to form eigenstates with both fractional bright and dark state character. As a result, excitation into an optically bright state necessarily prepares a coherent superposition of eigenstates, which in turn results in a time dependent transfer of vibrational energy into nearby states, or, expressed equivalently in the time domain, intramolecular vibrational redistribution (IVR). The critical question of interest is therefore whether typical off-diagonal IVR coupling matrix elements (i.e.,  $V_{ij} = \langle \Psi_{\text{dark}} | H | \Psi_{\text{bright}} \rangle$ ) are sufficiently large with respect to the inverse density of vibrational states ( $1/\rho(E_{\text{vib}})$ ) for such intramolecular coupling effects to become evident in the high-resolution spectrum. Experimentally, the  $\nu_{19}$  rovibrational spectrum of phenyl radical appears completely assignable and shows no effects from IVR at sub-Doppler spectroscopic resolution ( $\Delta\nu_{\text{FWHM}} \approx 50 \text{ MHz} = 0.00167 \text{ cm}^{-1}$ ) under Ne slit discharge expansion conditions. The relevant issue is whether the i) vibrational state density and ii) coupling matrix elements in phenyl radical are each sufficiently small to rationalize this behavior.

The vibrational state density of a molecule at a given excitation energy grows exceptionally rapidly with number of vibrational degrees of freedom, and in particular, the number of low vibrational modes.<sup>[3, 45-50]</sup> Due to the presence of  $3N-6 = 27$  vibrational normal modes, phenyl radical might be expected to suffer substantial loss of spectral simplicity from IVR induced fragmentation of isolated eigenstates of the lower order and largely separable Hamiltonian. Note that such intramolecular vibrational dynamics does not necessarily imply any true homogeneous broadening of lines beyond the sub-Doppler linewidth, as could occur for the case of strong predissociative coupling with the continuum. However, clearly neither scenario is the correct description, which we

would experience as partial blurring in each of the high-resolution spectral samples (Fig. 3.3 - 3.6). Instead, based on efficient backtracking state counting algorithms by Kemper *et al.* and simple harmonic predictions,<sup>[48]</sup> the vibrational state density per symmetry group in phenyl radical can be readily predicted to be  $\rho(E_{\text{vib}}) \cong 0.15$  states/cm<sup>-1</sup> at  $E_{\text{vib}} \sim 3000$  cm<sup>-1</sup>, which is clearly unusually small for a molecule with 11 atoms. The obvious reason for this is its aromatic C<sub>6</sub> ring conformation, which constrains proliferation of low frequency bends and internal torsional modes that can dramatically increase the density of states in linear hydrocarbon systems and thus the impact of mode-mode coupling.<sup>[51]</sup> In a closed C<sub>6</sub> ring structure, on the other hand, the lowest frequency vibrational modes are considerably higher than for a linear C<sub>6</sub> chain structure, which considerably decreases the state density at typical CH stretch frequencies.

To provide some additional quantitative context, there have been systematic high-resolution IR studies of IVR coupling dynamics for hydrocarbons such as terminal CH stretch excited substituted acetylenes.<sup>[31, 47, 52]</sup> By virtue of jet cooling and sub-Doppler resolution, these studies were able to resolve the true molecular eigenstates arising from these bright state/dark state interactions in the CH stretch manifold, which thus permitted coupling matrix elements to be extracted directly from the spectra. A typical coupling matrix element size was found to be on the order of  $\langle V_{ij} \rangle \sim 0.01$  cm<sup>-1</sup>, which was consistent with an empirical threshold of state density on the order of  $\rho(E_{\text{vib}}) \sim 10^2$  symmetry selected states per cm<sup>-1</sup> for onset of additional spectral complexity due to IVR mixing.<sup>[43, 53]</sup> Note that this critical threshold state density is nearly 3 orders of magnitude *smaller* than predicted for phenyl radical at 3000 cm<sup>-1</sup> levels of internal excitation. Thus, if one were to assume a similar range of coupling matrix elements for

fundamental CH stretch excitation in aromatic ring systems, this would indeed be entirely consistent with the observed lack of IVR induced fragmentation of bright states with near resonant dark states in the current phenyl radical spectra.

As a final comment, we briefly consider the future prospects for extending such high-resolution IR studies to even larger polyatomic aromatic hydrocarbon systems. Fig. 3.8 summarizes vibrational state density predictions ( $\rho(E_{\text{vib}})$ ) as a function of internal energy for a series of single, double and larger aromatic ring systems, based on simple harmonic frequency predictions (B3LYP/6-311++g(3df,3pd)) and the Kemper backtracking algorithm.<sup>[33, 48]</sup> Given that the arguments here rely on only approximate vibrational state densities, the choice of density functional theory predictions for these frequencies should be entirely adequate. For each of the single aromatic ring species, the density of states at fundamental CH stretch energies is roughly  $\rho(E_{\text{vib}}) \sim 0.1$  states/cm<sup>-1</sup>, with the corresponding numbers of  $\rho(E_{\text{vib}}) \sim 20$  states/cm<sup>-1</sup> and  $\rho(E_{\text{vib}}) \sim 1000$  states/cm<sup>-1</sup> for double (naphthalene) and triple (phenanthrene, anthracene) aromatic ring systems. Also indicated on this plot is the  $\sim 10^2$  states/cm<sup>-1</sup> threshold density of states empirically obtained from high-resolution studies for CH stretch excitation in the terminal acetylenes.<sup>[53]</sup> The predictions for the larger ring systems suggest that spectral congestion due to IVR coupling will be dominant, although results for double aromatic ring systems such as naphthalene may be sufficiently sparse to tackle with high-resolution methods. However, it is also worth noting that these state densities represent extremely rapidly growing functions of internal vibrational energy, and thus any such IVR imposed limits on molecular size in the CH stretch region could be considerably reduced for excitation at lower frequencies. In any event, the data for each of the *single* aromatic ring systems at the fundamental CH stretch excitation are already consistently

2-3 orders of magnitude below this threshold state density, which clearly bodes well for further study of the corresponding radical species via high-resolution IR spectroscopy.



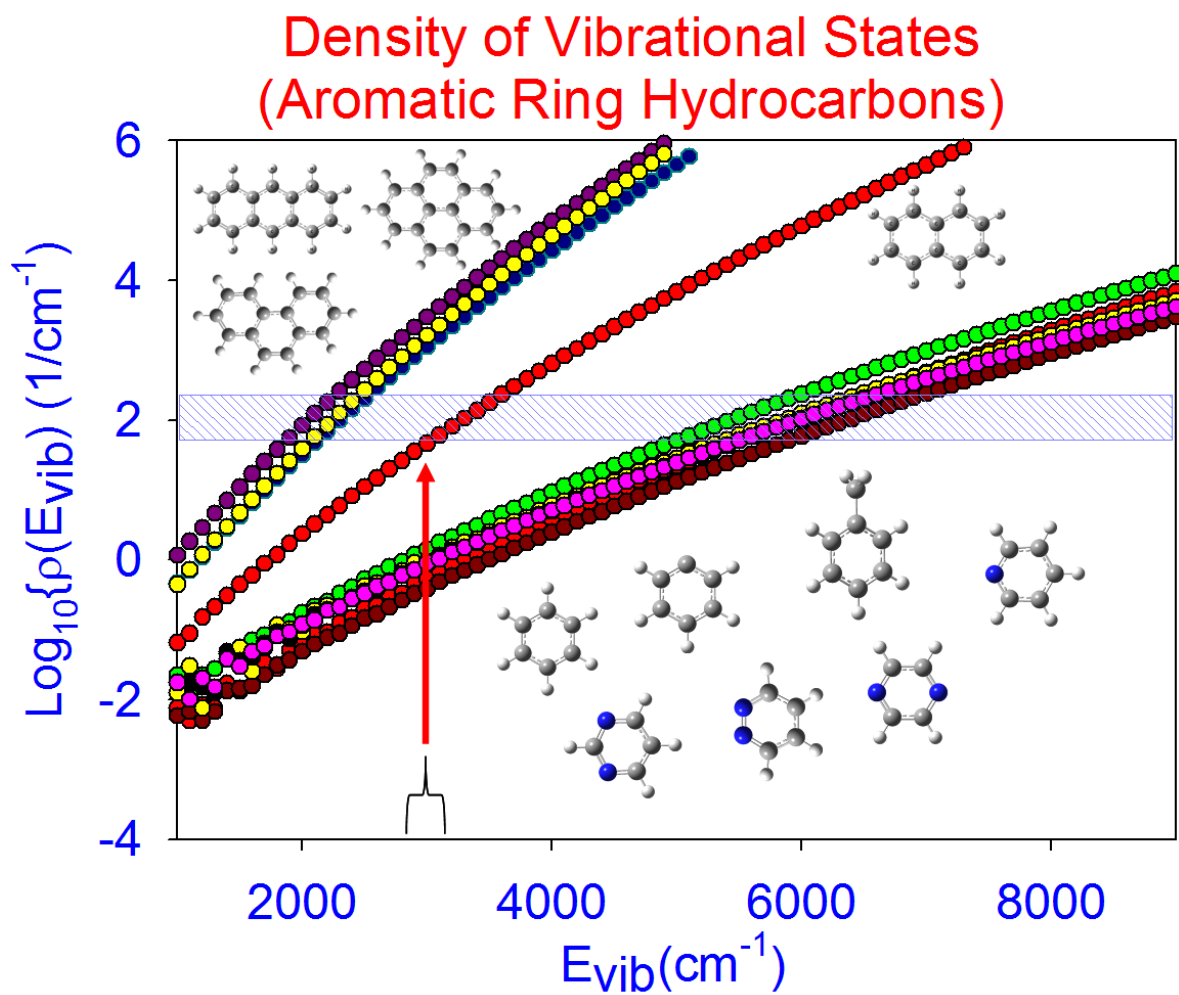


Fig. 3.8. Estimates of symmetry selected vibrational state density (i.e. scaled to point group order) for a series of aromatic and polycyclic aromatic hydrocarbon (PAH) molecules, based on simple density functional predictions (B3LYP/6-311++g(3df,3pd)) and an efficient backtracking algorithm by Kemper *et al.*<sup>[33, 48]</sup> The vertical arrow represents the fundamental CH stretch region, while the horizontal band indicates the threshold region of state density ( $\sim 100$  sym selected states/ $\text{cm}^{-1}$ ) suggested from high-resolution studies to be necessary for promoting IVR coupling between “bright” and “dark” zeroth order levels.<sup>[3, 28, 30, 43-44, 54]</sup> Color/shape coding for the calculations: single ring: phenyl (green circles), benzene (red circles), pyrazine (purple circles), pyridazine (grey circles), pyridine (dk red circles), naphthalene (red circles), phenanthrene (cyan circles), anthracene (dk blue circles), pyrene (yellow circles). Note that all the single ring species are well below this critical state density at  $\sim 3000 \text{ cm}^{-1}$ , which suggests the feasibility of high-resolution infrared detection for any of the corresponding single ring aromatic radical species under supersonically cooled conditions.

## V. Summary and Conclusions

The phenyl radical has been studied with high-resolution infrared spectroscopy enabling the identification of the  $\nu = 1 \leftarrow 0$  excitation of the C-H symmetric out-of-phase vibration,  $\nu_{19}$ . This assignment has been unambiguously confirmed via ground state combination difference band comparison with previously published microwave data,<sup>[27]</sup> with a vibrational band origin determined to high precision ( $\nu_0 = 3071.8915(4) \text{ cm}^{-1}$ ) and over 100 spectrally resolved transitions fit to near experimental uncertainty levels ( $\sigma = 11 \text{ MHz} = 0.0004 \text{ cm}^{-1}$ ). The band origin is in quite good agreement with matrix isolation studies ( $\nu_{19} = 3072 \text{ cm}^{-1}$ ) performed by Friderichsen *et al.*. This would be consistent with a red shift that is remarkably small (roughly  $0.96 \text{ cm}^{-1}$ ) and more typical of those observed under the more weakly perturbative conditions of rare gas Ne matrices or even van der Waals complexes.<sup>[25, 55-59]</sup> Given the relatively large number of atoms and normal modes in phenyl radical, the observed IR spectrum is surprisingly clean and lacks any additional structure and/or broadening due to intramolecular vibrational relaxation. Experimental and theoretical analysis of ground and excited state rotational constants help inform on changes in intramolecular bonding due to the half-filled  $s$  molecular orbital, with increased CCC bond angle and decreased bond CC lengths consistent with partial  $sp$  vs  $sp^2$  character for the radical-carbon atom. Analysis of nuclear spin statistical weights and experimental inertial defects confirms the vibrationally averaged planarity of phenyl as well as the  ${}^2A_1$  symmetry of the electronic ground state. The feasibility of such a spectral analysis constitutes an important step in progress towards high-resolution infrared spectroscopy of additional aromatic ring hydrocarbon radical systems, which likely play important roles in both combustion and interstellar chemistry.

### References for Chapter 3

- [1] P. M. Woods, T. J. Millar and A. A. Zijlstra. The synthesis of benzene in the proto-planetary nebula CRL 618. *Astrophysical Journal* **2002**, 574, L167-L170.
- [2] I. Glassman and R. A. Yetter, *Combustion, 4th Edition*, **2008**, p. 1-773.
- [3] G. A. Bethardy, X. L. Wang and D. S. Perry. The role of molecular flexibility in accelerating intramolecular vibrational-relaxation. *Canadian Journal of Chemistry* **1994**, 72, 652-659.
- [4] N. M. Marinov, W. J. Pitz, C. K. Westbrook, M. J. Castaldi and S. M. Senkan. Modeling of aromatic and polycyclic aromatic hydrocarbon formation in premixed methane and ethane flames. *Combustion Science and Technology* **1996**, 116, 211-287.
- [5] G. L. Agafonov, I. Naydenova, P. A. Vlasov and J. Warnatz. Detailed kinetic modeling of soot formation in shock tube pyrolysis and oxidation of toluene and n-heptane. *Proceedings of the Combustion Institute* **2007**, 31, 575-583.
- [6] T. Yu and M. C. Lin. Kinetics of the  $C_6H_5 + NO$  Association Reaction. *Journal of Physical Chemistry* **1994**, 98, 2105-2109.
- [7] J. Park, I. V. Dyakov and M. C. Lin. FTIR and mass-spectrometric measurements of the rate constant for the  $C_6H_5 + H_2$  reaction. *Journal of Physical Chemistry A* **1997**, 101, 8839-8843.
- [8] A. M. Mebel, M. C. Lin, T. Yu and K. Morokuma. Theoretical study of potential energy surface and thermal rate constants for the  $C_6H_5 + H_2$  and  $C_6H_6 + H$  reactions. *Journal of Physical Chemistry A* **1997**, 101, 3189-3196.
- [9] T. Yu and M. C. Lin. Kinetics of phenyl radical reactions studied by the cavity-ring-down method. *Journal of the American Chemical Society* **1993**, 115, 4371-4372.
- [10] M. J. Cohen, N. C. Handy, R. Hernandez and W. H. Miller. Cumulative reaction probabilities for  $H + H_2 \rightarrow H_2 + H$  from a knowledge of the anharmonic-force field. *Chemical Physics Letters* **1992**, 192, 407-416.

- [11] C. F. Logan and P. Chen. Ab initio calculation of hydrogen abstraction reactions of phenyl radical and *p*-benzyne. *Journal of the American Chemical Society* **1996**, *118*, 2113-2114.
- [12] R. I. Kaiser, O. Asvany, Y. T. Lee, H. F. Bettinger, P. V. Schleyer and H. F. Schaefer. Crossed beam reaction of phenyl radicals with unsaturated hydrocarbon molecules. I. Chemical dynamics of phenylmethylacetylene ( $C_6H_5CCCH_3$ ;  $X^1A'$ ) formation from reaction of  $C_6H_5(X^2A_1)$  with methylacetylene,  $CH_3CCH(X^1A_1)$ . *Journal of Chemical Physics* **2000**, *112*, 4994-5001.
- [13] M. Blitz, M. J. Pilling, S. H. Robertson and P. W. Seakins. Direct studies on the decomposition of the tert-butoxy radical and its reaction with NO. *Physical Chemistry Chemical Physics* **1999**, *1*, 73-80.
- [14] O. P. Strausz, T. W. Mojelsky, J. D. Payzant, G. A. Olah and G. K. S. Prakash. Upgrading of Alberta's heavy oils by superacid-catalyzed hydrocracking. *Energy & Fuels* **1999**, *13*, 558-569.
- [15] B. R. Cook, B. B. Wilkinson, C. C. Culross, S. M. Holmes and L. E. Martinez. Hydrogen transfer induced cleavage of biaryl bonds. *Energy & Fuels* **1997**, *11*, 61-75.
- [16] W. A. Morgan, E. D. Feigelson, H. Wang and M. Frenklach. A new mechanism for the formation of meteoritic kerogen-like material. *Science* **1991**, *252*, 109-112.
- [17] I. Cherchneff, J. R. Barker and A. Tielens. Polycyclic aromatic hydrocarbon formation in carbon-rich stellar envelopes. *Astrophysical Journal* **1992**, *401*, 269-287.
- [18] M. Frenklach and E. D. Feigelson. Formation of polycyclic aromatic-hydrocarbons in circumstellar envelopes. *Astrophysical Journal* **1989**, *341*, 372-384.
- [19] D. S. N. Parker, F. Zhang, Y. S. Kim, R. I. Kaiser, A. Landera, V. V. Kislov, A. M. Mebel and A. G. G. M. Tielens. Low temperature formation of naphthalene and its role in the synthesis of PAHs (Polycyclic Aromatic Hydrocarbons) in the interstellar medium. *Proceedings of the National Academy of Sciences of the United States of America* **2012**, *109*, 53-58.
- [20] J. Cernicharo, A. M. Heras, A. Tielens, J. R. Pardo, F. Herpin, M. Guelin and L. Waters. Infrared Space Observatory's discovery of  $C_4H_2$ ,  $C_6H_2$ , and benzene in CRL 618. *Astrophysical Journal* **2001**, *546*, L123-L126.

- [21] S. L. Widicus Weaver, A. J. Remijan, R. J. McMahon and B. J. McCall. A search for *ortho*-benzyne (*o*-C<sub>6</sub>H<sub>4</sub>) in CRL 618. *Astrophysical Journal Letters* **2007**, 671, L153-L156.
- [22] B. Magnelli, D. Lutz, P. Santini, A. Saintonge, S. Berta, M. Albrecht, B. Altieri, P. Andreani, H. Aussel, F. Bertoldi, M. Bethermin, A. Bongiovanni, P. Capak, S. Chapman, J. Cepa, A. Cimatti, A. Cooray, E. Daddi, A. L. R. Danielson, H. Dannerbauer, J. S. Dunlop, D. Elbaz, D. Farrah, N. M. F. Schreiber, R. Genzel, H. S. Hwang, E. Ibar, R. J. Ivison, E. Le Floch, G. Magdis, R. Maiolino, R. Nordon, S. J. Oliver, A. Perez Garcia, A. Poglitsch, P. Popesso, F. Pozzi, L. Riguccini, G. Rodighiero, D. Rosario, I. Roseboom, M. Salvato, M. Sanchez-Portal, D. Scott, I. Smail, E. Sturm, A. M. Swinbank, L. J. Tacconi, I. Valtchanov, L. Wang and S. Wuyts. A Herschel view of the far-infrared properties of submillimetre galaxies. *Astronomy & Astrophysics* **2012**, 539.
- [23] M. Harwit in *The Herschel Mission, Vol. 34* Eds.: P. R. Wesselius and H. Olthof, **2004**, pp. 568-572.
- [24] G. L. Pilbratt, J. R. Riedinger, T. Passvogel, G. Crone, D. Doyle, U. Gageur, A. M. Heras, C. Jewell, L. Metcalfe, S. Ott and M. Schmidt. Herschel Space Observatory An ESA facility for far-infrared and submillimetre astronomy. *Astronomy & Astrophysics* **2010**, 518, 1-6.
- [25] A. V. Friderichsen, J. G. Radziszewski, M. R. Nimlos, P. R. Winter, D. C. Dayton, D. E. David and G. B. Ellison. The Infrared Spectrum of the Matrix-Isolated Phenyl Radical. *Journal of the American Chemical Society* **2001**, 123, 1977-1988.
- [26] E. N. Sharp, M. A. Roberts and D. J. Nesbitt. Rotationally resolved infrared spectroscopy of a jet-cooled phenyl radical in the gas phase. *Physical Chemistry Chemical Physics* **2008**, 10, 6592-6596.
- [27] R. J. McMahon, M. C. McCarthy, C. A. Gottlieb, J. B. Dudek, J. F. Stanton and P. Thaddeus. The radio spectrum of the phenyl radical. *Astrophysical Journal* **2003**, 590, L61-L64.
- [28] A. McIlroy and D. J. Nesbitt. High-resolution, slit jet infrared spectroscopy of hydrocarbons: Quantum state specific mode mixing in CH stretch-excited propyne. *The Journal of Chemical Physics* **1989**, 91, 104-113.

- [29] S. Davis, M. Farnik, D. Uy and D. J. Nesbitt. Concentration modulation spectroscopy with a pulsed slit supersonic discharge expansion source. *Chemical Physics Letters* **2001**, *344*, 23-30.
- [30] K. K. Lehmann, G. Scoles and B. H. Pate. Intramolecular dynamics from eigenstate-resolved infrared-spectra. *Annual Review of Physical Chemistry* **1994**, *45*, 241-274.
- [31] J. B. Hopkins, D. E. Powers and R. E. Smalley. Vibrational-relaxation in jet-cooled alkylbenzenes .1. Absorption-spectra. *Journal of Chemical Physics* **1980**, *72*, 5039-5048.
- [32] F. Dong, S. Davis and D. J. Nesbitt. Slit discharge IR spectroscopy of a jet-cooled cyclopropyl radical: Structure and intramolecular tunneling dynamics. *Journal of Physical Chemistry A* **2006**, *110*, 3059-3070.
- [33] M. Frisch, G. Trucks, H. Schlegel, G. Scuseria, M. Robb, J. Cheeseman, V. Zakrzewski, J. Montgomery Jr, R. Stratmann and J. Burant in *Gaussian 98, revision A. 7; Gaussian, Inc, Vol. 12* Pittsburgh, Pa, **1998**.
- [34] A. S. Pine. High-resolution methane nu-3-band spectra using a stabilized tunable difference-frequency laser system. *Journal of the Optical Society of America* **1976**, *66*, 97-108.
- [35] P. R. Bunker, P. Jensen, N. R. C. Canada and N. R. C. C. M. P. Program, *Molecular Symmetry and Spectroscopy*, NRC Research Press, **2006**, p. 752.
- [36] T. Oka and Y. Morino. Calculation of inertia defect .1. General formulation. *Journal of Molecular Spectroscopy* **1961**, *6*, 472-482.
- [37] T. Oka. On negative inertial defect. *Journal of Molecular Structure* **1995**, *352*, 225-233.
- [38] M. F. Jagod and T. Oka. Inertial defects of planar symmetric top molecules. *Journal of Molecular Spectroscopy* **1990**, *139*, 313-327.
- [39] J. Pliva and A. S. Pine. Analysis of the 3-mu-m bands of benzene. *Journal of Molecular Spectroscopy* **1987**, *126*, 82-98.
- [40] J. Pliva and A. S. Pine. The spectrum of benzene in the 3-mu-m region - the nu-12 fundamental-band. *Journal of Molecular Spectroscopy* **1982**, *93*, 209-236.

- [41] A. Langseth and B. P. Stoicheff. High resolution raman spectroscopy of gases .6. Rotational spectrum of symmetric benzene-d-3. *Canadian Journal of Physics* **1956**, 34, 350-353.
- [42] P. J. K. H.-J. Werner, G. Knizia, F. R. Manby, M. Schütz, P. Celani, W. Györfy, D. Kats, T. Korona, R. Lindh, A. Mitrushenkov, G. Rauhut, K. R. Shamasundar, T. B. Adler, R. D. Amos, A. Bernhardsson, A. Berning, D. L. Cooper, M. J. O. Deegan, A. J. Dobbyn, F. Eckert, E. Goll, C. Hampel, A. Hesselmann, G. Hetzer, T. Hrenar, G. Jansen, C. Köppl, Y. Liu, A. W. Lloyd, R. A. Mata, A. J. May, S. J. McNicholas, W. Meyer, M. E. Mura, A. Nicklaß, D. P. O'Neill, P. Palmieri, D. Peng, K. Pflüger, R. Pitzer, M. Reiher, T. Shiozaki, H. Stoll, A. J. Stone, R. Tarroni, T. Thorsteinsson, M. Wang in *Molpro, Version 2002.6, Vol.* University of Birmingham: Birmingham, UK, **2003**.
- [43] D. J. Nesbitt and R. W. Field. Vibrational energy flow in highly excited molecules: Role of intramolecular vibrational redistribution. *Journal of Physical Chemistry* **1996**, 100, 12735-12756.
- [44] A. McIlroy, D. J. Nesbitt, E. R. T. Kerstel, B. H. Pate, K. K. Lehmann and G. Scoles. Sub-doppler, infrared-laser spectroscopy of the propyne 2-nu(1) band - evidence of z-axis coriolis dominated intramolecular state mixing in the acetylenic ch stretch overtone. *Journal of Chemical Physics* **1994**, 100, 2596-2611.
- [45] C. S. Parmenter and B. M. Stone. The methyl rotor as an accelerating functional-group for ivr. *Journal of Chemical Physics* **1986**, 84, 4710-4711.
- [46] D. B. Moss and C. S. Parmenter. Acceleration of intramolecular vibrational redistribution of methyl internal-rotation - a chemical timing study of *p*-fluorotoluene and *p*-fluorotoluene-D<sub>3</sub>. *Journal of Chemical Physics* **1993**, 98, 6897-6905.
- [47] R. A. Coveleskie, D. A. Dolson and C. S. Parmenter. A direct view of intramolecular vibrational redistribution in s1 para-difluorobenzene. *Journal of Chemical Physics* **1980**, 72, 5774-5775.
- [48] M. J. H. Kemper, J. M. F. Vandijk and H. M. Buck. Backtracking algorithm for exact counting of internal molecular energy-levels. *Chemical Physics Letters* **1978**, 53, 121-124.
- [49] G. Z. Whitten and B. S. Rabinovitch. Accurate and Facile Approximations for Vibrational Energy-Level Sums. *Journal of Chemical Physics* **1963**, 38, 2466-2473.

- [50] D. C. Tardy, B. S. Rabinovitch and G. Z. Whitten. Vibration-Rotation Energy-Level Density Calculations. *Journal of Chemical Physics* **1968**, *48*, 1427-1429.
- [51] A. Callegari, U. Merker, P. Engels, H. K. Srivastava, K. K. Lehmann and G. Scoles. Intramolecular vibrational redistribution in aromatic molecules. I. Eigenstate resolved CH stretch first overtone spectra of benzene. *Journal of Chemical Physics* **2000**, *113*, 10583-10596.
- [52] J. B. Hopkins, D. E. Powers and R. E. Smalley. Predissociation probes of vibrational-energy localization. *Journal of Chemical Physics* **1981**, *74*, 745-747.
- [53] A. McIlroy and D. J. Nesbitt. Large-amplitude skeletal isomerization as a promoter of intramolecular vibrational-relaxation in ch stretch excited hydrocarbons. *Journal of Chemical Physics* **1994**, *101*, 3421-3435.
- [54] B. H. Pate, K. K. Lehmann and G. Scoles. The onset of intramolecular vibrational-energy redistribution and its intermediate case - the nu-1 and 2-nu-1 molecular-beam, optothermal spectra of trifluoropropyne. *Journal of Chemical Physics* **1991**, *95*, 3891-3916.
- [55] A. McIlroy, R. Lascola, C. M. Lovejoy and D. J. Nesbitt. Structural dependence of hydrogen fluoride vibrational red shifts in argon-hydrogen fluoride ( $\text{Ar}_n\text{HF}$ ,  $n=1-4$ ), via high-resolution slit jet infrared spectroscopy. *The Journal of Physical Chemistry* **1991**, *95*, 2636-2644.
- [56] D. C. Clary, C. M. Lovejoy, S. V. Oneil and D. J. Nesbitt. Infrared-spectrum of NeHF. *Physical Review Letters* **1988**, *61*, 1576-1579.
- [57] C. M. Lovejoy and D. J. Nesbitt. Mode specific internal and direct rotational predissociation in HeHF, HeDF, and HeHCl - vanderwaals complexes in the weak binding limit. *Journal of Chemical Physics* **1990**, *93*, 5387-5407.
- [58] C. M. Lovejoy and D. J. Nesbitt. Rotational predissociation, vibrational mixing, and vanderwaals intermolecular potentials of NeDF. *Journal of Chemical Physics* **1991**, *94*, 208-223.
- [59] M. E. Jacox and W. E. Thompson. The infrared spectroscopy and photochemistry of  $\text{NO}_3$  trapped in solid neon. *Journal of Chemical Physics* **2008**, *129*, 2043061-2043015.





## Chapter 4

### Observation of the $a_1$ C-H Stretching Modes of Phenyl Radical, $\nu_1$ and $\nu_2$

#### Abstract

High-resolution infrared rovibrational transitions of the C-H stretching modes in phenyl radical ( $C_6H_5$ ) are investigated in the slit-jet supersonic expansion with sub-Doppler resolution (roughly 60 MHz). Two new fundamental modes have been studied that have never before been observed with rovibrational resolution. These  $b$ -type vibrational bands originate from the  $\nu_1$  and  $\nu_2$  mode of phenyl radical. The band origins are determined to be  $\nu_1 = 3073.96850(8) \text{ cm}^{-1}$  and  $\nu_2 = 3062.26480(7) \text{ cm}^{-1}$ , which agree to within  $5 \text{ cm}^{-1}$  with the theoretical anharmonic scaling prediction (B3LYP/6-311g++(3df,3dp) basis set). The assignments show slightly larger ( $11 \text{ cm}^{-1}$ ) red shift compared to the corresponding experimental Ar matrix isolation [Friderichsen *et al.* J. Am. Chem. Soc., **123**, 1977(2001) ]. Intensities for the three bands ( $\nu_1$ ,  $\nu_2$ , and  $\nu_{19}$ ) are also analyzed and the relative intensities agree well with theoretical calculations. The physical interpretation of the inertial defect and perturbation of the position of the band origin in the matrix are also discussed.

#### I. Introduction

The cyclic phenyl radical ( $C_6H_5$ ), shown in Fig. 4.1, plays a crucial role in combustion and soot formation processes.<sup>[1-2]</sup> It is also proposed that the formation of

the phenyl radical is an early stage in the further processing of polycyclic aromatic hydrocarbons (PAH).<sup>[3-5]</sup> The reaction of the phenyl radical with unsaturated hydrocarbons is proposed as an elementary step in soot formation in oxygen-poor environments as well as in the outflow of carbon rich stars in the interstellar medium.<sup>[6]</sup>

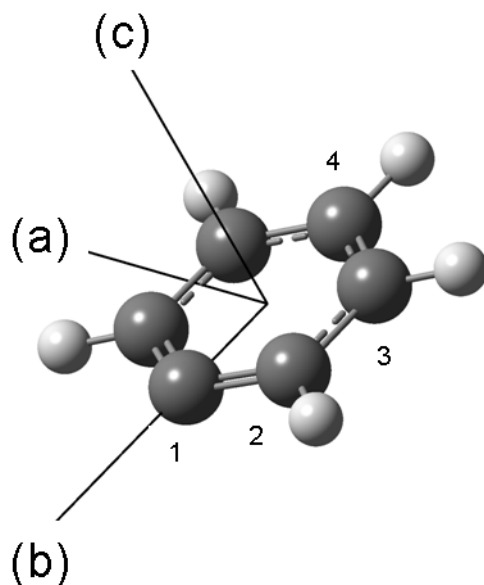


Fig. 4.1. Structure of phenyl radical with carbon atom positions labeled. The  $b$  axis is the  $C_{2v}$  axis and the  $c$  axis is defined out-of-plane.

Studies of the electron spin resonance for phenyl radical in an Ar matrix by Kasai *et al.*<sup>[7]</sup> and Bennett and Thomas<sup>[8]</sup> have revealed that after cleavage of the C–H bond, the unpaired electron is found to be localized in the nonbonding  $\sigma$  orbital at the  $C_1$  position, rather than in the six center  $\pi$  orbital. Initially, lower resolution infrared spectroscopy of phenyl radical had been reported by Pacansky and Bargon<sup>[9]</sup> in an Ar matrix environment and only the CH out-of-plane bending mode was assigned, at  $710\text{ cm}^{-1}$ . Matrix isolation Fourier Transform infrared (FTIR) was used to study phenyl radical along with five deuterated isotopomers, as reported by Ellison and coworker.<sup>[10-11]</sup>

Linear dichroism was employed to explore the polarization of each vibration and to distinguish the symmetry for each mode. The characterization of the electronic transition of phenyl radical had been studied by Ikeda *et al.*<sup>[12]</sup> and Radziszewski,<sup>[13]</sup> and the results indicated that there are three main electronic transitions of phenyl radical in the UV-VIS region,  ${}^2B_1$ ,  ${}^2A_1$ , and  ${}^2B_2$  at 510.5 nm, 235.1 nm, and 211.5 nm, respectively. The  ${}^2B_1$  band was tracked by the Lin group<sup>[14-15]</sup> to study the kinetic of reactions of the phenyl radical with a series of other species *via* cavity ring-down laser spectroscopy. Their recent rotationally resolved spectrum indicated that the lifetime of the  ${}^2B_1$  excited state is about 96 ps due to predissociation.<sup>[16]</sup> The only pure rotational spectroscopy of phenyl radical was performed by McMahon *et al.*<sup>[17]</sup> from a pulsed supersonic beam in the mm-wave region between 9–40 GHz and 150–330 GHz. The rotational constants for the  ${}^2A_1$  ground state as well as spin rotation constant ( $\epsilon_{cc}=4.78(2)$  MHz) were reported for the first time. Their studies provide the fingerprint information for this primary candidate in the field of astronomical detection.

Recent work in our group<sup>[18]</sup> reported on the a-type rovibrational transition in the C–H stretching mode,  $\nu_{19}$ . The assignment of this C–H mode is based on theoretical calculations and band type comparison with the Ar matrix results. In addition, the assignment is confirmed by excited state rotational constants, which show elongation along the a-axis consistent with the displacement vectors of  $\nu_{19}$ . The band origin for this mode was reported as 3071.8907(10)  $\text{cm}^{-1}$  in the gas-phase, very close to the Ar matrix assignment of 3071  $\text{cm}^{-1}$ . These experimental results indicated that the  $\nu_{19}$  vibrational mode is very minimally perturbed by the inert gas matrix environment. The experimental results of the gas-phase, Ar matrix, and theoretical predictions are

summarized in Table 4.1. The quantum chemical structure and frequencies for the phenyl radical had been investigated with density functional methods (B3LYP) over a series of the correlation consistent Dunning basis set function and 6-311g++(3df,3dp) basis set. The empirical anharmonic scaling factor<sup>[19]</sup> (0.964) was guided by the previous study of a series of CH stretching modes of hydrocarbon radical in the gas-phase, where experimental results were correlated with theoretical harmonic predictions.

The displacement vectors for each hydrogen atom in the five different C-H stretch vibrational modes are shown in Fig.4. 2. The excitation of the  $\nu_1$ ,  $\nu_2$  and  $\nu_3$  stretching modes correspond to the generation of the derivative of the dipole moment along the molecular  $b$  axis, as defined in Fig. 4.1. The  $\nu_{19}$  and  $\nu_{20}$  modes generate the dipole moment derivative along the  $a$ -axis. For the previous study of the  $\nu_{19}$  band, theoretical calculations of the out-of-phase motion of the C-H stretching for the ortho-position CH group predicted the integrated IR intensity of  $17.1 \text{ km mol}^{-1}$ . For the  $\nu_{20}$  mode, cancelation of the motion at the ortho-position C-H group results in only about  $4.0 \text{ km mol}^{-1}$  infrared intensity. For the  $a_1$  symmetry of the vibrational modes, such as  $\nu_1$ ,  $\nu_2$ , and  $\nu_3$  modes, the motion of the H atoms that superimpose each other with respect to the  $C_{2v}$  rotation cancel out and generate net zero projection along this  $a$  axis. For the  $\nu_1$  band, the main motion of the hydrogen atom that contributes to the infrared intensity comes from the hydrogen motion at the  $C_4$  position. The combination of the three C-H displacement vectors along the  $b$ -axis generates about  $3.7 \text{ km mol}^{-1}$  of IR intensity in the  $\nu_2$  mode. For the  $\nu_3$  mode, the C-H stretching at the  $C_4$  position diminishes the contribution of the other four C-H motions and should carry less oscillator strength as an infrared transition.

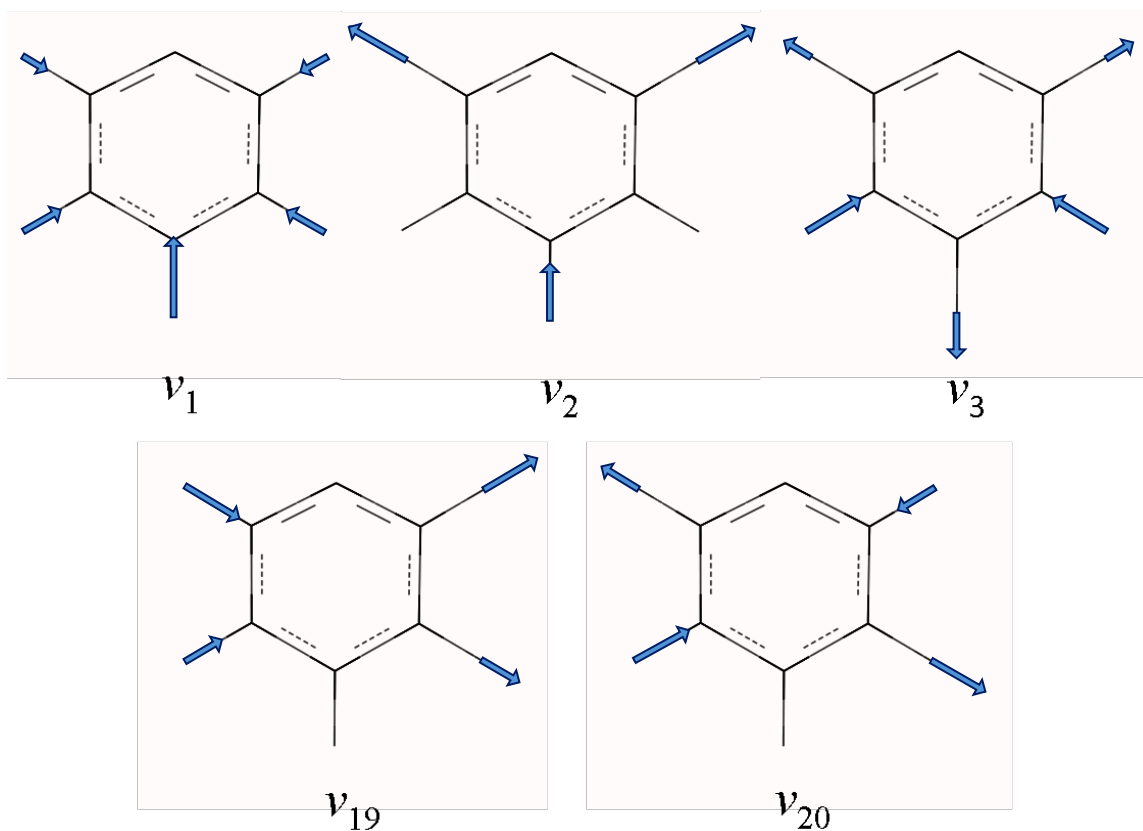


Fig. 4.2. The displacement vectors for each vibrational mode in the region of C-H stretching of phenyl radical.

In our previous studies of the infrared transitions of the phenyl radical in the region of  $3068 - 3075 \text{ cm}^{-1}$ , only one of these modes was observed it was and assigned as the excitation of  $\nu_{19}$ , characterized as an *a*-type band transition. Analysis of the moment of inertia also agrees well with the mm-wave result showing that the phenyl radical maintains planar geometry. This observation is reasonable since the excitation induces C-H stretching motion in the molecular plane. Compared with the Ar matrix results and theoretical intensity predictions, as indicated in Table 4.1, it is promising that we should be able to detect the other C-H stretching mode in the nearby transition region. Table 4.1 also shows that the other four modes, except the  $\nu_3$  mode with only 0.8 km

mol<sup>-1</sup>, should be detectable in our quantum-shot limit approach infrared spectrometer. Further, the band type associated with the different symmetry modes should allow for straightforward band assignments. In this work, we report the successful acquisition of the other two *b*-type bands of the C–H stretching mode in addition to the previously observed  $\nu_{19}$  band. The improvements in signal-to-noise ratio (S/N) reveal more detailed structure not observed previously. Spectral analysis indicates that the excitations of the  $\nu_1$  and  $\nu_2$  modes are responsible for these two additional observed bands. However, there are a few rovibrational lines that cannot be cleanly assigned, thus implying perturbation in the excited vibrational state.

## II. Experimental

The details of the sub-Doppler resolution of the infrared spectrometer have been described in previous work and the<sup>[20-21]</sup> preceding chapter. The infrared laser is generated by nonlinear difference frequency generation (DFG) using the single mode of the dye laser and the Ar<sup>+</sup> laser within a thin (10 mm×50 mm) periodically poled LiNbO<sub>3</sub> (PPLN) crystal. The frequency range available is 2500 to 5000 cm<sup>-1</sup>, which can easily be extended with the Ar<sup>+</sup> laser lasing at either 488 nm or 514 nm. The crystal is positioned in a precisely temperature-controlled oven housing, which is tuned during scanning to complement the quasi-phase matching conditions. The DFG laser that exits the crystal is split into two parts, signal and reference beams. These are monitored on separate N<sub>2</sub>(*l*) cooled InSb detectors to achieve fast electronic subtraction of the common-mode amplitude noise. The signal beam, before being imaged on the detector, traverses 16 times between two mirrors in a Herriot cell configuration downstream of a slit jet (4 cm × 300 μm) expansion with concentration modulation at 50 kHz resulting from the

electric discharge source. The attenuated modulation signal is decoupled with a lock-in detection scheme to improve the signal-to-noise ratio. Relative frequency is estimated to about 8 MHz through interpolation of an optical transfer market cavity with free spectral range (FSR) of 250 MHz. The absolute frequency is calibrated with respect to the CH<sub>4</sub> R(4) line at 3067.300 cm<sup>-1</sup>.<sup>[22]</sup>

Phenyl radical is generated through electron associative detachment in the electric discharge as illustrated in equation 4.1.



The products of the discharge are then adiabatically cooled in a supersonic expansion at the exit of the discharge source. A dilute sample of the precursor bromobenzene (0.3 %) is prepared in a 70:30 Ne:He mixed carrier gas. The discharge source makes use of a 50 kHz square modulating 500 Volt DC (current = 0.28 A) in a 1.2 ms pulse duration that is operated at 19 Hz. This instrument achieves signal-to-noise of about 70 for the strongest transitions of the phenyl radical.

### III. Results and Discussion

#### A. Spectral Observation and Analysis

In our previous studies of the infrared absorption of the C–H stretching mode of phenyl radical in the same spectral region, only one of these modes was observed ( $\nu_{19}$ ) due to its significant infrared absorption intensity (17.1 km mol<sup>-1</sup>) and the distinctive spectroscopic signature of a Q branch. The preliminary results of the assignment and analysis were reported and discussed in the previous studies.<sup>[18]</sup> Improvements in



signal-to-noise permitted acquisition of the spectrum shown in Fig. 4.3, which enabled further analysis to update results for the  $\nu_{19}$  band, as summarized in our 2013 work<sup>[23]</sup>.

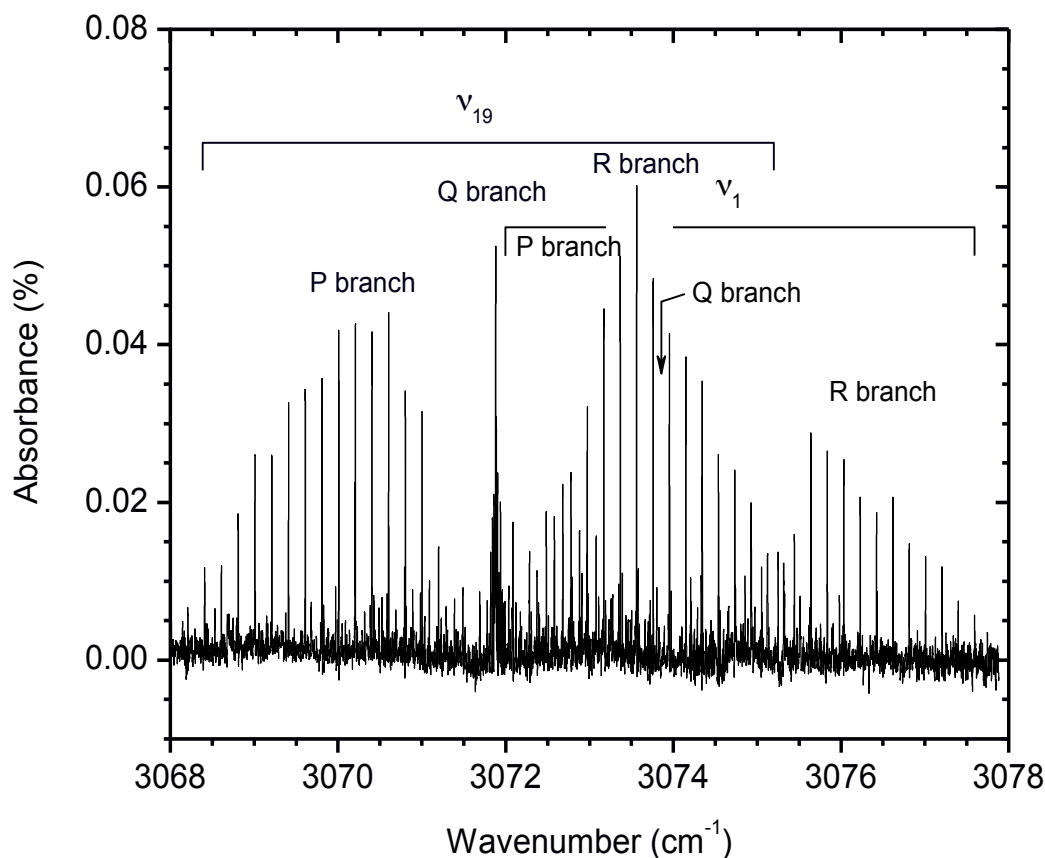


Fig. 4.3. Rotationally resolved spectrum of the phenyl radical in the region of 3068–3078  $\text{cm}^{-1}$ . The cluster of lines near 3072  $\text{cm}^{-1}$  is the Q branch of the  $\nu_{19}$  mode. Another progression in the rovibrational spectrum is clear at the blue end of this region, assigned as the R branches of the  $\nu_1$  band. The P and Q branches of the  $\nu_1$  band are interspersed with the R branch of the  $\nu_{19}$  mode.

In addition to the observed  $\nu_{19}$  band, we observe another transition that arises from the other band on the blue end of the spectrum, near 3076  $\text{cm}^{-1}$ . The P branch of this progression overlaps with the R branch of the  $\nu_{19}$  band and was thus difficult to identify initially. The Q branch of this progression does not stand out as it does with the  $\nu_{19}$  progression, indicating that the second observed transition has a different band

type. More information can be gleaned by comparing the intensities of the two bands; the second band shows non-negligible absorption intensity, about 70–80 % compared with the  $\nu_{19}$  band. As shown in Table 4.1, there are five C–H stretching modes in the spectral region accessible with our laser system. The band type of the transition for these five modes can be classified as either *a*-type or *b*-type according to the vibrational symmetry ( $a_1$  and  $b_2$ ).

Symmetry	mode	Phenyl radical				Cation
		6-311g++(3df,3dp)	Anharmonic Prediction <sup>b</sup>	Ar matrix <sup>c</sup>	Gas phase <sup>d</sup>	Ar matrix <sup>e</sup>
$a_1$	$\nu_1$	3192.84 [8.6] <sup>a</sup>	3077	3086 [3.1] <sup>a</sup>	3073.96850(8)	3110
$a_1$	$\nu_2$	3180.11 [3.4]	3065	3072 [0.2]	3062.26480(7)	
$a_1$	$\nu_3$	3160.53 [0.8]	3046	3037 [0.2]		
$b_2$	$\nu_{19}$	3182.28 [17.2]	3067	3071 [10.6]	3071.89150(7)	
$b_2$	$\nu_{20}$	3166.64 [3.9]	3052	3060 [0.1]		

Table 4.1. The symmetry and band origin frequencies ( $\text{cm}^{-1}$ ) from theoretical predictions, gas-phase, and Ar matrix studies of phenyl radical and cation in the region of C–H stretching frequencies

<sup>a</sup>. Numbers in brackets represent intensity in  $\text{km mol}^{-1}$

<sup>b</sup>. The anharmonic prediction is scaled from the theoretical calculation of density functional B3LYP/6-311g++(3df,3pd) calculations scaled by a factor of 0.964

<sup>c</sup>. Friderichsen *et al.* 2001.<sup>[11]</sup>

<sup>d</sup>. This work.

<sup>e</sup>. Winkler and Sander.<sup>[24]</sup>

Theoretical calculations predict that the  $\nu_1$  vibration is the second strongest C-H stretching band ( $8.6 \text{ km mol}^{-1}$ ) and that  $\nu_1$  has a different band-type than  $\nu_{19}$ . This justifies assigning the new progression as  $\nu_1$ . In our survey of this spectral region ( $\pm 20 \text{ cm}^{-1}$ ), there is also a weak band observed to the red of the features in Fig. 4.3. The transition position of this weak absorption is about  $12 \text{ cm}^{-1}$  red-shifted with respect to the  $\nu_{19}$  band. The rovibrational lines of this weak band are shown in Fig. 4.4 as well as the corresponding vibrational displacement vectors of hydrogen motion in  $\nu_2$ . The intensity of this weak band is about an order of magnitude smaller than that for the  $\nu_1$  and  $\nu_{19}$  bands. In Fig. 4.4 we clearly see weak *P* and *R* branches, but no observation of the *Q* branch, consistent with a *b*-type band.

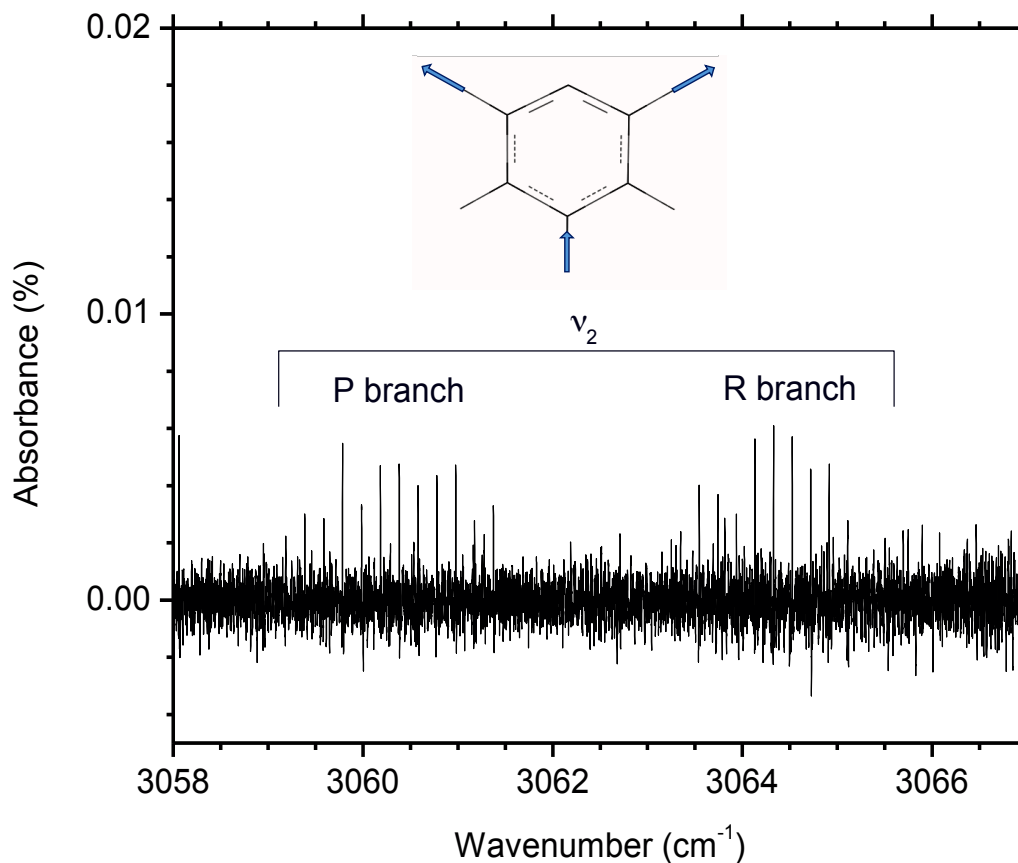


Fig. 4.4. Spectrum of the weak band observed at  $3062\text{ cm}^{-1}$  with the corresponding vibrational assignment. The rovibrational lines of the *P* and *R* branch are clearly visible but the *Q* branch is not easily identified. The corresponding hydrogen displacement vectors and the induced dipole moment are also shown in the top of the figure.

The assignments of rotational structure for the fundamental C–H stretching associated with  $\nu_1$  and  $\nu_{19}$  also are further confirmed *via* the two line ground state combination difference based on the result from the mm-wave studies of McMahon *et al.*,<sup>[17]</sup> which enables us to eliminate the possibility of the excitation from a hot band transition. Unlike the prominent *Q* branch in the *a*-type band transition, the structure of the *Q* branch for the *b*-type band is diffuse, thus not easily identified upon first

examination. Due to the highly oblate asymmetric top nature of phenyl radical, the strong lines observed in the  $P$  and  $R$  branches of  $\nu_1$  originate from the overlap between the two dominant progressions of  $N'_{1N} \leftarrow N_{0N}$  and  $N'_{0N} \leftarrow N_{1N}$  following the  $b$ -type selection rules,  $\Delta K_a \neq 0$ ,  $\Delta K_c \neq 0$ . Part of the spectrum is shown in Fig. 4.5 along with the rotational assignments and the simulated spectrum below in red.

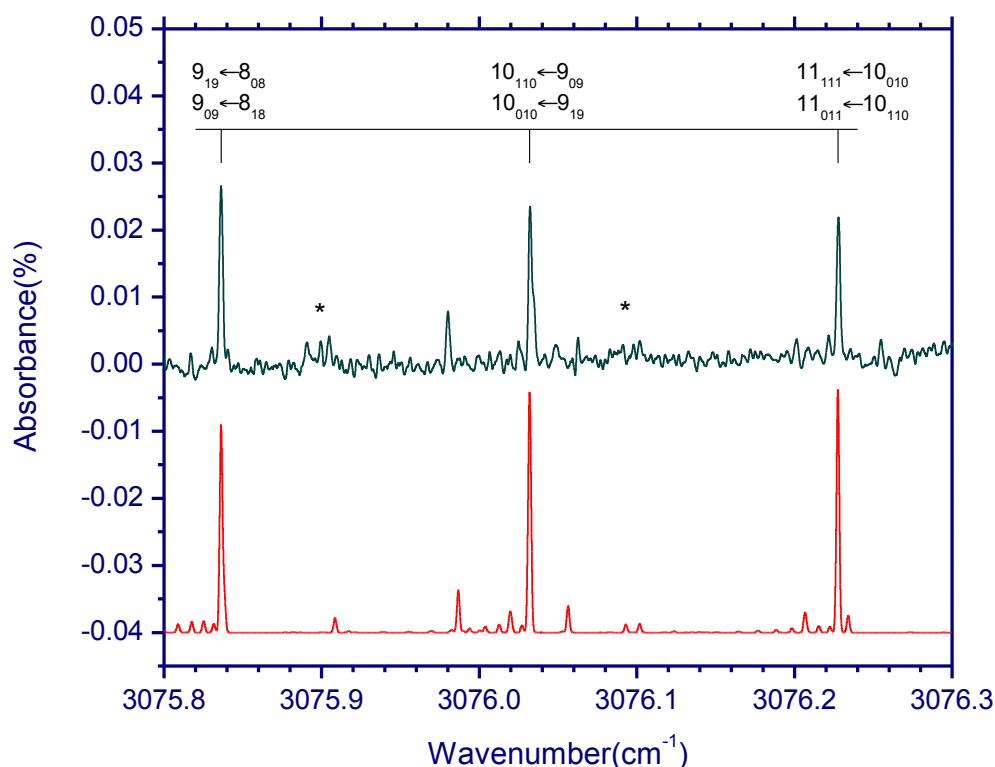


Fig. 4.5. A portion of the rotationally resolved rovibrational (black) spectrum in the vicinity of  $3076 \text{ cm}^{-1}$ . These features arise from excitation of the C–H stretching mode  $\nu_1$ , with the label of the rotational quantum number ( $N_{KaKc}$ ). The star (\*) indicates transition lines associated with the  $\nu_{19}$  band. The spectrum shown below in red is predicted based on the rotational constant and a rotational temperature of 15 K.

The asymmetric splitting of  $K_c$  is not clear and cannot be resolved within the sub-Doppler resolution (roughly 60 MHz) and thus provides no further information about the upper state structure. However, due to the planarity of phenyl radical ( $B \cong 2C$ ), a

further overlap structure arises from the  $\Delta N = \Delta K_a = \pm 1$  transition out of the levels with  $K_c=N, N-2, N-4$ , etc. Due to this overlap, we cannot eliminate the contribution from other rotational transitions. Overall, the analysis is first guided by the prediction of the frequency position with line width convolution, and nuclear spin statistical weighting (10 for  $K_a+K_c = \text{even}$  level, and 6 for  $K_a+K_c = \text{odd}$  level) are also included. The constants for the ground state are fixed to the previously published values<sup>[17]</sup> while  $A'$ ,  $B'$ ,  $C'$ , and band origin parameters are allowed to vary during the process of the fitting. The final fitting results for the  $\nu_1$  and  $\nu_2$  bands in this work are summarized in Table 4.2, with other results from the theoretical calculation and mm-wave studies. The result of the previous  $\nu_{19}$  band analysis is also included for comparison. The excited state centrifugal distortional constants ( $\Delta_{N'}$ ,  $\Delta_{NK'}$ ,  $\Delta_{K'}$ ) could be tentatively fit but the results for these parameters are an order of magnitude larger than expected by comparison with the ground state constants. Instead, these constants are fixed to be the same as the ground state values in the fitting process.

	Prediction <sup>a</sup>	Ground level <sup>b</sup>	$\nu_1$	$\nu_2$	$\nu_{19}$
A	0.211218	0.209471(10)	0.209365(23)	0.209342(5)	0.209380(4)
B	0.188434	0.186792(66)	0.186528(17)	0.186553(4)	0.186578(4)
C	0.099588	0.098714988(20)	0.09863866(64)	0.0986364(7)	0.0986098(8)
$\Delta_N \times 10^8$		4.733(13)			
$\Delta_{NK} \times 10^8$		-7.972(33)			
$\Delta_K \times 10^8$		3.63(20)			
$\nu_0$			3073.96850(8)	3062.26480(7)	3071.89150(7)
$\Delta$ (amu $\cdot\text{\AA}^2$ )		0.046(5)	0.009	0.016	0.089
$\Delta A/A$ (%)			-0.05	-0.06	-0.04
$\Delta B/B$ (%)			-0.13	-0.12	-0.11
$\Delta C/C$ (%)			-0.08	-0.08	-0.10

Table 4.2. Spectroscopic parameters of the phenyl radical in the ground state and excited CH stretching modes from this work

<sup>a</sup>. Ref. [18]

<sup>b</sup>. Ref. [17]

<sup>c</sup>. The centrifugal distortion constants are kept the same as the ground state values.

In this work, the band origins for the  $\nu_1$  and  $\nu_2$  modes are determined for the first time in the gas-phase to be  $3073.96850(8) \text{ cm}^{-1}$  and  $3062.26480(7) \text{ cm}^{-1}$ , respectively. In the Ar matrix study, Friderichsen *et al.* assigned the band origins for these two modes as  $3086$  and  $3072 \text{ cm}^{-1}$ , which are  $12$  and  $10 \text{ cm}^{-1}$  higher in energy than the results in this work. These shifts are considerably larger than that of  $\nu_{19}$ , which was  $3071.89150(7) \text{ cm}^{-1}$  in the gas-phase compared to  $3072 \text{ cm}^{-1}$  in the condensed phase. In an Ar matrix, the radical is entrapped in an inert gas matrix and is often perturbed, which can affect the observed transition frequencies and infrared intensities. Friderichsen *et al.*<sup>[11]</sup> estimated that the line widths of the IR band in the matrix spectra about  $0.5\text{--}0.8 \text{ cm}^{-1}$  due to matrix inhomogeneous line broadening. They considered the effect of broadening and matrix shift and estimated that the deviation from the gas-phase to be about  $\pm 1 \%$  ( $30 \text{ cm}^{-1}$  for C-H stretches) for the corresponding transition frequencies. A recent review by Jacobs<sup>[25]</sup> provided a guideline for polyatomic free radicals in Ar matrices, indicating that shifts are usually less than  $1 \%$  and often occur at lower energy.

Table 4.1 summarizes findings from experimental results (gas-phase and matrix isolation) and calculations (performed with B3LYP/6-311g++(3df,3dp) basis set including an anharmonic scaling (0.964) for the  $\nu_1, \nu_2$ , and  $\nu_{19}$  bands). One interesting finding is that the difference bands have different gas-phase to matrix shifts. One physical interpretation for this observation is provided by examining the displacement vectors for the different modes. Fig. 4.2 indicates that the vibrational motion of the H atoms in  $\nu_1, \nu_2$  and  $\nu_3$  tend to expand the molecule's physical size. In contrast, the H motion in  $\nu_{19}$  and  $\nu_{20}$  does less to affect the effective size of the radical. The shift in frequency could be through an effective increase in a force constant when the H atoms



must work against the rigid environment along the specific normal mode, and result in the blue shift of the transition.

The effective rotational constants are also determined from the fitting process (shown in Table 4.2.) and analysis for the  $\nu_1$  and  $\nu_2$  bands agrees well with the mm-wave study. The effect for the three molecular constants upon excitation of  $\nu_1$  is estimated to be  $\Delta A/A = -0.05\%$ ,  $\Delta B/B = -0.18\%$ , and  $\Delta C/C = -0.08\%$ , consistent with in-plane C–H motion. The behaviors for the  $\nu_2$  band are also listed in Table 4.2. The  $\Delta C/C$  of the  $\nu_{19}$  band is  $-0.10\%$ , larger than for the  $\nu_1$  and  $\nu_2$  bands analyzed here ( $-0.08\%$ ), indicating a larger change along the C axis, the out of plane rotational axis. Further information can be extracted from the inertia defect ( $\Delta \equiv I_c - I_a - I_b$ ) for the upper state. Our result indicates that the vibrational excited states maintain a planar structure, with  $\Delta(\nu_1) = 0.009 \text{ amu}\cdot\text{\AA}^2$ ,  $\Delta(\nu_2) = 0.016 \text{ amu}\cdot\text{\AA}^2$ , and  $\Delta(\nu_{19}) = 0.089 \text{ amu}\cdot\text{\AA}^2$ . These are all non-zero but small, similar to the ground vibrationless level ( $\Delta = 0.046 \text{ amu}\cdot\text{\AA}^2$ ). The inertial defects for the three vibrationally excited states also support the assignment of in-plane vibrational modes. Any mode with significant out-of-plane displacement or combination bands with out-of-plane motion would have excited state  $\Delta$  values that are much larger.

In our analysis of the spectrum in this region, there are still a few features that cannot be assigned. It is plausible that there exists coupling to other vibrational modes that have no oscillator strength (dark modes). For such a large molecule as phenyl radical, the density of vibrational state is estimated to be about 5–10 states/ $\text{cm}^{-1}$ .<sup>[18]</sup> This mainly arises from counting the various low-frequency bending modes. The spectrum

will become complex due to the mixing of rovibrational levels of the bright and dark states when the oscillation character is shared by two eigenstates. However, in our analysis, we do not observe spectroscopic signatures of any given coupling to specific states.

## B. Intensity Analysis

Since we have observed three gas-phase C-H vibrations,  $\nu_1$ ,  $\nu_2$ , and  $\nu_{19}$ , it is interesting to compare the experimental integrated intensity for the vibrational bands. Besides the predicted band origin for each mode, the predicted intensity (in  $\text{km mol}^{-1}$ ) is also included in Table 4.1. The values are  $\nu_1 = 8.5$ ,  $\nu_2 = 3.7$ ,  $\nu_3 = 0.8$ ,  $\nu_{19} = 17.1$  and  $\nu_{20} = 4.0 \text{ km mol}^{-1}$ . As mentioned in the previous section, due to overlap of the dominant features in the *P* and *R* branches, extracting the total integrated intensity for each band is challenging. However, there are still many single isolated rovibrational features that can be analyzed.

For a given single isolated rovibrational feature, the integrated line absorption coefficient is defined as:  $S_i = \int \varepsilon(\nu) d\nu$ , which is proportional to the number density of the radical in the initial level, the rotational partition function and the Hönl-London factor. The explicit formula<sup>[26]</sup> is given in equation 4.2.

$$S_i = \int \varepsilon(\nu) d\nu = \frac{8\pi^2}{3hc} \frac{1}{4\pi\epsilon_0} N_A \cdot \nu_{fi} \cdot \frac{g_{ns} g_N e^{-E_{rot}/kT} \cdot \text{HL} \cdot |\mu_v|^2}{Q_{rot}} \left(1 - e^{-h\nu_{fi}/kT}\right) \quad (4.2)$$

Here  $N_A$  is Avogadro's number,  $g_{ns}$  and  $g_J$  are the nuclear spin statistical weighting and degeneracy of the rotational level, HL is the Hönl-London factor, and  $\mu_v$

is the transition dipole moment for the specific vibrational transition. Here, we adapted the function for a symmetric top rather than an asymmetric top.

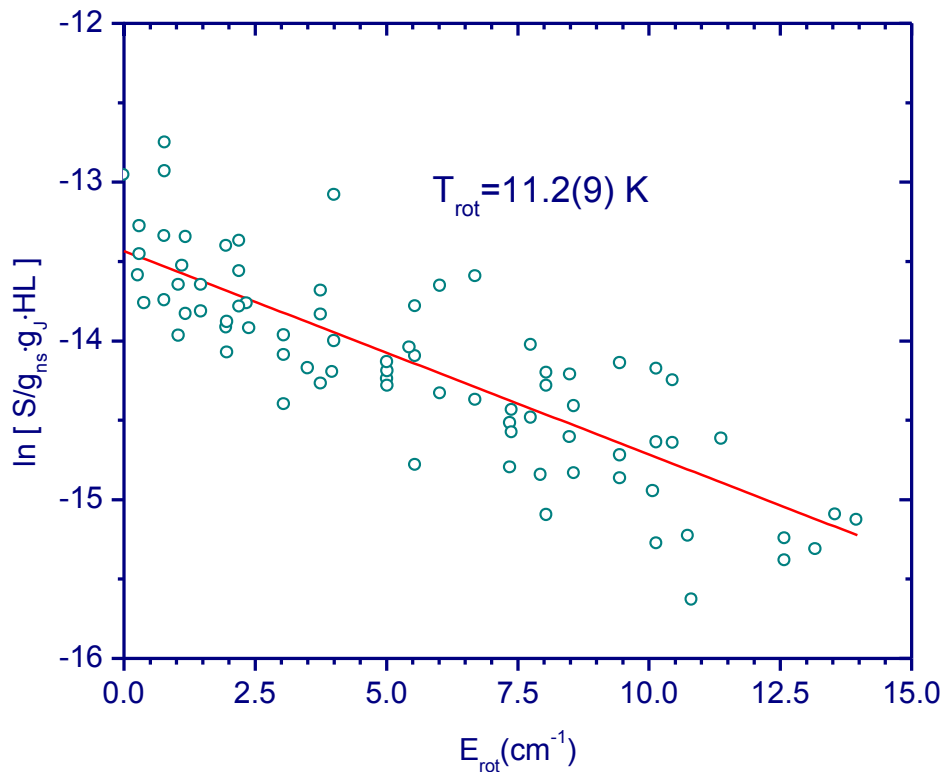


Fig. 4.6. Boltzmann plot of the single isolated lines in the  $\nu_{19}$  band leading to a rotational temperature of about 11.2 K.

The Boltzmann plot, which analyzes single rovibrational absorption features in the  $\nu_{19}$  band, is shown in Fig. 4.6. The slope of the Boltzmann plot indicates a rotational temperature of  $11.2 \pm 0.9 \text{ K}$ . A comparison between the experimental intensity observation and theoretical prediction offers a good test of the quality of the theoretical method and basis set used in the calculation. In order to avoid the bias of the overlapping structure in the  $P$  and  $R$  branches, we first predicted the rovibrational lines for each band based on the previous fitting rotational constants, rotational temperature (11.2 K), and linewidth convolution (60 MHz). The predicted intensity for each band is

scaled with the experimental observation to match the whole spectrum. Then the integrated band absorption coefficient is obtained by the sum of the individual lines as seen in equation 4.3

$$S \equiv \sum_{i=1}^n S_i = \left(8\pi^2/3hc \cdot 4\pi\epsilon_0\right) N \cdot \nu_{fi} \cdot |\mu_v|^2. \quad (4.3)$$

The results are normalized to the strongest  $\nu_{19}$  band and shown and are summarized in Fig. 4.7. Also included in Fig. 4.7 are the intensities reported from the Ar matrix study of the phenyl radical.<sup>[17]</sup> Disparities between gas-phase and condensed phase are due to perturbations from the matrix likely causing some fluctuation in absorbance. The experimental observations agree well with the ratio of the theoretical predictions indicating that the high level of basis set and method in used with density functional theory provide reliable predictions of the absorbance intensity. The intensity of the  $\nu_{19}$ ,  $\nu_{20}$  and  $\nu_{21}$  bands is related to the derivative of the dipole moment, which for  $\nu_{19}$  is dominated by the H atom motion in the  $C_4$  position. In the  $\nu_{21}$  mode, the effect of H atom motions at the  $C_3$ ,  $C_4$  and  $C_5$  cancel since they are out-of-phase during the motion. Unfortunately, we did not observe any signature of the  $\nu_{20}$  band. The reason may be due to its weak intensity ( $3.9 \text{ km mol}^{-1}$ ).

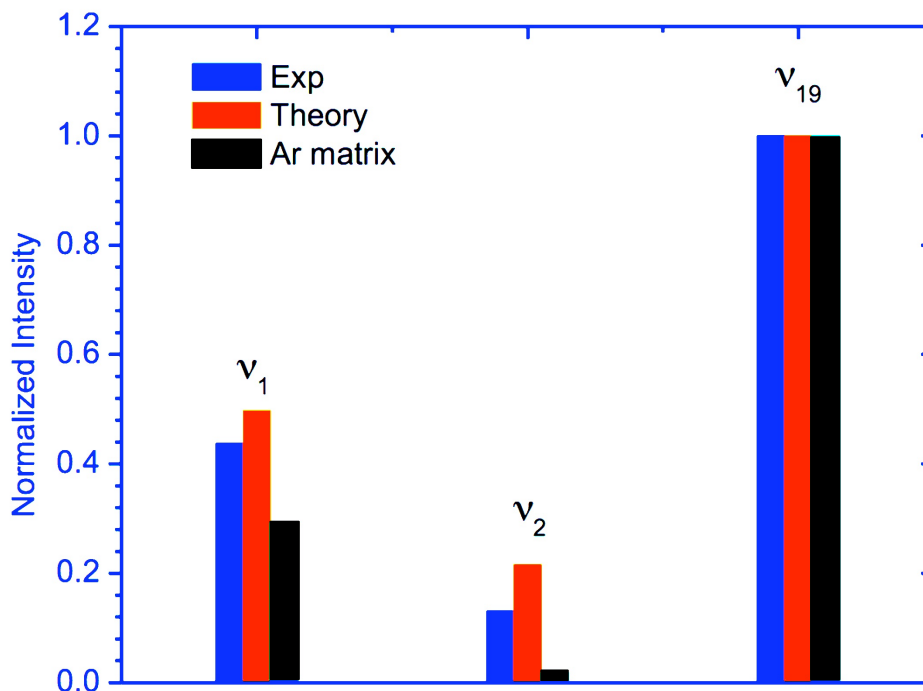


Fig. 4.7. The normalized integrated band intensity for the experimental (gas-phase and Ar matrix) observations and the theoretical predictions.

The infrared spectrum of the phenyl cation has been studied by Winkler and Sander<sup>[24]</sup> with Ar matrix isolation techniques. They reported that the corresponding  $\nu_{19}$  band for the cation species is found at  $3110\text{ cm}^{-1}$  in the condensed environment. No other transitions have been reported for this isolated species in the gas-phase. The calculated infrared intensity based on the B3LYP/cc-pVDZ method predicted that this mode carries an intensity of  $204\text{ km mol}^{-1}$ . The identification of rovibrational transitions of this cation with sub-Doppler resolution should be feasible using the radical spectroscopy presented here as a starting point. An open question currently exists regarding the ground state multiplicity of the phenyl cation; there is some debate regarding the gap between the  $^1A_1$  and  $^3B_1$  states.<sup>[27]</sup> Experimental studies of the phenyl cation in the gas-phase should be able to shed new light on this issue.

#### IV. Summary and Conclusions

The infrared absorption of the rovibrational transitions of the in-plane C–H stretching mode of the phenyl radical have been investigated in a slit-jet supersonic expansion. With the improvement of the absorption sensitivity since studying the  $\nu_{19}$  mode, two new *b*-type bands resulting from C-H stretches have been observed. The new bands are assigned as  $\nu_1$  and  $\nu_2$  and these assignments are confirmed via two-line combination difference. The band origins for these two modes are reported  $\nu_1 = 3073.96850(8) \text{ cm}^{-1}$  and  $\nu_2 = 3062.26480(7) \text{ cm}^{-1}$ . This constitutes the first observation of these bands in the gas-phase and the observed values agree well with theoretical anharmonic predictions accompanying these findings. Physical interpretations are given regarding the discrepancy between the results of theoretical prediction, Ar matrix, and gas-phase, both for band origins and absorbance intensities. The inertial defects for each are also discussed and indicate planarity of the excited vibrational states. The band intensities of the  $\nu_1$ ,  $\nu_2$  and  $\nu_{19}$  bands have been compared and the results agree well with theoretical predictions. The capability to measure the infrared spectroscopic signatures of aromatic radical species offers a promising probe for identification of the ubiquitous PAHs in the interstellar medium and provides spectroscopic information relevant for combustion models.

## References for Chapter 4

- [1] A. Kazakov and M. Frenklach. Dynamic modeling of soot particle coagulation and aggregation: Implementation with the method of moments and application to high-pressure laminar premixed flames. *Combustion and Flame* **1998**, *114*, 484-501.
- [2] J. A. Miller and C. F. Melius. Kinetic and thermodynamic issues in the formation of aromatic-compounds in flames of aliphatic fuels. *Combustion and Flame* **1992**, *91*, 21-39.
- [3] R. I. Kaiser, O. Asvany, Y. T. Lee, H. F. Bettinger, P. V. Schleyer and H. F. Schaefer. Crossed beam reaction of phenyl radicals with unsaturated hydrocarbon molecules. I. Chemical dynamics of phenylmethylacetylene ( $C_6H_5CCCH_3$ ;  $X^1A'$ ) formation from reaction of  $C_6H_5$  ( $X^2A_1$ ) with methylacetylene,  $CH_3CCH$  ( $X^1A_1$ ) *Journal of Chemical Physics* **2000**, *112*, 4994-5001.
- [4] P. Ehrenfreund. Astrophysical chemistry: Molecules on a space odyssey. *Science* **1999**, *283*, 1123-1124.
- [5] H. Bohm and H. Jander. PAH formation in acetylene-benzene pyrolysis. *Physical Chemistry Chemical Physics* **1999**, *1*, 3775-3781.
- [6] E. Herbst. Chemistry in the interstellar-medium. *Annual Review of Physical Chemistry* **1995**, *46*, 27-53.
- [7] P. H. Kasai, E. Hedaya and E. B. Whipple. Electron spin resonance study of phenyl radicals isolated in an argon matrix at 4 K. *Journal of the American Chemical Society* **1969**, *91*, 4364-4368.
- [8] J. E. Bennett, B. Mile and A. Thomas. Electron spin resonance spectrum of phenyl radical prepared by chemical reaction at 77 K. *Chemical Communications* **1965**, 265-267.
- [9] J. Pacansky and J. Bargon. Low-temperature photochemical studies on acetyl benzoyl peroxide - observation of methyl and phenyl radicals by matrix-isolation infrared spectroscopy. *Journal of the American Chemical Society* **1975**, *97*, 6896-6897.

- [10] J. G. Radziszewski, M. R. Nimlos, P. R. Winter and G. B. Ellison. Infrared absorption spectroscopy of the phenyl radical. *Journal of the American Chemical Society* **1996**, *118*, 7400-7401.
- [11] A. V. Friderichsen, J. G. Radziszewski, M. R. Nimlos, P. R. Winter, D. C. Dayton, D. E. David and G. B. Ellison. The infrared spectrum of the matrix-isolated phenyl radical. *Journal of the American Chemical Society* **2001**, *123*, 1977-1988.
- [12] N. Ikeda, N. Nakashima and K. Yoshihara. Observation of the ultraviolet-absorption spectrum of phenyl radical in the gas-phase. *Journal of the American Chemical Society* **1985**, *107*, 3381-3382.
- [13] J. G. Radziszewski. Electronic absorption spectrum of phenyl radical. *Chemical Physics Letters* **1999**, *301*, 565-570.
- [14] T. Yu and M. C. Lin. Kinetics of phenyl radical reactions studied by the cavity-ring-down method. *Journal of the American Chemical Society* **1993**, *115*, 4371-4372.
- [15] T. Yu and M. C. Lin. Kinetics of the C<sub>6</sub>H<sub>5</sub> + O<sub>2</sub> Reaction at Low-Temperatures. *Journal of the American Chemical Society* **1994**, *116*, 9571-9576.
- [16] K. Freel, M. C. Lin and M. C. Heaven. Cavity ring-down spectroscopy of the phenyl radical in a pulsed discharge supersonic jet expansion *Chemical Physics Letters* **2011**, *507*, 216-220.
- [17] R. J. McMahon, M. C. McCarthy, C. A. Gottlieb, J. B. Dudek, J. F. Stanton and P. Thaddeus. The radio spectrum of the phenyl radical. *Astrophysical Journal* **2003**, *590*, L61-L64.
- [18] E. N. Sharp, M. A. Roberts and D. J. Nesbitt. Rotationally resolved infrared spectroscopy of a jet-cooled phenyl radical in the gas phase. *Physical Chemistry Chemical Physics* **2008**, *10*, 6592-6596.
- [19] F. Dong, S. Davis and D. J. Nesbitt. Slit discharge IR spectroscopy of a jet-cooled cyclopropyl radical: Structure and intramolecular tunneling dynamics. *Journal of Physical Chemistry A* **2006**, *110*, 3059-3070.
- [20] A. S. Pine. High-resolution methane nu-3-band spectra using a stabilized tunable difference-frequency laser system. *Journal of the Optical Society of America* **1976**, *66*, 97-108.



- [21] S. Davis, M. Farnik, D. Uy and D. J. Nesbitt. Concentration modulation spectroscopy with a pulsed slit supersonic discharge expansion source. *Chemical Physics Letters* **2001**, *344*, 23-30.
- [22] J. Pliva and A. S. Pine. Analysis of the 3- $\mu$ m bands of benzene. *Journal of Molecular Spectroscopy* **1987**, *126*, 82-98.
- [23] G. T. Buckingham, C.-H. Chang and D. J. Nesbitt. High-Resolution Rovibrational Spectroscopy of Jet-Cooled Phenyl Radical: The  $\nu_{19}$  Out-of-Phase Symmetric CH Stretch. *The Journal of Physical Chemistry A* **2013**, *117*, 10047-10057.
- [24] M. Winkler and W. Sander. Isolation of the phenyl cation in a solid argon matrix. *Angewandte Chemie-International Edition* **2000**, *39*, 2014-2016.
- [25] M. E. Jacox. The vibrational-energy levels of small transient molecules isolated in neon and argon matrices. *Chemical Physics* **1994**, *189*, 149-170.
- [26] P. R. Bunker, P. Jensen, N. R. C. Canada and N. R. C. C. M. P. Program, *Molecular Symmetry and Spectroscopy*, NRC Research Press, **2006**, p. 90-92.
- [27] A. Nicolaidis, D. M. Smith, F. Jensen and L. Radom. Phenyl radical, cation, and anion. The triplet-singlet gap and higher excited states of the phenyl cation. *Journal of the American Chemical Society* **1997**, *119*, 8083-8088.

## Chapter 5

### Hydropyrolysis of Ethylbenzene in a Heated Micro-Reactor

#### Abstract

We have investigated the role that gas-phase hydrogen atoms can play in the pyrolysis of ethylbenzene ( $C_6H_5CH_2CH_3$ ) in a heated micro-reactor. Methyl nitrite ( $CH_3ONO$ ) thermally decomposes to form formaldehyde ( $CH_2O$ ), nitric oxide (NO), hydrogen atom at reactor temperatures of 800 K and higher. Gas-phase methyl nitrite can be mixed with ethylbenzene and the pyrolytically formed hydrogen atoms are shown to alter the pyrolysis of ethylbenzene. Hydrogen mediated pyrolysis, or hydropyrolysis, is studied using both photoionization mass spectrometry and matrix isolation infrared spectroscopy. The products observed during hydropyrolysis of ethylbenzene are styrene ( $C_6H_5CH=CH_2$ ), toluene, ( $C_6H_5CH_3$ ), benzene ( $C_6H_6$ ), and ethylene ( $CH_2=CH_2$ ).

#### I. Introduction

As the world's energy usage continues to grow, the use of fossil fuels has been under increasing scrutiny due to its one-directional deposition of carbon from the solid phase into the gas phase in the form of greenhouse gasses. Alternate fuel sources such as biofuels provide an attractive alternative since the fuel precursor, plants, remove carbon from the air rather than from inside the earth. However, biofuel globalization is still limited in part due to the difficulty of rendering the stored energy in plants

chemically available and industrially practical. Efforts have been marginally successful to utilize cellulose based plant matter but utilization of the second largest polymer component of plants, lignin,<sup>[1]</sup> has proven elusive due to challenges in liquefaction and deoxygenation of lignin fuel stock. Discovery of a more efficient de-polymerization mechanism will be necessary before any lignin derived liquid fuel can become a viable energy source in our current environment.

To this end, scientists have studied techniques to process lignin from its raw form into a more useful, monocyclic form. Lignin is made up of three phenylpropanoids with varying degrees of methoxylation (see Chapter 1). These monomers combine to form a complex network of cross linkages that make up lignin as it is found in nature.<sup>[1]</sup> Previous efforts to process lignocellulosic biomass have explored fast pyrolysis,<sup>[2-3]</sup> metal-catalyzed decarboxylation,<sup>[4]</sup> metal-catalyzed hydrogenation<sup>[5]</sup> and hydrogenolysis.<sup>[6]</sup> One of the more successful techniques thus far has been fast pyrolysis, where high pressures (1500-2500 psig) produce pyrolysis oils that require subsequent upgrading due to their high acidity, low heating value, and high oxygen content.

Recent work at the Gas Technology Institute has demonstrated a promising new technique to convert raw plant matter to gasoline and diesel fuel through a process called integrated hydrolysis and hydroconversion (IH<sup>2</sup>).<sup>[7]</sup> In this process, biomass feedstock is fed into a fluidized catalyst bed under 14–35 bar of hydrogen gas at temperatures between 350°C and 480°C. During hydrolysis, the biomass is deoxygenated to less than 1 % oxygen content and carbon that is bound in complex lignin linkages is converted to liquid phase hydrocarbons that are easily separated from aqueous phase products. These hydrolysis oils are lighter than pyrolysis oils and

show smooth boiling point distributions in the ranges of gasoline, diesel and jet fuel. These advances are particularly promising because the hydrogen responsible for hydrolysis is regenerated in the process, whereby hydrogen acts as a catalyst rather than a reagent. As this promising research demonstrates a potential future in biofuel gasification, more work must be done to gain a more detailed understanding of the chemistry that underlies IH<sup>2</sup>.

Recent work by Vasiliou *et al.* has begun to elucidate the chemical mechanisms in play during the hydrolysis process.<sup>[8]</sup> Gas phase benzaldehyde was pyrolyzed in a heated tubular reactor and the fragments were investigated using photoionization mass spectrometry and matrix isolation spectroscopy. It was found that benzaldehyde reacts with hydrogen atom to produce benzene and HCO, the latter of which further decomposes to CO and H, thus establishing a hydrogen atom chain reaction. Fig. 5.1 summarizes the chemical pathways discovered.

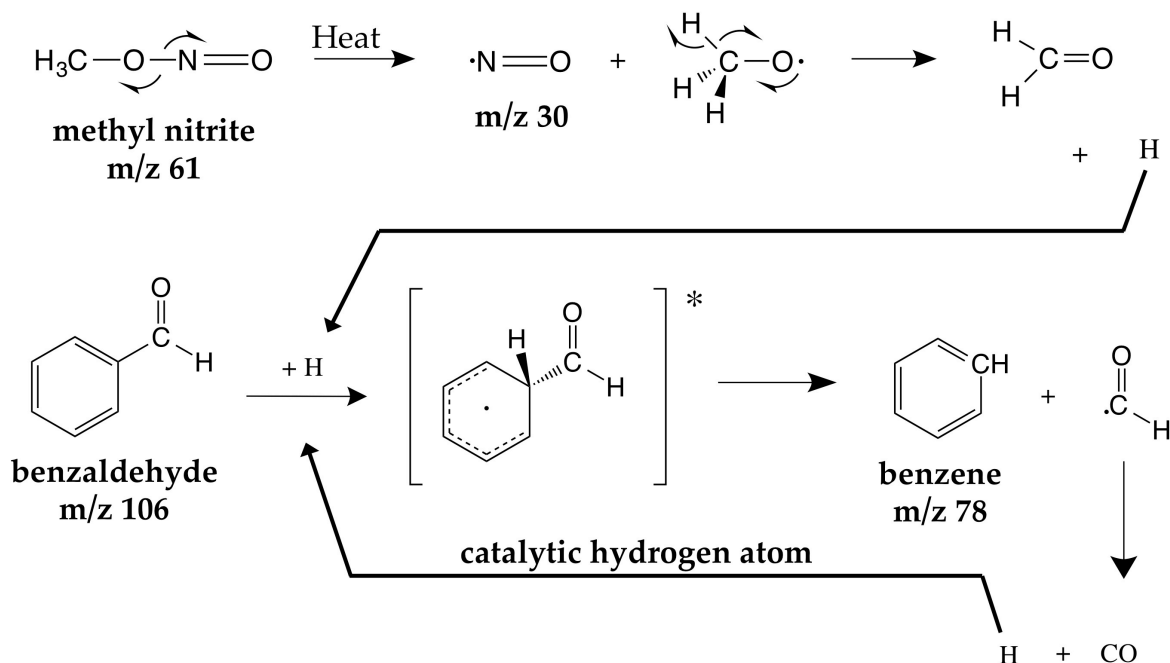


Fig. 5.1. Schematic of the chemical pathways confirmed for the pyrolysis of benzaldehyde ( $\text{C}_6\text{H}_5\text{CHO}$ ) mixed with methyl nitrite ( $\text{CH}_3\text{ONO}$ ). The methyl nitrite can decompose at low temperatures (900 K) in the micro-reactor to produce hydrogen atom. Hydrogen atom can replace the aldehyde group from benzaldehyde but another hydrogen atom is formed in the process, making this process catalytic.

As shown in Fig. 5.1, to confirm that the decomposition was hydrogen atom mediated, a chemical source of H atom was employed. Methyl nitrite is an attractive hydrogen atom source because the first step of decomposition is facilitated by a very weak bond dissociation enthalpy. The  $\text{CH}_3\text{O}-\text{NO}$  bond can be calculated from experimental heats of formation<sup>[9-10]</sup> to be  $42.7 \pm 0.6 \text{ kcal mol}^{-1}$ , which is sufficiently small to begin decomposition at temperatures lower than most other thermal decomposition pathways. This is a convenient source of hydrogen atom for pyrolysis that is available at lower temperatures than those at which target molecules (in this case benzaldehyde) begin to decompose.

In the absence of a low-temperature hydrogen source, pyrolysis of benzaldehyde required heating the reactor to sufficiently high temperatures (1600 K) to provide unbound hydrogen atoms. Establishing similar mechanisms at lower pyrolysis temperatures and for a broad array of substituent groups will aid in determining a mechanistic description of the hydrolysis that converts biomass feedstock into viable gasoline or diesel fuel sources.

In order to gain a deeper understanding of catalytic hydrolysis, a detailed study of the simplest biofuel molecules has been performed in our labs, starting with ethylbenzene ( $C_6H_5CH_2CH_3$ ), n-propylbenzene ( $C_6H_5CH_2CH_2CH_3$ ), and isopropylbenzene ( $C_6H_5CH(CH_3)_2$ ). These alkylbenzene molecules function as surrogates for the aromatic ring/side-chain bonding found in lignin polymers. To isolate the effects of hydrogen atoms on the thermal decomposition of these relatively small molecules, a dilute hydrogen atom source has been developed and characterized that allows for the presence of hydrogen atoms at much lower temperatures than those used in the study of benzaldehyde.

Pyrolysis reactions of these alkylbenzene molecules in a micro-tubular reactor are studied using the combination of photoionization mass spectrometry and matrix isolation Fourier transform infrared spectroscopy to identify the fragments formed as a result of heating, both in the presence and absence of the hydrogen atom source. In this way, the products that form as a result of hydrolysis can be isolated from those that occur during the un-catalyzed pyrolysis. The data show that through both hydrogen atom abstraction and addition to the parent molecule, the catalytic hydrogen atoms promote chemical pathways that were previously inaccessible until much higher pyrolysis temperatures. These findings will hopefully be used to modify and optimize

current hydrolysis practices in the conversion of lignin containing biomass to fungible fuel sources in the future.

## II. Experimental

Ethylbenzene ( $C_6H_5CH_2CH_3$ ) and methyl nitrite ( $CH_3ONO$ ) are pyrolyzed in a heated SiC micro-reactor as described in Chapter 2. At the exit of the reactor, the pyrolysis products are entrained in a supersonic expansion of either helium or argon and are then detected using either photoionization mass spectrometry (PIMS) or argon matrix isolation infrared (IR) spectroscopy. The reactor wall temperature is monitored using a Type-C thermocouple and temperature is controlled using a variable transformer to run current through the SiC reactor to cause resistive heating.

Methyl nitrite was synthesized daily for each set of experiment. Sodium nitrite and methanol were mixed in a round bottom flask and 37 % hydrochloric acid was slowly added in using a dropping funnel and the reaction flask was cooled in an ice bath. The gas-phase methyl nitrite was collected in a cold finger submerged in liquid nitrogen and the pale yellow solid methyl nitrite was purified by a few freeze-pump-thaw cycles. The sample gas cylinder was prepared by removing the cold finger from the liquid nitrogen for roughly 1 minute and collecting the vapor-phase methyl nitrite and diluting with helium or argon. Dilute ethylbenzene samples are prepared simply by collecting the room temperature vapor pressure above liquid ethylbenzene.

PIMS is performed by tripling the tripled (355 nm) output of an Nd:YAG laser and intersecting the light with the skimmed output of the heated micro-reactor. The 9<sup>th</sup> harmonic is generated by nonlinear sum frequency generation in a stagnant Xe:Ar (pressure ratio 10:90) cell mounted to the PIMS vacuum chamber. Upon ionization by

10.487 eV photons, cations are accelerated into a commercial time-of-flight spectrometer and PIMS spectra are recorded by monitoring the microchannel plate (MCP) detector signal over time. Matrix isolation IR spectra were recorded by seeding the target molecules in argon and then aiming the output of the reactor at a cryogenically cooled CsI window maintained at roughly 20 K. Argon condenses onto the window trapping all dilute species in an inert matrix where local densities of IR absorbers can be built up without reaction or degradation of the pyrolysis products. After roughly two hours of dosing onto the CsI window, the reactor assembly is rotated 90° and the sample is moved into the beam path of a commercial Fourier transform IR spectrometer.

### **III. Results and Discussion**

#### **A. Ethylbenzene Decomposition**

The first molecule investigated was ethylbenzene ( $C_6H_5CH_2CH_3$ ), which is the simplest alkyl benzene after toluene ( $C_6H_5CH_3$ ). This molecule has a sufficient vapor pressure at room temperature to make dilute pre-made mixes in helium. The dilution discussed here is 0.1 % but further dilution shows similar decomposition pathways. A more recent study on benzyl radical decomposition<sup>[11]</sup> has made use of ethylbenzene as the main precursor for pyrolytic production of benzyl radical. The pyrolysis of ethylbenzene at temperatures up to 1300 K is shown in Fig. 5.2.



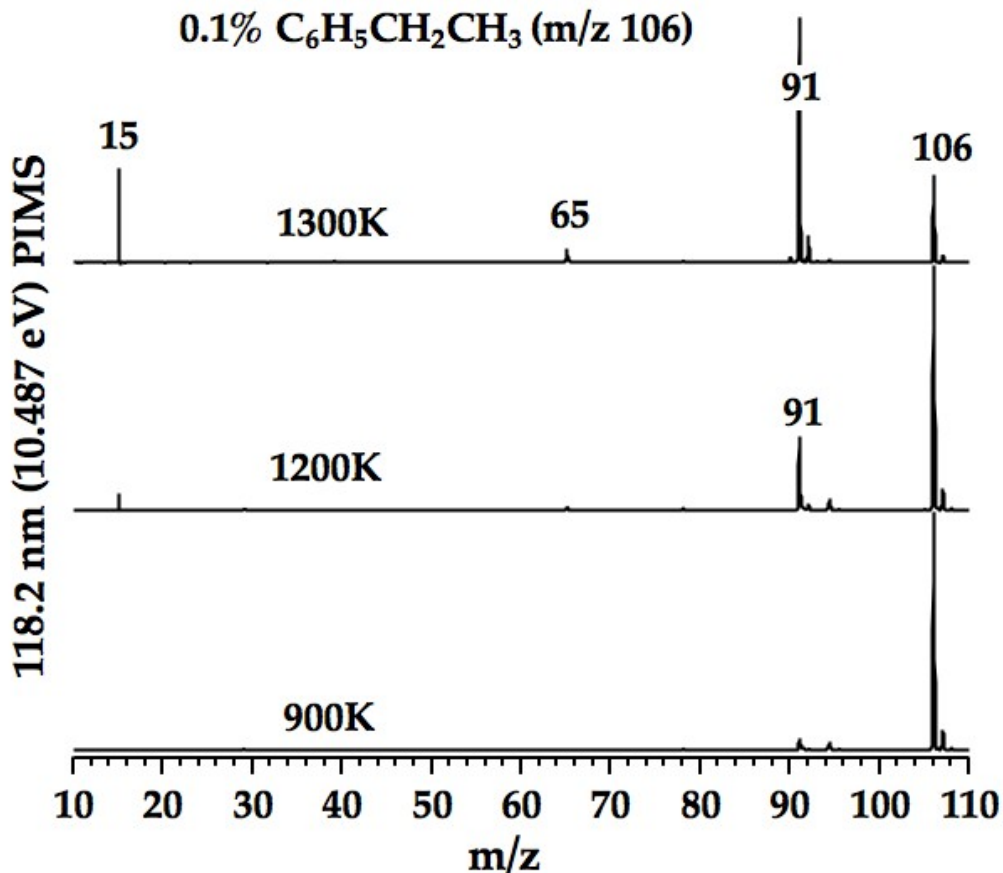


Fig. 5.2. Thermal decomposition of dilute ethylbenzene (0.1 % in He) at 900 K, 1200 K and 1300 K. The only major products observed are benzyl radical (m/z 91) and methyl radical (m/z 15) at 1200 K. Upon heating to 1300 K, a third decomposition product is observed at m/z 65.

The decomposition of ethylbenzene observed using PIMS is relatively simple for temperatures up to 1300 K. The first products are benzyl radical and methyl radical, which is predictable given the weak C<sub>6</sub>H<sub>5</sub>CH<sub>2</sub>—CH<sub>3</sub> bond<sup>[11]</sup> (DH<sub>298</sub> = 77.6 ± 0.7 kcal mol<sup>-1</sup>). At 1300 K a third feature appears at m/z 65 that has been confirmed to be cyclopentadienyl radical (*c*-C<sub>5</sub>H<sub>5</sub>).

To identify the effects of hydrogen atom on ethylbenzene pyrolysis, methyl nitrite was added to the premixed sample volume and PIMS was recorded duplicating all other experimental conditions. Methyl nitrite has been used as pyrolytic hydrogen

atom source previously<sup>[8]</sup> but the process was confirmed here. Fig. 5.3 shows the PIMS spectra of methyl nitrite pyrolysis between 600 K and 1200 K. Pyrolysis is initiated at 800 K as indicated by the feature at  $m/z$  30. Following the chemical diagram in Fig. 5.1, this is assumed to be nitric oxide (NO). The co-produced fragment methoxy radical ( $IE(CH_3O) = 10.726 \pm 0.008$  eV)<sup>[12]</sup> is likely responsible for the small peak at  $m/z$  31 but is expected to be short lived. Loss of a hydrogen atom forms formaldehyde ( $m/z$  30), which is very stable but has an ionization energy too large for the 118.2 nm PIMS ( $IE(CH_2O) = 10.8850 \pm 0.0002$  eV).<sup>[13]</sup> At 900 K and 1200 K, a feature emerges at  $m/z$  15, presumed to be methyl radical ( $IE(CH_3) = 9.8380 \pm 0.0004$  eV),<sup>[14]</sup> which indicates another chemical pathway is also active. Methyl nitrite can also fragment as shown in equation 5.1.



This pathway is higher in energy than the hydrogen atom forming route ( $DH_{298}(CH_3-ONO) = 59.1 \pm 0.3$  kcal mol<sup>-1</sup>)<sup>[9-10]</sup> but can explain the observed  $m/z$  15 feature. The other product generated by the reaction in equation 5.1 would be NO<sub>2</sub>, which, despite its ionization energy being less than 10.482 eV ( $IE(ONO) = 9.586 \pm 0.002$  eV)<sup>[15]</sup>, is not observed, which may be the result of bimolecular reactions or a small absorption cross section at 10.487 eV. The thermal decomposition of methyl nitrite has been the topic of recent computational investigation,<sup>[16]</sup> where equation 5.1 is indicated as well as direct formation of HNO ( $m/z$  31). For this reason, the small feature at  $m/z$  31 in Fig. 5.3 could be HNO. The potential existence of bimolecular chemistry further clouds this issue. For these purposes, however, the formation of hydrogen atom is indicated by its role in hydrolysis, *i.e.*, the formation of benzene from

benzaldehyde. The presence or absence of other mechanisms is not relevant to the present work but could be the subject of further investigation.

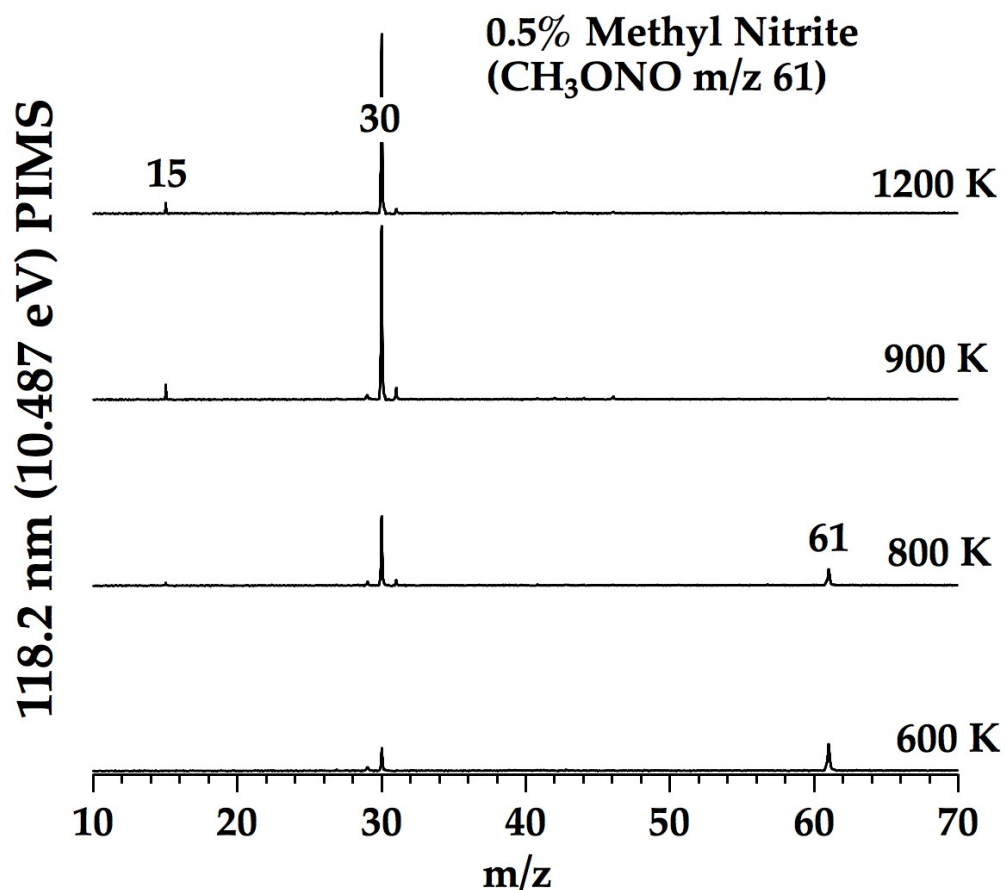


Fig. 5.3. Thermal decomposition of 0.5 % methyl nitrite (CH<sub>3</sub>ONO) in a pulsed He micro-reactor. PIMS was used to identify the parent peak at m/z 61 and decomposition to NO is indicated starting at temperatures of 800 K. By 900 K, no parent methyl nitrite is observed, although at 1200 K, a small feature at m/z 15 is observed, indicating a secondary decomposition pathway to form methyl radical (CH<sub>3</sub>).

## B. Hydropyrolysis of Ethylbenzene

When ethylbenzene is pyrolyzed in the presence of methyl nitrite, a few new product features are observed compared to the simple decomposition shown in Fig. 5.2.

These PIMS spectra are shown in Fig. 5.4. By comparing the products in Fig. 5.2 and Fig 5.3 with those found in Fig. 5.4, we conclude that any new features are a result from reactions between ethylbenzene and hydrogen atom.

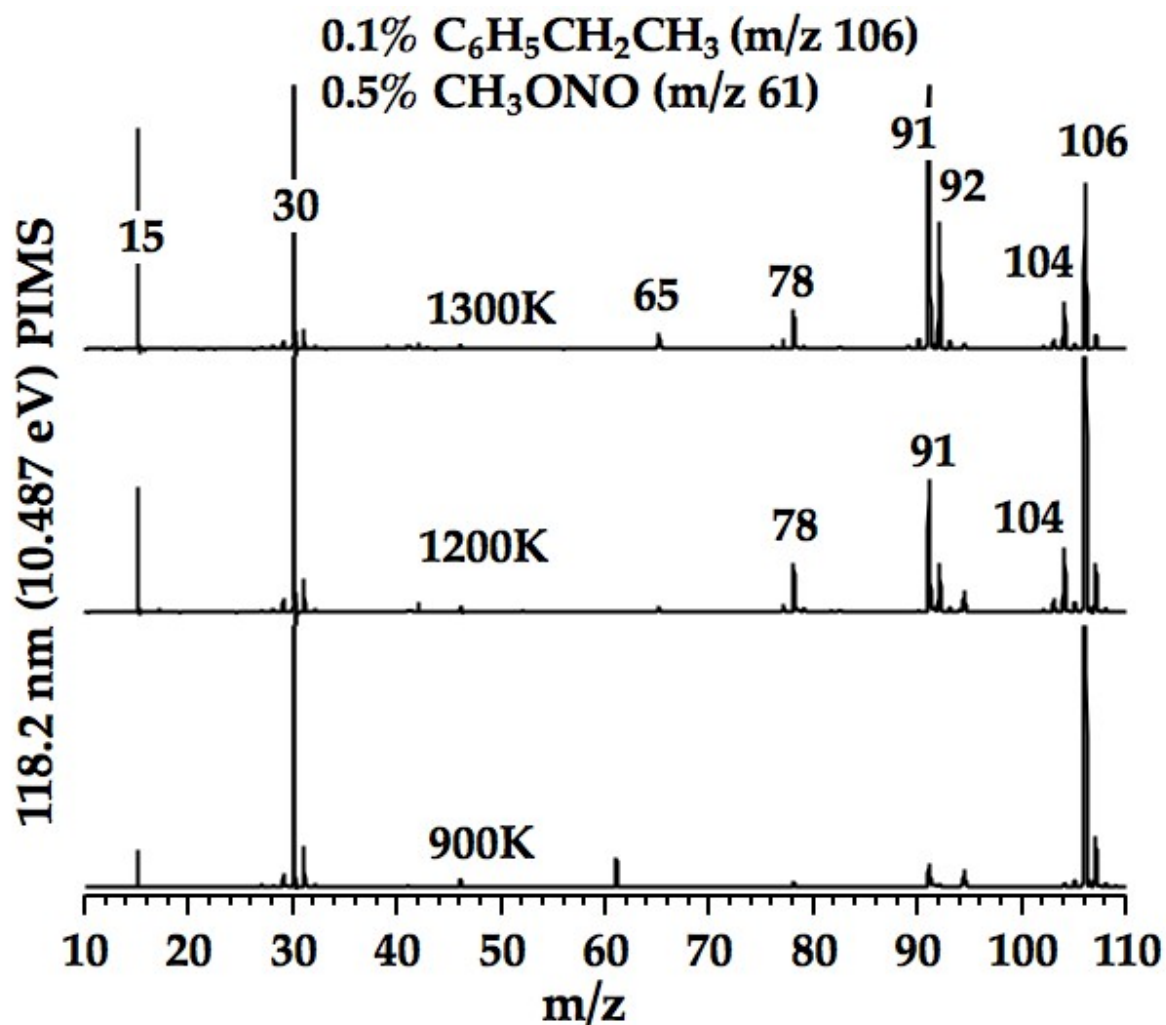
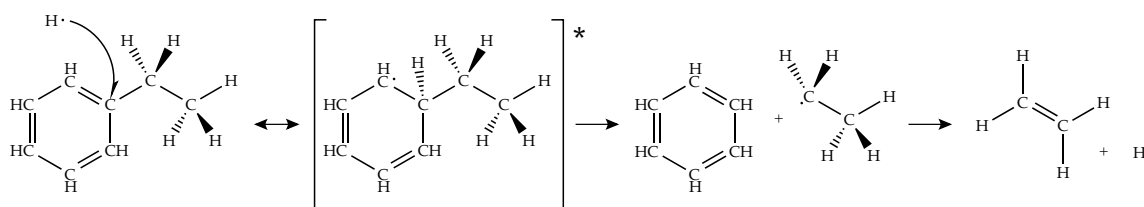


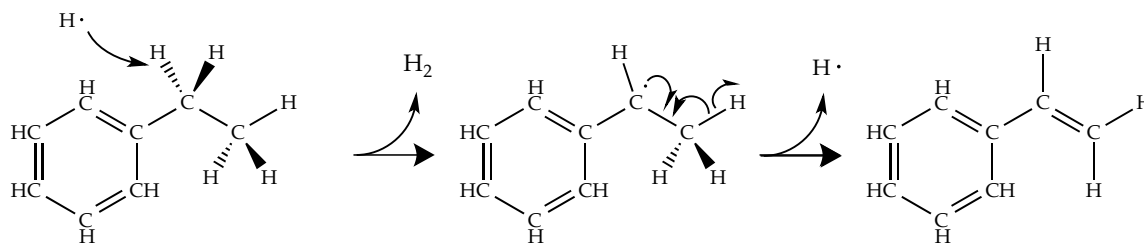
Fig. 5.4. A mixture of 0.1 % ethylbenzene and 0.5 % methyl nitrite was pyrolyzed at 900 K, 1200 K, and 1300 K in a micro-reactor and the products were detected using 118.2 nm PIMS. The features at m/z 78, 92, and 104 are only seen when the two precursors are mixed and are concluded to be the result of hydroperoxylation.

The features in Fig. 5.4 that are not found in Fig. 5.2 or Fig 5.3 are  $m/z$  78, 92, and 104, which are each consistent with hydrogen mediated reaction pathways. Assuming a similar pathway to that deduced in benzaldehyde pyrolysis (Fig. 5.1), hydrogen atom can add to the *ipso* position carbon atom in ethylbenzene to form an  $sp^3$  hybridized carbon atom. Formation of this adduct is stabilized by the doubly allylic radical formed among the remaining five carbon atoms in the ring. This intermediate can regain aromaticity by losing either the hydrogen atom or the ethyl group. The former leads to no observable reaction but the latter will produce benzene and ethyl radical ( $CH_3CH_2$ ). Ethyl radical will likely form ethylene ( $IE(CH_2=CH_2) = 10.51268 \pm 0.00003$  eV),<sup>[17]</sup> thus reproducing a hydrogen atom. By replenishing the hydrogen atom, the hydroxyrolysis is catalytic. This mechanism is illustrated in Scheme 5.1.



Scheme 5.1.

Another result of hydroxyrolysis shown in Fig. 5.4 is the creation of a product with  $m/z$  104. This is assigned to be styrene ( $IE(C_6H_5CH=CH_2) = 8.464 \pm 0.001$  eV),<sup>[18]</sup> the mechanisms for which is shown in Scheme 5.2. Rather than hydrogen addition onto carbon, this mechanism indicates hydrogen abstraction to form  $H_2$  and the resultant radical eliminates another hydrogen atom to form styrene ( $m/z$  104). Here again, the hydrogen atom is catalytic.



Scheme 5.2.

The intermediate radical in Scheme 5.2 is in fact a benzyl radical with the formula  $C_6H_5-CR_2$ . As will be seen in Chapters 6 and 7 of this work, benzyl radicals have a set of decomposition pathways identified. Two products from the fulvenallene pathway<sup>[11]</sup> are consistent with features in Fig. 5.4, namely  $m/z$  104 (coincident with styrene) and  $m/z$  103. Since  $m/z$  103 is quite small and 104 cannot be disambiguated without further experiments, these pathways will not be addressed in detail.

A third change observed as a result of methyl nitrite addition is a dramatic increase in the relative ratio of  $m/z$  92 to 91. Due to the natural abundance of  $^{13}C$ , all features in PIMS spectra corresponding to species containing carbon ( $m/z = N$ ) have a small feature at  $m/z = N+1$  that results from roughly 1.08 % of molecules containing a single  $^{13}C$  atom. In Fig. 5.4, the  $N+1$  feature of  $m/z$  91 at 1300 K is much larger than  $^{13}C$  natural abundance would imply 3.79 %. This enhancement is significantly larger than the experimentally determined standard deviation on  $^{13}C$  peaks ( $1.02 \pm 0.16$  %), which found by comparing 15 different hydrocarbon molecules studied with our apparatus. Given the hydrogen atom formed in the reactor, it seems that we are observing radical-radical recombination between H atom and benzyl radical ( $m/z$  91) to form toluene ( $m/z$  92). Bond forming reactions like this are often too exothermic<sup>[11]</sup> ( $DH_{298}(C_6H_5CH_2-H) = 89.8 \pm 0.6$  kcal mol<sup>-1</sup>) and the chemically activated adduct will undergo homolytic bond cleavage. In this case, the statistically relevant enhancement

of  $m/z$  92 indicates that with a sufficiently large recombination partner, the excess energy can be redistributed into available degrees of freedom and the adduct survives.

To confirm the hydroxyrolytic conversion from ethylbenzene to benzene and ethylene (Scheme 5.1), it is important to ensure that the products in the PIMS spectra are the correct isomers. Further, ethylene cannot be ionized by 118.2 nm light ( $IE(\text{CH}_2=\text{CH}_2) = 10.51268 \pm 0.00003 \text{ eV}$ )<sup>[17]</sup> so a complementary technique is required to corroborate the chemical mechanism. Matrix isolation spectroscopy is ideal for this since the predicted products are both well studied and stable enough to be prepared in pre-mixed samples. Dilute benzene and dilute ethylene were both studied individually so that their IR matrix spectra can be directly compared to the pyrolysis products of ethylbenzene under the same spectroscopic and pyrolytic conditions. Fig. 5.5 shows that benzene is formed by hydroxyrolysis of ethylbenzene. When ethylbenzene is decomposed at 1200 K, vibrational bands for benzene are not observed. However, when methyl nitrite is added to the mixture and then decomposed with the same conditions, three vibrational modes assigned to benzene are observed as indicated with black arrows.

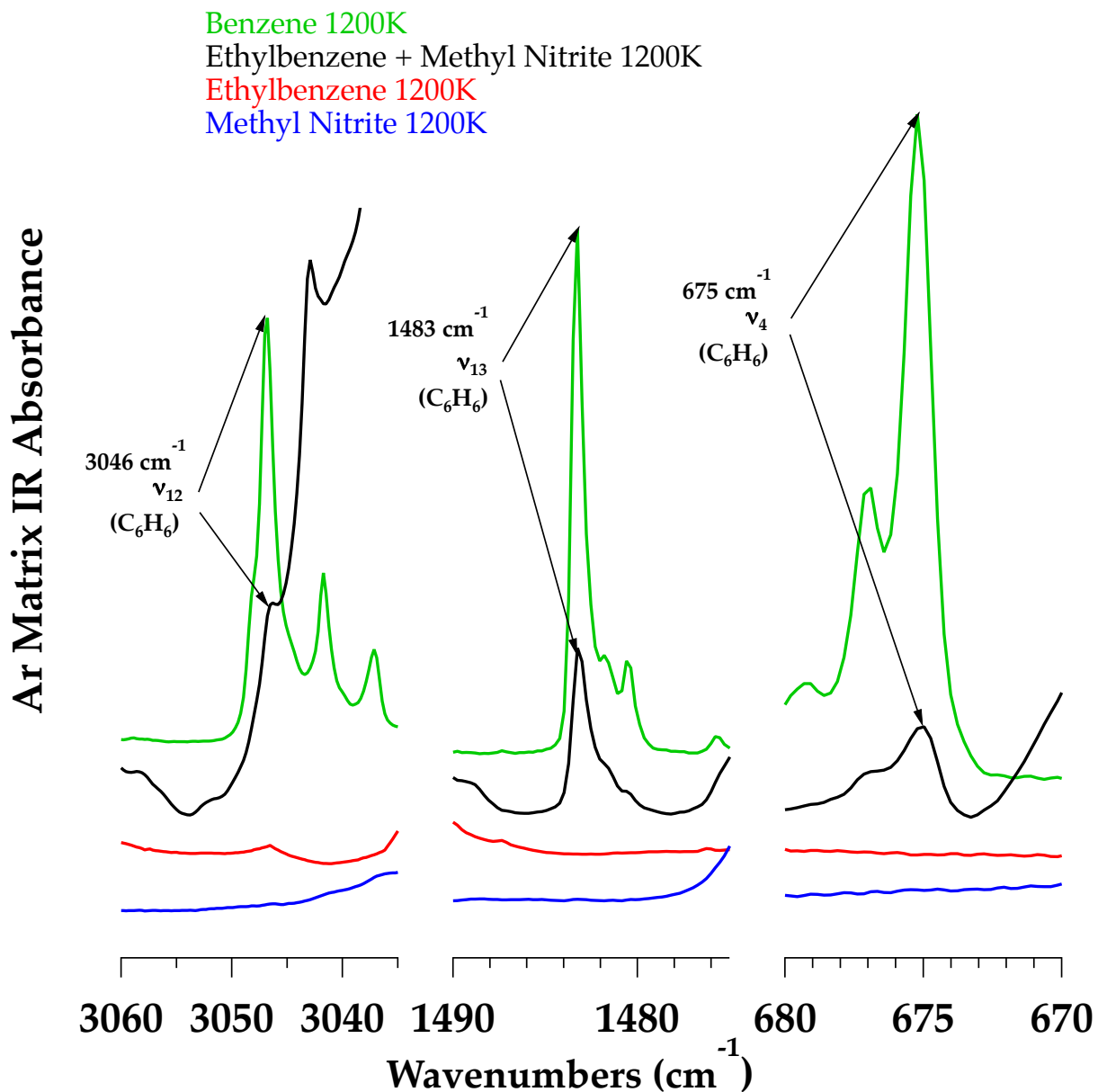


Fig. 5.5. Matrix isolation IR spectra of gas mixtures flowed through a heated micro-reactor. The green trace is from dilute benzene heated to 1200 K, the black trace is ethylbenzene and methyl nitrite heated to 1200 K, the red trace is ethylbenzene heated to 1200 K and the blue trace is methyl nitrite heated to 1200 K. Arrows indicate vibrational modes assigned<sup>[19]</sup> to benzene that are only seen when ethylbenzene and methyl nitrite are pyrolyzed together.



Similarly, to confirm the other product from Scheme 5.1 (ethylene), the hydrolysis of ethylbenzene is compared to pure ethylene in matrix IR spectra in Fig. 5.6. After ethyl radical is ejected from the H and ethylbenzene adduct, loss of one hydrogen atom allows the formation of ethylene, replenishing the catalytic hydrogen atom that can then react another ethylbenzene molecule. In Fig. 5.6 we can see that the mixture of ethylbenzene and methyl nitrite heated to 1200 K reproduces two vibrational modes of ethylene that are not observed when ethylbenzene or methyl nitrite are pyrolyzed alone.

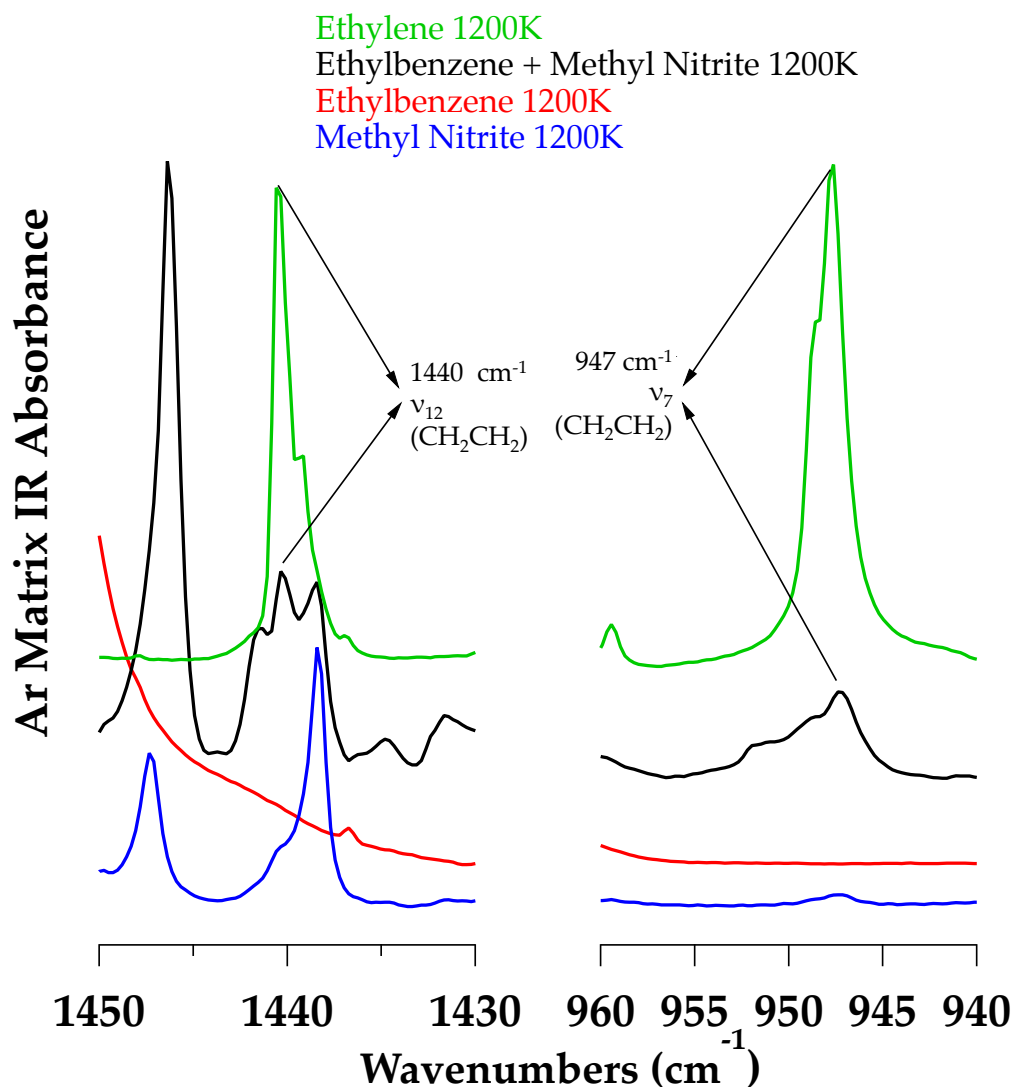


Fig. 5.6. Matrix isolation IR spectra of gas mixtures flowed through a heated micro-reactor. The green trace is from dilute ethylene heated to 1200 K, the black trace is ethylbenzene and methyl nitrite heated to 1200 K, the red trace is ethylbenzene heated to 1200 K and the blue trace is methyl nitrite heated to 1200 K. Arrows indicate vibrational modes assigned<sup>[19]</sup> to ethylene that are only seen when ethylbenzene and methyl nitrite are pyrolyzed together.

Matrix IR spectroscopy can also be used to confirm the recombination reaction of H and benzyl radical. The vibrational spectrum of toluene has been assigned in the IR spectrum from hydrolysis of ethylbenzene by comparing to spectra taken in a neon

matrix as is described in Chapter 7. The precursor cycloheptatriene ( $C_7H_8$ ) has been shown in previous work<sup>[20]</sup> and in our reactor to isomerize to toluene. Direct comparison between spectra recorded in argon matrices and neon matrices is complicated by the fact that the two carrier gases perturb vibrational band origins by different amounts, often differing by 5 to 10  $cm^{-1}$ . Many strong vibrational features assigned to toluene from the cycloheptatriene precursor are found in a congested region of the spectrum in the hydrolysis experiment and thus cannot be assigned unambiguously. Between the Ar and Ne matrices and gas phase assignments from previous work,<sup>[21]</sup> four observed vibrational features can be assigned (see Table 5.1). One features observed at 1383  $cm^{-1}$  in the neon spectrum is an overtone band of toluene ( $\nu_4 = 695 \text{ cm}^{-1}$ ) that cannot be directly identified in the hydrolysis spectra due to a strong nearby absorbance feature originating directly from heated methyl nitrite. Many other strong features assigned to toluene in the neon spectrum are also observed in the hydrolysis spectra but are omitted from Table 5.1 due to absorption features within 5  $cm^{-1}$  that originate from either precursors or other known products.

Mode	Gas <sup>(a)</sup>	Neon <sup>(b)</sup>	Argon <sup>(c)</sup>
$2 \times \nu_4$	1384	1383	1376
$\nu_{19b}$	1472	1472	1470
$\nu_{8a}$	1611	1610	1611
$\nu_{7b}$	3032	3036	3035
$\nu_4$	695	696	congested

Table 5.1. Vibrational band assignments of toluene <sup>(a)</sup> Experimental values and mode numbering from previous work.<sup>[21]</sup>

<sup>(b)</sup> Present work, cycloheptatriene precursors 1300 K.

<sup>(c)</sup> Present work, hydrolysis of ethylbenzene using methyl nitrite mixture, reactor at 1200 K.

The formation of styrene is also confirmed using IR spectroscopy. The liquid-phase and IR and Raman vibrational spectra of styrene were assigned<sup>[22]</sup> by comparing the d0, d3, d5 and d8 isotopomers. The 14 strongest features assigned are summarized in Table 5.2 alongside corresponding features in the hydropyrolysis Ar matrix spectrum. All 14 of the strongest modes can be identified as a unique feature in the hydropyrolysis spectrum or are in a region too congested with absorptions from other molecules to make a distinct assignment.

Mode	Liquid <sup>(a)</sup>	Argon <sup>(b)</sup>
v <sub>37</sub>	698	congested
v <sub>25</sub>	776	778
v <sub>33</sub>	909	909
v <sub>31</sub>	992	992
v <sub>23</sub>	1019	1016
v <sub>21</sub>	1083	1086
v <sub>14</sub>	1412	1409
v <sub>13</sub>	1450	1446
v <sub>12</sub>	1494	congested
v <sub>11</sub>	1575	1580
v <sub>9</sub>	1630	congested
v <sub>6</sub>	3029	congested
v <sub>4</sub>	3061	congested
v <sub>3</sub>	3084	congested

Table 5.2. Vibrational band assignments of styrene

<sup>(a)</sup> Experimental values and mode numbering from previous work.<sup>[22]</sup>

<sup>(b)</sup> Present work, hydropyrolysis of ethylbenzene using methyl nitrite mixture, reactor at 1200 K.

#### IV. Conclusions

The pyrolysis of dilute ethylbenzene in a heated micro-reactor at temperatures up to 1300 K shows relatively few decomposition products, namely m/z 15, 65, and 91.

Cleavage of the ethyl C—C bond forms methyl radical ( $m/z$  15) and benzyl radical ( $m/z$  91) at wall temperatures of 1200 K and further decomposition to  $m/z$  65 is observed upon heating to 1300 K. Cyclopentadienyl radical is shown to be the fragment with  $m/z$  65 (as will be discussed in more detail in Chapter 6) and the co-produced fragment acetylene ( $m/z$  26) cannot be observed using our 118.2 nm ionization source. Upon addition of the hydrogen atom source, methyl nitrite, pyrolysis is clearly affected. Two new fragments are observed,  $m/z$  78 and  $m/z$  104, and we observe an increase in the signal at  $m/z$  92 in excess of the natural abundance  $^{13}\text{C}$  peak for  $m/z$  91. Scheme 5.1 illustrates how hydrogen atom can catalytically produce benzene and ethylene by displacing the ethyl side chain from ethylbenzene and the two products are both confirmed using matrix isolation IR spectroscopy. Styrene is formed via hydrogen abstraction of a side-chain hydrogen atom but subsequent H atom loss (regenerating the catalytic hydrogen atom) forms the carbon double bond of styrene, see Scheme 5.2. Matrix IR vibrational spectroscopy also confirms the identity of the species at  $m/z$  104 as styrene. Finally, we show that radical-radical recombination occurs between benzyl radical and hydrogen atom to form toluene. Despite the large exothermicity of this process ( $D_{298}\text{H}(\text{C}_6\text{H}_5\text{CH}_2\text{—H}) = 89.8 \pm 0.6 \text{ kcal mol}^{-1}$ ) the chemically activated toluene is able to redistribute energy and exits the nozzle to be detected by both PIMS and matrix IR. Similar hydrolysis experiments have been performed on other substituted phenyl systems including n-propylbenzene ( $\text{C}_6\text{H}_5\text{CH}_2\text{CH}_2\text{CH}_3$ ), isopropylbenzene ( $\text{C}_6\text{H}_5\text{CH}(\text{CH}_3)_2$ ), styrene ( $\text{C}_6\text{H}_5\text{CH}=\text{CH}_2$ ), phenol ( $\text{C}_5\text{H}_6\text{OH}$ ), anisole ( $\text{C}_6\text{H}_5\text{OCH}_3$ ), and benzyl phenyl ether ( $\text{C}_6\text{H}_5\text{CH}_2\text{OC}_6\text{H}_5$ ). PIMS spectra for these are shown in Appendix A.

## References for Chapter 5

- [1] G. Knothe. Analyzing biodiesel: Standards and other methods. *Journal of the American Oil Chemists Society* **2006**, *83*, 823-833.
- [2] A. V. Bridgwater, D. Meier and D. Radlein. An overview of fast pyrolysis of biomass. *Organic Geochemistry* **1999**, *30*, 1479-1493.
- [3] A. V. Bridgwater. Review of fast pyrolysis of biomass and product upgrading. *Biomass & Bioenergy* **2012**, *38*, 68-94.
- [4] S. Ohyama, K. E. Popp, M. C. Kung and H. H. Kung. Effect of vanadia on the performance of NiO in vapor-phase oxidative decarboxylation of benzoic acid to phenol. *Catalysis Communications* **2002**, *3*, 357-362.
- [5] T. Q. Hu, B. R. James, S. J. Rettig and C. L. Lee. Stereoselective hydrogenation of lignin degradation model compounds. *Canadian Journal of Chemistry-Revue Canadienne De Chimie* **1997**, *75*, 1234-1239.
- [6] E. Furimsky. Catalytic hydrodeoxygenation. *Applied Catalysis a-General* **2000**, *199*, 147-190.
- [7] T. L. Marker, L. G. Felix, M. B. Linck and M. J. Roberts. Integrated Hydrolysis and Hydroconversion (IH<sub>2</sub>) for the Direct Production of Gasoline and Diesel Fuels or Blending Components from Biomass, Part 1: Proof of Principle Testing. *Environmental Progress & Sustainable Energy* **2012**, *31*, 191-199.
- [8] A. K. Vasiliou, J. H. Kim, T. K. Ormond, K. M. Piech, K. N. Urness, A. M. Scheer, D. J. Robichaud, C. Mukarakate, M. R. Nimlos, J. W. Daily, Q. Guan, H.-H. Carstensen and G. B. Ellison. Biomass Pyrolysis: Thermal Decomposition Mechanisms of Furfural and Benzaldehyde *Journal of Chemical Physics* **2013**, *139*, 104310.
- [9] S. J. Blanksby and G. B. Ellison. Bond dissociation energies of organic molecules. *Accounts of Chemical Research* **2003**, *36*, 255-263.
- [10] J. B. Pedley, R. D. Naylor and S. P. Kirby, *Thermochemistry of Organic Compounds*, Chapman and Hall, New York, **1986**, p. 87-222.

- [11] G. T. Buckingham, T. K. Ormond, J. P. Porterfield, P. Hemberger, O. Kostko, M. Ahmed, D. J. Robichaud, M. R. Nimlos, J. W. Daily and G. B. Ellison. The thermal decomposition of the benzyl radical in a heated micro-reactor. I. Experimental findings. *The Journal of Chemical Physics* **2015**, *142*, 044307.
- [12] B. Ruscic and J. Berkowitz. Photoionization mass-spectrometric studies of the isomeric transient species  $\text{CD}_2\text{OH}$  and  $\text{CD}_3\text{O}$ . *Journal of Chemical Physics* **1991**, *95*, 4033-4039.
- [13] A. M. Schulenburg, M. Meisinger, P. P. Radi and F. Merkt. The formaldehyde cation: Rovibrational energy level structure and Coriolis interaction near the adiabatic ionization threshold. *Journal of Molecular Spectroscopy* **2008**, *250*, 44-50.
- [14] J. A. Blush, P. Chen, R. T. Wiedmann and M. G. White. Rotationally resolved threshold photoelectron-spectrum of the methyl radical. *Journal of Chemical Physics* **1993**, *98*, 3557-3559.
- [15] K. S. Haber, J. W. Zwanziger, F. X. Campos, R. T. Wiedmann and E. R. Grant. Direct determination of the adiabatic ionization potential of  $\text{NO}_2$  by multiresonant optical absorption. *Chemical Physics Letters* **1988**, *144*, 58-64.
- [16] R. S. Zhu, P. Raghunath and M. C. Lin. Effect of Roaming Transition States upon Product Branching in the Thermal Decomposition of  $\text{CH}_3\text{NO}_2$ . *The Journal of Physical Chemistry A* **2013**, *117*, 7308-7313.
- [17] X. Xing, B. Reed, M. K. Bahng and C. Y. Ng. Infrared-vacuum ultraviolet pulsed field ionization-photoelectron study of  $\text{C}_2\text{H}_4^+$  using a high-resolution infrared laser. *Journal of Physical Chemistry A* **2008**, *112*, 2572-2578.
- [18] J. M. Dyke, H. Ozeki, M. Takahashi, M. C. R. Cockett and K. Kimura. A study of phenylacetylene and styrene, and their argon complexes PA-Ar and ST-Ar with laser threshold photoelectron spectroscopy. *The Journal of Chemical Physics* **1992**, *97*, 8926-8933.
- [19] T. Shimanouchi *Tables of Vibrational Frequencies, Consolidated Volume I*, NSRDS-NBS **39**, **1972**.
- [20] S. H. Luu, K. Glänzer and J. Troe. Thermal isomerization in shock waves and flash photolysis of cycloheptatriene, III. *Berichte der Bunsengesellschaft für physikalische Chemie* **1975**, *79*, 855-858.

- [21] N. Fuson, C. Garrigou-Lagrange and M. L. Josien. Spectre infrarouge et attribution des vibrations des toluènes  $C_6H_5CH_3$ ,  $C_6H_5CD_3$  et  $C_6D_5CD_3$ . *Spectrochimica Acta* **1960**, *16*, 106-127.
- [22] D. A. Condirston and J. D. Laposa. Vibrational-spectra of styrene-H8, styrene-D3, styrene-D5, and styrene-D8. *Journal of Molecular Spectroscopy* **1976**, *63*, 466-477.





## Chapter 6

### The Thermal Decomposition of the Benzyl Radical in a Heated Micro-Reactor: I. Experimental Findings

#### Abstract

The pyrolysis of the benzyl radical has been studied in a set of heated micro-reactors. A combination of photoionization mass spectrometry (PIMS) and matrix isolation infrared (IR) spectroscopy has been used to identify the decomposition products. Both benzyl bromide and ethyl benzene have been used as precursors of the parent species,  $C_6H_5CH_2$ , as well as a set of isotopically labeled radicals:  $C_6H_5CD_2$ ,  $C_6D_5CH_2$ , and  $C_6H_5^{13}CH_2$ . The combination of PIMS and IR spectroscopy has been used to identify the earliest pyrolysis products from benzyl radical as:  $C_5H_4=C=CH_2$ , H atom,  $C_5H_4-C\equiv CH$ ,  $C_5H_5$ ,  $HC\equiv CCH_2$ , and  $HC\equiv CH$ . Pyrolysis of the  $C_6H_5CD_2$ ,  $C_6D_5CH_2$  and  $C_6H_5^{13}CH_2$  benzyl radicals produces a set of methyl radicals, cyclopentadienyl radicals, and benzyne that are not predicted by a fulvenallene pathway. Explicit PIMS searches for the cycloheptatrienyl radical were unsuccessful; there is no evidence for the isomerization of benzyl and cycloheptatrienyl radicals:  $C_6H_5CH_2 \rightleftharpoons C_7H_7$ . These labeling studies suggest that there must be other thermal decomposition routes for the  $C_6H_5CH_2$  radical that differ from the fulvenallene pathway.

## I. Introduction

Benzyl radical,  $C_6H_5CH_2$ , is a long-lived combustion species and is an important soot-precursor. Reaction with oxygen is quite slow because the resulting adduct,  $C_6H_5CH_2OO$ , is not very stable:  $C_6H_5CH_2 + O_2 \rightleftharpoons C_6H_5CH_2OO$ . Consequently the oxidation of  $C_6H_5CH_2$  is sluggish, which leaves benzyl radicals available to contribute to further chemical reactions including soot formation.

This chapter is focused on the thermal decomposition pathways of the benzyl radical itself. Pyrolysis of benzyl bromide and ethyl benzene in a set of heated micro-reactors produced samples of  $C_6H_5CH_2$  that were observed to decompose to a complex set of atoms, radicals, and metastables. A combination of photoionization mass spectrometry (PIMS) and matrix infrared spectroscopy (IR) has been used to identify the initial decomposition products.

In 1948 pioneering shock tube measurements<sup>[1]</sup> decomposed the aromatics toluene and xylene. About 30 years later, a set of experiments was reported<sup>[2]</sup> in which toluene was decomposed in a Knudsen cell. The Knudsen cell was heated to 2100 K and coupled to an electron impact (EI) mass spectrometer. The resulting mass spectra identified the presence of  $C_2H_2$ ,  $C_3H_3$ ,  $C_4H_2$ ,  $C_4H_4$ ,  $C_5H_5$ , and  $C_6H_6$  and all species were assigned as thermal decomposition products of  $C_6H_5CH_2$ . Subsequent shock tube studies were carried out on a variety of aromatic precursors and the decomposition products were monitored by vacuum ultraviolet (VUV) absorption spectroscopy.<sup>[3-5]</sup> It was demonstrated<sup>[5]</sup> that ethylbenzene decomposes to the radical pair, ( $C_6H_5CH_2$  and  $CH_3$ ) and not to ( $C_6H_5CHCH_3$  plus H). In 1986, Rao and Skinner<sup>[6]</sup> presented the results of shock tube measurements for the decomposition of ethylbenzene- $d_{10}$  and ethyl- $\alpha,\alpha$ -

$d_2$ -benzene in argon behind incident shock waves at temperatures of 1430-1740 K. Progress of the reaction was followed by analysis for H and D atoms by atomic resonance absorption spectroscopy (ARAS). ARAS spectroscopy demonstrated that benzyl radicals decompose to hydrogen atoms and other unknown products. Benson made the imaginative suggestion<sup>[6]</sup> that the pyrolysis of benzyl radical proceeded by rearrangement to a bicyclic species followed by fragmentation to fulvenallene ( $C_5H_4=C=CH_2$ ) and H atom. Fulvenallene could further decompose to the fulvenallenyl radical,  $C_5H_4-C\equiv CH$ . Rather than Benson's stepwise rearrangement to fulvenallene, benzyl could suffer a concerted fragmentation to the cyclopentadienyl radical and vinylidene. Vinylidene ( $CH_2=C:$ ) is known<sup>[7-8]</sup> to rapidly isomerize to  $HC\equiv CH$ . Finally classical organic chemistry might expect rearrangement of benzyl to the cycloheptatrienyl radical; subsequent  $C_7H_7$  fragmentation could directly provide  $HC\equiv CH$  and  $C_5H_5$ . These suggestions are outlined in Fig. 6.1.

## Possible Pathways for Benzyl Radical Thermal Decomposition

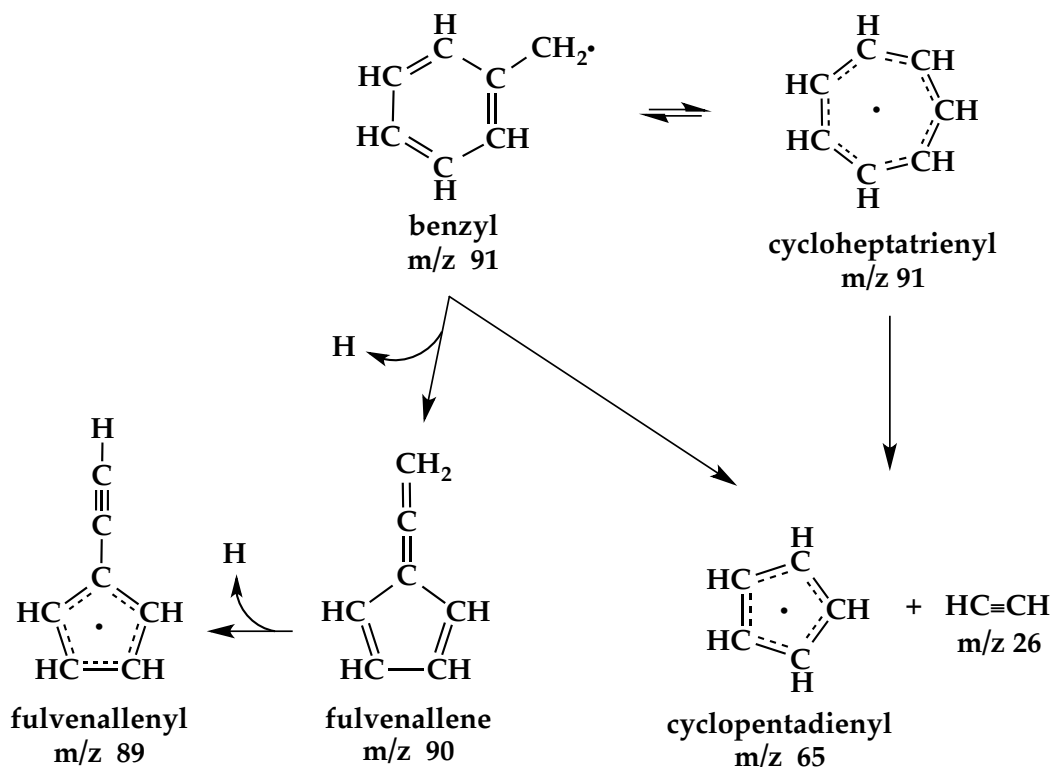


Fig. 6.1. Benzyl radical is proposed to decompose not through direct bond breakage but through isomerization(s) reactions. Loss of one hydrogen atom can lead to fulvenallene ( $C_5H_4=C=CH_2$ ,  $m/z$  90) and a second hydrogen atom loss would produce the fulvenallenyl radical ( $C_5H_4-C\equiv CH$ ,  $m/z$  89). Isomerization to cycloheptatrienyl radical has also been proposed.

Decomposition of benzyl radical has also been investigated by photochemistry. Molecular beams of either toluene or cycloheptatriene were irradiated with UV light to form "hot" benzyl radicals that underwent immediate unimolecular decomposition. Fragmentation products were detected using EI mass spectrometry<sup>[9]</sup> and the first direct detection of  $C_7H_6$  ( $m/z$  90) was reported as the product of  $C_7H_7 \rightarrow C_7H_6 + H$ .

Later experiments were reported to pursue Benson's suggested mechanism.<sup>[10-11]</sup> In the work of Jones *et al.*<sup>[12]</sup>, shock tube measurements of the decomposition of benzyl

bromide were coupled with computational studies to suggest multiple benzyl radical decomposition mechanisms. Four mechanisms were proposed: 1) formation of the norbornadienyl radical followed by  $C_5H_5 + HCCH$  formation, 2) ring opening leading to linear  $C_7H_6 + H$  and further fragmentation, 3) Benson's isomerization to the bicyclic intermediate, 6-methylenebicyclo[3.1.0]hex-3-en-2-yl radical that subsequently decomposes to the fulvenallenyl radical ( $C_5H_4-C\equiv CH$ ) + H atom or  $C_5H_5 + HCCH$  and, 4) isomerization to a seven-membered ring followed by formation of  $C_5H_5 + HCCH$ . Further computational studies have reported<sup>[13]</sup> fulvenallene formation as the major decomposition route for benzyl radical. Density functional theory (DFT) calculations<sup>[14]</sup> found that hydrogen addition to fulvenallene would result in  $C_5H_5 + C_2H_2$ . Recently there has been extensive work<sup>[15-19]</sup> performed on potential energy surfaces for each of the species  $C_7H_7$ ,  $C_7H_6$ , and  $C_7H_5$  and their interplay during benzyl radical decomposition. Because of their likely importance during the decomposition of benzyl, both fulvenallene and fulvenallenyl radical,<sup>[20-21]</sup> as well as the cycloheptatrienyl radical<sup>[22]</sup> have been detected and identified by photoionization mass spectrometry.

To explore the thermal decomposition of the benzyl radical, we have prepared  $C_6H_5CH_2$  from both ethylbenzene and benzyl bromide in a heated micro-reactor. By increasing the temperature of the reactor, pyrolysis of the benzyl radical was observed. Our goal is to identify the nascent fragmentation products:  $C_6H_5CH_2 (+ M) \rightarrow$  products.

Over the last decade, we have used a set of micro-reactors to examine the pyrolysis of complex organic molecules. These resistively heated silicon carbide (SiC) reactors are typically 0.5 – 1 mm inner diameter and 2 – 3 cm long. Target molecules are delivered to the reactor as dilute mixtures (typically 0.1 % or less) in He, Ar, or Ne buffer gases with entrance pressures of 200 – 300 Torr. The micro-reactors can be

operated in either pulsed or continuous flow (CW) modes and are heated to temperatures up to 1800 K. Residence times in the micro-reactors are in the range of 25 – 150  $\mu\text{sec}$ . Gases exit the hot micro-reactors into a vacuum of  $10^{-6}$  Torr where all reactions are quenched. A combination of photoionization mass spectrometry, matrix isolation infrared spectroscopy, resonance-enhanced multiphoton ionization spectroscopy, and microwave spectroscopy has been used to identify all the decomposition products. This package of spectroscopies is very powerful and enables identification of all products (atoms, radicals, metastables) that are formed in the first 100  $\mu\text{sec}$  of complex fuel pyrolysis.<sup>[23-29]</sup> The goal of the present study is to produce clean samples of benzyl and to observe the temperature-dependent decomposition of the radical. With care, the set of micro-reactors can be used to confirm the fragmentation products from benzyl radical and indicate which mechanism(s) are activated first.

The experimental thermochemical and electronic properties of benzyl radical ( $\text{C}_6\text{H}_5\text{CH}_2, \tilde{X}^2\text{B}_1$ ) have been compiled in Table 6.1, alongside data for its isomer, the cycloheptatrienyl radical ( $\text{C}_7\text{H}_7, \tilde{X}^2\text{E}_2''$ ). Experimental information is included for three precursors of benzyl radical: toluene, benzyl bromide, and ethylbenzene.

## Experimental Properties of Benzyl and Cycloheptatrienyl Radicals

$IE(C_6H_5CH_2, \tilde{X}^2B_1)$	$7.2487 \pm 0.0006$	eV	[30-31]	
$\Delta_f H_{298}(C_6H_5CH_2, \tilde{X}^2B_1)$	49.7 (208)	$\pm 0.6$ $\pm 3$	kcal mol <sup>-1</sup> kJ mol <sup>-1</sup>	[32]
$\Delta_{rxn} H_{298}(C_6H_5CH_2 \rightarrow HCCH + C_5H_5)$	68 (284)	$\pm 2$ $\pm 6$	kcal mol <sup>-1</sup> this work kJ mol <sup>-1</sup>	
$\Delta_{acid} H_{298}(C_6H_5CH_2-H)$	382.3 (1600)	$\pm 0.5$ $\pm 2$	kcal mol <sup>-1</sup> kJ mol <sup>-1</sup>	[33]
$EA(C_6H_5CH_2, \tilde{X}^2B_1)$	$0.912 \pm 0.006$	eV	[34]	
$\Delta_{isomerization} H_{298}(C_6H_5CH_2, \tilde{X}^2B_1 \rightarrow C_7H_7, \tilde{X}^2E_2'')$	15.3 (64)	$\pm 0.9$ $\pm 4$	kcal mol <sup>-1</sup> this work kJ mol <sup>-1</sup>	
$IE(C_7H_7, \tilde{X}^2E_2'')$	$6.221 \pm 0.006$	eV	[22, 35]	
$\Delta_f H_{298}(C_7H_7, \tilde{X}^2E_2'')$	65.0 (272)	$\pm 0.7$ $\pm 3$	kcal mol <sup>-1</sup> kJ mol <sup>-1</sup>	[32]
$\Delta_{rxn} H_{298}(C_7H_7 \rightarrow HCCH + C_5H_5)$	53 (220)	$\pm 2$ $\pm 7$	kcal mol <sup>-1</sup> this work kJ mol <sup>-1</sup>	
$AE(C_7H_8 \rightarrow C_7H_7^+ + H)$	$9.36 \pm 0.02$	eV	[36]	
$\Delta_f H_{298}(C_5H_5, \tilde{X}^2E_1'')$	63 (264)	$\pm 1$ $\pm 6$	kcal mol <sup>-1</sup> kJ mol <sup>-1</sup>	[37]
$DH_{298}(C_6H_5CH-H)$	106 (444)	$\pm 4$ $\pm 15$	kcal mol <sup>-1</sup> kJ mol <sup>-1</sup>	[38-39]
$DH_{298}(C_6H_5-CH_2)$	124.3 (520)	$\pm 0.9$ $\pm 4$	kcal mol <sup>-1</sup> kJ mol <sup>-1</sup>	[32]
$DH_{298}(C_6H_5CH_2-H)$	89.8 (376)	$\pm 0.6$ $\pm 3$	kcal mol <sup>-1</sup> kJ mol <sup>-1</sup>	[33]
$DH_{298}(C_7H_7-H)$	73.9 (309)	$\pm 0.5$ $\pm 2$	kcal mol <sup>-1</sup> kJ mol <sup>-1</sup>	[36]



DH <sub>298</sub> (C <sub>6</sub> H <sub>5</sub> CH <sub>2</sub> -Br)	61 (255)	± 1 ± 4	kcal mol <sup>-1</sup> kJ mol <sup>-1</sup>	[32]
DH <sub>298</sub> (C <sub>6</sub> H <sub>5</sub> CH <sub>2</sub> -CH <sub>3</sub> )	77.6 (325)	± 0.7 ± 3	kcal mol <sup>-1</sup> kJ mol <sup>-1</sup>	[32]
DH <sub>298</sub> (C <sub>6</sub> H <sub>5</sub> -CH <sub>2</sub> CH <sub>3</sub> )	102.3 (428)	± 0.7 ± 3	kcal mol <sup>-1</sup> kJ mol <sup>-1</sup>	[32]

### Important Ionization Energies

CH <sub>3</sub>	9.8380	± 0.0004	eV	[40]
HC≡CH	11.40081	± 0.00001	eV	[41]
HC≡CCH <sub>2</sub>	8.7006	± 0.0002	eV	[42]
C <sub>5</sub> H <sub>5</sub>	8.4268	± 0.0005	eV	[43]
o-C <sub>6</sub> H <sub>4</sub>	9.03	± 0.05	eV	[44]
C <sub>6</sub> H <sub>5</sub>	8.32	± 0.04	eV	[45]
C <sub>5</sub> H <sub>4</sub> -C≡CH	8.19	± 0.02	eV	[20]
C <sub>5</sub> H <sub>4</sub> =C=CH <sub>2</sub>	8.22	± 0.01	eV	[20]
C <sub>6</sub> H <sub>5</sub> CH <sub>2</sub>	7.2487	± 0.0006	eV	[30-31]
C <sub>7</sub> H <sub>7</sub>	6.221	± 0.006	eV	[22, 35]
C <sub>6</sub> H <sub>5</sub> CH <sub>2</sub> CH <sub>3</sub>	8.7734	± 0.0007	eV	[46]
C <sub>6</sub> H <sub>5</sub> CH <sub>2</sub> Br	8.990	± 0.015	eV	[47]

Table 6.1. Experimental properties of benzyl and cycloheptatrienyl radicals and important ionization energies

## II. Experimental

The thermal decomposition of benzyl radical is studied by entraining a dilute sample of precursor in helium, neon, or argon. The precursors used in this study are benzyl bromide ( $C_6H_5CH_2Br$ ) and ethylbenzene ( $C_6H_5CH_2CH_3$ ). Both precursors are available from Sigma-Aldrich with reported purities of 98 % and 99 %, respectively, and are liquid at room temperature. Additionally, multiple isotopomers have been examined including  $C_6H_5CD_2Br$ ,  $C_6D_5CH_2Br$ ,  $C_6H_5CD_2CD_3$ ,  $C_6D_5CH_2CH_3$ , and  $C_6H_5^{13}CH_2CH_3$ , all of which were purchased from CDN Isotopes, with reported isotopic enrichment of 98 % for the deuterium isotopomers and 99 % for the  $^{13}C$  isotopomer;  $^{13}C$  NMR was used to confirm that the  $\alpha$ -carbon is  $98.9 \pm 0.1$  %  $^{13}C$ . The vapor pressure of ethylbenzene is sufficiently large to prepare static sample volumes of between 0.1 % and 0.01 % ethylbenzene in up to 1500 Torr of noble gas. Benzyl bromide, however, requires flowing pure carrier gas over a sample of liquid precursor. The benzyl bromide sample was never heated so as to avoid higher  $C_6H_5CH_2Br$  concentrations that would trigger bimolecular chemistry. The ratio of the vapor pressure at the sample temperature to the backing pressure was used to approximate the concentration of benzyl bromide in the beam. A careful dilution study with ethylbenzene shows that as concentrations were lowered from 0.1 % to 0.02 %, some peaks in the mass spectra lost signal intensity more rapidly than other peaks, thus indicating their higher order dependence on concentration. As a result, all of the PIMS peaks discussed herein are believed to be solely a result of unimolecular decomposition.

Benzyl radical, its precursors, and its fragmentation products are detected by means of PIMS and IR spectroscopy. We have carried out 118.2 nm PIMS with a pulsed

micro-reactor as well as synchrotron-based PIMS with continuous flow micro-reactors at the Lawrence Berkeley National Lab's (LBNL) Advanced Light Source (ALS) in Berkeley, CA, USA and the Swiss Light Source (SLS) at the Paul Scherrer Institute in Villigen Switzerland.

PIMS with a pulsed micro-reactor<sup>[48]</sup> combines the 9<sup>th</sup> harmonic of a Nd:YAG laser (118.2 nm or 10.487 eV). The laser is synchronized to a Parker general pulsed valve backed by a helium-hydrocarbon mixture. The pulsed valve operates at 10 Hz and is open for about 1 msec. A skimmer is placed about 1 cm from the exit of the SiC reactor to select only the component of the expansion traveling in the longitudinal direction with respect to the reactor tube. The internally frequency-tripled output of a Nd:YAG laser is directed into a cell that is pressurized to 150 Torr with a 10:1 argon:xenon mixture. This mixture is optimized to promote sum frequency generation that creates 118.2 nm VUV photons, which have sufficient energy to ionize most hydrocarbon molecules. Generation of 118.2 nm photons by Xe/Ar tripling cells has been studied at great length.<sup>[49]</sup> Based on the use of 30 mJ pulse<sup>-1</sup> power at 355 nm from the YAG laser and the established tripling efficiency of  $1 \times 10^{-5}$  in pure xenon<sup>[50-51]</sup> as well as the transmission efficiency of the MgF<sub>2</sub> lens, we expect to produce roughly 30 nJ pulse<sup>-1</sup> of 118.2 nm light. This VUV laser light is directed into a vacuum chamber maintained at 10<sup>-7</sup> Torr by a 1200 L/s Pfeiffer TPU 1201 P turbomolecular pump and is then intersected with the skimmed output of the supersonic expansion. After ionization the molecules in the expansion are accelerated into a Jordan reflectron time-of-flight spectrometer with an MCP detector producing PIMS spectra at 10.487 eV.

Other experiments employ a tunable ionization source that is used with a set of continuous flow micro-reactors to measure photoionization efficiency (PIE) curves.

These PIMS experiments were conducted at the Advanced Light Source using the beamline's 9.0.2 molecular beam end-station. The gas mixture of product molecules entrained in helium emerging from the hot micro-reactor is formed into a molecular beam. The skimmed molecular beam is intersected with tunable synchrotron light and the nascent ions are detected in a Jordan reflectron time-of-flight apparatus. Utilization of pseudo-CW ionizing radiation requires that voltages on the repeller plate be pulsed to allow discrete data acquisition. The ALS synchrotron does not easily permit scans below 7.4 eV so in order to distinguish the isomers, benzyl (7.2 eV) and cycloheptatrienyl radicals (6.2 eV), tunable light down to 6 eV was required. These photon energies are available at the Swiss Light Source, where tunable synchrotron light extends to energies as low as 6 eV. During the SLS experiments<sup>[52]</sup> a continuous stream of Ar and precursor was expanded through a micro-reactor forming a molecular beam, which was skimmed. The products were detected applying imaging photoelectron photoion coincidence (iPEPICO) techniques.<sup>[53]</sup>

Matrix isolation Fourier Transform infrared spectroscopy is a complementary detection method performed to help identify individual isomers present at the exit of the reactor. A similar pulse valve and tubular reactor assembly is coupled to a helium compressor-cooled cesium iodide (CsI) window that is enclosed and pumped to  $10^{-6}$  Torr during pulse valve operation. Gas mixtures consist of dilute samples of molecular precursor entrained in neon. Neon is used rather than argon because its smaller atomic radius and lower electronic polarizability has been shown to create inert solid matrices that have smaller perturbations than comparable matrices using argon. Gas mixtures pulsed through the heated reactor are then directed towards the CsI window that is maintained at 5.4 K. Gas is pulsed for 1 to 2 hours with the pulse valve opening time

set to 1 msec and a repetition rate of roughly 10 Hz. Repetition rate and opening time are tuned to maintain a consistent dose rate as measured by upstream pressure decrease over time. After dosing is completed, the pulse valve assembly can be rotated out of the way to allow the CsI window to be lowered into the beam path of a commercial FTIR, where between 200 and 1000 scans can be averaged to achieve a single composite absorbance spectrum from 400 to 4000  $\text{cm}^{-1}$  with 0.25  $\text{cm}^{-1}$  resolution. Spectra taken in a solid neon matrix can then be compared directly to published neon matrix spectra or carefully assigned using similar spectra taken in argon matrices or in the gas phase to allow vibrational assignments. The band origin assignments in neon matrices show shifts from the gas-phase values of around 5  $\text{cm}^{-1}$ , while argon matrix assignments often have shifts on the scale of 10  $\text{cm}^{-1}$ . A complete list of vibrational assignments for molecules detected during the decomposition of benzyl radical (which was prepared using ethylbenzene as the precursor) is included in supplementary material (see Appendix B).

The micro-reactor assembly used for pyrolysis is described in more detail elsewhere<sup>[48, 54-58]</sup> and consists of a 0.6 mm or 1 mm inner diameter SiC tubular reactor that can be resistively heated up to 1800 K. Carbon discs are fitted to the outer diameter of the reactor approximately 1 cm apart and these form the contact points for the electrical circuit used to resistively heat the reactor. A Type C thermocouple with 0.005" diameter wires is tightly attached to the SiC reactor between the two electrical contacts so that the surface temperature can be monitored directly. Backing pressures and downstream pressures vary between experiments. Table 6.2 is provided to summarize the conditions across all experiments performed in this work.

	Carrier Gas	Flow	Ionization Source	Backing Pressure	Outlet Pressure	Reactor Geometry
Photoionization Mass Spectrometry in Colorado	Helium	Pulsed	118.2 nm (10.487 eV) Laser	1500 Torr	$2 \times 10^{-6}$ Torr	I.D. 1 mm Heated Length: 15 mm
Photoionization Mass Spectrometry at the ALS	Helium	Continuous	Tunable Synchrotron	50 Torr	$2 \times 10^{-5}$ Torr	I.D. 0.6 mm Heated Length: 10 mm
Photoionization Mass Spectrometry at the SLS	Argon	Continuous	Tunable Synchrotron	50 Torr	$5 \times 10^{-6}$ Torr	I.D. 1 mm Heated Length: 15 mm
Matrix Isolation IR Spectroscopy in Colorado	Neon	Pulsed	none	1000 Torr	$2 \times 10^{-6}$ Torr	I.D. 1 mm Heated Length: 10 mm

Table 6.2. Summary of Experimental Conditions

Recent computational fluid dynamics (CFD) simulations<sup>[59]</sup> have dramatically clarified the nature of the pyrolysis in the micro-reactors. These devices operate in a steady-state (CW) mode when using synchrotron photons (LBNL Advanced Light Source and Paul Scherrer Institute Swiss Light Source) or in a pulsed mode for 10.487 eV PIMS and IR studies. During a CW experiment, the volumetric flow rate is controlled using a mass flow controller, and the pressure is measured just upstream of the reactor and in the downstream vacuum chambers. The upstream pressure typically ranges from 10 Torr to 400 Torr depending on the heating temperature and flow rate. In the CW case, an interesting result of these simulations was the discovery of a “sweet-spot”, which emerges from the interaction of the rising gas temperature and the rapidly falling gas pressure, as will be discussed later in the paper. For a pulsed reactor, the flow rate is determined by the time-dependent geometry of the valve pintle and orifice, which unfortunately is not well known.

The characteristics of CW and pulsed flows are quite different. In steady-state laminar flow, the time-dependent terms in the Navier-Stokes equation drop out of the equation. In our situation the geometry is fixed and the mass flow rate is controlled, thus making CFD numerical solutions tractable<sup>[59]</sup> and detailed flow field information attainable. Given a reaction mechanism and kinetic parameters, one can include chemistry in the simulations, predicting, for example, the overall conversion percentage of the reactant. As a result, simulations can be used to test reaction mechanisms. In pulsed flow, the geometry is varying in time due to motion of the pintle within the valve and the instantaneous mass flow rate is thus unknown. Furthermore, the duty cycle is such that the tubular reactor is completely purged of gas between pulses resulting in a highly complex transient flow that transitions from collisionless to collision-dominated over the course of a few milliseconds. This is a formidable problem to model and is the subject of current research.

### III. Results

We have chosen benzyl bromide and ethylbenzene as convenient precursors of the benzyl radical.

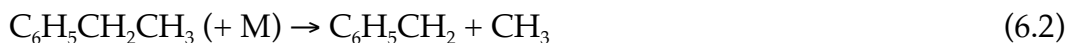


Table 6.1 shows that  $\Delta_{\text{rxn}}H_{298}(1)$  is  $61 \pm 1 \text{ kcal mol}^{-1}$  ( $260 \pm 4 \text{ kJ mol}^{-1}$ ) while  $\Delta_{\text{rxn}}H_{298}(2)$  is  $77.6 \pm 0.7 \text{ kcal mol}^{-1}$  ( $325 \pm 3 \text{ kJ mol}^{-1}$ ). Because of the differing thermochemistry between reactions (6.1) and (6.2), benzyl radicals are observed at lower decomposition

temperatures when using  $C_6H_5CH_2Br$  than with  $C_6H_5CH_2CH_3$ . However the higher vapor pressure of ethylbenzene makes sample preparation comparatively simpler. An important experimental difficulty associated with benzyl bromide is dissociative ionization. The IE of  $C_6H_5CH_2Br$  is 9.0 eV (see Table 6.1) and so 10.5 eV (118.2 nm) PIMS is 1.5 eV above the ionization threshold. Consequently the ion resulting from irradiating  $C_6H_5CH_2Br$  with 118.2 nm,  $[C_6H_5CH_2Br]^+$  ( $m/z$  170/172), commonly fragments to  $C_6H_5CH_2^+$  ( $m/z$  91) and Br. This dissociative ionization process obscures the  $m/z$  91 signal that results from thermally formed benzyl radicals. While the IE( $C_6H_5CH_2CH_3$ ) is 8.8 eV (see Table 6.1), very few of the  $C_6H_5CH_2CH_3^+$  ( $m/z$  106) cations subsequently fragment, which produces cleaner PIMS spectra. Synchrotron radiation is especially useful for taking PIMS spectra of benzyl bromide because the ionization source can be lowered to just above the ionization energy of the precursor, 9 eV.

### A. Decomposition of Benzyl- $d_0$ Radical

Fig. 6.2 shows the 118.2 nm PIMS spectrum that results from pyrolysis of a dilute sample of  $C_6H_5CH_2CH_3$  (0.02 % in He). The bottom scan was recorded with the reactor at 350 K and the spectrum only shows ions resulting from the parent at  $m/z$  106 and an appropriate isotope peak at  $m/z$  107. There is a small feature at  $m/z$  91 resulting from dissociative ionization of the  $C_6H_5CH_2CH_3^+$  cation ( $C_6H_5CH_2CH_3^+ \rightarrow C_6H_5CH_2^+ + CH_3$ ).



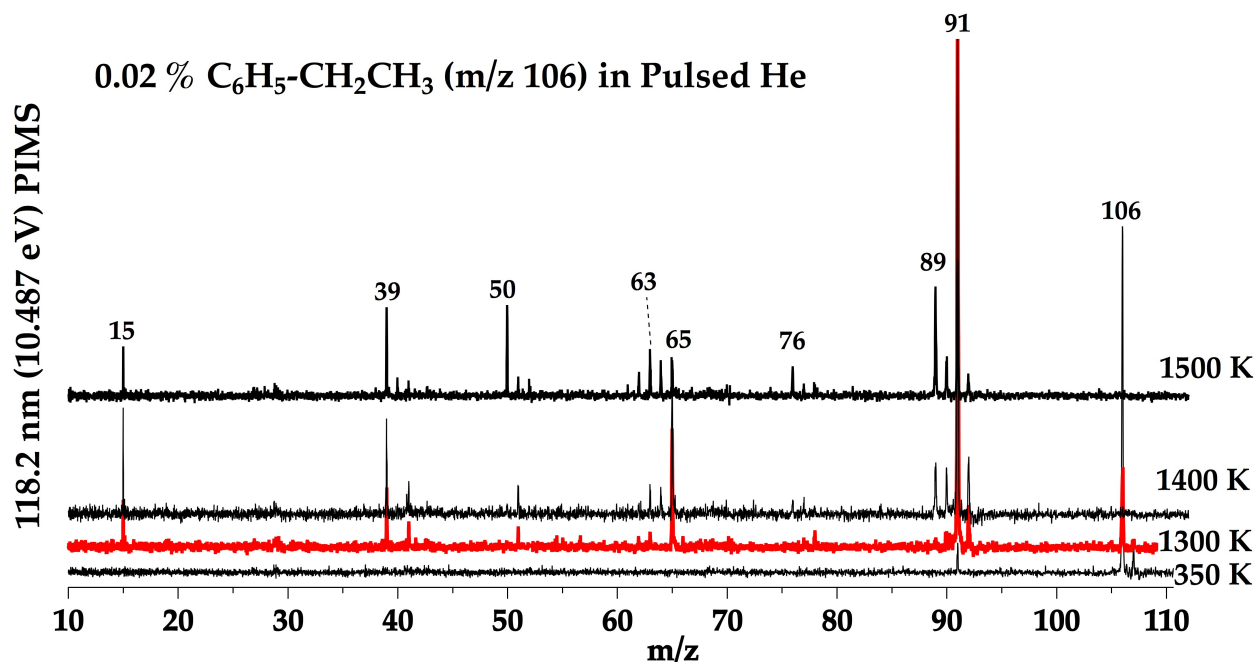
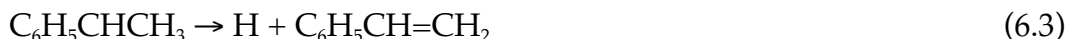


Fig. 6.2. Dilute ethylbenzene (C<sub>6</sub>H<sub>5</sub>CH<sub>2</sub>CH<sub>3</sub>) heated in a pulsed helium tubular micro-reactor studied using PIMS at four different reactor temperatures, 350 K, 1300 K, 1400 K, and 1500 K. At 1300 K (shown in red), the large peak at m/z 91 is benzyl radical, along with the associated fragment methyl radical (m/z 15). Some decomposition to m/z 65 and 39 is observed. Further heating to 1400 K and 1500 K shows significant destruction of benzyl radical and a host of fragment peaks. The y-axis is arbitrarily scaled to allow easier comparison between temperatures.

Pyrolysis of ethylbenzene is more likely to occur by reaction (6.2) but formation of the methylbenzyl radical, C<sub>6</sub>H<sub>5</sub>CH-CH<sub>3</sub>, is also a possibility. In a hot micro-reactor, the methylbenzyl radical will rapidly decompose to styrene and H atoms.



In Fig. 6.2, heating the reactor to 1300 K triggers the decomposition of ethylbenzene to produce the benzyl (m/z 91) and methyl radicals (m/z 15). There is no evidence for the presence of styrene, C<sub>6</sub>H<sub>5</sub>CH=CH<sub>2</sub>, m/z 104, which indicates there is no formation of the C<sub>6</sub>H<sub>5</sub>CH-CH<sub>3</sub> radical.

Once the benzyl-d<sub>0</sub> radical is produced, it begins to fragment. At 1300 K, pyrolysis of C<sub>6</sub>H<sub>5</sub>CH<sub>2</sub> is underway and ions at m/z 39, 41, 51, and 65, appear. Raising the micro-reactor temperature to 1400 K leads to the appearance of ions at m/z 63, 64, 89, and 90. The pyrolysis scheme in Fig. 6.1 suggests that an assignment for these features is fulvenallene (C<sub>5</sub>H<sub>4</sub>=C=CH<sub>2</sub>), m/z 90, and the fulvenallenyl radical (C<sub>5</sub>H<sub>4</sub>-C≡CH), m/z 89. The IE(C<sub>5</sub>H<sub>4</sub>=C=CH<sub>2</sub>) is 8.22 eV while IE(C<sub>5</sub>H<sub>4</sub>-C≡CH) is 8.19 eV (see Table 6.1) so the 118.2 nm VUV laser can ionize both. The strong band at m/z 65 is cyclopentadienyl with IE(C<sub>5</sub>H<sub>5</sub>) of 8.4 eV (see Table 6.1), m/z 39 is likely propargyl radical with IE(HCCCH<sub>2</sub>) of 8.7 eV, and m/z 15 is methyl radical, IE(CH<sub>3</sub>) of 9.8 eV. The weak features at m/z 41 are very likely CH<sub>2</sub>CHCH<sub>2</sub><sup>+</sup> and m/z 51 is probably protonated diacetylene, (HC≡C-C≡CH, H<sup>+</sup>).

The top trace in Fig. 6.2 is pyrolysis of ethylbenzene at 1500 K and it is apparent that new chemistry is taking place. At 1500 K benzyl radical (m/z 91) is largely consumed and new features at m/z 40, 50, 52, 62, 63, 64, 76, and 77 grow in. Possible assignments for some of the new species are CH<sub>3</sub>C≡CH (m/z 40), HC≡C-C≡CH (m/z 50), HC≡C-CH=CH<sub>2</sub> (m/z 52), o-benzyne (o-C<sub>6</sub>H<sub>4</sub>, m/z 76), and phenyl (C<sub>6</sub>H<sub>5</sub>, m/z 77). The vexing problem is to apportion the source of these products. They could be new, higher temperature decomposition products of C<sub>6</sub>H<sub>5</sub>CH<sub>2</sub> or they could be fragmentation products from the pyrolysis of fulvenallene (C<sub>5</sub>H<sub>4</sub>=C=CH<sub>2</sub>), fulvenallenyl radical (C<sub>5</sub>H<sub>4</sub>-C≡CH), or cyclopentadienyl radical (C<sub>5</sub>H<sub>5</sub>).

### 0.05% C<sub>6</sub>H<sub>5</sub>-CH<sub>2</sub>CH<sub>3</sub> in Pulsed Neon

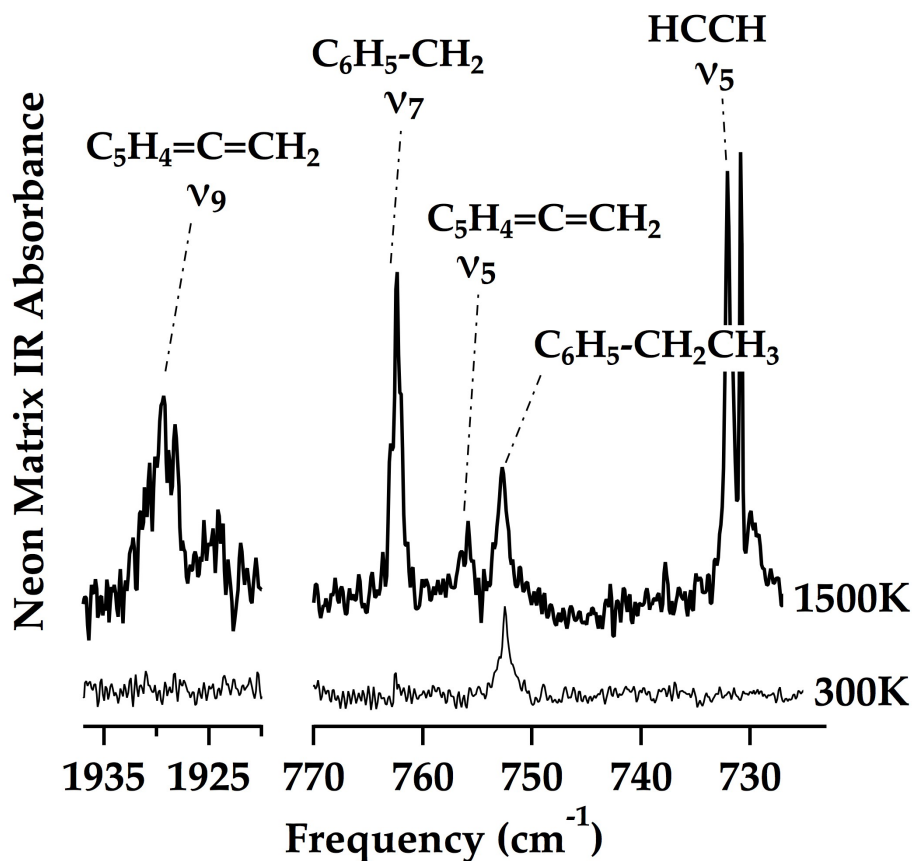


Fig. 6.3. Matrix isolation IR absorbance spectra of dilute ethylbenzene (C<sub>6</sub>H<sub>5</sub>CH<sub>2</sub>H<sub>3</sub>) in a pulsed neon reactor at 300 K (thin line) and 1500 K (thick black line). At 300 K, the only peak in this frequency window is from the precursor, ethylbenzene. Upon heating to 1500 K, peaks grow in for fulvenallene, benzyl radical and acetylene.

To confirm many of these assignments, we turn to IR spectroscopy and PIE measurements. Fig. 6.3 is a matrix IR spectrum of the results of pyrolysis of a 0.05 % mixture of C<sub>6</sub>H<sub>5</sub>CH<sub>2</sub>CH<sub>3</sub> in a pulsed Ne micro-reactor. The spectrum at the bottom is a control scan at 300 K. Heating C<sub>6</sub>H<sub>5</sub>CH<sub>2</sub>CH<sub>3</sub> to 1500 K produces the spectrum shown above. In previous work the infrared spectra of fulvenallene was reported<sup>[60]</sup> and 22 fundamentals and 2 overtone bands were assigned. The five strongest vibrational bands of fulvenallene have been identified in our Ne matrix isolation spectrum taken

during benzyl radical decomposition. These bands include  $\nu_4$ ,  $\nu_{11}$ ,  $\nu_{22}$ ,  $\nu_{28}$ , and  $\nu_9$ , the last of which is diagnostic of a  $>C=C=C<$  allenic stretch. The IR spectrum in Fig. 6.3 demonstrates the presence of  $\nu_9(C_5H_4=C=CH_2)$  and  $\nu_5(C_5H_4=C=CH_2)$  as well as  $\nu_7(C_6H_5CH_2)$ . The intense  $\nu_5(HC\equiv CH)$  bend is also present and is consistent with the scheme in Fig. 6.1. The CH stretching region of the IR spectrum is shown in Fig. 6.4. The presence of acetylene is again confirmed by observation of  $\nu_3(HC\equiv CH)$  and its Darling-Dennison Resonance. The intense  $\nu_1(HCCCH_2)$  band of propargyl radical<sup>[61]</sup> is detected as well. Fig. 6.4 also has a number of strong CH bands around the acetylenic stretching region,  $3330 - 3340\text{ cm}^{-1}$ , that are marked by bullets ( $\bullet$ ). These IR transitions have not yet been assigned since the candidate  $-C\equiv C-H$  molecules have not yet been assigned. In addition to IR identification of  $C_5H_4=C=CH_2$ ,  $C_6H_5CH_2$ ,  $HCCCH_2$ , and  $HC\equiv CH$ , we have tentative IR evidence for the  $C_5H_5$  radical. One complication is that the two vibrations of  $C_5H_5$  with the strongest IR intensities have been assigned<sup>[62-63]</sup> to within  $5\text{ cm}^{-1}$  of intense bands of benzyl radical,<sup>[62]</sup> making exact identification impossible at our spectral resolution. However, other fundamentals of the  $C_5H_5$  radical,  $\nu_2$ ,  $\nu_3$ ,  $\nu_6$ , and  $\nu_{14}$ , have been observed following the pyrolysis of  $C_6H_5CH_2CH_3$ . Many of the vibrational modes that are assigned in this study are collected together in the supplementary material (see Appendix B).

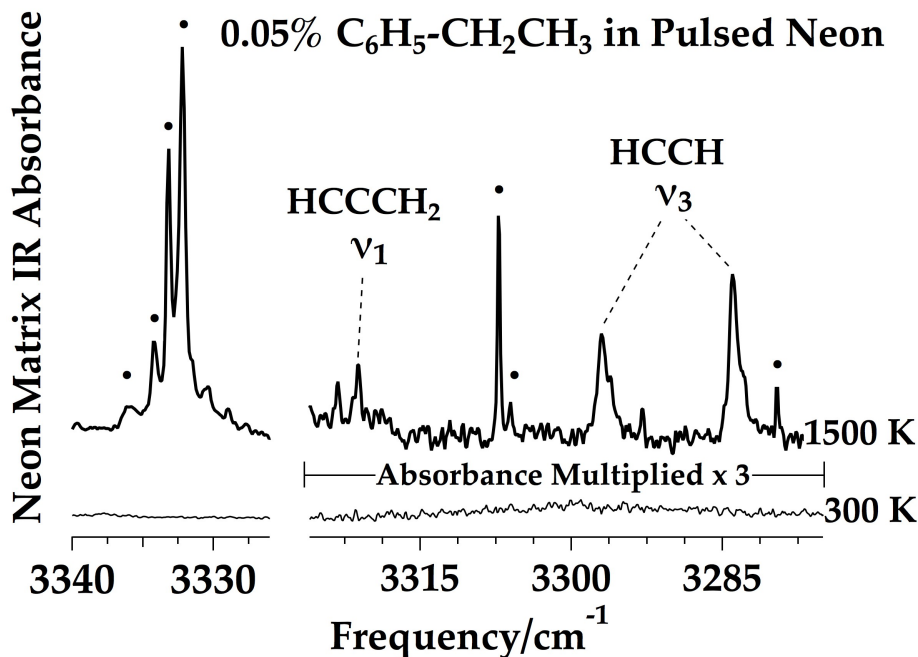


Fig. 6.4. The acetylenic stretch region of the vibrational spectrum is shown for the decomposition of ethylbenzene ( $C_6H_5CH_2CH_3$ ) in pulsed neon at 300 K (thin line) and 1500 K (thick black line). Peaks for propargyl radical ( $\nu_1$ ) and acetylene ( $\nu_3$ ) are shown, and the Darling-Denison splitting of  $\nu_3$ (HCCH) is evident. Multiple peaks in this region remain unassigned. Molecular assignments are collected in the Supplementary IR table (see Appendix B). Many candidates exist but the vibrational spectra for these molecules have not been measured. In the right panel, the absorbance is multiplied by three to highlight the assigned peaks.

In addition to IR spectroscopy, the measurement of PIE curves can be used to identify products. Fig. 6.5 shows the PIE( $m/z$  76) and PIE( $m/z$  65) that result when a 0.2 % mixture of  $C_6H_5CH_2CH_3$  in a CW He reactor is thermally decomposed at 1500 K. The photoionization efficiency curve for  $m/z$  76 has an ionization threshold that is consistent with that<sup>[44]</sup> of *o*-benzyne,  $9.03 \pm 0.05$  eV. Likewise the PIE( $m/z$  65) is consistent with the measured<sup>[43]</sup> IE( $C_5H_5$ ) of  $8.4268 \pm 0.0005$  eV; the PIE( $m/z$  65) in Fig. 6.5 shows good agreement with the measured<sup>[64]</sup> photoionization efficiency curve for the cyclopentadienyl radical,  $C_5H_5$ .

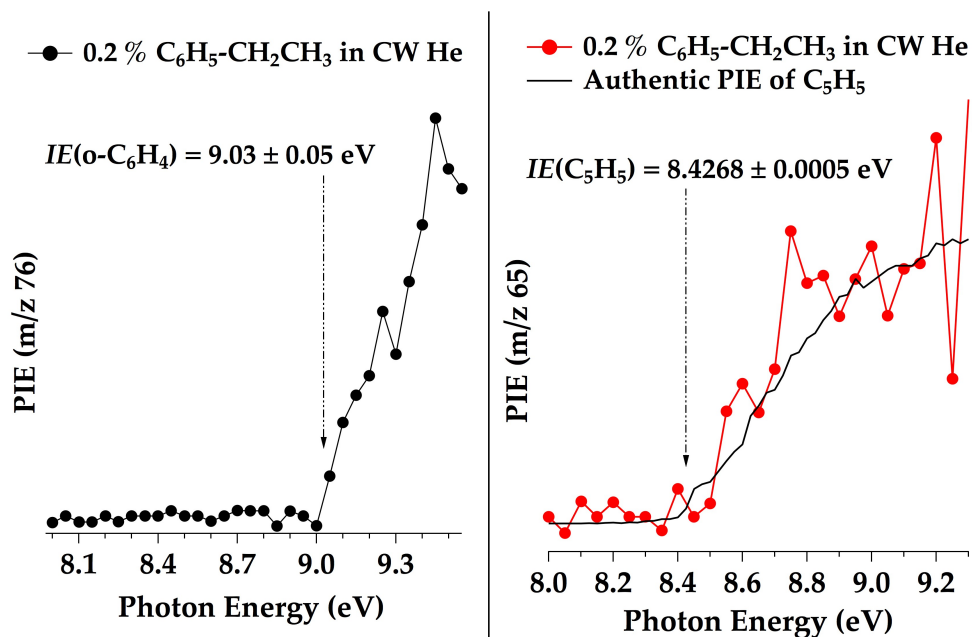


Fig. 6.5. Photoionization efficiency curves (PIE) for  $m/z$  76 (left) and  $m/z$  65 (right) measured during the 1500 K decomposition of 0.2 % ethylbenzene ( $C_6H_5CH_2CH_3$ ) in a CW helium reactor. The ionization energy<sup>[44]</sup> of ortho-benzyne ( $C_6H_4$ ) is included and the signal at  $m/z$  76 shows good agreement with this value. Published IE values of benzyne and cyclopentadienyl radical are collected in Table 6.1. To confirm that  $m/z$  65 is cyclopentadienyl radical, the authentic<sup>[64]</sup> PIE of  $C_5H_5$  is overlaid with the experimental trace.

Figs. 6.6 and 6.7 illustrate important experimental complications. As mentioned in the introduction, these heated micro-reactors are complex, nonlinear devices predicted<sup>[59]</sup> to have a reaction “sweet-spot.” This results from the interaction of the rapidly rising gas temperature and the falling gas pressure. Consequently kinetic properties of the reactor will be very sensitive to changes in gas pressure, flow rates, nature of the buffer gas, dimensions of the reactor, and potentially other factors that have not yet been considered.

In Figs. 6.6 and 6.7, benzyl bromide has been used as a source of the  $C_6H_5CH_2$  radical because the thermochemistry [in reaction (6.1) and Table 6.1] implies ease of decomposition of  $C_6H_5CH_2Br$ ; consequently benzyl bromide provides a lower temperature source of benzyl radical. In Fig. 6.6 a CW SiC micro-reactor is used with a high flow rate of He (right panel) as well as a low flow rate (left panel). It is apparent that reactors with different flow rates decompose the  $C_6H_5CH_2Br$  sample to different extents. The synchrotron at the ALS is operating at 9.4 eV so the signals in the PIMS should not arise from dissociative ionization. The low flow rate scan (5 sccm) in Fig. 6.6 is consistent with the 1300 K scan in Fig. 6.2, which uses  $C_6H_5CH_2CH_3$  as a benzyl source in a pulsed He reactor with 118.2 nm PIMS. Signals corresponding to fulvenallene ( $m/z$  90), fulvenallenyl ( $m/z$  89), cyclopentadienyl ( $m/z$  65), and propargyl ( $m/z$  39) are evident. However the right panel in Fig. 6.6 shows that when the micro-reactor is operated at higher flow (100 sccm) conditions,  $C_5H_4=C=CH_2$  ( $m/z$  90) is present but only weak signals at  $m/z$  65 or  $m/z$  39 are detected. The two scans in Fig. 6.6 were measured under the same experimental conditions except for the flow rate. It appears that different chemistry occurs in the CW reactor with different flow rates even though the wall temperature is the same.

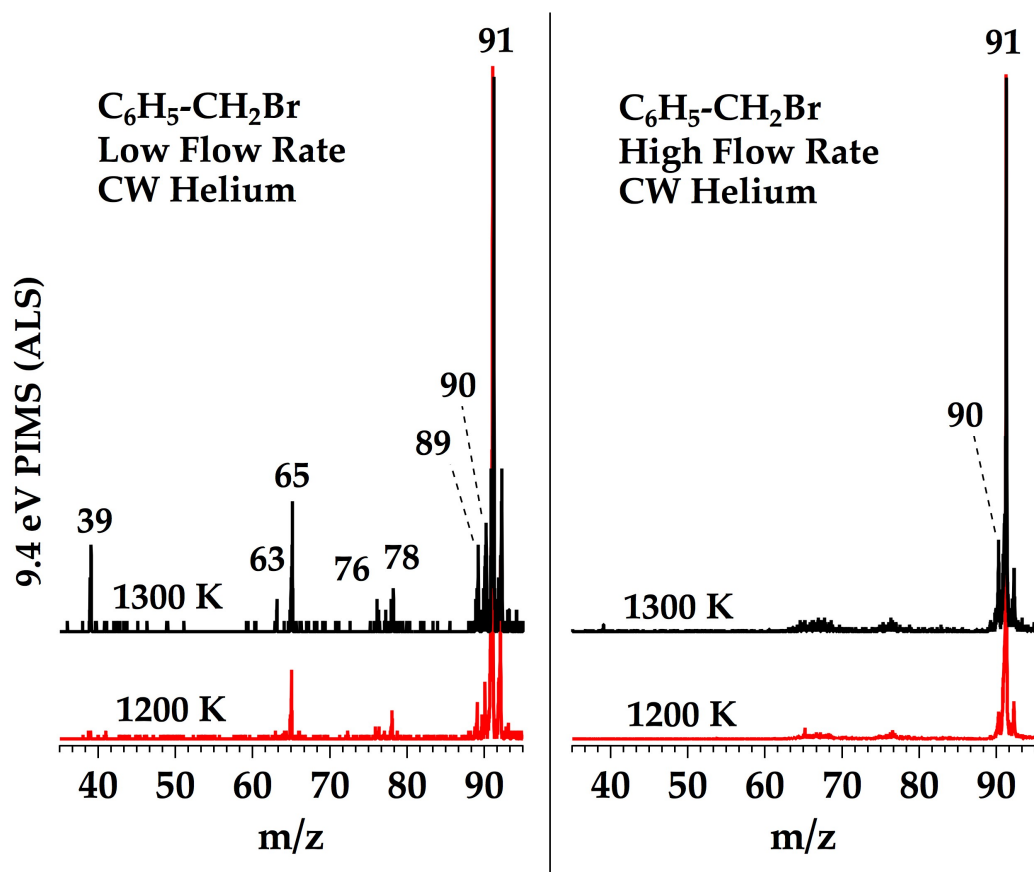


Fig. 6.6. PIMS spectra recorded during the decomposition of benzyl bromide at 1200 K (red) and 1300 K (black) in a CW reactor. Helium gas was flowed over the liquid sample of benzyl bromide at two different mass flow rate settings, 5 sccm and 100 sccm. Aside from the different flow rates, the scans are otherwise identical and peaks at  $m/z$  39 and 65 clearly depend dramatically on the flow rate setting. All spectra shown are normalized relative to the peak at  $m/z$  91.

Changing the buffer gas from helium to argon can also lead to variability in experimental findings. Fig. 6.7 shows the pyrolysis of  $C_6H_5CH_2Br$  entrained in Ar in a CW SiC micro-reactor measured at the Swiss Light Source. The left panel in Fig. 6.7 demonstrates that the initial decomposition products of  $C_6H_5CH_2$  at 1150 K in a CW Ar source are  $C_5H_4=C=CH_2$  ( $m/z$  90) and  $C_5H_4-C\equiv CH$  ( $m/z$  89). The decomposition scheme in Fig. 6.1 indicates that  $C_5H_4-C\equiv CH$  originates from  $C_5H_4=C=CH_2$  via loss of a H atom. The right panel in Fig. 6.7 uses the SLS synchrotron at 13.8 eV to photoionize hydrogen



atom and it is apparent that there are H atoms present at 1150 K. Figs 6.6 and 6.7 imply that differences in operational conditions (temperature, pressure) or carrier gas (He, Ar) are very important to the product distributions of thermal fragmentation.

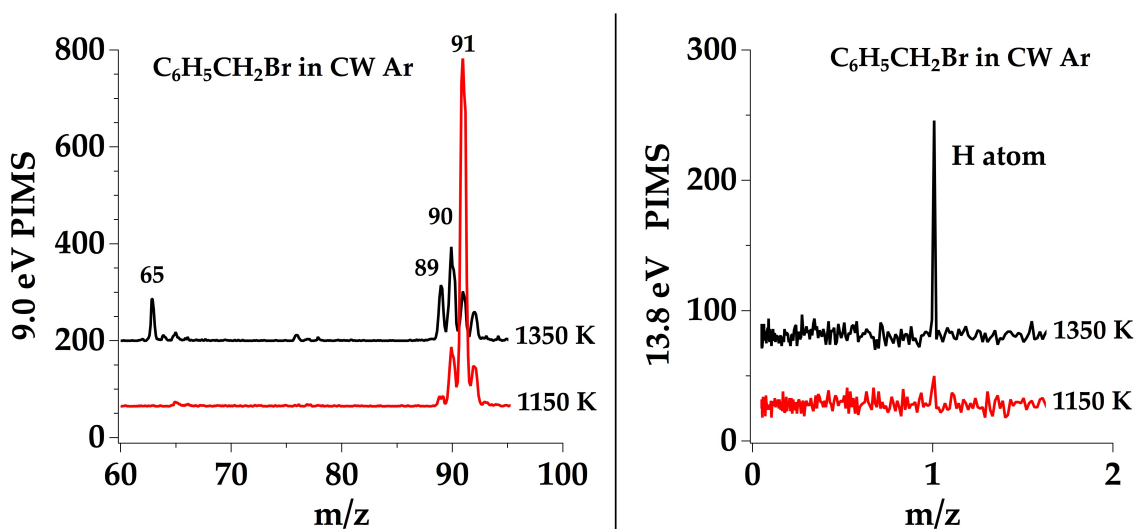


Fig. 6.7. Thermal decomposition of benzyl bromide in a CW argon reactor measured at the tunable synchrotron light source at the SLS. The left panel shows the formation of  $m/z$  90 ( $C_5H_4=C=CH_2$ ) and 89 ( $C_5H_4-C\equiv CH$ ) during the 1150 K decomposition of benzyl radical ( $m/z$  91). The photon energy was set to 9.0 eV, just high enough to ionize these products. The right panel shows the appearance of hydrogen atom produced ( $m/z$  1) at the same temperature ( $C_6H_5CH_2 \rightarrow C_5H_4=C=CH_2 + H$ ). To ionize hydrogen atom, 13.8 eV photons were used.

Recent CFD simulations<sup>[59]</sup> are currently limited to CW reactors but are able to provide insight into the comparison between experiments using Ar or He as a carrier gas. Given similar conditions, a reactor using He will exhibit considerably hotter temperature profiles along the reactor length, showing both higher peak temperature and more rapid heating. Furthermore, the residence time is a function of the mass flow rate. Both of these flow dependencies will alter the decomposition environment present and may explain the differences indicated by Figs. 6.6 and 6.7. Since decomposition

pathways have differing temperatures dependence, varying the reactor environment may dramatically alter the decomposition products.

## B. Decomposition of Benzyl-d<sub>2</sub> Radical

Fig. 6.8 shows the result of pyrolysis of C<sub>6</sub>H<sub>5</sub>CD<sub>2</sub>CD<sub>3</sub>; the predicted fragmentation of C<sub>6</sub>H<sub>5</sub>CD<sub>2</sub> is presented in the supplementary figure (see Appendix B), Fig. B.1. The signals at m/z 111 and m/z 112 are present from photoionization of C<sub>6</sub>H<sub>5</sub>CD<sub>2</sub>CD<sub>3</sub> and its natural abundance isotope peak. Small peaks at m/z 93 (dissociative ionization) and an impurity peak at m/z 110 are also present. At 1300 K, the decomposition of C<sub>6</sub>H<sub>5</sub>CD<sub>2</sub>CD<sub>3</sub> is demonstrated by the presence of CD<sub>3</sub> (m/z 18) and C<sub>6</sub>H<sub>5</sub>CD<sub>2</sub> (m/z 93). Complications with the scheme in Fig. 6.1 are immediately evident. This scheme would predict C<sub>6</sub>H<sub>5</sub>CD<sub>2</sub> to lose H atom and produce fulvenallene-d<sub>2</sub> (m/z 92) followed by loss of D atom to generate fulvenallenyl radical (m/z 90). Fig. 6.1 would also predict formation of cyclopentadienyl radical-d<sub>0</sub> (m/z 65) plus DCCD (m/z 28). Fig. 6.8 clearly shows the presence of the unexpected peak m/z 91 as well as formation of intense signals at m/z 66 and 67 in addition to the expected peak at m/z 65. Also present are ions at m/z (39, 40, 41, 42, and 43). As the micro-reactor is heated to 1500 K, numerous unexpected species appear. Among these new peaks at 1500 K is m/z 17, CHD<sub>2</sub>.

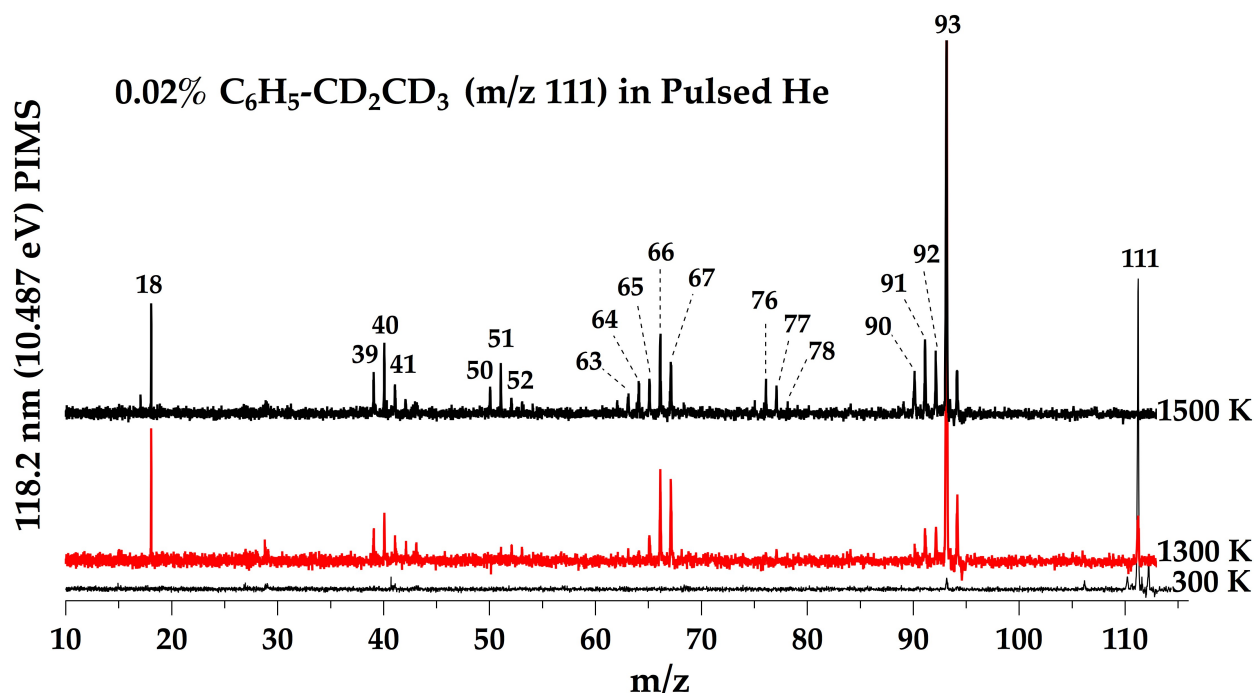


Fig. 6.8. Dilute ethylbenzene- $d_5$  ( $C_6H_5CD_2CD_3$ ,  $m/z$  111) heated in a pulsed helium tubular micro-reactor studied using PIMS at three different reactor temperatures, 300 K, 1300 K, and 1500 K. At 1300 K (shown in red), the large peak at  $m/z$  93 is benzyl radical- $d_2$ , along with the counter fragment methyl radical- $d_3$  ( $m/z$  18). Some decomposition is observed resulting in cyclopentadienyl radical ( $m/z$  65 is  $d_0$ , 66 is  $d_1$ , and 67 is  $d_2$ ) and 39, 40 and 41 (presumed to be propargyl radical) are observed. At 1500 K we see peaks at 90, 91, and 92, 50, 51, and 52, and a triplet at 76, 77, and 78. Comparison to Fig 6.2 (the  $d_0$  case) is useful. The y-axis is arbitrarily scaled to allow easy comparison between temperatures.

A potential factor for many of these new peaks is the fact that radical-radical processes in these micro-reactors have been observed earlier. In a study of the pyrolysis of isotopically substituted acetaldehydes,<sup>[65]</sup> rapid isotope exchanges were observed:  $CD_3$  ( $m/z$  18) + H  $\rightleftharpoons$   $CHD_2$  ( $m/z$  17) + D. Likewise in an earlier study of the pyrolysis of furan,<sup>[66]</sup> it was observed that H atoms attacked  $CH_3C\equiv CH$  to produce  $CH_3$  radicals ( $m/z$  15) and HCCH. Careful dilution of the furan sample to 0.01 % (or lower) in He was required<sup>[66]</sup> to suppress this H atom chemistry. The reaction scheme in Fig. 6.1

predicts the formation of H atoms and confirmation of this is found in Fig. 6.7, which shows PIMS detection of H atoms following pyrolysis of  $C_6H_5CH_2$ .

One explanation of the unexpected sets of peaks in Fig. 6.8 could be rapid radical/radical bimolecular chemistry. Many radical/radical reactions are very fast.<sup>[67]</sup>



To find more direct evidence for H/D atom chemistry, we have examined the chemistry of D atoms reacting with cyclopentadienyl radicals. In an earlier study<sup>[25]</sup> of the pyrolysis of benzaldehyde, methyl nitrite- $d_3$  was used as a chemical source of D atoms.



Additionally, anisole ( $C_6H_5OCH_3$ ) is known<sup>[28]</sup> to be a convenient source of  $C_5H_5$  radicals so we can test for rapid D atom reactions with cyclopentadienyl radical. Fig. 6.9 shows the results of this examination. The thin trace is from thermal decomposition of anisole at 1300 K.



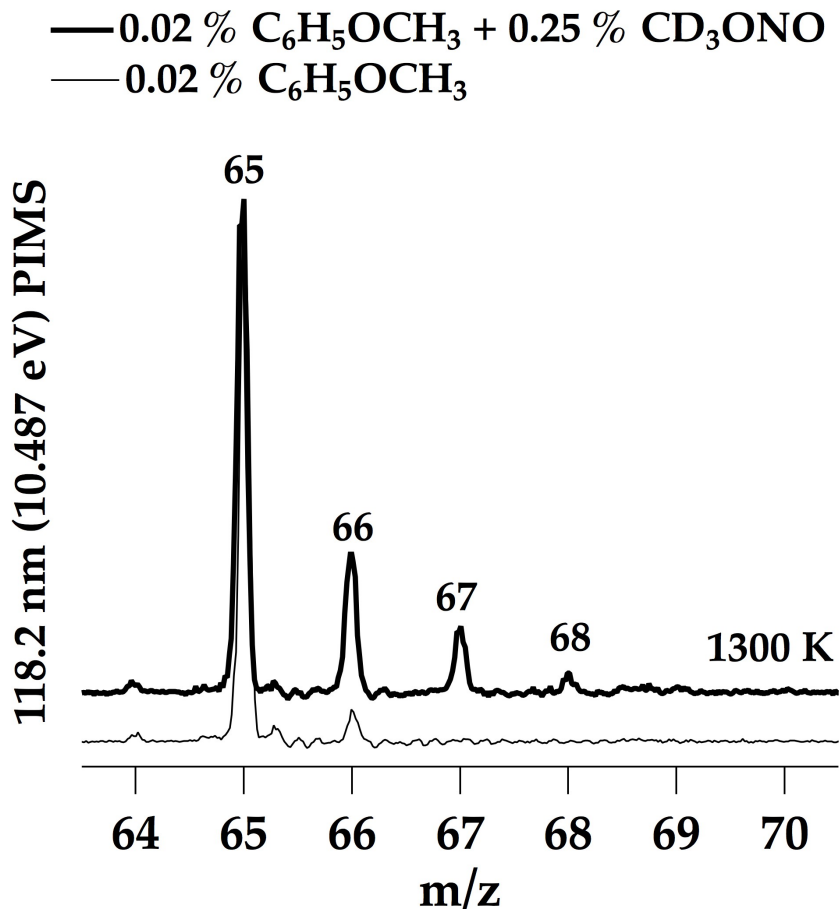
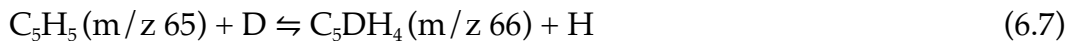


Fig. 6.9. The thin black trace is the PIMS spectrum of C<sub>6</sub>H<sub>5</sub>OCH<sub>3</sub> decomposition at 1300 K yielding cyclopentadienyl radical (C<sub>5</sub>H<sub>5</sub>, m/z 65) observed with a small natural abundance <sup>13</sup>C peak at m/z 66. Shown above is the outcome of mixing 0.02 % C<sub>6</sub>H<sub>5</sub>OCH<sub>3</sub> with 0.25 % CD<sub>3</sub>ONO, a known D atom source, in pulsed helium. We can clearly see significant incorporation of D atom up to C<sub>5</sub>D<sub>3</sub>H<sub>2</sub> due to bimolecular radical-radical reactions (C<sub>5</sub>H<sub>5</sub> + D → C<sub>5</sub>DH<sub>5</sub>\* → C<sub>5</sub>DH<sub>4</sub> + H). Note the monotonic decrease in signal observed with increasing deuteration events.

The thicker trace in Fig. 6.9 is the result of pyrolysis of a mixture of 0.02 % C<sub>6</sub>H<sub>5</sub>OCH<sub>3</sub> and 0.25 % CD<sub>3</sub>ONO in a pulsed He reactor at 1300 K. Since pyrolysis of CD<sub>3</sub>ONO produces CD<sub>2</sub>O (m/z 32) plus NO (m/z 30) and D atoms, radical-radical reactions ensue that lead to scrambling of the cyclopentadienyl radical.



In addition to  $C_5DH_4$ , Fig. 6.9 demonstrates that D atom chemistry can exchange multiple H atoms to produce both the  $C_5D_2H_3$  and  $C_5D_3H_2$  radicals as well.

This set of complementary data helps in the interpretation of the H/D ratios in peaks in Fig. 6.8. In the 1300 K trace for  $C_6H_5CD_2CD_3$ , instead of one peak at  $m/z$  65 (assigned as  $C_5H_5$  in Fig 6.2) features at 65, 66, and 67 are observed; in Fig. 6.8 the peaks at 66 and 67 are surprisingly intense. Decomposition of  $C_6H_5CD_2$  via Fig. 6.1 predicts formation of  $C_5H_5$  only. It may seem initially attractive to assign  $m/z$  66 and 67 in Fig. 6.8 to H/D scrambling but the intensities are inconsistent with this process. Bimolecular scrambling produces monotonically decreasing intensity for subsequent deuteration of  $C_5H_5$ , as evident in Fig 6.9. Due to the qualitative differences between Fig 6.8 and Fig 6.9, it seems likely that the intensities for  $C_5H_4D$  ( $m/z$  66) and  $C_5H_3D_2$  ( $m/z$  67) result from different pathways than those shown in Fig. 6.1 and not simple bimolecular H/D scrambling.

Additional indication that our experiments follow unimolecular decomposition is found in the absence of styrene formation. If hydrogen atoms were present in large enough densities to facilitate bimolecular chemistry, a likely target would be H-atom abstraction from ethylbenzene of the  $\alpha$ -carbon, yielding methylbenzyl radical ( $C_6H_5CH-CH_3$ ), which would rapidly undergo hydrogen atom loss to produce styrene, see reaction (6.3). This process was observed during the decomposition of ethylbenzene in shock tubes and was commonly observed when bimolecular reactions dominate.<sup>[68]</sup> Since no  $C_6H_5-CH=CH_2$  ( $m/z$  104) is observed in the PIMS spectra (Fig. 6.2), it is unlikely that H atom chemistry is prevalent under the operating conditions of the micro-reactor.

## D. Decomposition of Benzyl-d<sub>5</sub> Radical

Fig. 6.10 shows the results of pyrolysis of a 0.02 % mixture of C<sub>6</sub>D<sub>5</sub>CH<sub>2</sub>CH<sub>3</sub> in a pulsed micro-reactor; the predicted fragmentation for C<sub>6</sub>D<sub>5</sub>CH<sub>2</sub> is shown in the supplementary figure (see Appendix B), Fig. B.2. The initial trace at 350 K shows the parent peak for C<sub>6</sub>D<sub>5</sub>CH<sub>2</sub>CH<sub>3</sub> at m/z 111. The small feature at m/z 110 reveals a slight impurity (C<sub>6</sub>HD<sub>4</sub>CH<sub>2</sub>CH<sub>3</sub>) of the benzyl-d<sub>5</sub> precursor as well as a small amount of dissociation ionization producing C<sub>6</sub>D<sub>5</sub>CH<sub>2</sub><sup>+</sup> at m/z 96. At 1300 K a large portion of C<sub>6</sub>D<sub>5</sub>CH<sub>2</sub>CH<sub>3</sub> decomposes to generate C<sub>6</sub>D<sub>5</sub>CH<sub>2</sub> (m/z 96) as well as the methyl radical, m/z 15. Instead of the expected feature for C<sub>5</sub>D<sub>5</sub> (m/z 70) there are additional signals at m/z 65, 68, and 69 similar to Fig 6.8. There are also a number of peaks at (m/z 40, 41, 42, 44, and 45) as well as (m/z 52 and 53) which remain unassigned. As the reactor is heated to 1400 K, benzyl-d<sub>5</sub> radical pyrolyzes to fragments at m/z 92, 93, 94, and 95. A decomposition scheme based on Fig. 6.1 predicts that C<sub>6</sub>D<sub>5</sub>CH<sub>2</sub> (m/z 96) generates fulvenallene-d<sub>4</sub> (m/z 94) and the fulvenallenyl radical-d<sub>4</sub> (m/z 93); the production of radicals at m/z 95 is not anticipated. Additionally, a number of new, unexpected peaks grow in that are comparable to those found during benzyl-d<sub>2</sub> radical decomposition.

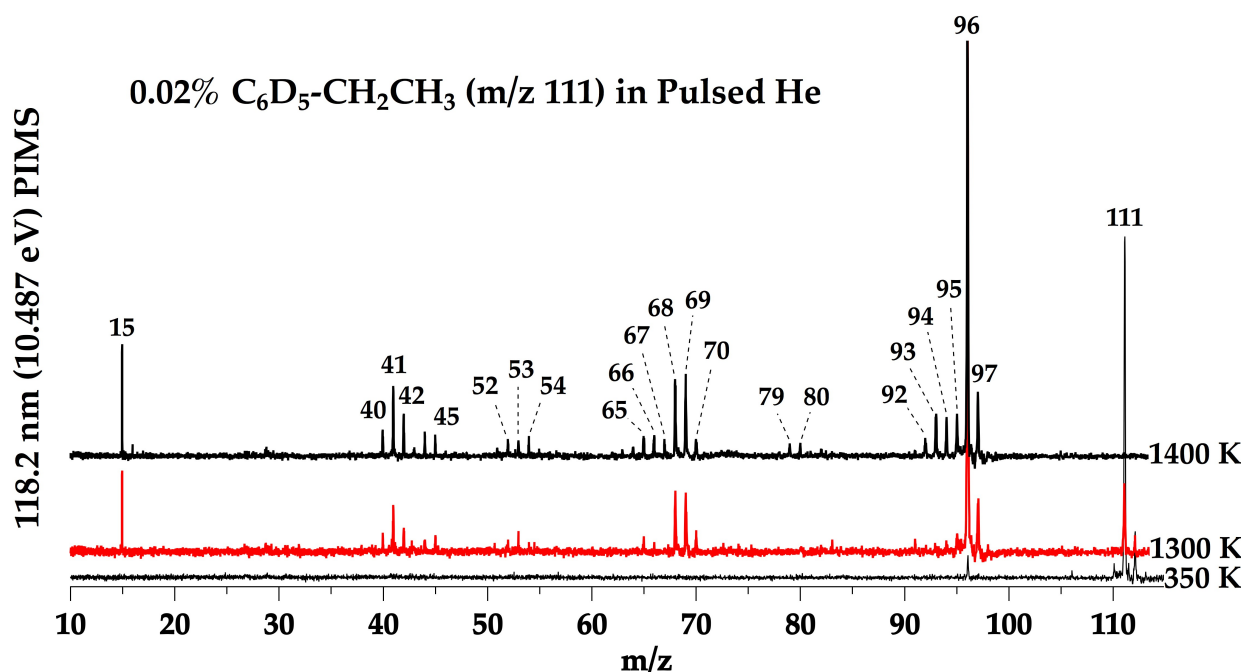


Fig. 6.10. Dilute ethylbenzene-d<sub>5</sub> (C<sub>6</sub>D<sub>5</sub>CH<sub>2</sub>CH<sub>3</sub>, m/z 111) heated in a pulsed helium tubular micro-reactor studied using PIMS at three different reactor temperatures, 350 K, 1300 K, and 1400 K. The peaks here are to be compared to the d<sub>0</sub> case and the d<sub>2</sub> shown in Fig 6.2 and Fig 6.8, respectively. At 1300 K (shown in red), the large peak at m/z 96 is benzyl radical-d<sub>5</sub>, along with the counter fragment methyl radical (m/z 15). At 1300 K we see some decomposition to cyclopentadienyl radical (m/z 68 is d<sub>3</sub>, 69 is d<sub>4</sub>, and 70 is d<sub>5</sub>) and 40, 41, and 42 are observed (likely isotopomers of propargyl radical). Further heating to 1400 K shows significant destruction of benzyl radical and the appearance of a set of new peaks from m/z 65 – 70 and 92 – 95, now assumed to be isotopomers of C<sub>5</sub>H<sub>4</sub>=C=CH<sub>2</sub> and C<sub>5</sub>H<sub>4</sub>-C≡CH. The y-axis is arbitrarily scaled to allow easy comparison between temperatures.

#### D. Decomposition of <sup>13</sup>C-Benzyl Radical, C<sub>6</sub>H<sub>5</sub><sup>13</sup>CH<sub>2</sub>

To circumvent the complications with H/D atom chemistry entirely, <sup>13</sup>C was used as an isotopic label. Shown in Fig. 6.11 is the 118.2 nm PIMS of the products of thermal fragmentation of 0.02 % C<sub>6</sub>H<sub>5</sub><sup>13</sup>CH<sub>2</sub>CH<sub>3</sub> in He in a pulsed SiC micro-reactor; the decomposition predictions for C<sub>6</sub>H<sub>5</sub><sup>13</sup>CH<sub>2</sub> are shown in the supplementary figure (see Appendix B), Fig. B.3. The bottom scan at 300 K reveals the parent peak for



$C_6H_5^{13}CH_2CH_3$  at  $m/z$  107. There is a trace impurity in the  $^{13}C$  sample,  $C_6H_5^{12}CH_2CH_3$  at  $m/z$  106, and a small amount of dissociative ionization,  $C_6H_5^{13}CH_2^+$ , at  $m/z$  92. Heating the sample to 1300 K induces the formation of  $^{13}C$ -benzyl radical ( $C_6H_5^{13}CH_2$  at  $m/z$  92) along with its co-product  $CH_3$  ( $m/z$  15). Upon formation the  $^{13}C$ -benzyl radical begins decomposition to  $^{13}C$ -fulvenallene ( $m/z$  91) and the  $^{13}C$ -fulvenallenyl radical ( $m/z$  90). In stark contrast to expectations from Fig. 6.1, not only  $^{12}C_5H_5$  ( $m/z$  65) is present but also  $^{13}C_5H_5$  ( $m/z$  66). There is also a group of products present at  $m/z$  39, 40, 41, and 42. Further heating of  $C_6H_5^{13}CH_2CH_3$  to 1500 K leads to other peaks that are not predicted by Fig. 6.1. The peak at  $m/z$  16 is certainly  $^{13}CH_3$ . Likewise a cluster of peaks at  $m/z$  (50, 51, and 52) appears as well as the set at  $m/z$  (76, 77, and 78). Based on measured PIE curves, we assign  $m/z$  76 as  $o$ - $C_6H_4$  and  $m/z$  78 as benzene;  $m/z$  77 is likely the phenyl radical,  $C_6H_5$ . Many of these features are inconsistent with the mechanisms depicted in Fig. 6.1. From these PIMS scans we notice that  $m/z$  76, 77, and 78 are still present and show no sign of  $^{13}C$  incorporation. This is important to note because benzene has been shown<sup>[28]</sup> to form from dimerization of propargyl radicals, ( $HCCCH_2 + HCCCH_2$ ), and from reactions of methyl radical with the cyclopentadienyl radical ( $CH_3 + C_5H_5$ ). If these pathways were the source of the benzene observed, then the  $^{13}C:^{12}C$  ratio would match that of the two radicals reacting. Both  $^{13}(HCCCH_2)$  and  $^{13}(C_5H_5)$  are present in the reactor so the absence of peaks at  $m/z$  79 and 80 indicates that, however benzene is formed, it does so without  $^{13}C$  atom incorporation.

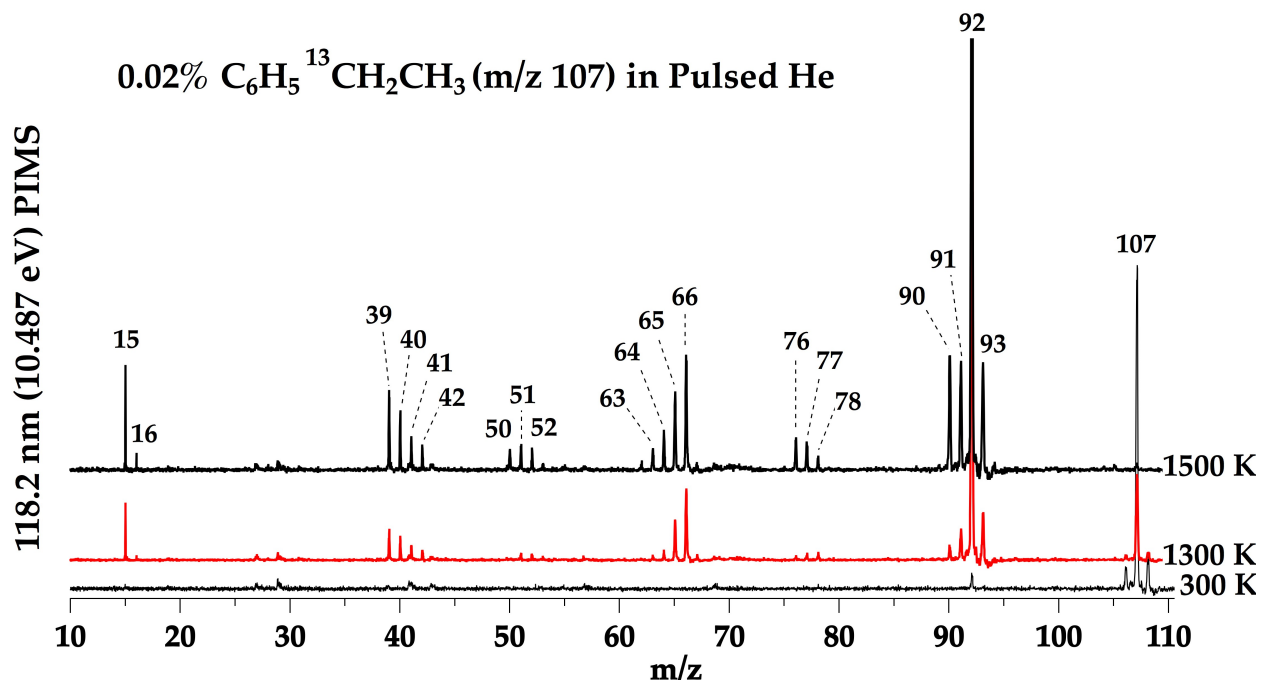


Fig. 6.11. Dilute ethylbenzene-<sup>13</sup>C (C<sub>6</sub>H<sub>5</sub><sup>13</sup>CH<sub>2</sub>CH<sub>3</sub>, m/z 107) heated in a pulsed helium tubular micro-reactor studied using PIMS at three different reactor temperatures, 300 K, 1300 K, and 1500 K. At 1300 K (shown in red), the large peak at m/z 92 is benzyl radical-<sup>13</sup>C along with the counter fragment methyl radical (m/z 15). Decomposition to cyclopentadienyl radical shows surprising incorporation of <sup>13</sup>C at m/z 66. At 1500 K, <sup>13</sup>C isotopomers are observed for propargyl radical (m/z 40) and unexpectedly, methyl radical (m/z 16) but not in the triplet at 76-78, indicating unimolecular formation of these three peaks from C<sub>6</sub>H<sub>5</sub><sup>13</sup>CH<sub>2</sub>. The y-axis is arbitrarily scaled to allow easy comparison between temperatures.

To confirm the identification of the ions at m/z 90 and 91 in Fig. 6.11, PIEs were measured with the synchrotron at the ALS. Shown in Fig. 6.12 are the PIE curves for m/z 90 and m/z 91 measured during the pyrolysis of a dilute mixture of C<sub>6</sub>H<sub>5</sub><sup>13</sup>CH<sub>2</sub>CH<sub>3</sub> in He in a CW SiC micro-reactor. Both of these PIE curves are consistent with the assignment of m/z 90 as the <sup>13</sup>C isotopomer of the fulvenallenyl radical (C<sub>5</sub>H<sub>4</sub>-C≡CH) while m/z 91 is identified as <sup>13</sup>C-fulvenallene (C<sub>5</sub>H<sub>4</sub>=C=CH<sub>2</sub>). The ionization thresholds agree with the published<sup>[20]</sup> values and the known PIE curves as indicated by black

lines. Fig 6.13 shows a pair of PIE curves from the same  $C_6H_5^{13}CH_2CH_3$  decomposition that identify both the  $m/z$  65 and  $m/z$  66 signals as cyclopentadienyl radicals,  $^{12}C_5H_5$  and  $(^{13}C)C_4H_5$ .

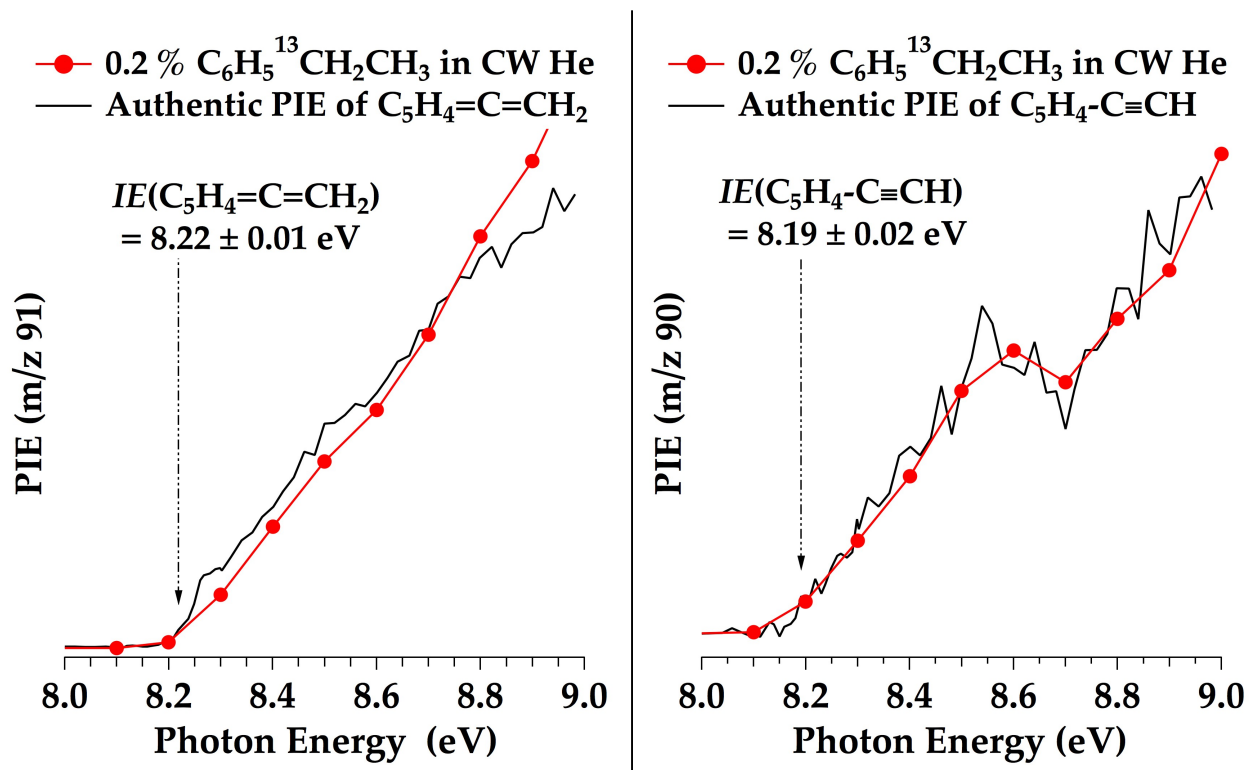


Fig. 6.12. PIEs confirming the identity of  $m/z$  91 as  $C_5H_4=C=CH_2$  and  $m/z$  90 as  $C_5H_4-C\equiv CH$  each containing one  $^{13}C$ . Red data points are from ethylbenzene- $^{13}C$  decomposition at 1500 K in a CW helium reactor. In black are previously reported<sup>[21]</sup> PIEs for the two molecules with their IE's labeled on the plots. Y-axis values are scaled so that signal intensities are approximately equal.

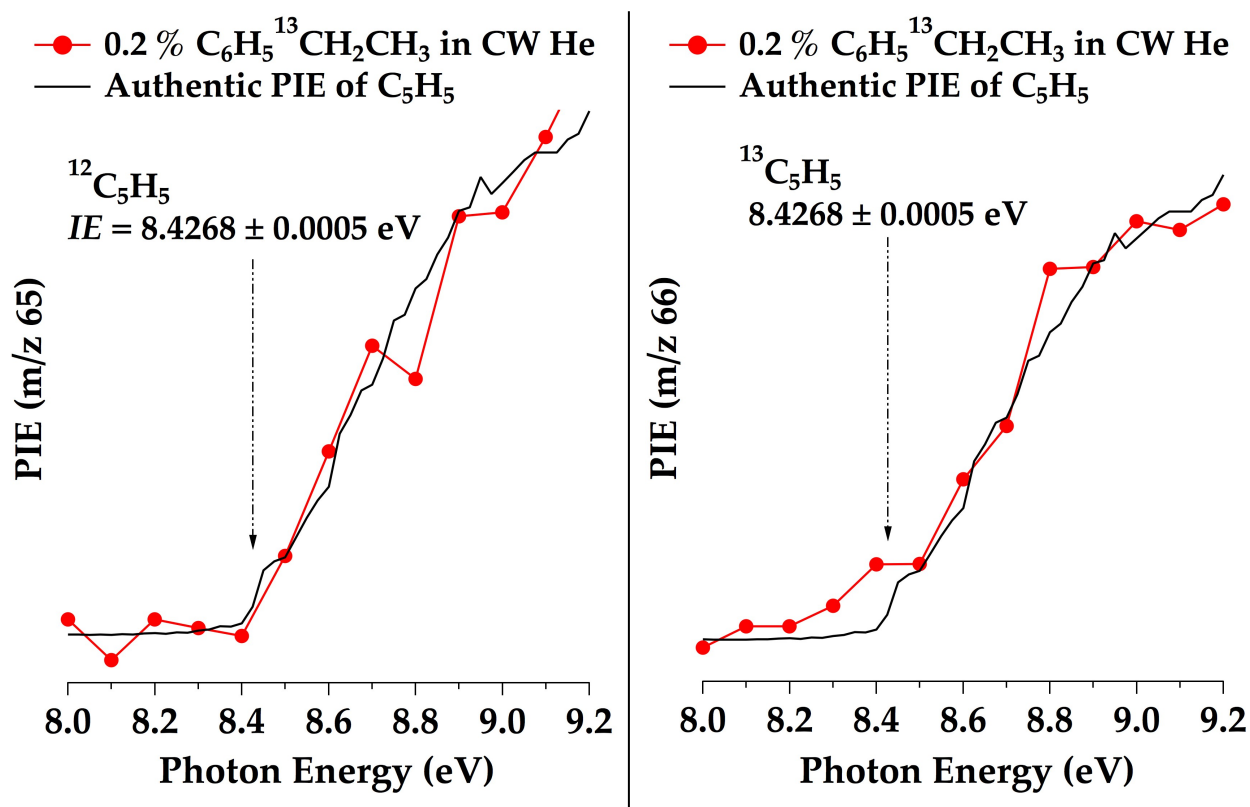


Fig. 6.13. PIEs confirming the identity of  $m/z$  65 and 66 as cyclopentadienyl radical ( $C_5H_5$ ). Red data points are from ethylbenzene- $^{13}C$  decomposition at 1500 K in a CW He reactor. In black are the previously reported<sup>[64]</sup> PIEs for  $C_5H_5$  with the IE labeled on the plots;  $^{13}C$  substitution should have no effect on the IE. Y-axis values are scaled so that signal intensities are approximately equal.

Fig. 6.1 illustrates that benzyl radical could isomerize to cycloheptatrienyl radical,  $C_6H_5CH_2, \tilde{X}^2B_1 (+ M) \rightleftharpoons C_7H_7, \tilde{X}^2E_2$  and this isomerization is consistent with many of the ratios of isotopomers detected during the D/H and  $^{13}C$  precursors decomposition. Because the ionization energies for both benzyl (7.2 eV) and cycloheptatrienyl (6.2 eV) radicals are known (Table 6.1), PIMS can differentiate these two isotopomers. Fig. 6.14 shows the PIMS spectra that result from pyrolysis of  $C_6H_5CD_2Br$  in an effusive, CW Ar micro-reactor at 1250 K taken at the SLS. The species at  $m/z$  93 could be either benzyl ( $C_6H_5CD_2$ ) or cycloheptatrienyl ( $C_7H_5D_2$ ). As the synchrotron is tuned from 7.5 eV down to 7.0 eV and on to 6.8 eV, the  $m/z$  93 signal

collapses. The scans at 6.8 eV and 7.0 eV in Fig. 6.14 have been multiplied by a factor of 10. We conclude that all of the  $m/z$  93 radicals that result from pyrolysis of benzyl bromide- $d_2$  at 1250 K in a CW Ar micro-reactor are benzyl radicals ( $C_6H_5CD_2$ ). No cycloheptatrienyl radicals ( $C_7H_5D_2$ ) are present in the CW Ar micro-reactor. It is worth noting, however, that while the isomerization,  $C_6H_5CD_2 (+ M) \rightleftharpoons C_7H_5D_2$ , was not observed in the effusive, CW Ar reactor in Switzerland, different results could be found with pulsed reactors or with the use of different carrier gasses.

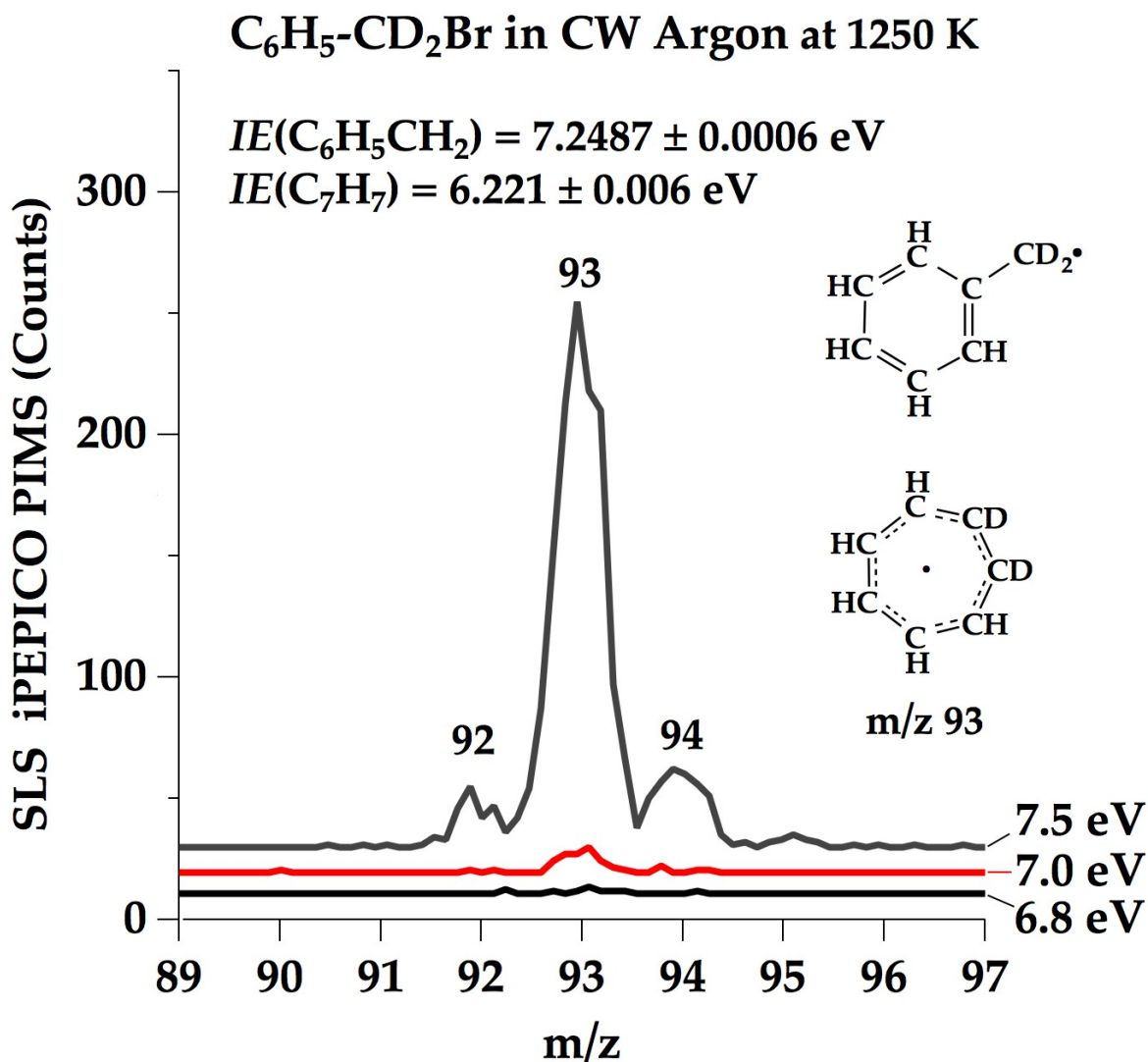


Fig. 6.14. PIMS for the decomposition of C<sub>6</sub>H<sub>5</sub>CD<sub>2</sub>Br at 1250 K in a CW Ar reactor at the SLS. Benzyl radical (C<sub>6</sub>H<sub>5</sub>CD<sub>2</sub>) and cycloheptatrienyl radical (C<sub>7</sub>H<sub>5</sub>D<sub>2</sub>) have the same mass but IEs that differ by around 1 eV. The signal intensity at m/z 93 (benzyl radical-d<sub>2</sub>) drops off significantly at photon energies below the IE of benzyl radical, indicating that cycloheptatrienyl radical is not present.

#### IV. Discussion and Conclusions

This chapter describes an experimental study of the pyrolysis of the benzyl radical carried out in a set of heated micro-reactors. We have used both benzyl bromide and ethylbenzene as precursors of the parent species, C<sub>6</sub>H<sub>5</sub>CH<sub>2</sub>, as well as a set of

isotopically labeled radicals:  $C_6H_5CD_2$ ,  $C_6D_5CH_2$ , and  $C_6H_5^{13}CH_2$ . A combination of PIMS, PIE measurements, and IR spectroscopy has been used to identify the thermal decomposition products. Before making any mechanistic assessments there are at least two serious complications that must be resolved. These are the non-linear properties of the micro-reactors and the unknown pyrolysis mechanisms of the nascent metastables and radicals: fulvenallene, fulvenallenyl radical, and the cyclopentadienyl radical.

The experiments in this chapter made use of four different micro-reactors: a pulsed He reactor, a pulsed Ne reactor, a CW He reactor, and a CW Ar reactor. All of these reactors are slightly different. Recent computational fluid dynamics (CFD) simulations<sup>[59]</sup> have revealed that the heated micro-reactors are complex, non-linear devices. The chemical reactions in the micro-reactors vary exponentially with the gas temperature (which is rising) and quadratically with the pressure (which is falling). Consequently there is only a small region of the micro-reactor in which chemical reactions occur. The size and location of the “sweet-spot” can vary dramatically with changes in reactor dimensions (diameter, length), material (SiC, quartz, or  $Al_2O_3$ ), the nature of the buffer gas (He, Ne, or Ar), mass flow-rate, mode of operation (pulsed vs. continuous), or other factors that have not yet been anticipated. Consequently, care must be taken when comparing results from different micro-reactors.

The products  $C_5H_4=C=CH_2$ , H atom,  $C_5H_4-C\equiv CH$ ,  $C_5H_5$ ,  $HCCCH_2$  and  $HC\equiv CH$  have all been detected. Consequently we must contend with subsequent thermal cracking processes of the products:  $C_5H_4=C=CH_2$  and the radicals  $C_5H_4-C\equiv CH$  and  $C_5H_5$ . Several earlier experiments (see Fig. 6.5 in ref.<sup>[26]</sup>) and a computational paper<sup>[69]</sup> have demonstrated that the cyclopentadienyl radical thermally decomposes to propargyl and acetylene:  $C_5H_5 (+ M) \rightarrow HCCCH_2$  and  $HC\equiv CH$ . The dynamics of fulvenallene pyrolysis

are even more complicated.<sup>[16-17]</sup> When the bicyclic molecule phthalide (1-isobenzofuranone,  $C_6H_4COOCH_2$ ) was used as a fulvenallene precursor, pyrolysis in a CW Ar micro-reactor reported decomposition of  $C_5H_4=C=CH_2$  ( $m/z$  90) to  $C_5H_4-C\equiv CH$  ( $m/z$  89) and thence to the expected  $HCCCH_2$  ( $m/z$  39) and  $HC\equiv C-C\equiv CH$  ( $m/z$  50). However Fig. 6.3 in ref. <sup>[16]</sup> also reveals the presence of  $HC\equiv CH$  ( $m/z$  26), a set of products at  $m/z$  63-65, as well as (76, 78). In this work, we have also observed many of these products but we cannot determine if they result from  $C_6H_5CH_2$  decomposition or from  $C_5H_5$  and  $C_5H_4=C=CH_2$  decomposition. Until the fragmentation of fulvenallene and the cyclopentadienyl radical are properly understood, it will be difficult to confirm the products of  $C_6H_5CH_2$  pyrolysis.

Even with these two complexities — the non-linear nature of the reactors and the obscuring products from cyclopentadienyl and fulvenallene decomposition — there is compelling isotopic evidence that the fulvenallene-decomposition pathway in Fig. 6.1 is not the sole route for  $C_6H_5CH_2$  decomposition. The enhanced D/H ratio on  $C_5H_5$  observed during  $C_6H_5CD_2CD_3$  decomposition (Fig. 6.8) reveals an unexpected incorporation of D into the cyclopentadienyl radical. The deuteration pattern resulting from bimolecular D-atom chemistry displayed in Fig. 6.9 is not present in  $C_6H_5CD_2$  decomposition. The presence of  $C_5H_5$  ( $m/z$  65) predicted by Fig. 6.1 is dwarfed by signals at  $m/z$  66 ( $C_5H_4D$ ) and  $m/z$  67 ( $C_5H_3D_2$ ). Likewise for the case of  $C_6H_5^{13}CH_2$  in Fig. 6.11, intense signals for both  $^{12}C_5H_5$  ( $m/z$  65) and  $^{13}CC_4H_5$  ( $m/z$  66) are present. The PIE curves in Fig. 6.13 confirm the identity of both of these peaks as cyclopentadienyl radicals. The  $^{13}C$  experiments in Fig. 6.11 also clearly show formation of both  $CH_3$  ( $m/z$  15) and  $^{13}CH_3$  ( $m/z$  16) radicals at 1500 K during  $C_6H_5^{13}CH_2$  decomposition. Fig. 6.11 also shows clear evidence for  $^{12}$ benzyne ( $m/z$  76),  $^{12}$ phenyl radical ( $m/z$  77), and



<sup>12</sup>benzene (m/z 78). None of these species incorporate <sup>13</sup>C, thus indicating their formation is from direct decay of parent. These results are not compatible with the fulvenallene pathway predicted in Fig. 6.1.

The failure to detect cycloheptatrienyl radicals (Fig. 6.14) is puzzling. An obvious route to scramble <sup>13</sup>C into the cyclopentadienyl radical (see Fig. 6.11) is through the cycloheptatrienyl radical, which could then decompose as summarized in reaction 6.8.



If there were a low barrier between the cycloheptatrienyl radical and its decomposition products (acetylene, cyclopentadienyl radical), there might only be a small pool of C<sub>7</sub>H<sub>7</sub> radicals. Consequently detection of C<sub>7</sub>H<sub>7</sub> could be very difficult. As a result, the implications of Fig. 6.14 are not completely clear at this time.

## References for Chapter 6

- [1] M. Szwarc. The C-H bond energy in toluene and xylenes. *Journal of Chemical Physics* **1948**, *16*, 128-136.
- [2] R. D. Smith. Direct mass-spectrometric study of the mechanism of toluene pyrolysis at high-temperatures. *Journal of Physical Chemistry* **1979**, *83*, 1553-1556.
- [3] D. C. Astholz, L. Brouwer and J. Troe. High-temperature ultraviolet-absorption spectra of polyatomic-molecules in shock-waves. *Berichte Der Bunsen-Gesellschaft-Physical Chemistry Chemical Physics* **1981**, *85*, 559-564.
- [4] D. C. Astholz and J. Troe. Thermal-decomposition of benzyl radicals in shock-waves. *Journal of the Chemical Society-Faraday Transactions II* **1982**, *78*, 1413-1421.
- [5] L. Brouwer, W. Müller-Markgraf and J. Troe. Thermal-decomposition of ethylbenzene in shock-waves. *Berichte Der Bunsen-Gesellschaft-Physical Chemistry Chemical Physics* **1983**, *87*, 1031-1036.
- [6] V. S. Rao and G. B. Skinner. Formation of hydrogen atoms in pyrolysis of ethylbenzene behind shock waves. Rate constants for the thermal dissociation of the benzyl radical. *Proceedings of the Combustion Institute* **1986**, *21*, 809-814.
- [7] A. H. Laufer. An excited-state of acetylene - photochemical and spectroscopic evidence. *Journal of Chemical Physics* **1980**, *73*, 49-52.
- [8] A. H. Laufer and A. Fahr. Reactions and kinetics of unsaturated C<sub>2</sub> hydrocarbon radicals. *Chemical Reviews* **2004**, *104*, 2813-2832.
- [9] R. Fröchtenicht, H. Hippler, J. Troe and J. P. Toennies. Photon-induced unimolecular decay of the benzyl radical - 1<sup>st</sup> direct identification of the reaction pathway to C<sub>7</sub>H<sub>6</sub>. *Journal of Photochemistry and Photobiology a-Chemistry* **1994**, *80*, 33-37.
- [10] M. Braun-Unkhoff, P. Frank and T. Just. High-temperature reactions of benzyl radicals. *Berichte Der Bunsen-Gesellschaft-Physical Chemistry Chemical Physics* **1990**, *94*, 1417-1425.
- [11] R. Sivaramakrishnan, M. C. Su and J. V. Michael. H- and D-atom formation from the pyrolysis of C<sub>6</sub>H<sub>5</sub>CH<sub>2</sub>Br and C<sub>6</sub>H<sub>5</sub>CD<sub>2</sub>Br: Implications for high-

- temperature benzyl decomposition. *Proceedings of the Combustion Institute* **2011**, 33, 243-250.
- [12] J. Jones, G. B. Bacskay and J. C. Mackie. Decomposition of the benzyl radical: Quantum chemical and experimental (shock tube) investigations of reaction pathways. *Journal of Physical Chemistry A* **1997**, 101, 7105-7113.
- [13] G. da Silva and J. W. Bozzelli. Benzoyl Radical Decomposition Kinetics: Formation of Benzaldehyde plus H, Phenyl + CH<sub>2</sub>O, and Benzene plus HCO. *Journal of Physical Chemistry A* **2009**, 113, 6979-6986.
- [14] C. Cavallotti, M. Derudi and R. Rota. On the mechanism of decomposition of the benzyl radical. *Proceedings of the Combustion Institute* **2009**, 32, 115-121.
- [15] G. da Silva. Oxidation of Carboxylic Acids Regenerates Hydroxyl Radicals in the Unpolluted and Nighttime Troposphere. *Journal of Physical Chemistry A* **2010**, 114, 6861-6869.
- [16] G. da Silva, A. J. Trevitt, M. Steinbauer and P. Hemberger. Pyrolysis of fulvenallene (C<sub>7</sub>H<sub>6</sub>) and fulvenallenyl (C<sub>7</sub>H<sub>5</sub>): Theoretical kinetics and experimental product detection. *Chemical Physics Letters* **2011**, 517, 144-148.
- [17] G. da Silva and A. J. Trevitt. Chemically activated reactions on the C<sub>7</sub>H<sub>5</sub> energy surface: propargyl plus diacetylene, i-C<sub>5</sub>H<sub>3</sub> + acetylene, and n-C<sub>5</sub>H<sub>3</sub> + acetylene. *Physical Chemistry Chemical Physics* **2011**, 13, 8940-8952.
- [18] D. Polino and C. Cavallotti. Fulvenallene Decomposition Kinetics. *Journal of Physical Chemistry A* **2011**, 115, 10281-10289.
- [19] D. Polino, A. Famulari and C. Cavallotti. Analysis of the Reactivity on the C<sub>7</sub>H<sub>6</sub> Potential Energy Surface. *Journal of Physical Chemistry A* **2011**, 115, 7928-7936.
- [20] M. Steinbauer, P. Hemberger, I. Fischer and A. Bodi. Photoionization of C<sub>7</sub>H<sub>6</sub> and C<sub>7</sub>H<sub>5</sub>: Observation of the Fulvenallenyl Radical. *Chem phys chem* **2011**, 12, 1795-1797.
- [21] J. Giegerich and I. Fischer. Photodissociation dynamics of fulvenallene, C<sub>7</sub>H<sub>6</sub>. *Physical Chemistry Chemical Physics* **2013**, 15, 13162-13168.

- [22] K. H. Fischer, P. Hemberger, A. Bodi and I. Fischer. Photoionisation of the tropyli radical. *Beilstein Journal of Organic Chemistry* **2013**, *9*, 681-688.
- [23] A. V. Friderichsen, E.-J. Shin, R. J. Evans, M. R. Nimlos, D. C. Dayton and G. B. Ellison. The Pyrolysis of Anisole (C<sub>6</sub>H<sub>5</sub>OCH<sub>3</sub>) Using a Hyperthermal Nozzle. *Fuel* **2001**, *80*, 1747-1755.
- [24] A. Vasiliou, M. R. Nimlos, J. W. Daily and G. B. Ellison. Thermal Decomposition of Furan Generates Propargyl Radicals. *Journal of Physical Chemistry A* **2009**, *113*, 8540-8547.
- [25] A. K. Vasiliou, J. H. Kim, T. K. Ormond, K. M. Piech, K. N. Urness, A. M. Scheer, D. J. Robichaud, C. Mukarakate, M. R. Nimlos, J. W. Daily, Q. Guan, H.-H. Carstensen and G. B. Ellison. Biomass Pyrolysis: Thermal Decomposition Mechanisms of Furfural and Benzaldehyde *Journal of Chemical Physics* **2013**, *139*, 104310.
- [26] A. M. Scheer, C. Mukarakate, D. J. Robichaud, M. R. Nimlos, H.-H. Carstensen and G. B. Ellison. Unimolecular Thermal Decomposition of Phenol and d<sub>5</sub>-Phenol: Direct Observation of Cyclopentadiene Formation via Cyclohexadienone. *Journal of Chemical Physics* **2012**, *136*, 044309-044320
- [27] A. M. Scheer, Ph.D. Thesis, *Thermal Decomposition Mechanisms of Lignin Model Compounds: From Phenol to Vanillin*, University of Colorado, Department of Chemistry and Biochemistry, **2011**
- [28] A. M. Scheer, C. Mukarakate, D. J. Robichaud, G. B. Ellison and M. R. Nimlos. Radical Chemistry in the Thermal Decomposition of Anisole and Deuterated Anisoles: An Investigation of Aromatic Growth. *Journal of Physical Chemistry A* **2010**, *114*, 9043-9056.
- [29] T. K. Ormond, A. M. Scheer, M. R. Nimlos, D. J. Robichaud, T. P. Troy, M. Ahmed, J. W. Daily, T. L. Nguyen, J. F. Stanton and G. B. Ellison. Pyrolysis of Cyclopentadienone: Mechanistic Insights from a Direct Measurement of Product Branching Ratios. *The Journal of Physical Chemistry A* **2015**, *119*, 7222-7234.
- [30] F. A. Houle and J. L. Beauchamp. Detection and investigation of allyl and benzyl radicals by photoelectron-spectroscopy. *Journal of the American Chemical Society* **1978**, *100*, 3290-3294.

- [31] G. C. Eiden, F. Weinhold and J. C. Weisshaar. Photoelectron-spectroscopy of free-radicals with  $\text{cm}^{-1}$  resolution - the benzyl cation. *Journal of Chemical Physics* **1991**, *95*, 8665-8668.
- [32] J. B. Pedley, R. D. Naylor and S. P. Kirby, *Thermochemistry of Organic Compounds*, Chapman and Hall, New York, **1986**, p. 87-222.
- [33] G. B. Ellison, G. E. Davico, V. M. Bierbaum and C. H. DePuy. Thermochemistry of the benzyl and allyl radicals and ions. *International Journal of Mass Spectrometry and Ion Processes* **1996**, *156*, 109-131.
- [34] R. F. Gunion, M. K. Gilles, M. L. Polak and W. C. Lineberger. Ultraviolet photoelectron-spectroscopy of the phenide, benzyl and phenoxide anions, with *ab initio* calculations. *International Journal of Mass Spectrometry and Ion Processes* **1992**, *117*, 601-620.
- [35] R. D. Johnson. Excited electronic states of the tropylium (*cyclo-C<sub>7</sub>H<sub>7</sub><sup>+</sup>*) radical. *Journal of Chemical Physics* **1991**, *95*, 7108-7113.
- [36] J. C. Traeger and R. G. McLoughlin. Threshold photoionization and dissociation of toluene and cycloheptatriene. *Journal of the American Chemical Society* **1977**, *99*, 7351-7352.
- [37] T. Ichino, S. W. Wren, K. M. Vogelhuber, A. J. Gianola, W. C. Lineberger and J. F. Stanton. The vibronic level structure of the cyclopentadienyl radical. *Journal of Chemical Physics* **2008**, *129*, 084310.
- [38] J. C. Poutsma, J. J. Nash, J. A. Paulino and R. R. Squires. Absolute heats of formation of phenylcarbene and vinylcarbene. *Journal of the American Chemical Society* **1997**, *119*, 4686-4697.
- [39] R. A. Seburg, B. T. Hill and R. R. Squires. Synthesis, properties and reactivity of the phenylcarbene anion in the gas phase. *Journal of the Chemical Society-Perkin Transactions 2* **1999**, 2249-2256.
- [40] J. A. Blush, P. Chen, R. T. Wiedmann and M. G. White. Rotationally resolved threshold photoelectron-spectrum of the methyl radical. *Journal of Chemical Physics* **1993**, *98*, 3557-3559.

- [41] S. T. Pratt, P. M. Dehmer and J. L. Dehmer. Zero-kinetic-energy photoelectron-spectroscopy from the A  $^1A_U$  state of acetylene - renner-teller interactions in the trans-bending vibration of  $C_2H_2^+ X^2\Pi_U$ . *Journal of Chemical Physics* **1993**, 99, 6233-6244.
- [42] H. Gao, Y. T. Xu, L. Yang, C. S. Lam, H. L. Wang, J. A. Zhou and C. Y. Ng. High-resolution threshold photoelectron study of the propargyl radical by the vacuum ultraviolet laser velocity-map imaging method. *Journal of Chemical Physics* **2011**, 135, 224304
- [43] H. J. Wörner and F. Merkt. Diradicals, antiaromaticity, and the pseudo-Jahn-Teller effect: Electronic and rovibronic structures of the cyclopentadienyl cation. *Journal of Chemical Physics* **2007**, 127, 034303.
- [44] X. Zhang and P. Chen. Photoelectron-spectrum of *o*-benzyne - ionization-potentials as a measure of singlet triplet gaps. *Journal of the American Chemical Society* **1992**, 114, 3147-3148.
- [45] V. Butcher, M. L. Costa, J. M. Dyke, A. R. Ellis and A. Morris. A study of the phenyl radical by vacuum ultraviolet photoelectron-spectroscopy. *Chemical Physics* **1987**, 115, 261-267.
- [46] S. Sato, T. Kojima, K. Byodo, H. Shinohara, S. Yanagihara and K. Kimura. ZEKE electron spectroscopy of alkylbenzene-argon van der Waals complexes. *Journal of Electron Spectroscopy and Related Phenomena* **2000**, 112, 247-255.
- [47] T. Baer, J. C. Morrow, J. D. Shao and S. Olesik. Gas-phase heats of formation of  $C_7H_7^+$  isomers - *meta*-tolyl, *para*-tolyl, and benzyl ions. *Journal of the American Chemical Society* **1988**, 110, 5633-5638.
- [48] X. Zhang, A. V. Friderichsen, S. Nandi, G. B. Ellison, D. E. David, J. T. McKinnon, T. G. Lindeman, D. C. Dayton and M. R. Nimlos. Intense, hyperthermal source of organic radicals for matrix-isolation spectroscopy. *Review of Scientific Instruments* **2003**, 74, 3077-3086.
- [49] N. P. Lockyer and J. C. Vickerman. Single photon ionisation mass spectrometry using laser-generated vacuum ultraviolet photons. *Laser Chemistry* **1997**, 17, 139-159.

- [50] J. Boyle and L. Pfefferle. Study of higher hydrocarbon production during ethylacetylene pyrolysis using laser-generated vacuum-ultraviolet photoionization detection. *Journal of Physical Chemistry* **1990**, *94*, 3336-3340.
- [51] R. E. Bandy, C. Lakshminarayan, R. K. Frost and T. S. Zwier. The Ultraviolet Photochemistry of Diacetylene - Direct Detection of Primary Products of the Metastable  $C_4H_2^* + C_4H_2$  Reaction. *Journal of Chemical Physics* **1993**, *98*, 5362-5374.
- [52] M. Johnson, A. Bodi, L. Schulz and T. Gerber. Vacuum ultraviolet beamline at the Swiss Light Source for chemical dynamics studies. *Nuclear Instruments & Methods in Physics Research Section a-Accelerators Spectrometers Detectors and Associated Equipment* **2009**, *610*, 597-603.
- [53] A. Bodi, M. Johnson, T. Gerber, Z. Gengeliczki, B. Sztaray and T. Baer. Imaging photoelectron photoion coincidence spectroscopy with velocity focusing electron optics. *Review of Scientific Instruments* **2009**, *80*, 034101.
- [54] P. Chen, S. D. Colson, W. A. Chupka and J. A. Berson. Flash Pyrolytic Production of Rotationally Cold Free-Radicals in a Supersonic Jet - Resonant Multiphoton Spectrum of the  $3P^2A_2''$  Origin Band of  $CH_3$ . *Journal of Physical Chemistry* **1986**, *90*, 2319-2321.
- [55] D. W. Kohn, H. Clauberg and P. Chen. Flash Pyrolysis Nozzle for Generation of Radicals in a Supersonic Jet Expansion. *Review of Scientific Instruments* **1992**, *63*, 4003-4005.
- [56] J. A. Blush, H. Clauberg, D. W. Kohn, D. W. Minsek, X. Zhang and P. Chen. Photoionization Mass and Photoelectron-Spectroscopy of Radicals, Carbenes, and Biradicals. *Accounts Chem. Res.* **1992**, *25*, 385-392.
- [57] P. Chen *Supersonic Jets of Organic Radicals*, Eds.: C. Y. Ng, T. Baer and I. Powis, John Wiley, Cambridge, UK, **1994**, pp. 371-397.
- [58] H. W. Rohrs, C. T. Wickham-Jones, D. Berry, G. B. Ellison and B. M. Argrow. FTIR Absorption Spectroscopy of Jet-Cooled Radicals. *Review of Scientific Instruments* **1995**, *66*, 2430.
- [59] Q. Guan, K. N. Urness, T. K. Ormond, D. E. David, G. B. Ellison and J. W. Daily. The Properties of a Micro-Reactor for the Study of the Unimolecular Decomposition of Large Molecules. *International Reviews in Physical Chemistry* **2014**, *33*, 447-487.

- [60] C. L. Angell. Vapor-phase infrared spectrum and structure of fulvenallene. *Journal of Molecular Structure* **1971**, *10*, 265-273.
- [61] E. B. Jochowitz, X. Zhang, M. R. Nimlos, M. E. Varner, J. F. Stanton and G. B. Ellison. Propargyl Radical: *ab initio* Anharmonic Modes and the Polarized Infrared Absorption Spectra of Matrix-Isolated HCCCH<sub>2</sub>. *Journal of Physical Chemistry A* **2005**, *109*, 3812-3821.
- [62] E. G. Baskir, A. K. Maltsev, V. A. Korolev, V. N. Khabashesku and O. M. Nefedov. Generation and ir spectroscopic study of benzyl radical. *Russian Chemical Bulletin* **1993**, *42*, 1438-1440.
- [63] B. E. Applegate, A. J. Bezant and T. A. Miller. The Jahn-Teller and related effects in the cyclopentadienyl radical. II. Vibrational analysis of the A <sup>2</sup>A<sub>2</sub>" - X <sup>2</sup>E<sub>1</sub>" electronic transition. *Journal of Chemical Physics* **2001**, *114*, 4869-4882.
- [64] J. D. Savee, Private communication, 2014
- [65] A. Vasiliou, K. M. Piech, X. Zhang, M. R. Nimlos, M. Ahmed, O. Kostko, A. Golan, D. L. Osborn, J. W. Daily, J. F. Stanton and G. B. Ellison. The products of the thermal decomposition of CH<sub>3</sub>CHO. *Journal of Chemical Physics* **2011**, *135*, 14306-14311.
- [66] K. N. Urness, Q. Guan, A. Golan, J. W. Daily, M. R. Nimlos, J. F. Stanton, M. Ahmed and G. B. Ellison. Pyrolysis of Furan in a Microreactor *Journal of Chemical Physics* **2013**, *139*, 124305-124314
- [67] D. M. Golden. Yet another look at the reaction CH<sub>3</sub> + H + M = CH<sub>4</sub> + M. *International Journal of Chemical Kinetics* **2008**, *40*, 310-319.
- [68] L. D. Brouwer, W. Müller-Markgraf and J. Troe. Thermal-decomposition of toluene - a comparison of thermal and laser-photochemical activation experiments. *Journal of Physical Chemistry* **1988**, *92*, 4905-4914.
- [69] L. V. Moskaleva and M. C. Lin. Unimolecular isomerization/decomposition of cyclopentadienyl and related bimolecular reverse process: Ab initio MO/statistical theory study. *Journal of Computational Chemistry* **2000**, *21*, 415-425.





## Chapter 7

### The Thermal Decomposition of the Benzyl Radical in a Heated Micro-Reactor: II. Pyrolysis of the Tropyl Radical

#### Abstract

Cycloheptatrienyl (tropyl) radical,  $C_7H_7$ , was cleanly produced in the gas-phase and subjected to pyrolysis in a set of flash-pyrolysis micro-reactors. The pyrolysis products resulting from  $C_7H_7$  were detected and identified by vacuum ultraviolet photoionization mass spectrometry. Complementary product identification was provided by infrared absorption spectroscopy. Pyrolysis pressures in the micro-reactor were roughly 200 Torr and residence times in the micro-reactors were approximately 100  $\mu$ sec. At 1100 K, pyrolysis begins and the products from pyrolysis of tropyl radicals are only acetylene and cyclopentadienyl radicals. Tropyl radicals do not isomerize to benzyl radicals at reactor temperatures up to 1600 K. Heating samples of either cycloheptatriene or norbornadiene never produced tropyl ( $C_7H_7$ ) radicals but rather only benzyl ( $C_6H_5CH_2$ ). The thermal decomposition of benzyl radicals has been reconsidered without participation of tropyl radicals. There are at least three distinct pathways for pyrolysis of benzyl radical: the Benson Fragmentation, the methyphenyl radical, and the bridgehead norbornadienyl radical. These three pathways account for the majority of the products detected following pyrolysis of all of the isotopomers:  $C_6H_5CH_2$ ,  $C_6H_5CD_2$ ,  $C_6D_5CH_2$ , and  $C_6H_5^{13}CH_2$ .

## I. Introduction

Resonance stabilized radicals are important in combustion processes because they are precursors to soot formation. Modern transportation fuels include a large number<sup>[1]</sup> of aromatics (benzene, toluene, xylenes, alkylbenzenes and the like); see Fig. 3 of ref.<sup>[2]</sup>. Consequently, benzyl radicals ( $C_6H_5CH_2$ ) are important intermediates in the high-temperature oxidation of these fuels. The pyrolysis of the benzyl radical has recently been examined<sup>[3-5]</sup> and evidence was found for several complex decomposition pathways. Fig. 1 is an overview<sup>[5]</sup> of the products that were detected following the pyrolysis of the  $C_6H_5CH_2$  radical. A pathway for fragmentation of benzyl radical to fulvenallene and the fulvenallenyl radical was suggested<sup>[6]</sup> by Benson in 1986. An isomer of the benzyl radical is the cycloheptatrienyl (or tropylium) radical,  $C_7H_7$ . The relationship of tropylium to the benzyl radical is shown in Fig. 7.1. In the early literature, the interconversion of benzyl to tropylium ( $C_6H_5CH_2 \rightleftharpoons C_7H_7$ ) was considered by several groups.<sup>[7-13]</sup> However all recent theoretical studies<sup>[14-16]</sup> find no pathways below 2000 K for the isomerization of benzyl to tropylium. A photoionization search for the isomerization of the  $C_6H_5CD_2$  benzyl radical to the  $C_7H_5D_2$  tropylium radical with tunable VUV radiation found no evidence for tropylium radical formation.<sup>[5]</sup> To date, there are no experimental studies of the thermal decomposition of the tropylium radical,  $C_7H_7 (+ M) \rightarrow$  products.

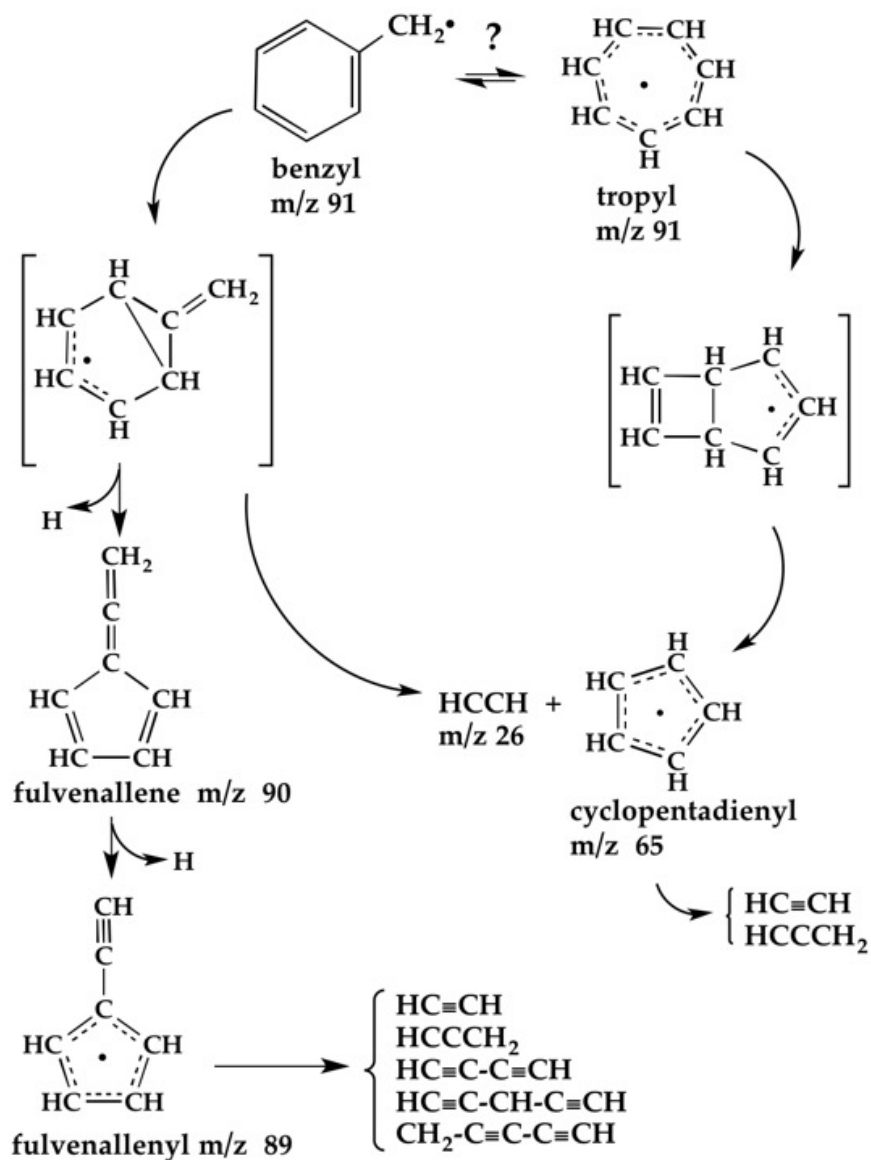


**Fig. 7.1** The Benson Pathway<sup>[6]</sup> for the pyrolysis of benzyl radical<sup>[5]</sup> is shown. A possible link of the  $\text{C}_6\text{H}_5\text{CH}_2$  radical to the  $\text{C}_7\text{H}_7$  radical is indicated.

The focus of this chapter is to generate authentic samples of the tropylium radical and to examine the pyrolysis pathways:  $\text{C}_7\text{H}_7 (+ \text{M}) \rightarrow$  products. Earlier photoionization studies<sup>[17]</sup> of the  $\text{C}_7\text{H}_7$  radical found bitropylium,  $\text{C}_7\text{H}_7-\text{C}_7\text{H}_7$ , to be a convenient thermal precursor for tropylium. As sources of tropylium radicals, we have investigated the flash-

pyrolysis of bitropyl, cycloheptatriene, and norbornadiene. The hydrocarbon samples were diluted in a carrier gas of He or Ar and subjected to pyrolysis in a heated silicon carbide (SiC) micro-reactor. The micro-reactor was resistively heated to temperatures up to 1600 K and operated at pressures of roughly 200 Torr. Approximate residence times<sup>[18]</sup> in the reactor are 100  $\mu$ sec after which the gas mixture exits into a vacuum chamber at a pressure of  $10^{-6}$  Torr. The resulting pyrolysis products are entrained in a molecular beam and are analyzed by a combination of photoionization mass spectroscopy (PIMS) and matrix infrared (IR) absorption spectroscopy.

Because of its importance in organic chemistry, atmospheric chemistry, and combustion processes, the benzyl radical ( $C_6H_5CH_2, \tilde{X}^2B_1$ ) has been extensively studied and a list of its properties is collected in Table 1 of ref.<sup>[5]</sup> The tropyli radical ( $C_7H_7, \tilde{X}^2E_2''$ ) is not as well characterized experimentally. Because the tropyli radical has no electric dipole moment, there are no microwave spectra. To date, there are published laser induced fluorescence (LIF) spectra<sup>[9-10]</sup> of the tropyli radical, an IR-UV double resonance study with a free electron laser,<sup>[13]</sup> and preliminary helium nanodroplet IR absorption spectra,<sup>[19]</sup> but there is no definitive analysis of the infrared spectrum of  $C_7H_7$ . Some of the available experimental properties of the tropyli radical are summarized in Table 7.1.

## Tropyl and Benzyl Radical Experimental Properties

$\Delta_f H_{298}(\text{C}_7\text{H}_8)$	43.2	$\pm 0.5$	kcal mol <sup>-1</sup>	[20]
	(181	$\pm 2$	kJ mol <sup>-1</sup> )	
$\Delta_f H_{298}(\text{C}_7\text{H}_7, \tilde{X}^2E_2'')$	65.0	$\pm 0.7$	kcal mol <sup>-1</sup>	[20]
	(272	$\pm 3$	kJ mol <sup>-1</sup> )	
$DH_{298}(\text{C}_7\text{H}_7\text{-H})$	73.9	$\pm 0.5$	kcal mol <sup>-1</sup>	[21]
	(309	$\pm 2$	kJ mol <sup>-1</sup> )	
$\Delta_f H_{298}(\text{C}_6\text{H}_5\text{CH}_3)$	12.0	$\pm 0.1$	kcal mol <sup>-1</sup>	[20]
	(50.4	$\pm 0.6$	kJ mol <sup>-1</sup> )	
$\Delta_f H_{298}(\text{C}_6\text{H}_5\text{CH}_2, \tilde{X}^2B_1)$	49.6	$\pm 0.6$	kcal mol <sup>-1</sup>	[20, 22]
	(208	$\pm 3$	kJ mol <sup>-1</sup> )	
$DH_{298}(\text{C}_6\text{H}_5\text{CH}_2\text{-H})$	89.8	$\pm 0.6$	kcal mol <sup>-1</sup>	[20, 22]
	(376	$\pm 3$	kJ mol <sup>-1</sup> )	
$\Delta_f H_{298}(\text{norbornadiene}, \text{C}_7\text{H}_8)$	58.8	$\pm 0.7$	kcal mol <sup>-1</sup>	[20]
	(246	$\pm 3$	kJ mol <sup>-1</sup> )	
$\Delta_f H_{298}(\text{C}_5\text{H}_6)$	32.1	$\pm 0.4$	kcal mol <sup>-1</sup>	[20]
	(134	$\pm 2$	kJ mol <sup>-1</sup> )	
$\Delta_f H_{298}(\text{C}_5\text{H}_5, \tilde{X}^2E_1'')$	63	$\pm 1$	kcal mol <sup>-1</sup>	[23]
	(264	$\pm 6$	kJ mol <sup>-1</sup> )	
$DH_{298}(\text{C}_5\text{H}_5\text{-H})$	83	$\pm 1$	kcal mol <sup>-1</sup>	[20, 23]
	(348	$\pm 6$	kJ mol <sup>-1</sup> )	
$DH_{298}(\text{C}_6\text{H}_5\text{-H})$	112.9	$\pm 0.5$	kcal mol <sup>-1</sup>	[20, 22]
	(472	$\pm 2$	kJ mol <sup>-1</sup> )	
$\Delta_{\text{rxn}} H_{298}(\text{C}_7\text{H}_7 \rightarrow \text{HC}\equiv\text{CH} + \text{C}_5\text{H}_5)$	53	$\pm 2$	kcal mol <sup>-1</sup>	[5]
	(220	$\pm 7$	kJ mol <sup>-1</sup> )	
$AE(\text{C}_7\text{H}_8 \rightarrow \text{C}_7\text{H}_7^+ + \text{H})$	9.36	$\pm 0.02$	eV	[21]
$\Delta_{\text{isomeriz'n}} H_{298}(\text{C}_6\text{H}_5\text{CH}_2, \tilde{X}^2B_1 \rightarrow \text{C}_7\text{H}_7, \tilde{X}^2E_2'')$	15.3	$\pm 0.9$	kcal mol <sup>-1</sup>	[5]
	(64	$\pm 4$	kJ mol <sup>-1</sup> )	

## Important Ionization Energies

$\text{CH}_3$	9.8380	$\pm 0.0004$	eV	[24]
---------------	--------	--------------	----	------

HC≡CH	11.40081 ± 0.00001 eV	[25]
HCCCH <sub>2</sub>	8.7006 ± 0.0002 eV	[26]
CH <sub>2</sub> CHCH <sub>2</sub>	8.13146 ± 0.00025 eV	[27-28]
<i>o</i> -C <sub>6</sub> H <sub>4</sub>	9.03 ± 0.05 eV	[29]
C <sub>5</sub> H <sub>5</sub>	8.4268 ± 0.0005 eV	[30]
C <sub>5</sub> H <sub>4</sub> -C≡CH	8.19 ± 0.02 eV	[31]
C <sub>5</sub> H <sub>4</sub> =C=CH <sub>2</sub>	8.22 ± 0.01 eV	[31]
C <sub>7</sub> H <sub>7</sub> , $\tilde{X}^2E_2''$	6.221 ± 0.006 eV	[7, 17]
C <sub>6</sub> H <sub>5</sub> CH <sub>2</sub> , $\tilde{X}^2B_1$	7.2487 ± 0.0006 eV	[28, 32]
C <sub>6</sub> H <sub>5</sub> CH <sub>3</sub>	8.8276 ± 0.0006 eV	[33]
C <sub>7</sub> H <sub>8</sub> (cycloheptatriene)	8.29 ± 0.01 eV	[34]
C <sub>7</sub> H <sub>8</sub> (2, 5 norbornadiene)	≤ 8.35 ± 0.01 eV	[34]

Table 7.1. Experimental properties of tropyli and benzyl radicals and important ionization energies.

This chapter will demonstrate that pyrolysis of the tropyli radical only produces acetylene and the cyclopentadienyl radical. Tropyli radical does not isomerize to benzyl radical under any conditions observed in this work. As part of the final Discussion, we will reconsider the thermal cracking of the C<sub>6</sub>H<sub>5</sub>CH<sub>2</sub> radical in the absence of C<sub>7</sub>H<sub>7</sub>. We present three separate pathways for the pyrolysis of the benzyl radical that seem to account for all of the current experimental findings, C<sub>6</sub>H<sub>5</sub>CH<sub>2</sub> (+ M) → products.

## II. Experimental

### A. Heated Micro-Reactor Pyrolysis Source

To carry out flash-pyrolysis of target molecules, we employ a resistively heated silicon carbide (SiC) reactor with an inner diameter (I.D.) of either 1.0 mm or 0.6 mm and a relatively short heated length, 10 to 15 mm. This geometry along with the present flow conditions allows<sup>[18]</sup> for short residence times of around 100  $\mu$ s. At the exit of the reactor the gas is cooled as it expands into a vacuum chamber pumped to  $10^{-4}$  to  $10^{-6}$  Torr, where reactive collisions cease. To monitor the temperature of the reactor, a Type-C thermocouple is attached to the reactor's outer wall using tantalum wire as described previously.<sup>[35]</sup> The fluid mechanics of the heated micro-reactors were the subject of a recent detailed computational fluid dynamics investigation<sup>[18]</sup> that modeled the pressure and temperature in the reactor at wall temperatures up to 1600 K. The findings in this study show that for a given set of reactor conditions and kinetic parameters, decomposition occurs within a small "sweet-spot" that can be as small as only a few mm of the total heated length. Another key finding was that the temperature, pressure, and thus decomposition rates can vary dramatically upon varying the experimental parameters, including: 1) carrier gas (argon, neon, and helium are all commonly used), 2) upstream and downstream pressure, and 3) mass flow rate, which can be controlled either by use of commercial mass flow controllers or with a pulsed valve. Therefore when comparing results from different experimental techniques, some variation is expected for the onset temperature of decomposition and/or the product ratios of competing decomposition pathways.



## B. Photoionization Mass Spectroscopy

### i. Pulsed Vacuum Ultraviolet Radiation

The 355 nm output light of a commercial Nd:YAG laser (Spectra Physics Pro-230-10) is focused into a tripling cell filled to 150 Torr with a 10:1 mixture of argon:xenon, which produces 118.2 nm (10.487 eV) photons. At the exit of the tripling cell is a MgF<sub>2</sub> lens used to focus the 118.2 nm light into the interaction region of the Jordan time-of-flight spectrometer. This tripling process has been well-studied<sup>[36]</sup> and has an efficiency<sup>[37-38]</sup> of around  $1 \times 10^{-5}$ . Additional losses are introduced by incomplete transmission of 118.2 nm light through the Mg<sub>2</sub>F lens and intentional off-axis alignment through the lens to spatially separate 118.2 nm light from the remaining 355 nm light that exits the tripling cell, which can cause unwanted multiphoton ionization. As a result, laser powers of 30 mJ pulse<sup>-1</sup> at 355 nm yield roughly 30 nJ pulse<sup>-1</sup> of 118.2 nm. The region where the ionizing radiation and molecular beam are intersected is maintained at 10<sup>-7</sup> Torr by a turbomolecular pump. Any molecule with ionization energy less than 10.487 eV is ionized and the resulting ions are accelerated into a reflectron time-of-flight spectrometer. In order to sustain sufficiently low pressure to maintain collisionless conditions, the gas flow must be pulsed with a Parker general valve operating at 10 Hz with 1 ms opening time. Backing pressures behind the pulsed valve are typically 2000 Torr of helium carrier gas and the pressure downstream of the reactor is typically 10<sup>-6</sup> Torr, maintained by an 11-inch diffusion pump. Spectra shown in this work are the result of signal averaging of 1000 scans.

## ii. Continuous Vacuum Ultraviolet Radiation

A similar experimental setup for the micro-reactor scheme is used at the Chemical Dynamics Beamline endstation (9.0.2) at the Advanced Light Source (ALS) in the Lawrence Berkeley National Laboratory. Using the synchrotron light for PIMS adds the experimental degree of freedom — tunable photon energy.<sup>[39]</sup> The energy of the synchrotron photons can be tuned between 7.4 eV and 30 eV, sufficiently high to ionize all species produced in the heated reactor. By measuring ion current at a single mass-to-charge ratio ( $m/z$ ) while varying the photon energy and normalizing to the measured VUV power, it is possible to record photoionization spectra, which can be used to identify individual isomers that may be present. Signal averaging is used to increase signal-to-noise ratio; typical spectra are the composite of between  $5 \times 10^4$  and  $2 \times 10^5$  sweeps. To control the flow of gas through the reactor, an MKS mass flow controller is used along with a slightly smaller SiC reactor with an I.D. of 0.6 mm. Typical flow conditions include setting the flow controller to 200 standard  $\text{cm}^3 \text{min}^{-1}$  (SCCM) backed by 5 atm of He. This yields pressures of 100 Torr between the mass flow controller and entrance of the reactor and roughly  $10^{-4}$  Torr at the exit of the nozzle. With a 1 mm skimmer, the pressure in the ionization chamber can be maintained at roughly  $5 \times 10^{-6}$  Torr by a large turbomolecular pump.

## C. Matrix Isolation Fourier Transform Infrared Spectroscopy

Since all polyatomic molecules possess characteristic vibrational spectra, IR spectroscopy is an excellent technique for identifying molecular species and serves as a valuable complement to the PIMS experiments. The matrix IR spectrometer has been

described before.<sup>[40-41]</sup> Briefly, a 1 mm I.D. SiC reactor is coupled to a pulsed valve assembly very similar to the PIMS system described above. The upstream pressure is between 800 and 1000 Torr, and with the pulsed valve operating with a roughly 1 ms opening time and 15 Hz repetition rate, the pressure at the reactor exit is typically  $10^{-6}$  Torr, which is maintained with a small turbomolecular pump. The output of the reactor impinges on a cryogenically cooled CsI window 4 cm downstream that is maintained at 5 K by a helium cryostat. The carrier gas for this experiment is neon, which condenses into a solid matrix upon colliding with the 5 K window. A standard matrix is formed by flowing 200 Torr of sample mixture from a roughly 3 L gas manifold, which leads to a deposition time of around one hour. After dosing is complete, the reactor assembly is rotated  $90^\circ$  out of the way and the CsI window is lowered into the beampath of a commercial Fourier transform IR spectrometer (Nicolet 6700). The MCT-A detector has a spectral range of 4000 to  $600\text{ cm}^{-1}$  and is operated with  $0.25\text{ cm}^{-1}$  resolution, with typical spectra constructed by averaging 500 scans. Although the neon matrix is chemically inert, it does affect the vibrational spectra of entrained molecules. Average matrix shifts are on the order of 1 to  $5\text{ cm}^{-1}$  from the unperturbed, gas-phase values.

#### D. Sample Preparation

Pyrolysis of bitropyl (7,7'-bi(1,3,5-cycloheptatriene)) is a good source of the tropyli radical.<sup>[17]</sup> Cleavage of the C-C bond produces two tropyli radicals.



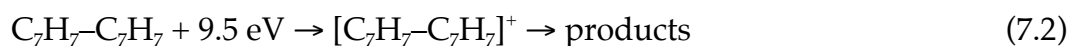
The bond energy,  $DH_{298}(\text{C}_7\text{H}_7\text{-C}_7\text{H}_7)$ , was measured<sup>[42]</sup> to be  $43 \pm 1\text{ kcal mol}^{-1}$  ( $1.86 \pm 0.05\text{ eV}$ ). Bitropyl is solid at room temperature and was purchased from Sigma-Aldrich and

used without further purification. Another tropyli precursor, cycloheptatriene ( $C_7H_8$ ), was explored. The C-H bond strength<sup>[21]</sup> of cycloheptatriene is 74 kcal mol<sup>-1</sup> and this implies that  $C_7H_8$  could be an attractive thermal precursor for tropyli radical; see Table 7.1. Cycloheptatriene is a liquid at room temperature and was purchased from Sigma-Aldrich with a purity of 95 % and used without further purification. A final potential precursor for tropyli radical to be considered is 2,5-norbornadiene. This hydrocarbon was purchased from Sigma-Aldrich with 98 % purity and was used without further purification. All of the pyrolysis experiments use dilute gas samples with either helium or neon as the carrier gas. Previous work with SiC reactors<sup>[5, 43-44]</sup> has shown that bimolecular chemistry can obscure decomposition spectra so samples were made as dilute as possible while maintaining sufficient signal-to-noise. Typical dilutions are 0.1 – 0.01 %. For some experiments the dilution is difficult to control because the solid bitropyli precursor must be heated to 50 – 65 °C to achieve sufficient vapor pressure, depending on the gas flow rate and amount of sample surface area present. At the ALS, the sample was heated in a 1 cm I.D. glass test tube and He carrier gas was directed over the surface before traveling downstream to the reactor. The matrix IR experiments make use of a 1 mm I.D. glass vial that is inserted directly behind the pulse valve, where it is then heated. Pyrolysis appears to be unimolecular since no change in products was observed over a range of sample temperatures.

### III. Results and Discussion

#### A. Photoionization Mass Spectrometry

Fig. 7.2 shows the 9.5 eV PIMS that results from a dilute sample of bitropyl heated to 600 K in a continuous flow micro-reactor. Earlier threshold photoelectron spectra of bitropyl reported<sup>[17]</sup> ions at both  $m/z$  91 and 182 with VUV photons of 8.7 eV. The 9.5 eV spectrum in Fig. 7.2 shows signals at  $m/z$  91 and 104 only; there are no parent ions at  $m/z$  182 indicating that the bitropyl sample is completely dissociatively ionized.



The  $m/z$  91 ion is  $\text{C}_7\text{H}_7^+$  while the smaller feature at  $m/z$  104 remains unidentified. The results in Fig. 7.2 are consistent with earlier PIMS studies<sup>[42]</sup> that revealed the appearance energy for the  $\text{C}_7\text{H}_7^+$  ion from bitropyl was  $8.09 \pm 0.05$  eV. The extensive dissociative ionization in Fig. 7.2 results from the fragmentation of the  $[\text{C}_7\text{H}_7\text{-C}_7\text{H}_7]^+$  cation into a pair of exceptionally stable products:  $\tilde{X}^2\text{E}_2''$   $\text{C}_7\text{H}_7$  and  $\tilde{X}^+{}^1\text{A}_1'$   $\text{C}_7\text{H}_7^+$ , which is an aromatic cation.

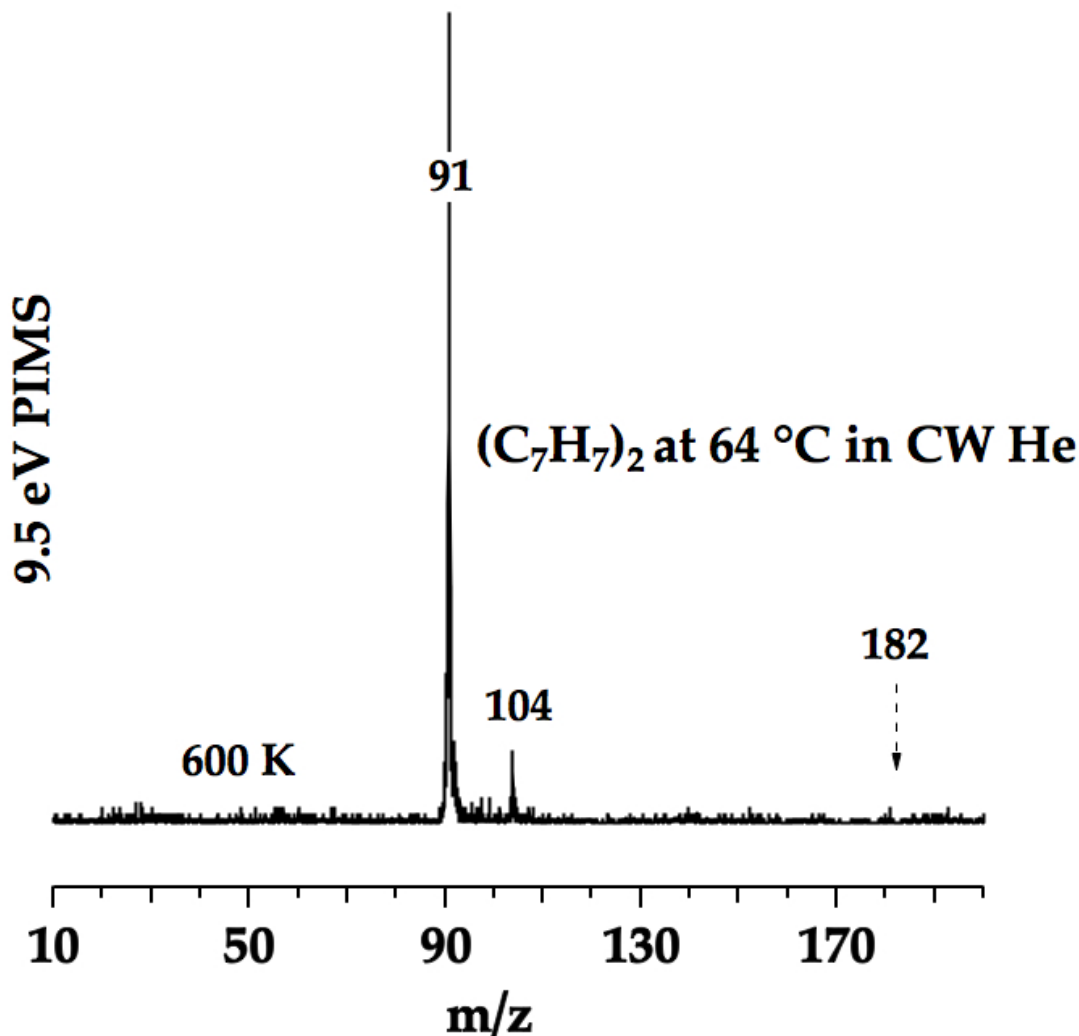
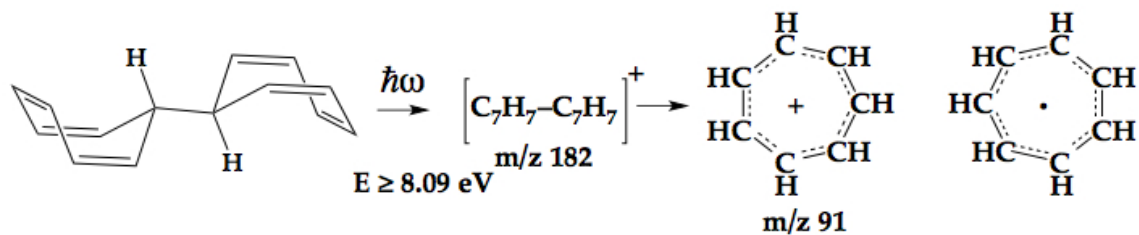
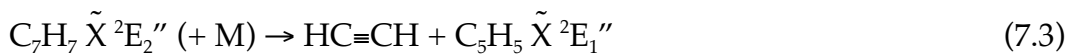


Fig. 7.2. The 9.5 eV PIMS spectra of bitropyl ( $\text{C}_7\text{H}_7\text{-C}_7\text{H}_7$   $m/z$  182) pyrolyzed in a continuous flow micro-reactor heated to 600 K. The absence of a signal at  $m/z$  182 indicates that the bitropyl sample is dissociatively ionized. The feature at 104 is the result of dissociative ionization of the precursor and is probably  $[\text{styrene}]^+$ .

Fig. 7.3 shows the PIMS spectra that result as bitropyl is heated in the micro-reactor up to 1500 K. As the sample is heated to 1100 K, the 11.8 eV PIMS reveals the

appearance of a peak at  $m/z$  26 (circled in red) that is shown to be  $\text{HCCH}^+$  by PIE spectra. The signal at  $m/z$  65 is assigned to  $\text{C}_5\text{H}_5^+$  via PIE spectra at reactor temperatures of 1100 K and higher. At temperature below 1100 K, signals at  $m/z$  65 arise from dissociative ionization. Since the ionization energy of acetylene is so large (11.4 eV, see Table 7.1), signal at  $m/z$  26 will only arise from photoionization of thermally produced acetylene and not from dissociative ionization. When molecules are ionized with excess photon energy, cations are formed with internal energy that can fragment to a daughter ion and a neutral fragment(s). By recording PIMS at 11.8 eV, we conclude that the feature at  $m/z$  65 results from dissociative ionization whenever the co-produced fragment,  $\text{HC}\equiv\text{CH}$ , is not detected. At 1100 K and hotter, the spectra imply thermal cracking of tropylium to acetylene and cyclopentadienyl.



As the reactor temperature is increased to 1500 K, the pyrolysis of tropylium radical is complete and  $m/z$  91 is no longer present. At 1400 K, a 10.0 eV PIMS signal at  $m/z$  39 is detected that is assigned to propargyl radical; the  $IE(\text{HCCCH}_2)$  is 8.7 eV (see Table 7.1). In earlier studies,<sup>[5, 45-46]</sup> it was observed that at 1300 K the cyclopentadienyl radical thermally dissociates to propargyl radical and acetylene.



$(C_7H_7)_2$  at 64 °C in CW Helium

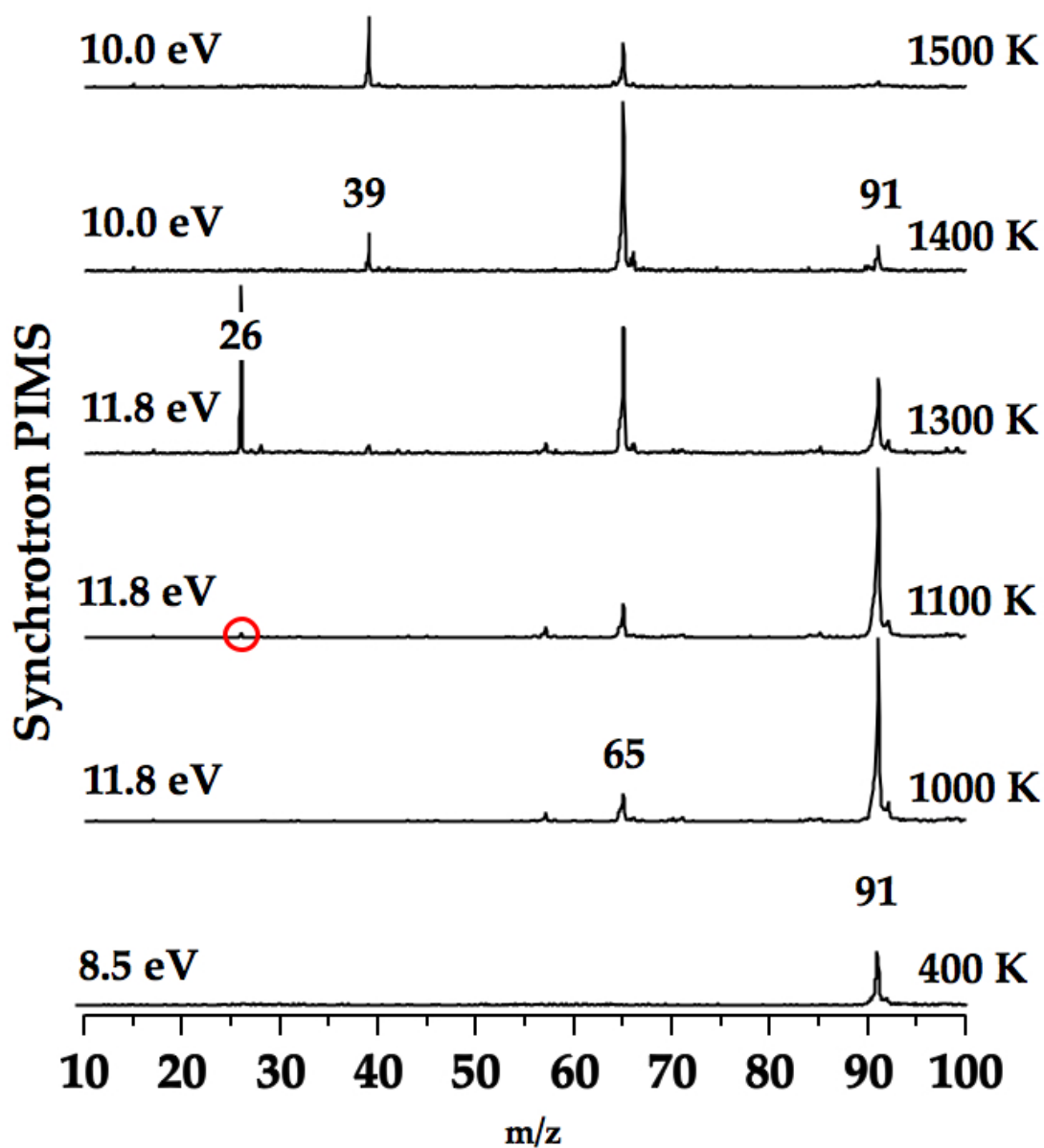


Fig. 7.3. PIMS spectra of bitropyl ( $C_7H_7-C_7H_7$ ) recorded in a continuous flow micro-reactor at temperatures of: 400 K, 1100 K, 1200 K, 1300 K, 1400 K, and 1500 K. Pyrolysis of tropyl ( $C_7H_7 (+ M) \rightarrow HC\equiv CH + C_5H_5$ ) commences at 1100 K as indicated by the small signal for  $HC\equiv CH^+$  at  $m/z$  26 (denoted with a red circle).



The thermal decomposition of the tropyli radical from 1200 K up to 1500 K is remarkably simple. We observe features at  $m/z$  65 and 26 that are predicted to be cyclopentadienyl and acetylene, consistent with eq. (7.3) and Fig. 7.1. To confirm the identity of the feature at  $m/z$  65, the PIE spectrum of  $m/z$  65 was recorded between 8.0 and 10.5 eV; see Fig. 7.4. At 900 K and below, there is no signal for PIE( $m/z$  65). At temperatures of 1200 K and above, the PIE for  $m/z$  65 shows a threshold at  $8.5 \pm 0.1$  eV, consistent with the observed<sup>[30]</sup>  $IE(C_5H_5)$  of 8.4 eV (see Table 7.1). The PIE( $m/z$  65) at 1200 K and 1500 K in Fig. 7.4 agree with the PIE of an authentic sample<sup>[47]</sup> of  $C_5H_5$ . The assignment of  $m/z$  39 to the propargyl radical in Fig. 7.3 is also confirmed by a measurement of the PIE( $m/z$  39). Both the threshold and the shape of the PIE( $m/z$  39) match the known<sup>[26]</sup>  $IE(HCCCH_2)$  and photoionization cross section<sup>[48]</sup> of the propargyl radical.

## Bitropyl ( $C_7H_7$ )<sub>2</sub> Decomposition in CW He

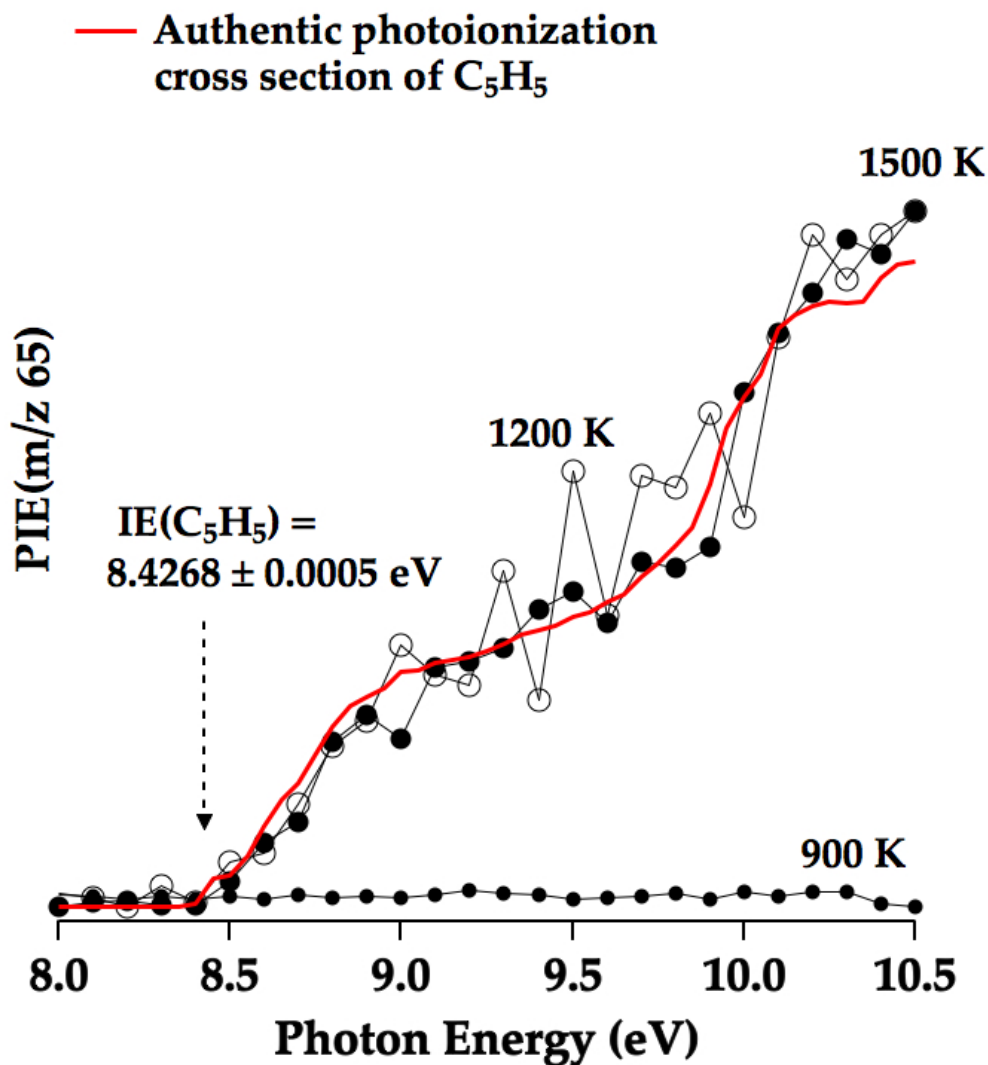


Fig. 7.4. PIE (m/z 65) recorded during the thermal decomposition of bitropyl ( $C_7H_7$ - $C_7H_7$ ) in a continuous flow micro-reactor in He at 900 K, 1200 K, and 1500 K. The red trace is the PIE spectrum of the  $C_5H_5$  radical recorded previously.<sup>[47]</sup> The ionization threshold<sup>[30]</sup> for  $\tilde{X}^2E_1''$   $C_5H_5$  is indicated. There is no evidence for cyclopentadienyl radical being present at 900 K.

Fig. 7.5 shows the neon matrix IR spectrum of the products of the thermal decomposition of bitropyl in a pulsed reactor at 1200 K. This vibrational spectrum confirms HC≡CH as a pyrolysis product of tropyli radical. Both the PIE( $m/z$  65) spectrum in Fig. 7.4 and the IR spectrum in Fig. 7.5 confirm the products in eq. (7.3).

## Bitropyl ( $C_7H_7$ )<sub>2</sub> Decomposition in Pulsed Neon

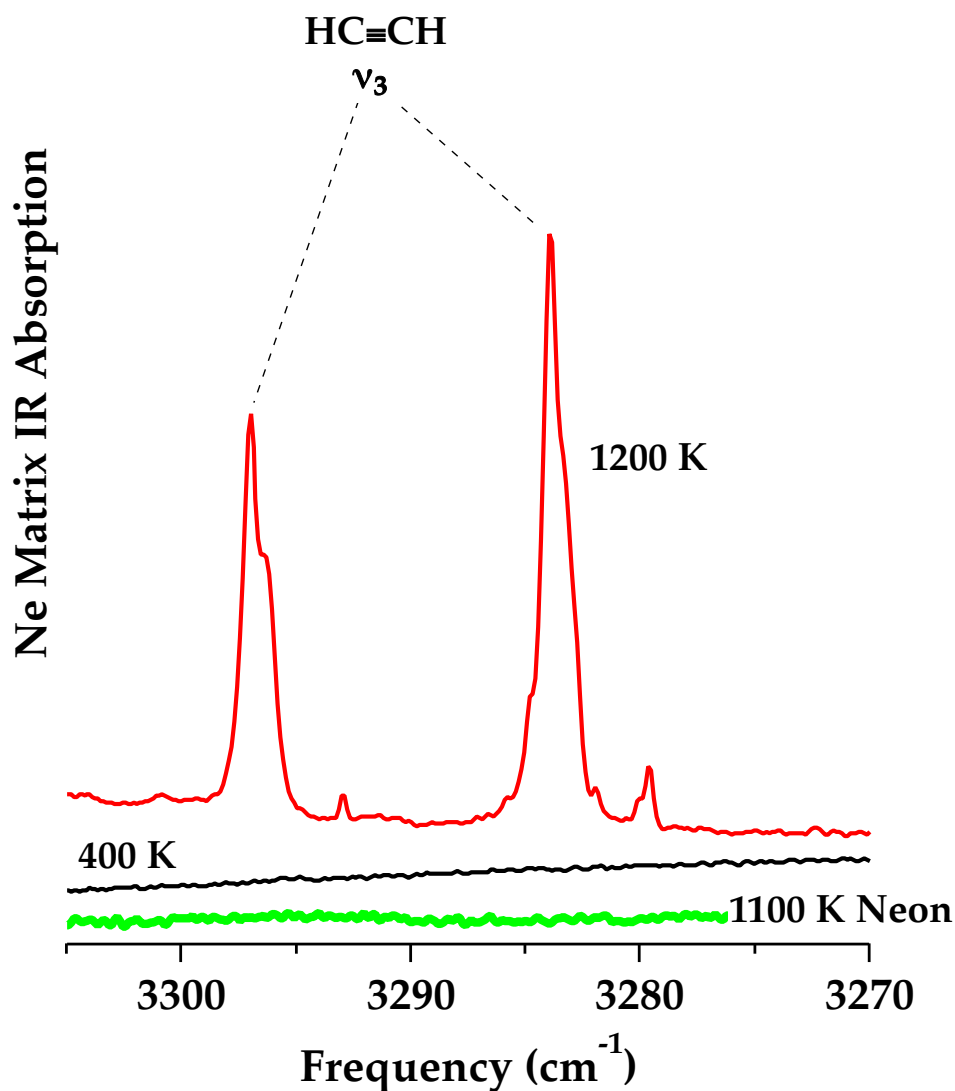


Fig. 7.5. Neon matrix absorption IR spectrum of the 1200 K pyrolysis of bitropyl ( $C_7H_7$ - $C_7H_7$ ) in a pulsed micro-reactor is shown in red. The presence of acetylene<sup>[49]</sup> is demonstrated by observation of the intense bands of  $\nu_3(\text{HC}\equiv\text{CH})$ . The black trace is that of the bitropyl precursor, which is un-pyrolyzed at 400 K. The green trace is the background spectrum of pure Ne heated to 1100 K.

Fig. 7.6 is a contrast between the pyrolysis products of ethylbenzene (top) and bitropyl (bottom). Both samples are thermally decomposed in a 0.6 mm I.D., continuous flow micro-reactor that is heated to 1500 K. The thermal cracking of  $C_6H_5CH_2CH_3$  initially generates<sup>[5]</sup> methyl radicals ( $m/z$  15) and benzyl radicals ( $m/z$  91). Subsequent fragmentation of the  $C_6H_5CH_2$  radical leads to the complex set of products at  $m/z$  26, 39, 50, 63, 65, 76, 78, 89, and 90 that are discussed in ref. <sup>[5]</sup>. Pyrolysis of bitropyl at the bottom of Fig. 7.6 produces  $C_7H_7$  ( $m/z$  91) and the fragmentation products from tropylium,  $C_5H_5$  ( $m/z$  65) and  $HC\equiv CH$  ( $m/z$  26). Propargyl radical,  $HCCCH_2$  ( $m/z$  39), results from the thermal cracking of the cyclopentadienyl radical, eq. (7.4). The dramatic differences between these two PIMS spectra in Fig. 7.6 provide strong evidence that the tropylium radical does not isomerize to the benzyl radical.

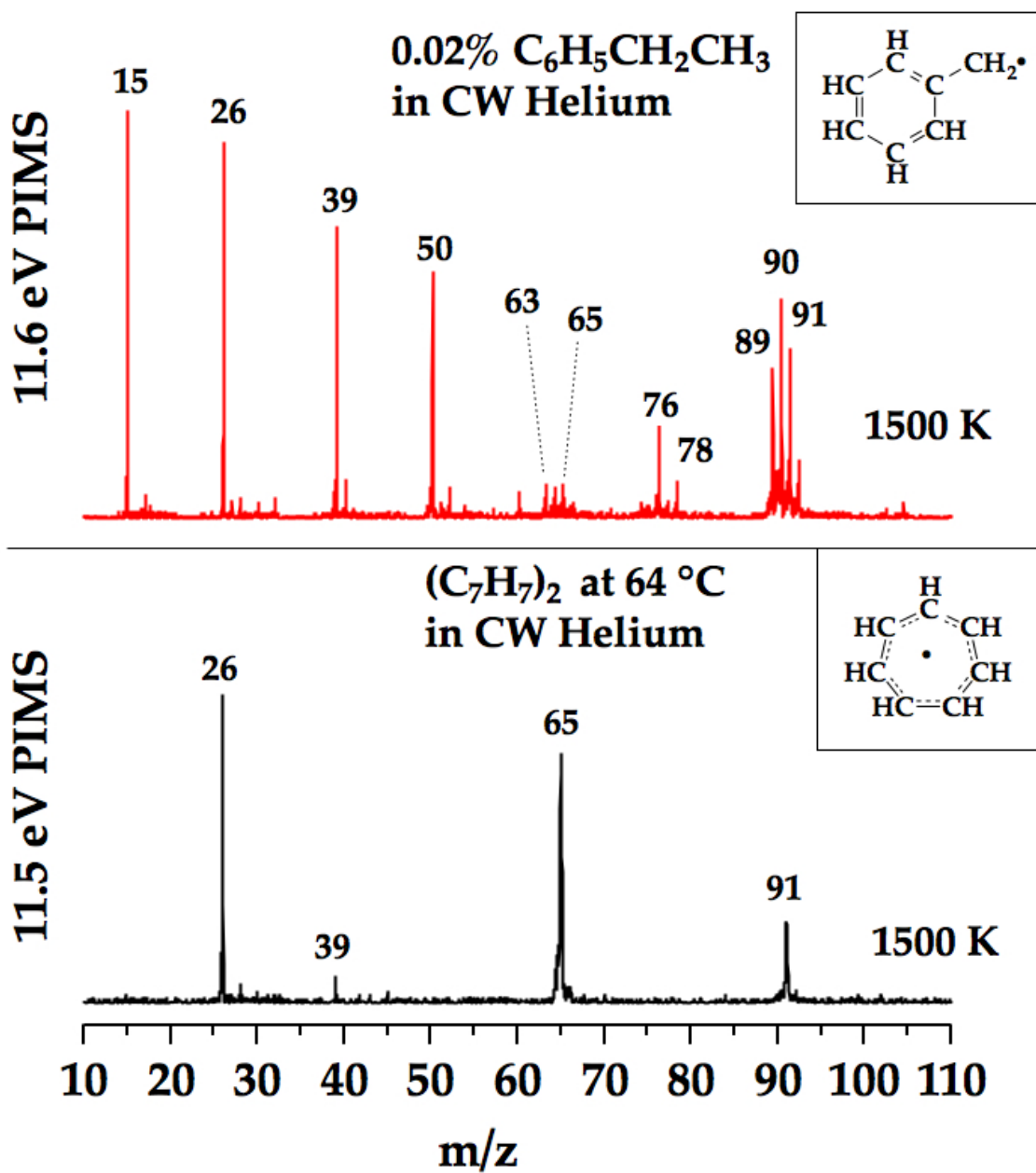


Fig. 7.6. PIMS spectra comparing the thermal decomposition of the benzyl radical and the tropylyl radical. In both experiments the precursors (ethyl benzene and bitropylyl) are decomposed in a continuous, 0.6 mm I.D. micro-reactor that is heated to 1500 K. No isomerization from the C<sub>7</sub>H<sub>7</sub> radical to the more stable C<sub>6</sub>H<sub>5</sub>CH<sub>2</sub> is observed, as indicated by the paucity of benzyl decomposition products found in tropylyl decomposition spectra.

## B. Matrix Isolation Spectroscopy

Because of the extensive dissociative ionization of the tropylium radical precursor,  $C_7H_7^+-C_7H_7$ , the application of PIMS to study tropylium radical pyrolysis is somewhat limited. Photo-ions of the pyrolysis products will always be partially obscured by fragments of dissociative ionization. Consequently IR spectroscopy is a very useful complementary detection tool.

However the matrix IR spectroscopy of tropylium radical has its own set of complications. There are no definitive vibrational spectra of the  $C_7H_7$  radical in a matrix environment. The gas phase IR spectrum was recorded for the tropylium radical (formed in a discharge from cycloheptatriene) with an IR-UV double resonance technique<sup>[13]</sup> that used the free electron laser "FELIX". Several vibrational modes of tropylium were observed in the fingerprint region but none could be assigned. LIF spectroscopy<sup>[10]</sup> has been used to identify some of the modes of  $C_7H_7, \tilde{X}^2E_2''$ . This study presented a vibrational analysis of the  $\tilde{A}^2E_3'' \leftarrow \tilde{X}^2E_2''$  electronic spectrum and several gas phase modes of the ground  $^2E_2''$  state were reported. Unfortunately, because of the nature of LIF spectroscopy, there is no information available regarding IR intensities for the ground state  $C_7H_7, \tilde{X}^2E_2''$  fundamentals. An important complication for studying tropylium radical in a neon matrix is the presence of the Jahn–Teller effect, which distorts the tropylium radical from the  $D_{7h}$  surface to the  $C_{2v}$  surface. The effect of inert gas matrices on Jahn–Teller distorted molecules is not easy to predict and is expected to cause perturbations from any gas-phase fundamentals greater than usual matrix to gas-phase frequencies shifts.

In spite of these difficulties, matrix isolation IR spectroscopy is useful as a secondary confirmation for tropyyl radical decomposition. The precursor used is bitropyyl and the experiments were performed using neon as the carrier gas. Fig. 7.7 shows 4 scans taken at different reactor temperatures for bitropyyl decomposition: 400 K, 1000 K, 1100 K, and 1200 K; as well as a scan of pure neon run at 1100 K as a control to rule out any systematic contaminants. The thin black trace shows an absorption feature from the precursor, which has not undergone decomposition at 400 K. This peak is significantly depleted upon heating to 1000 K (thick black line) and a strong, broad feature has developed centered at  $3056 \pm 6 \text{ cm}^{-1}$ . Upon heating to 1100 K (thin red trace) and 1200 K (thick red trace), this new peak is depleted as tropyyl radical thermally decomposes. The feature from the bitropyyl precursor is completely absent by 1100 K. This temperature dependence is in qualitative agreement with that observed in Fig. 7.3, although one could expect minor discrepancies due to differing carrier gas (Ne vs. He) and flow conditions (pulsed vs. continuous).



## Bitropyl ( $C_7H_7$ )<sub>2</sub> Decomposition in Pulsed Neon

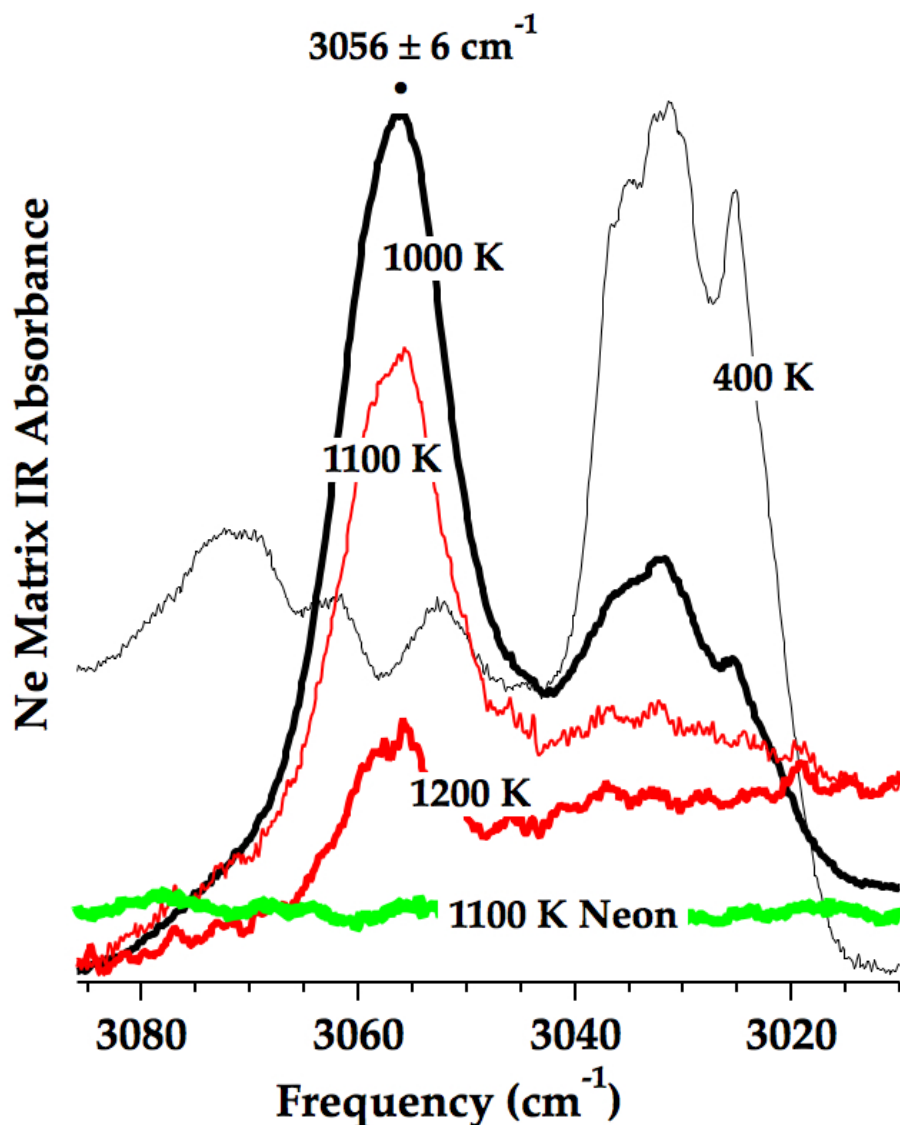


Fig. 7.7. Neon matrix absorbance IR spectra of the pyrolysis of bitropyl ( $C_7H_7$ - $C_7H_7$ ) in a pulsed micro-reactor at 400 K (thin black), 1000 K (thick black), 1100 K (thin red), and 1200 K (thick red). The feature at 3030  $cm^{-1}$  is assigned as the bitropyl precursor. A new band at  $3056 \pm 6 cm^{-1}$  is assigned to the  $C_7H_7$  radical. This assignment is corroborated by the temperature dependence observed here and in the PIMS of Fig. 7.3. The green trace is a background spectrum of Ne heated to 1100 K.

None of the vibrational features for tropyli radical in the CH stretch region have been previously assigned. A recent helium nanodroplet<sup>[19]</sup> study observed a pair of vibrational bands at 3052.9 cm<sup>-1</sup> and 3057.4 cm<sup>-1</sup> that are assigned to the tropyli radical. The helium nanodroplet spectra agree well with the matrix IR feature illustrated in Fig. 7.7.

Fig. 7.8 shows an additional intense absorption feature appearing in the decomposition of bitropyli at 1451 cm<sup>-1</sup>. This feature exhibits similar temperature dependence to that shown in Fig. 7.7; it is not observed at 400 K, is strongest at 1000 K and begins to decay at 1100 K and 1200 K.

## Bitropyl ( $C_7H_7$ )<sub>2</sub> Decomposition in Pulsed Neon

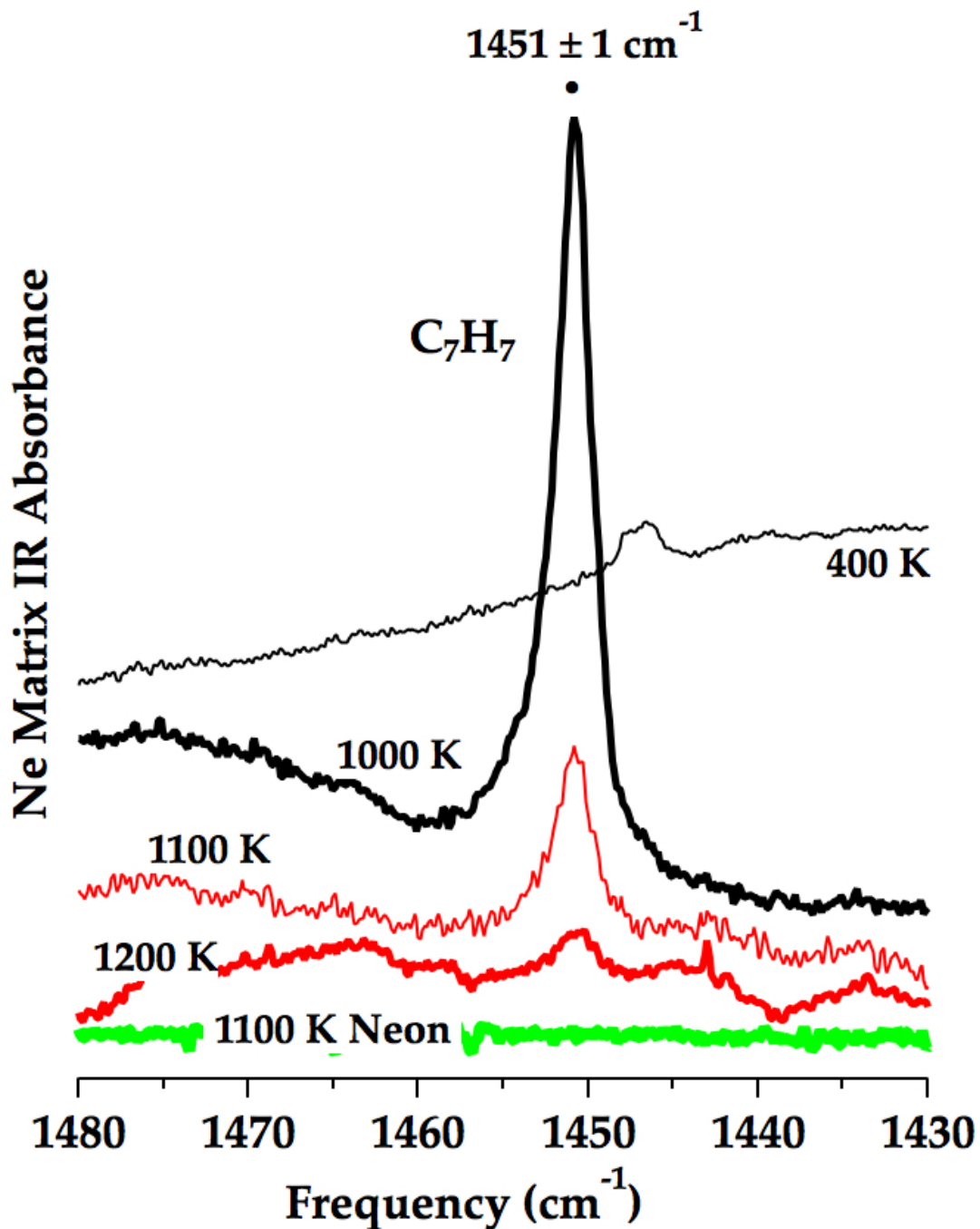


Fig. 7.8. Neon matrix absorbance IR spectra of the pyrolysis of bitropyl at 400 K (thin black), 1000 K (thick black), 1100 K (thin red), and 1200 K (thick red). The absorption feature at  $1451 \pm 1 \text{ cm}^{-1}$  is assigned to the tropyli radical. The green scan is a background spectrum of Ne heated to 1100 K.

Neither the  $3056\text{ cm}^{-1}$  nor the  $1451\text{ cm}^{-1}$  bands were observed in the spectra from benzyl decomposition,<sup>[5]</sup> nor were any vibrational assignments for benzyl radical observed in the tropylium radical decomposition spectra. This provides further confirmation that the benzyl and tropylium radicals do not interconvert, even at temperatures where both radicals thermally decompose.

### C. Cycloheptatriene or Norbornadiene as Tropylium Precursors?

In addition to bitropylium, cycloheptatriene ( $\text{C}_7\text{H}_8$ ) was considered as a pyrolytic source of  $\text{C}_7\text{H}_7$ . Cycloheptatriene has been successfully used as a precursor to prepare gas-phase tropylium radicals in discharge sources.<sup>[8, 10, 13]</sup> However, shock tube studies<sup>[50]</sup> of high-temperature pyrolysis of cycloheptatriene demonstrate complete conversion of  $\text{C}_7\text{H}_8$  to  $\text{C}_6\text{H}_5\text{CH}_3$ . A gas-phase, stirred-flow reactor was used<sup>[51]</sup> to explore the isomerizations of norbornadiene, cycloheptatriene, and toluene. No intermediate radicals could be detected in this early study because the reaction products were detected by gas chromatography with flame ionization detection. Fig. 7.9 is a summary<sup>[52]</sup> of the interconversions of norbornadiene, cycloheptatriene, and toluene. Norcaradiene<sup>[53]</sup> has been predicted as an intermediate in the equilibration of norbornadiene and cycloheptatriene. The first decomposition pathway of norbornadiene is the retro-Diels-Alder fragmentation to cyclopentadiene and acetylene. At higher temperatures, norbornadiene, norcaradiene, cycloheptatriene, and toluene all interconvert, where toluene is the most stable isomer.<sup>[51]</sup>

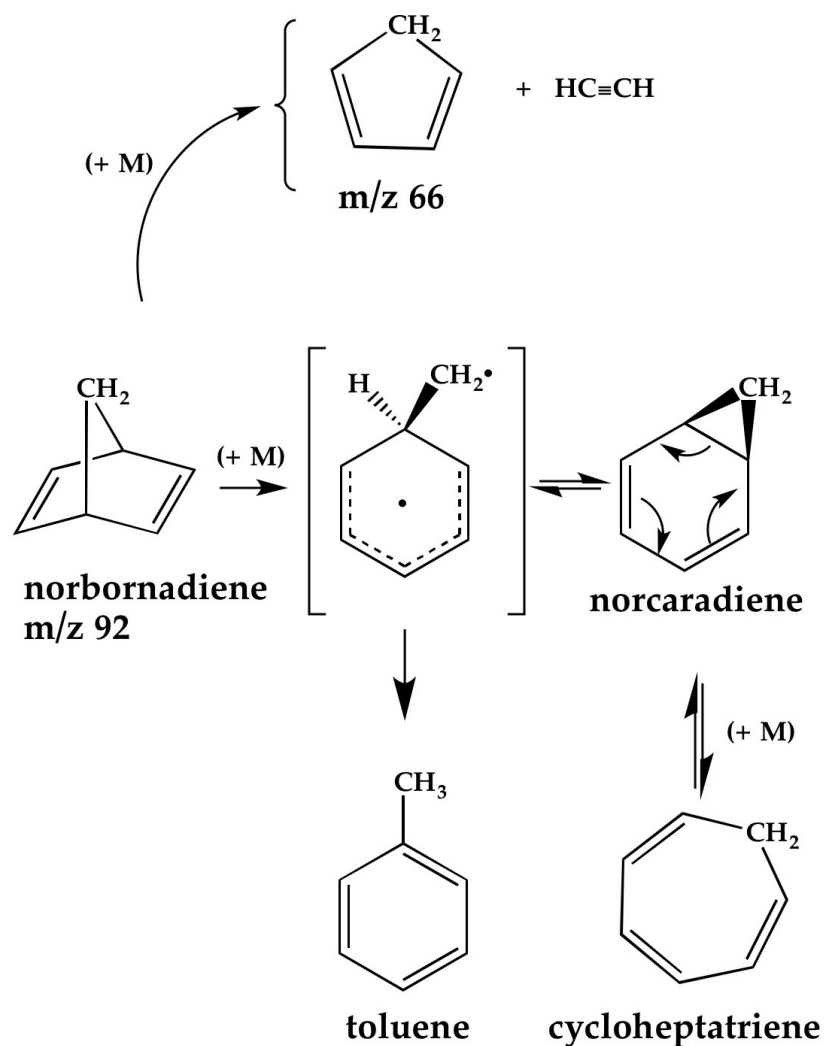


Fig. 7.9. Isomerizations<sup>[50-53]</sup> of norbornadiene, norcaradiene, cycloheptatriene, and toluene.

Fig. 7.10 shows the IR spectra of a dilute mixture of 0.05 % cycloheptatriene in neon that was thermally decomposed in a pulsed micro-reactor. As predicted,<sup>[50]</sup>  $\text{C}_7\text{H}_8$  isomerizes to toluene rather than forming tropyli radical. This finding was confirmed by assigning 11 absorption features to gas-phase<sup>[54]</sup>  $\text{C}_6\text{H}_5\text{CH}_3$ . At 300 K the only feature in this spectral window is due to the precursor, cycloheptatriene, but upon heating, three new bands emerge. The three peaks are assigned<sup>[54]</sup> as  $\nu_{11}$  at  $730\text{ cm}^{-1}$ ,  $\nu_4$  at  $695\text{ cm}^{-1}$ , and

$\nu_{18b}$  at  $1083\text{ cm}^{-1}$ , which agree well with the gas-phase values:  $\nu_{11} = 728\text{ cm}^{-1}$ ,  $\nu_4 = 695\text{ cm}^{-1}$ , and  $\nu_{18b} = 1080\text{ cm}^{-1}$ . At the highest temperature (1500 K), a few small features are observed that are assigned to  $\text{C}_6\text{H}_5\text{CH}_2$  including  $\nu_7$  ( $762\text{ cm}^{-1}$ ) and  $\nu_{13}$  ( $1308\text{ cm}^{-1}$ ), in agreement with the argon matrix spectrum of benzyl radical.<sup>[55]</sup>

**0.05% Cycloheptatriene (C<sub>7</sub>H<sub>8</sub>)  
in Pulsed Neon**

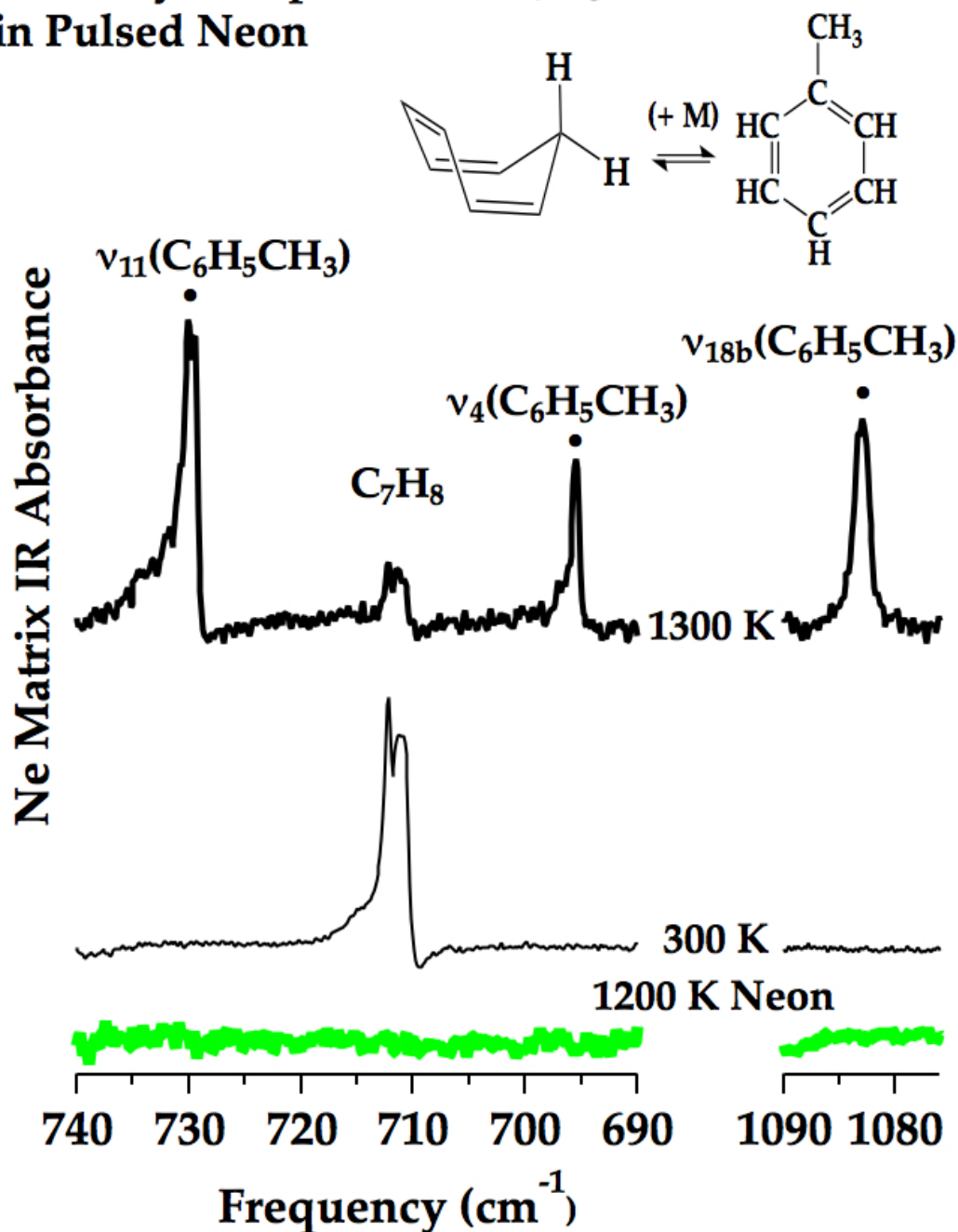


Fig. 7.10. The neon matrix absorbance IR spectrum of cycloheptatriene (C<sub>7</sub>H<sub>8</sub>) pyrolysis in a pulsed micro-reactor at 1300 K is shown in thick black. The thin black line is the absorbance spectrum of cycloheptatriene at 300 K. The 300 K spectrum shows only one feature belonging to C<sub>7</sub>H<sub>8</sub>. Upon heating to 1300 K, the precursor feature has diminished and new bands are observed. All three are assigned as vibrations of toluene.<sup>[55]</sup>

The isomerization of  $C_7H_8$  to  $C_6H_5CH_3$  is confirmed by the 118.2 nm PIMS, shown in Fig. 7.11. In this experiment, cycloheptatriene is subjected to pyrolysis in a pulsed micro-reactor heated to 300 K, 1400 K, and 1600 K. The products shown at 1600 K are nearly identical to those observed from benzyl radical precursors<sup>[5]</sup> but with a higher temperature for decomposition onset; compare with top panel of Fig. 7.6.



## 0.1% Cycloheptatriene (C<sub>7</sub>H<sub>8</sub>)/He

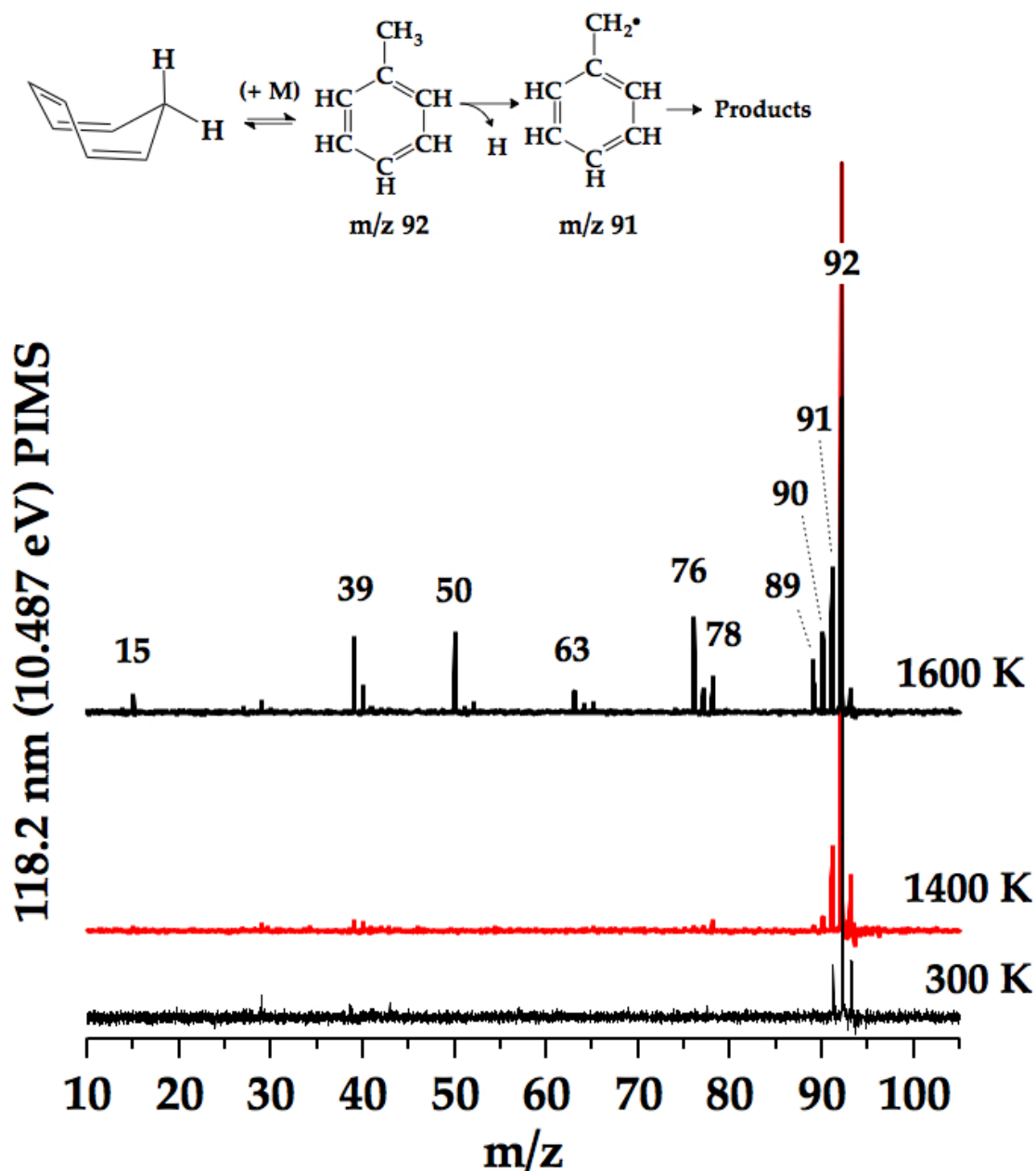


Fig. 7.11. PIMS spectra from the pyrolysis of cycloheptatriene in pulsed helium are shown at three reactor temperatures, 300 K, 1400 K, and 1600 K. At 1400 K the expected fragmentation of tropylium radical (see Fig. 7.3) is not observed. At 1600 K a set of products appears that is very similar to those characteristic<sup>[5]</sup> of benzyl radical decomposition (see Fig. 7.6).

We also studied the decomposition of 2,5-norbornadiene (Fig. 7.12). The  $IE(2,5\text{-norbornadiene})$  is less than 8.35 eV (Table 7.1) and the initial scan (400 K) reveals a small amount of dissociative ionization:  $\text{norbornadiene} + 118.2 \text{ nm} \rightarrow \text{C}_6\text{H}_5\text{CH}_2^+ (m/z 91) + \text{H}$  atom. At 1300 K, it is observed that norbornadiene undergoes a retro-Diels-Alder reaction:  $\text{norbornadiene} (+ \text{M}) \rightarrow \text{C}_5\text{H}_6 (m/z 66) + \text{HC}\equiv\text{CH}$  (see Fig. 7.9). As the reactor is heated to 1600 K, it appears that 2,5-norbornadiene isomerize to  $\text{C}_6\text{H}_5\text{CH}_3$ , which thermally dissociates to H atom and benzyl radical. The fragmentation of  $\text{C}_6\text{H}_5\text{CH}_2$  (top scan in Fig. 7.12) is very close to the pyrolysis pattern observed for norbornadiene (bottom Fig. 7.12).

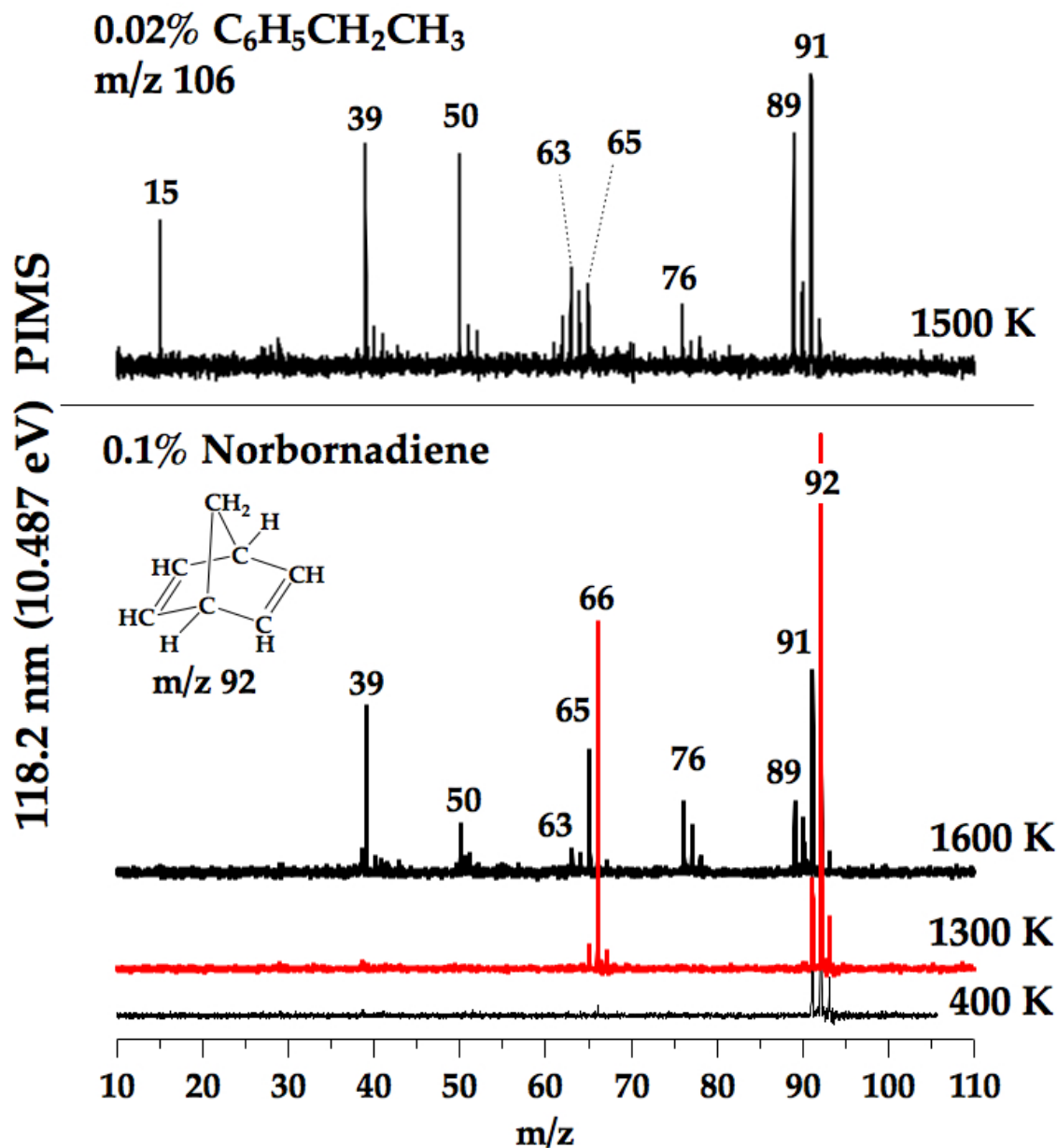


Fig. 7.12. PIMS spectra from the pyrolysis of norbornadiene in pulsed helium are shown at three reactor temperatures, 400 K, 1300 K, and 1600 K. At 1300 K norbornadiene undergoes a retro-Diels-Alder fragmentation and produces HC≡CH and C<sub>5</sub>H<sub>6</sub> (m/z 66); bottom scan. At 1600 K a set of products appears that is very similar to those characteristic<sup>[5]</sup> of benzyl radical decomposition; top scan uses C<sub>6</sub>H<sub>5</sub>CH<sub>2</sub>CH<sub>3</sub> as a source of benzyl radical.

## IV. Conclusions

The results of Figs. 7.3 – 7.8 eliminate any participation of the  $C_7H_7$  radical from the pyrolysis pathways of the  $C_6H_5CH_2$  radical at temperatures up to 1600 K. Tropyli radical only decomposes to acetylene and the cyclopentadienyl radical, eq. (7.3). These findings are consistent with the failure<sup>[5]</sup> of tunable PIMS to detect  $C_7H_7$  radicals as benzyl undergoes pyrolysis. We conclude this chapter with a reconsideration of the pathways for the thermal fragmentation of benzyl radical based on all experimental findings.<sup>[5-6, 11, 56-61]</sup>

The pyrolysis of the benzyl radical is a complex problem. None of the early experimental papers<sup>[61-66]</sup> describing the pyrolysis of  $C_6H_5CH_2$  were able to identify any of the thermal fragments except for the H atoms detected by ARAS.<sup>[6, 11]</sup> The only organic radicals resulting from pyrolysis of benzyl radical come from a few studies using heated micro-reactors outfitted with VUV PIMS.<sup>[3-5]</sup>

The pyrolysis of toluene was studied<sup>[3]</sup> in a quartz flow tube reactor at pressures of 8 – 15 Torr and temperatures of 1136 – 1507 K. A more recent study<sup>[4]</sup> of toluene pyrolysis used a heated alumina ( $Al_2O_3$ ) micro-reactor coupled to a VUV PIMS driven by tunable radiation from a synchrotron. The 248 nm photochemistry of benzyl radical has been studied<sup>[67]</sup> by photofragment translational spectroscopy. Dissociation occurs following relaxation from the excited state<sup>[68]</sup> to the ground state,  $C_6H_5CH_2, \tilde{X}^2B_1$ , producing benzyl radicals ( $C_6H_5CH_2$ )\* excited by 5 eV radiation. The benzyl\* radicals fragment to  $H + C_7H_6$  and  $CH_3 + C_6H_4$  radicals.

As mentioned in the introduction, pyrolysis of either ethylbenzene or benzyl bromide in a heated SiC micro-reactor<sup>[5]</sup> revealed an extended set of products that are

summarized in Fig. 7.1. When  $C_6H_5^{13}CH_2CH_3$  was heated<sup>[5]</sup> to 1200 K, the labeled benzyl radical,  $C_6H_5^{13}CH_2$ , was produced. Decomposition of  $C_6H_5^{13}CH_2$  at 1300 K produced a mixture of <sup>12</sup>[cyclopentadienyl] and <sup>13</sup>[cyclopentadienyl] radicals. One pathway to incorporate the <sup>13</sup>C label into the cyclopentadienyl radical would be isomerization of  $C_6H_5^{13}CH_2$  to <sup>13</sup>C-labeled  $C_7H_7$  (see Fig. 7.1). However the use<sup>[5]</sup> of 6.5 eV photons to search for the isomerization  $C_6H_5CD_2 \rightarrow C_7H_5D_2$  detected no tropyli radicals. This failure to observe  $C_7H_7$  radicals did not conclusively prove that tropyli is not present during the thermal cracking of benzyl radical. However, the current results in Figs. 7.3 – 7.8 demonstrates that clean samples of  $C_7H_7$  radicals can be produced and that they fragment by a pathway independent of benzyl.

### A. Pyrolysis of Benzyl Radical without Tropyli

In all of the experiments to scrutinize the pyrolysis of benzyl radicals<sup>[5]</sup> or tropyli radicals (this chapter), care was taken to study dilute samples (0.1 % — 0.02 % hydrocarbons in He or Ne). In the analysis of these results, we assume all fragmentation products result from unimolecular chemistry; there is no bimolecular chemistry to be analyzed. Pathways for the unimolecular, thermal decomposition of the benzyl radical are shown in Figs. 7.13 and 7.14. These schemes are based on the experimental findings from shock tubes with ARAS detection<sup>[6, 11]</sup> and heated micro-reactors monitored by PIMS and IR spectroscopy.<sup>[5]</sup> Heating the  $C_6H_5CH_2$  radical to 1300 K triggers an “extended” Benson fragmentation. The original suggestion<sup>[6]</sup> was only to offer pathways for H atom loss and formation of the fulvenallenyl radical,  $C_5H_4-C\equiv CH$ . This mechanism<sup>[6]</sup> also implies formation of the cyclopentadienyl radical and acetylene. The bicyclic radicals and vinylidene<sup>[69-70]</sup> ( $:C=CH_2$ ) in Fig. 7.13 will not be stable in the hot

micro-reactor and are enclosed in brackets. The production of H atoms is known from both<sup>[6, 11]</sup> ARAS and PIMS spectra.<sup>[5]</sup>

## Benson Fragmentation: benzyl- $d_0$

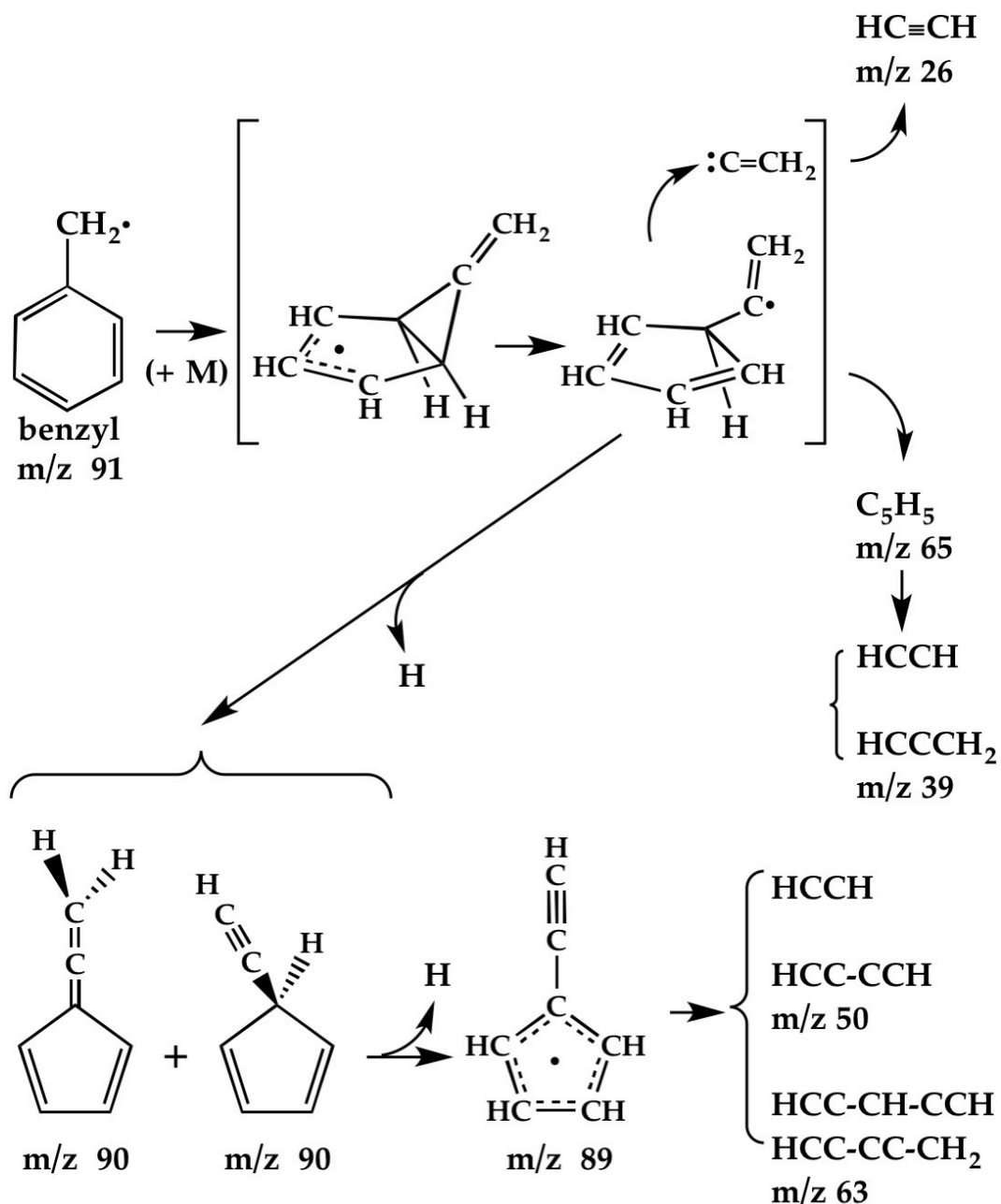
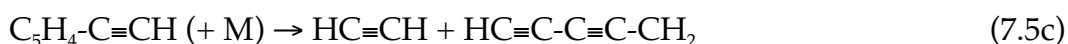
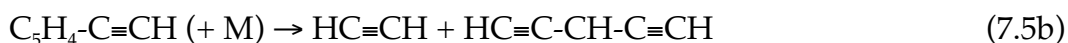
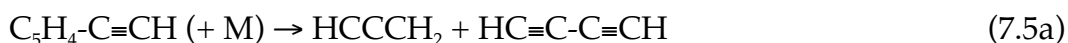


Fig. 7.13. The “extended” Benson Fragmentation of the benzyl radical,  $\text{C}_6\text{H}_5\text{CH}_2$ ,  $\tilde{\text{X}}^2\text{B}_1$ . The original suggestion<sup>[6]</sup> provided pathways for H atom loss and formation of the fulvenallenyl radical,  $\text{C}_5\text{H}_4\text{-C}\equiv\text{CH}$ . This suggestion also implies formation of the cyclopentadienyl radical and acetylene. The bicyclic radicals and vinylidene ( $\text{:C}=\text{CH}_2$ ) will not be stable in the hot micro-reactor and are enclosed in brackets. The tropyli radical,  $\text{C}_7\text{H}_7$ ,  $\tilde{\text{X}}^2\text{E}_2''$ , does not participate.

The Benson fragmentation in Figs. 7.13 leads to formation of the cyclopentadienyl and the fulvenallenyl radicals. (One could view  $C_5H_4-C\equiv CH$  as a substituted cyclopentadienyl radical.) As shown in eq. (7.4),  $C_5H_5$  decomposes to acetylene and propargyl radicals at 1300 K. Likewise the fulvenallenyl radical has been observed<sup>[71-72]</sup> to decompose to propargyl radical and diacetylene. This can be summarized.



The presence of the cyclopentadienyl radical and  $HC\equiv CH$  are confirmed by PIMS, PIE, and IR spectroscopy.<sup>[5]</sup> PIMS and PIE spectroscopy also detect both  $C_5H_4=C=CH_2$  and  $C_5H_4-C\equiv CH$ . The presence of fulvenallene is additionally confirmed by IR spectroscopy. PIMS and IR spectroscopy clearly identify the propargyl radical,  $HCCCH_2$ . PIMS signals at  $m/z$  50 and 63 are consistent with the presence of  $HC\equiv C-C\equiv CH$  and the two radicals,  $CH_2-C\equiv C-C\equiv CH$  and  $HC\equiv C-CH-C\equiv CH$ . However neither the PIE nor IR spectra could distinguish between the ( $CH_2-C\equiv C-C\equiv CH$ ,  $HC\equiv C-CH-C\equiv CH$ ) pair.

The Benson fragmentation predicts loss of H atom from  $C_6H_5CH_2$  to produce a pair of isomers,  $C_5H_4=C=CH_2$  and  $C_5H_5-C\equiv CH$ , both at  $m/z$  90. Recently pyrolysis of  $C_6H_5CD_2$  in a shock tube with ARAS detection<sup>[11]</sup> revealed the formation of both H and D atoms in agreement with this prediction. Pyrolysis of  $C_6H_5CD_2CD_3$  in a micro-



reactor<sup>[5]</sup> provided further support with the detection of both  $C_5H_4=C=CD_2$  ( $m/z$  92) and  $C_5H_5-C\equiv CD$  ( $m/z$  91).

The Benson fragmentation shown in Fig. 7.13 cannot be the complete story for the thermal cracking of the benzyl radical. PIMS and PIE spectra confirm<sup>[5]</sup> that heating  $C_6H_5^{13}CH_2$  radicals to 1300 K produces  $^{13}CH_3$ ,  $^{13}C_5H_5$ , and  $o-C_6H_4$ ; these products are incompatible with Benson's suggestion.<sup>[6]</sup> Fig. 7.14 shows two additional pathways for thermal cracking of benzyl radicals that address these products.

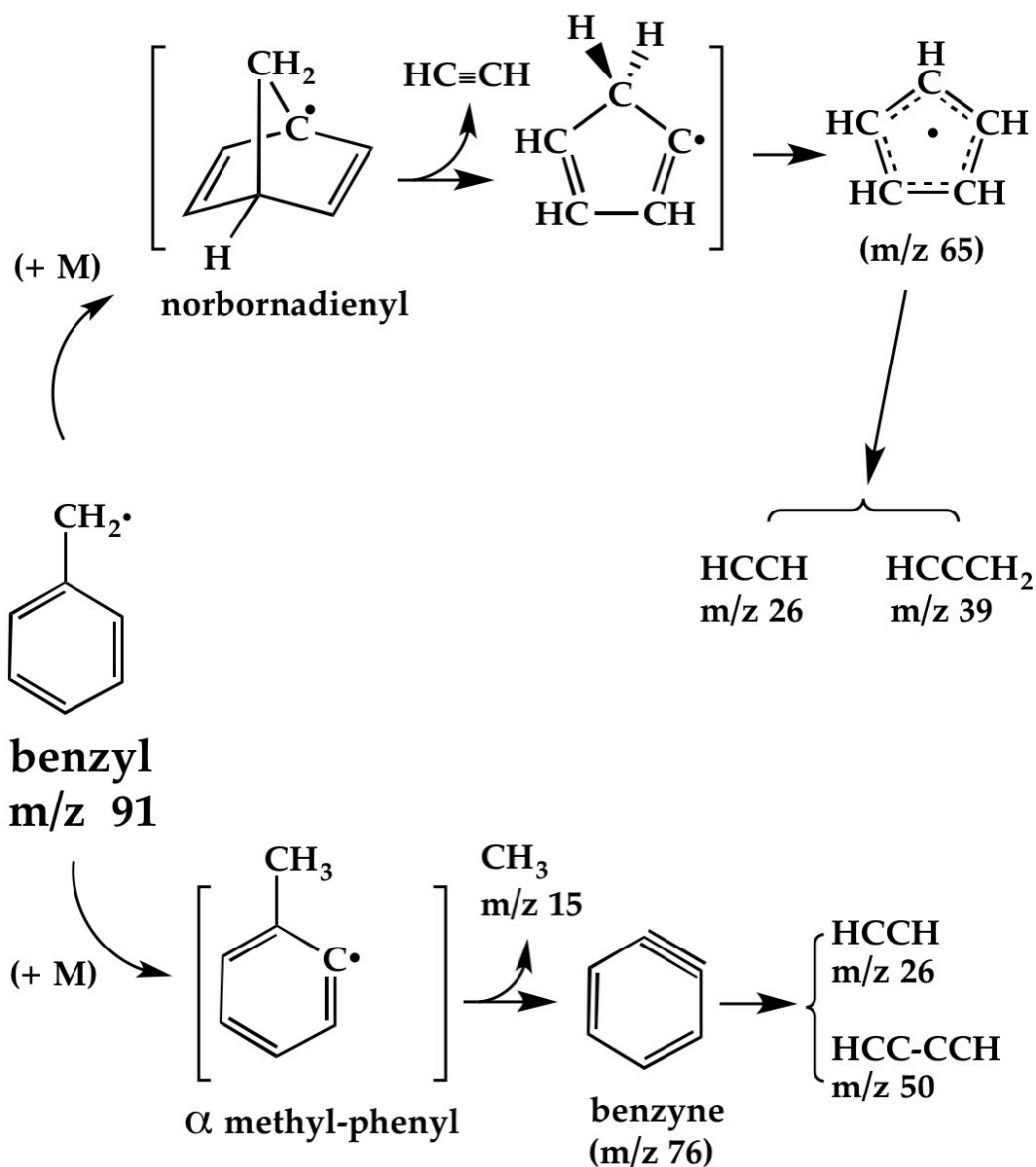


Fig. 7.14. Fragmentation pathways of the benzyl radical,  $\text{C}_6\text{H}_5\text{CH}_2 \tilde{\text{X}}^2\text{B}_1$ , are shown. The internal H-atom abstraction from the ring that leads to the formation of the  $\alpha$  methyl-phenyl radical will be endothermic<sup>[22]</sup> by roughly 1 eV. It also requires a curve-crossing from the  $^2\text{B}_1$  benzyl ( $\pi$  radical) to the  $^2\text{A}'$  methyl-phenyl ( $\sigma$  radical). Decomposition of the  $\alpha$  methyl-phenyl radical produces  $\text{CH}_3$  and  $o\text{-C}_6\text{H}_4$ . A second pathway is the isomerization of benzyl to the bridgehead norbornadienyl radical. The  $\alpha$  methyl-phenyl radicals, bridgehead norbornadienyl radicals, and  $^2\text{A}'$  cyclopentadienyl radicals will not be stable in the hot micro-reactor and are enclosed in brackets. The tropylium radical,  $\text{C}_7\text{H}_7 \tilde{\text{X}}^2\text{E}_2''$ , does not participate.

The pyrolysis of  $C_6H_5^{13}CH_2$  produces<sup>[5]</sup> both  $^{13}CH_3$  ( $m/z$  16) and  $o-C_6H_4$  ( $m/z$  76). These products could be the result of an isomerization of the  $^{13}$ [benzyl] radicals to the [ $\alpha$   $^{13}$ methyl-phenyl] radicals in Fig. 7.14. The isomerization would be initiated by H-abstraction from the aromatic ring by the  $-CH_2$  side chain. Such an abstraction would be difficult because of a required ( $\pi \rightarrow \sigma$ ) curve-crossing ( $C_6H_5CH_2, {}^2B_1 \rightarrow C_6H_4CH_3, {}^2A'$ ). In addition the internal abstraction will be endothermic by about 1 eV because of the difference in the  $C_6H_5CH_2-H$  and  $C_6H_5-H$  bond energies (see Table 7.1). Formation of the  $C_6H_4CH_3, {}^2A'$  radical in Fig. 7.14 will be followed by rapid fragmentation to the methyl and  $o$ -benzyne radicals and both are confirmed to be present. Heating  $o-C_6H_4$  to high temperatures is known<sup>[73]</sup> to trigger fragmentation to  $HC\equiv CH$  and  $HC\equiv C-C\equiv CH$ . The pyrolysis of both the  $C_6H_5CD_2$  and  $C_6D_5CH_2$  radicals are consistent with this pathway.<sup>[5]</sup> Decomposition of  $C_6H_5CD_2$  radicals at 1500 K forms small quantities of the  $CD_2H$  ( $m/z$  17) radicals while heating  $C_6D_5CH_2$  radicals to 1400 K leads to appearance of  $CH_2D$  ( $m/z$  16) radicals.

A second pathway for fragmentation of the benzyl radical shown in Fig. 4.14 is isomerization of  $C_6H_5CH_2$  to the bridgehead, norbornadienyl radical. Such a bridgehead radical would undergo a retro-Diels-Alder fragmentation producing  $HC\equiv CH$  and the  ${}^2A'$   $C_5H_5$  radical. The planar ( $\sigma$ )  ${}^2A'$   $C_5H_5$  radical is certainly the initial adduct in the reaction<sup>[74-75]</sup> of propargyl with acetylene and it rapidly isomerizes to the ground state, cyclopentadienyl radical,  $C_5H_5 \tilde{X} {}^2E_1''$ . A  $^{13}$ [norbornadienyl] radical will automatically incorporate the  $^{13}C$  label into the cyclopentadienyl radical, as observed in Fig. 13 of ref. <sup>[5]</sup>.

The pyrolysis pathways for  $C_6H_5CH_2$  shown in Figs. 7.13 and 7.14 are consistent with all of the major peaks of the PIMS in Fig. 2 of ref. <sup>[5]</sup>. The corresponding pathways for the isotopically substituted benzyl radicals,  $C_6H_5CD_2$ ,  $C_6D_5CH_2$ , and  $C_6H_5^{13}CH_2$  are contained in Figs E.1 – E.6 (see Appendix E). As in the case of the parent benzyl radical, these predicted  $C_6H_5CD_2$ ,  $C_6D_5CH_2$ , and  $C_6H_5^{13}CH_2$  pathways (see Appendix E) can be used to assign the major peaks of the experimental PIMS spectra in Fig. 8, Fig. 10, and Fig. 11 of ref. <sup>[5]</sup>.

A recent paper<sup>[16]</sup> applied *metadynamics* to the pyrolysis of benzyl. These calculations suggested that both  $C_5H_5$  and its isomer,  $(CH_2)_2C-C\equiv CH$ , are intermediates in the high temperature pyrolysis of benzyl. The  $IE(C_5H_5)$  is measured to be 8.4 eV (see Table 7.1) and the measured<sup>[5]</sup> PIE(m/z 65) has its threshold at  $8.4 \pm 0.1$  eV. The  $IE((CH_2)_2C-C\equiv CH)$  is not measured but it is likely less than that of the allyl radical, 8.1 eV (see Table 7.1). The PIE(m/z 65) resulting from the thermal cracking of the  $C_6H_5CH_2$  radical indicates that there is little (or no)  $(CH_2)_2C-C\equiv CH$  present in the pyrolysis of benzyl. It was also predicted by the *metadynamics* calculations<sup>[16]</sup> that the starting  $C_6H_5CH_2$  radicals could isomerize to a pair of isomeric, dimethylene-cyclopentenyl radicals. The spectroscopic probes of ref. <sup>[5]</sup> could not confirm the presence of these two isomers.

There are small features at m/z 41, 51, 64, 77, and 78 present in the PIMS of  $C_6H_5CH_2$  (Fig. 2 of ref. <sup>[5]</sup>) that cannot be rationalized by either pathways of Figs. 7.13 and 7.14. The peaks at m/z 77 and 78 are likely the phenyl radical ( $C_6H_5$ ) and benzene. There is a theoretical calculation that<sup>[72]</sup> predicts a small channel for pyrolysis of fulvenallene to  $C_5H_4\cdot + HC\equiv CH$ . The singlet carbene ( $C_5H_4\cdot$ ) is consistent with the peak

at  $m/z$  64.

There are small bands in the 118.2 nm PIMS spectra of  $C_6H_5CD_2$  and  $C_6D_5CH_2$  (Figs. 8 and 10 of ref. [5]) that suggest an interesting subtlety to the  $\alpha$  methyl-phenyl radical in Fig. 7.14. Perhaps there is some equilibration of benzyl radicals with the  $\alpha$  methyl-phenyl radicals? If so, then the  $C_6H_5CD_2$  and  $C_6D_5CH_2$  radicals will scramble:  $C_6H_5CD_2 \rightleftharpoons [C_6H_4-CHD_2] \rightleftharpoons C_6H_4D-CHD$ . Application of the [Benson fragmentation, methyl-phenyl, norbornadienyl] pathways to the  $o$ - $C_6H_4D-CHD$  radical leads to the formation of complex set of labeled (fulvenallenes, ethynyl cyclopentadienes, and fulvenallenyl) radicals. Fragmentation of these radicals predicts formation of  $C_5H_4-C\equiv CH$  ( $m/z$  89),  $C_5H_4D$  (cyclopentadienyl radical- $d_1$ ,  $m/z$  66),  $o$ - $C_6H_3D$  ( $o$ -benzyne,  $m/z$  77),  $HC\equiv C-CH-C\equiv CH$  ( $m/z$  63), and  $DC\equiv C-C\equiv CD$  ( $m/z$  52). There are signals in Fig. 8 of ref. [5] that are compatible with these radicals. A similar scrambling of benzyl radical- $d_5$  ( $C_6D_5CH_2 \rightleftharpoons [C_6D_4H-CDH_2] \rightleftharpoons C_6D_4H-CHD$ ) leads to production of  $C_5H_3D-CCH$  ( $m/z$  92),  $C_5D_4H$  ( $m/z$  69),  $o$ - $C_6D_3H$  ( $m/z$  79), and ( $DC\equiv C-C\equiv C-CD_2$  or  $DC\equiv C-CD-C\equiv CD$ )  $m/z$  66. Weak features for all of these radicals are present in Fig. 10 of ref. [5].

The three distinct pathways for pyrolysis of benzyl radical in Figs. 7.13 and 7.14 are complicated. Nevertheless they offer a set of predictions for the thermal cracking of more complex aromatic compounds that are included in surrogate fuel mixtures. Aviation fuels are mixtures of a very large number of chemical components<sup>[76]</sup>. The detailed numerical simulation of real combustion fuels is too difficult to apply to any fuel that is not a pure component or a mixture of more than a few species. One way to circumvent this problem is to study a surrogate fuel. Such surrogate fuels should be comprised of a handful of components but be capable of emulating the gas phase

combustion characteristics of the real fuel of interest. The advantage, of course, is that the resulting reaction mechanism is of much more manageable size.

A surrogate fuel for aviation diesels has been proposed<sup>[76]</sup> that is a mixture of ten compounds. This mixture includes 6 alkanes (*n*-decane, *n*-dodecane, *iso*-octane, *iso*-cetane, and methyl cyclohexane) and 4 aromatic species (toluene, *n*-propyl benzene, 1,3,5-trimethyl benzene, and 1-methyl naphthalene). Three of these species ( $C_6H_5-CH_3$ ,  $C_6H_3(CH_3)_3$ , and  $C_6H_5-CH_2CH_2H_3$ ) would be predicted to pyrolyze to benzyl radicals. The decomposition pathways for  $C_6H_5CH_2$  in Figs. 7.13 and 7.14 will be relevant to these surrogates.

## Reference for Chapter 7

- [1] J. L. Burger, T. M. Lovestead and T. J. Bruno. Composition of the C-6+ Fraction of Natural Gas by Multiple Porous Layer Open Tubular Capillaries Maintained at Low Temperatures. *Energy & Fuels* **2016**, *30*, 2119-2126.
- [2] C. J. Mueller, W. J. Cannella, T. J. Bruno, B. Bunting, H. D. Dettman, J. A. Franz, M. L. Huber, M. Natarajan, W. J. Pitz, M. A. Ratcliff and K. Wright. Methodology for Formulating Diesel Surrogate Fuels with Accurate Compositional, Ignition-Quality, and Volatility Characteristics. *Energy & Fuels* **2012**, *26*, 3284-3303.
- [3] B. Shukla, A. Susa, A. Miyoshi and M. Koshi. *In Situ* Direct Sampling Mass Spectrometric Study on Formation of Polycyclic Aromatic Hydrocarbons in Toluene Pyrolysis. *Journal of Physical Chemistry A* **2007**, *111*, 8308-8324.
- [4] T. Zhang, L. Zhang, X. Hong, K. Zhang, F. Qi, C. K. Law, T. Ye, P. Zhao and Y. Chen. An Experimental and Theoretical Study of Toluene Pyrolysis With Tunable Synchrotron VUV Photoionization and Molecular-Beam Mass Spectrometry. *Combustion and Flame* **2009**, *156*, 2071-2083.
- [5] G. T. Buckingham, T. K. Ormond, J. P. Porterfield, P. Hemberger, O. Kostko, M. Ahmed, D. J. Robichaud, M. R. Nimlos, J. W. Daily and G. B. Ellison. The Thermal Decomposition of the Benzyl Radical in a Heated Micro-Reactor: I. Experimental Findings. *Journal of Chemical Physics* **2015**, *142*, 044307-044320.
- [6] V. S. Rao and G. B. Skinner. Formation of Hydrogen Atoms in Pyrolysis of Ethylbenzene Behind Shock Waves. Rate Constants for the Thermal Dissociation of the Benzyl Radical. *Proceedings of the Combustion Institute* **1986**, *21*, 809-814.
- [7] R. D. Johnson. Excited Electronic States of the Tropyli (cyclo-C<sub>7</sub>H<sub>7</sub>) Radical. *Journal of Chemical Physics* **1991**, *95*, 7108-7113.
- [8] T. Pino, F. Guthe, H. Ding and J. P. Maier. Gas-Phase Electronic Spectrum of the Tropyli C<sub>7</sub>H<sub>7</sub> Radical. *Journal of Physical Chemistry A* **2002**, *106*, 10022-10026.
- [9] V. L. Stakhursky, I. Sioutis, G. Tarczay and T. A. Miller. Computational Investigation of the Jahn-Teller Effect in the Ground and Excited Electronic States of the Tropyli Radical. Part I. Theoretical Calculation of Spectroscopically Observable Parameters. *Journal of Chemical Physics* **2008**, *128*, 084310-084323.

- [10] I. Sioutis, V. L. Stakhursky, G. Tarczay and T. A. Miller. Experimental Investigation of the Jahn-Teller Effect in the Ground and Excited Electronic States of the Tropylium Radical. Part II. Vibrational Analysis of the A  $^2E_3$ "-X  $^2E_2$ " Electronic Transition. *Journal of Chemical Physics* **2008**, *128*, 084311 - 084329.
- [11] R. Sivaramakrishnan, M. C. Su and J. V. Michael. H- and D-Atom Formation from the Pyrolysis of C<sub>6</sub>H<sub>5</sub>CH<sub>2</sub>Br and C<sub>6</sub>H<sub>5</sub>CD<sub>2</sub>Br: Implications for High-Temperature Benzyl Decomposition. *Proceedings of the Combustion Institute* **2011**, *33*, 243-250.
- [12] J. Jones, G. B. Bacskay and J. C. Mackie. Decomposition of the Benzyl Radical: Quantum Chemical and Experimental (Shock Tube) Investigations of Reaction Pathways. *Journal of Physical Chemistry A* **1997**, *101*, 7105-7113.
- [13] R. G. Satink, G. Meijer and G. von Helden. Infrared Spectroscopy of Neutral C<sub>7</sub>H<sub>7</sub> Isomers: Benzyl and Tropylium. *Journal of the American Chemical Society* **2003**, *125*, 15714-15715.
- [14] C. Cavallotti, M. Derudi and R. Rota. On the Mechanism of Decomposition of the Benzyl Radical. *Proceedings of the Combustion Institute* **2009**, *32*, 115-121.
- [15] M. Derudi, D. Polino and C. Cavallotti. Toluene and Benzyl Decomposition Mechanisms: Elementary Reactions and Kinetic Simulations. *Physical Chemistry Chemical Physics* **2011**, *13*, 21308-21318.
- [16] D. Polino and M. Parrinello. Combustion Chemistry via Metadynamics: Benzyl Decomposition Revisited. *Journal of Physical Chemistry A* **2015**, *119*, 978-989.
- [17] K. H. Fischer, P. Hemberger, A. Bodi and I. Fischer. Photoionisation of the Tropylium Radical. *Beilstein Journal of Organic Chemistry* **2013**, *9*, 681-688.
- [18] Q. Guan, K. N. Urness, T. K. Ormond, D. E. David, G. B. Ellison and J. W. Daily. The Properties of a Micro-Reactor for the Study of the Unimolecular Decomposition of Large Molecules. *International Reviews in Physical Chemistry* **2014**, *33*, 447-487.
- [19] M. Kaufmann, B. M. Broderick and G. E. Douberly, *70<sup>th</sup> International Symposium on Molecular Spectroscopy* **2015**.
- [20] J. B. Pedley, R. D. Naylor and S. P. Kirby, *Thermochemistry of Organic Compounds*, Chapman and Hall, New York, **1986**, p. 87-222.



- [21] J. C. Traeger and R. G. McLoughlin. Threshold Photoionization and Dissociation of Toluene and Cycloheptatriene. *Journal of the American Chemical Society* **1977**, *99*, 7351-7352.
- [22] S. J. Blanksby and G. B. Ellison. Bond Dissociation Energies of Organic Molecules. *Accounts of Chemical Research* **2003**, *36*, 255-263.
- [23] T. Ichino, S. W. Wren, K. M. Vogelhuber, A. J. Gianola, W. C. Lineberger and J. F. Stanton. The Vibronic Level Structure of the Cyclopentadienyl Radical. *Journal of Chemical Physics* **2008**, *129*, 084310.
- [24] J. A. Blush, P. Chen, R. T. Wiedmann and M. G. White. Rotationally Resolved Threshold Photoelectron-Spectrum of the Methyl Radical. *Journal of Chemical Physics* **1993**, *98*, 3557-3559.
- [25] S. T. Pratt, P. M. Dehmer and J. L. Dehmer. Zero-Kinetic-Energy Photoelectron-Spectroscopy from the  $\tilde{a}^1A_u$  State of Acetylene - Renner-Teller Interactions in the Trans-Bending Vibration of  $C_2H_2^+ X^2\Pi_u$ . *Journal of Chemical Physics* **1993**, *99*, 6233-6244.
- [26] H. Gao, Y. T. Xu, L. Yang, C. S. Lam, H. L. Wang, J. A. Zhou and C. Y. Ng. High-Resolution Threshold Photoelectron Study of the Propargyl Radical by the Vacuum Ultraviolet Laser Velocity-Map Imaging Method. *Journal of Chemical Physics* **2011**, *135*, 224304-224311.
- [27] X. Xing, B. Reed, K. C. Lau, C. Y. Ng, X. Zhang and G. B. Ellison. Vacuum Ultraviolet Laser Pulsed Field Ionization-Photoelectron Study of Allyl Radical  $CH_2CHCH_2$ . *Journal of Chemical Physics* **2007**, *126*, 171170-171174.
- [28] F. A. Houle and J. L. Beauchamp. Detection and Investigation of Allyl and Benzyl Radicals by Photoelectron-Spectroscopy. *Journal of the American Chemical Society* **1978**, *100*, 3290-3294.
- [29] X. Zhang and P. Chen. Photoelectron-Spectrum of *o*-Benzyne - Ionization-Potentials as a Measure of Singlet Triplet Gaps. *Journal of the American Chemical Society* **1992**, *114*, 3147-3148.
- [30] H. J. Wörner and F. Merkt. Diradicals, Antiaromaticity, and the Pseudo-Jahn-Teller Effect: Electronic and Rovibronic Structures of the Cyclopentadienyl Cation. *Journal of Chemical Physics* **2007**, *127*, 034303-034319.

- [31] M. Steinbauer, P. Hemberger, I. Fischer and A. Bodi. Photoionization of  $C_7H_6$  and  $C_7H_5$ : Observation of the Fulvenallenyl Radical. *Chem Phys Chem* **2011**, *12*, 1795-1797.
- [32] G. C. Eiden, F. Weinhold and J. C. Weisshaar. Photoelectron-Spectroscopy of Free-Radicals with  $cm^{-1}$  Resolution - The Benzyl Cation. *Journal of Chemical Physics* **1991**, *95*, 8665-8668.
- [33] K. T. Lu, G. C. Eiden and J. C. Weisshaar. Toluene Cation - Nearly Free Rotation of the Methyl-Group. *Journal of Physical Chemistry* **1992**, *96*, 9742-9748.
- [34] J. C. Traeger and R. G. McLoughlin. Photo-ionization study of energetics of  $C_7H_7^+$  ion formed from  $C_7H_8$  precursors. *International Journal of Mass Spectrometry and Ion Processes* **1978**, *27*, 319-333.
- [35] X. Zhang, A. V. Friderichsen, S. Nandi, G. B. Ellison, D. E. David, J. T. McKinnon, T. G. Lindeman, D. C. Dayton and M. R. Nimlos. Intense, Hyperthermal Source of Organic Radicals for Matrix-Isolation Spectroscopy. *Review of Scientific Instruments* **2003**, *74*, 3077-3086.
- [36] N. P. Lockyer and J. C. Vickerman. Single Photon Ionisation Mass Spectrometry Using Laser-Generated Vacuum Ultraviolet Photons. *Laser Chemistry* **1997**, *17*, 139-159.
- [37] J. Boyle and L. Pfefferle. Study of Higher Hydrocarbon Production During Ethylacetylene Pyrolysis Using Laser-Generated Vacuum-Ultraviolet Photoionization Detection. *Journal of Physical Chemistry* **1990**, *94*, 3336-3340.
- [38] R. E. Bandy, C. Lakshminarayan, R. K. Frost and T. S. Zwier. The Ultraviolet Photochemistry of Diacetylene - Direct Detection of Primary Products of the Metastable  $C_4H_2^* + C_4H_2$  Reaction. *Journal of Chemical Physics* **1993**, *98*, 5362-5374.
- [39] P. A. Heimann, M. Koike, C. W. Hsu, D. Blank, X. M. Yang, A. G. Suits, Y. T. Lee, M. Evans, C. Y. Ng, C. Flaim and H. A. Padmore. Performance of the Vacuum Ultraviolet High-Resolution and High-Flux Beamline for Chemical Dynamics Studies at the Advanced Light Source. *Review of Scientific Instruments* **1997**, *68*, 1945-1951.
- [40] A. Vasiliou, K. M. Piech, X. Zhang, M. R. Nimlos, M. Ahmed, A. Golan, O. Kostko, D. L. Osborn, J. W. Daily, J. F. Stanton and G. B. Ellison. The Products of the

- Thermal Decomposition of CH<sub>3</sub>CHO. *Journal of Chemical Physics* **2011**, *135*, 14306-14311.
- [41] T. K. Ormond, A. M. Scheer, M. R. Nimlos, D. J. Robichaud, J. W. Daily, J. F. Stanton and G. B. Ellison. Polarized Matrix Infrared Spectra of Cyclopentadienone: Observations, Calculations, and Assignment for an Important Intermediate in Combustion and Biomass Pyrolysis. *J. Phys. Chem. A* **2014**, *118*, 708-718.
- [42] F. A. Elder and A. C. Parr. Photoionization of the Cycloheptatrienyl Radical. *Journal of Chemical Physics* **1969**, *50*, 1027-1028.
- [43] A. K. Vasiliou, K. M. Piech, B. Reed, X. Zhang, M. R. Nimlos, M. Ahmed, A. Golan, O. Kostko, D. L. Osborn, K. N. Urness, D. E. David, J. W. Daily, J. F. Stanton and G. B. Ellison. Thermal Decomposition of CH<sub>3</sub>CHO Studied by Matrix Infrared Spectroscopy and Photoionization Mass Spectroscopy *Journal of Chemical Physics* **2012**, *137*, 164308.
- [44] K. N. Urness, Q. Guan, A. Golan, J. W. Daily, M. R. Nimlos, J. F. Stanton, M. Ahmed and G. B. Ellison. Pyrolysis of Furan in a Microreactor *Journal of Chemical Physics* **2013**, *139*, 124305-124314
- [45] A. M. Scheer, C. Mukarakate, D. J. Robichaud, G. B. Ellison and M. R. Nimlos. Radical Chemistry in the Thermal Decomposition of Anisole and Deuterated Anisoles: An Investigation of Aromatic Growth. *Journal of Physical Chemistry A* **2010**, *114*, 9043-9056.
- [46] L. V. Moskaleva and M. C. Lin. Unimolecular Isomerization/Decomposition of Cyclopentadienyl and Related Bimolecular Reverse Process: *ab initio* MO/Statistical Theory Study. *Journal of Computational Chemistry* **2000**, *21*, 415-425.
- [47] J. D. Savee, Privately communicated., 2014
- [48] J. D. Savee, S. Soorkia, O. Welz, T. M. Selby, C. A. Taatjes and D. L. Osborn. Absolute photoionization cross-section of the propargyl radical. *Journal of Chemical Physics* **2012**, *136*, 134307-134317.
- [49] T. Shimanouchi, *Tables of Vibrational Frequencies, Consolidated Vol. I*, NSRDS-NBS 39, **1972**, p. 9-157.

- [50] S. H. Luu, K. Glanzer and J. Troe. Thermal Isomerization in Shock-Waves and Flash-Photolysis of Cycloheptatriene .3. *Berichte der Bunsen-Gesellschaft-Physical Chemistry Chemical Physics* **1975**, 79, 855-858.
- [51] W. C. Herndon and L. L. Lowry. Mechanism of Pyrolysis of Bicyclo [2.2.1] Heptadiene. Kinetics of Bicyclo [2.2.1] Heptadiene to Toluene Isomerization. *Journal of the American Chemical Society* **1964**, 86, 1922-1926.
- [52] R. Sustmann, D. Brandes, F. Lange and U. Nuchter. Rearrangements of Free-Radicals.11. Sigmatropic And Electrocyclic Reactions of Bicyclo [3.2.0] Heptadienyl Radicals, 3-Quadricyclanyl Radicals, and 7-Norbornadienyl Radical. *Chemische Berichte* **1985**, 118, 3500-3512.
- [53] C. Cavallotti, S. Mancarella, R. Rota and S. Carra. Conversion of C<sub>5</sub> Into C<sub>6</sub> Cyclic Species Through the Formation of C<sub>7</sub> Intermediates. *Journal of Physical Chemistry A* **2007**, 111, 3959-3969.
- [54] N. Fuson, C. Garrigoulagrange and M. L. Josien. Spectre Infrarouge et Attribution des Vibrations des Toluenes C<sub>6</sub>H<sub>5</sub>CH<sub>3</sub>, C<sub>6</sub>H<sub>5</sub>CD<sub>3</sub> et C<sub>6</sub>D<sub>5</sub>CD<sub>3</sub>. *Spectrochimica Acta* **1960**, 16, 106-127.
- [55] E. G. Baskir, A. K. Maltsev, V. A. Korolev, V. N. Khabashesku and O. M. Nefedov. Generation and IR Spectroscopic Study of Benzyl Radical. *Russian Chemical Bulletin* **1993**, 42, 1438-1440.
- [56] D. C. Astholz and J. Troe. Thermal-Decomposition of Benzyl Radicals in Shock-Waves. *Journal of the Chemical Society-Faraday Transactions II* **1982**, 78, 1413-1421.
- [57] L. Brouwer, W. Müller-Markgraf and J. Troe. Thermal-Decomposition of Ethylbenzene in Shock-Waves. *Berichte Der Bunsen-Gesellschaft-Physical Chemistry Chemical Physics* **1983**, 87, 1031-1036.
- [58] L. D. Brouwer, W. Müller-Markgraf and J. Troe. Thermal-Decomposition of Toluene - A Comparison of Thermal and Laser-Photochemical Activation Experiments. *Journal of Physical Chemistry* **1988**, 92, 4905-4914.
- [59] R. Fröchtenicht, H. Hippler, J. Troe and J. P. Toennies. Photon-Induced Unimolecular Decay of the Benzyl Radical - 1<sup>st</sup> Direct Identification of the Reaction Pathway to C<sub>7</sub>H<sub>6</sub>. *Journal of Photochemistry and Photobiology a-Chemistry* **1994**, 80, 33-37.

- [60] W. Müller-Markgraf and J. Troe. Thermal Decomposition of Benzyl Iodide and of Benzyl Radicals in Shock Waves. *The Journal of Physical Chemistry* **1988**, *92*, 4899-4905.
- [61] M. A. Oehlschlaeger, D. F. Davidson and R. K. Hanson. High-Temperature Thermal Decomposition of Benzyl Radicals. *Journal of Physical Chemistry A* **2006**, *110*, 6649-6653.
- [62] K. M. Pamidimukkala, R. D. Kern, M. R. Patel, H. C. Wei and J. H. Kiefer. High-Temperature Pyrolysis of Toluene. *Journal of Physical Chemistry* **1987**, *91*, 2148-2154.
- [63] A. Alexiou and A. Williams. Soot Formation in Shock-Tube Pyrolysis of Toluene, Toluene-Methanol, Toluene-Ethanol, and Toluene-Oxygen Mixtures. *Combustion and Flame* **1996**, *104*, 51-65.
- [64] P. Dagaut, G. Pengloan and A. Ristori. Oxidation, Ignition and Combustion of Toluene: Experimental and Detailed Chemical Kinetic Modeling. *Physical Chemistry Chemical Physics* **2002**, *4*, 1846-1854.
- [65] P. Dagaut, A. Ristori, A. El Bakali and M. Cathonnet. Experimental and Kinetic Modeling Study of the Oxidation of n-Propylbenzene. *Fuel* **2002**, *81*, 173-184.
- [66] R. Sivaramakrishnan, R. S. Tranter and K. Brezinsky. High Pressure Pyrolysis of Toluene. 1. Experiments and Modeling of Toluene Decomposition. *Journal of Physical Chemistry A* **2006**, *110*, 9388-9399.
- [67] M. Shapero, N. C. Cole-Filipiak, C. Haibach-Morris and D. M. Neumark. Benzyl Radical Photodissociation Dynamics at 248 nm. *Journal of Physical Chemistry A* **2015**, *119*, 12349-12356.
- [68] G. Porter and Savadatt.Mi. Electronic Spectra of Benzyl - A New Transition. *Spectrochimica Acta* **1966**, *22*, 803-806.
- [69] A. H. Laufer. An Excited-State of Acetylene - Photochemical and Spectroscopic Evidence. *Journal of Chemical Physics* **1980**, *73*, 49-52.
- [70] K. M. Ervin, J. Ho and W. C. Lineberger. A Study of the Singlet and Triplet-States of Vinylidene By Photoelectron-Spectroscopy of  $\text{H}_2\text{C}=\text{C}^-$ ,  $\text{D}_2\text{C}=\text{C}^-$ , and  $\text{HDC}=\text{C}^-$

- Vinylidene Acetylene Isomerization. *Journal of Chemical Physics* **1989**, *91*, 5974-5992.
- [71] G. da Silva, A. J. Trevitt, M. Steinbauer and P. Hemberger. Pyrolysis of fulvenallene ( $C_7H_6$ ) and fulvenallenyl ( $C_7H_5$ ): Theoretical kinetics and experimental product detection. *Chemical Physics Letters* **2011**, *517*, 144-148.
- [72] D. Polino and C. Cavallotti. Fulvenallene Decomposition Kinetics. *Journal of Physical Chemistry A* **2011**, *115*, 10281-10289.
- [73] X. Zhang, A. T. MacCarone, M. R. Nimlos, S. Kato, V. M. Bierbaum, G. B. Ellison, B. Ruscic, A. C. Simmonett, W. D. Allen and H. F. Schaefer. Unimolecular Thermal Fragmentation of *ortho*-Benzyne. *Journal of Chemical Physics* **2007**, *126*, 044312 - 044322.
- [74] V. D. Knyazev and I. R. Slagle. Kinetics of the Reaction Between Propargyl Radical and Acetylene. *Journal of Physical Chemistry A* **2002**, *106*, 5613-5617.
- [75] J. D. Savee, J. Zador, P. Hemberger, B. Sztaray, A. Bodi and D. L. Osborn. Threshold Photoelectron Spectrum of the Benzyl Radical. *Molecular Physics* **2015**, *113*, 2217-2227.
- [76] S. Dooley, S. H. Won, M. Chaos, J. Heyne, Y. Ju, F. L. Dryer, K. Kumar, C.-J. Sung, H. Wang, M. A. Oehlschlaeger, R. J. Santoro and T. A. Litzinger. A Jet Fuel Surrogate Formulated by Real Fuel Properties. *Combustion and Flame* **2010**, *157*, 2333-2339.



## Chapter 8

### Tabletop Vacuum Ultraviolet Laser-Based Photoionization Mass Spectrometry with Photoelectron Photoion Coincidence Detection of Pyrolysis Products

#### Abstract

Pyrolysis using a heated micro-reactor is combined with a tabletop vacuum ultraviolet (VUV) laser and photoelectron photoion coincidence (PEPICO) detector. This new combination of techniques provides for more powerful photoionization mass spectrometry (PIMS) by allowing isomer-specific identification of products and spectral simplification via reduction of unwanted dissociative ionization. These two advantages over previous PIMS experiments demonstrate a desirable means of studying the pyrolysis of gas phase molecules like combustion precursors and intermediates.

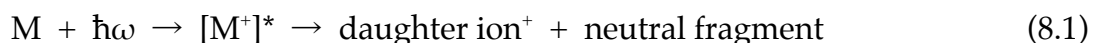
#### I. Introduction

Studying pyrolysis in a heated micro-reactor using photoionization mass spectrometry (PIMS) has advantages including short data acquisition time and the ability to detect all species with sufficiently energetic ionizing radiation. PIMS using an Nd:YAG laser ionization source is a well established technique that makes use of the 9<sup>th</sup> harmonic of the laser's fundamental frequency, which corresponds to  $\lambda = 118.2 \text{ nm}$  ( $E_{\text{photon}} = 10.487 \text{ eV}$ ). This frequency is useful because it is sufficiently energetic to ionize the overwhelming majority of organic molecules. Using a static gas



cell filled with a 10:1 mixture of argon and xenon, one can reproducibly and straightforwardly produce the 9<sup>th</sup> harmonic of a commercial Nd:YAG laser.

One major disadvantage of 118.2 nm photoionization techniques is that when ionizing molecules with ionization energies (IE) smaller than 10.487 eV, the excess energy can be redistributed in the molecule and result in bond breaking within the newly formed cation. This process is called dissociative ionization and is summarized in Equation 8.1. In extreme cases, dissociative ionization is so dramatic that none of the parent signal is detected and only fragment peaks survive to reach the detector.<sup>[1]</sup> In the cases of dissociative ionization, it is challenging to determine if a peak is the result of thermal decomposition of the parent that exited the micro-reactor or whether it is the result of dissociative ionization. Secondary confirmation may be required for a given fragment if dissociative ionization is suspected. If 118.2 nm PIMS were the only means of detecting pyrolysis products, many conclusions would be equivocal due to the limitations of the detection mechanisms.



Our research groups commonly use one of two secondary confirmation techniques before concluding chemical arguments based upon a 118.2 nm PIMS feature. The first method is matrix isolation IR spectroscopy, which removes the possibility of dissociative ionization since no ionizing radiation is needed. The second method is to utilize a synchrotron, which provides tunable ionizing light. Lowering the photon energy decreases the amount of excess energy available to fragment molecules but more importantly, scanning the photon energy while recording signal for a single mass peak provides photoionization spectra, which are diagnostic of a given species. If a feature in 118.2 nm PIMS is the result of dissociative ionization, the photoionization spectrum will

elucidate this. When a PIMS feature results from a pyrolysis product, the photoionization spectrum will agree with previously recorded photoionization spectra and ionization energy of that product, if such information is available. In many cases of dissociative ionization, the ionization onset in a photoionization spectrum differs substantially from that of the true molecule at that mass. The use of synchrotron radiation makes a PIMS experiment much more valuable, however, the effort involved to obtain synchrotron data is also much greater. The researchers must apply for and receive beam time at a synchrotron facility, travel to the location, construct a pyrolysis source, and take as much data as possible within their allotted beam time. These trips are often only a few days long and can only be done a few times per year, making synchrotron data both costly and challenging to acquire.

A more desirable method to provide dissociative ionization-free PIMS spectra is to produce vacuum ultraviolet (VUV) light without the need to travel to a synchrotron facility. Four-wave frequency mixing has been used<sup>[2]</sup> to study allyl radical ( $\text{CH}_2\text{CCH}_2$ ) from a micro-reactor. This method has a relatively low duty cycle (less than 100 Hz) so it is not commonly used for pyrolysis due to the large amount of time required to perform experiments. A recent collaboration with the group of Dr. Margaret Murnane and Dr. Henry Kapteyn has yielded a novel combination of experimental techniques that produces PIMS spectra where dissociative ionization can be identified and the spectra are collected with fast acquisition times yielding significant increase in experimentally available information.

The ionization source in these experiments is based on a femtosecond Ti:sapphire laser that can be upconverted to energies in the vacuum ultraviolet (VUV), the range relevant for molecular ionization. Rather than a standard Wiley-McLaren time-of-flight

(TOF) mass spectrometry setup,<sup>[3]</sup> the detection scheme in these experiments is a custom designed coincidence detector that allows for spatial imaging of the photoelectrons and the cations formed for each laser pulse.

Photoelectron photoion coincidence (PEPICO) detection has been used before in conjunction with a heated micro-reactor and synchrotron source.<sup>[4]</sup> PEPICO is accomplished in the present experiment by creating a static electric field that is roughly flat along the 25 cm long TOF axis, which is enforced by equally spaced copper plates wired in-series with resistors between each. This electric field scheme responds differently to dissociative ionization events than do Wiley-McLaren reflectron spectrometers. Given the specific geometry and varying electric fields found in Wiley-McLaren reflectron TOF, the spread in kinetic energy imparted by dissociative ionization is condensed back into narrow TOF peaks by the time the ions reach the detector. The static electric field found in the PEPICO detector does not refocus the ions in time and so dissociative ionization peaks are broad in TOF and PIMS spectra. This allows for straightforward identification of dissociative ionization peaks in the spectra and disambiguation in the case where thermal and dissociative ionization peaks are both present.

Two examples where the present experimental setup is especially useful are 1) cases where two or more isomers are present and 118.2 nm PIMS is unable to distinguish between them and 2) cases where dissociative ionization is strong enough to causes spurious assignments of thermal decomposition products. To demonstrate the utility of this combination of experimental techniques, we have investigated two sets of molecules. The first experiment shows that the isomers 1,3-butadiene ( $\text{CH}_2=\text{CHCH}=\text{CH}_2$ ) and 1-butyne ( $\text{CH}_3\text{CH}_2\text{C}\equiv\text{CH}$ ) can be distinguished in PEPICO

spectra due to their different IE. The IE of 1,3-butadiene<sup>[5]</sup> is  $9.082 \pm 0.004$  eV and the IE of 1-butyne<sup>[6]</sup> is  $10.20 \pm 0.02$  eV. In this experiment, pure samples of each isomer were flowed through an unheated micro-reactor. In a mixture of the two samples, photoelectron spectra clearly resolve the two isomers. The true test of this method is to prepare a precursor that forms both isomers pyrolytically and confirm that both isomers remain distinguishable. The second experiment compares a set of pyrolysis experiments done both with 118.2 nm PIMS and VUV PEPICO experiments. A set of molecules that is challenging to study with 118.2 nm PIMS is small alcohols: methanol, ethanol, 1-propanol, 2-propanol, 1-butanol, and 2-butanol. The OH groups are highly susceptible to dissociative ionization, as was shown by a comprehensive study<sup>[1]</sup> of alcohols using the 9<sup>th</sup> harmonic of an Nd:YAG ionization source. Here, we show that due to dissociative ionization, pyrolysis of these alcohols is challenging with 118.2 nm PIMS but when using VUV and PEPICO, dissociative ionization can be identified and thus the pyrolysis products can be identified.

## II. Experimental

In order to combat issues of dissociative ionization, isomer ambiguity, and inability to ionize molecules with large ionization energies, we have coupled the micro-reactor to a laser system that generates harmonics of 800 nm Ti:sapphire laser light. The laser system was built in the group of Dr. Margaret Murnane and Dr. Henry Kapteyn and is modeled after the KMLabs Inc. Dragon<sup>TM</sup> system. The laser system used here is able to perform with 10 kHz repetition rate, which is important due to the low count rates required for coincidence detection. After amplifying the 30 fs output of a

Ti:sapphire mode locked oscillator, the power of the IR light is on the order of 20 W. This is focused into a waveguide made of a fused silica capillary (150  $\mu\text{m}$  I.D.  $\times$  2.5 cm long) in which Xe is flowed, generating odd harmonics in the range of the 3<sup>rd</sup> harmonic (roughly 4.8 eV) up through the 9<sup>th</sup> harmonic (roughly 14.4 eV); the technique is capable of higher harmonics, up to at least the 17th harmonic. The highest IE relevant to our experiments<sup>[7]</sup> is 15.4 eV for H<sub>2</sub>, so only the 9<sup>th</sup> harmonic and lower are necessary here. By filtering of higher harmonics with different filter schemes, harmonics can be selected by making only minor alterations to the system. The laser system was not modified for these experiments and a more detailed description can be found in a previous publication and citations therein.<sup>[8]</sup>

The micro-reactor assembly in this experiment can be used without a pulse valve since the source chamber is pumped by a large turbomolecular pump (1650 L s<sup>-1</sup> Leybold MAG W 2010 C). Roughly 1 cm downstream of the reactor exit is a 300  $\mu\text{m}$  skimmer that separates the source chamber from the ionization chamber and insures that a narrow molecular beam reaches the laser interaction region. In order to keep the pressure low enough for the detector, a 50  $\mu\text{m}$  orifice was brazed into the stainless steel tubing just upstream of the reactor. This allows for a backing pressure of 1 to 2 atm, downstream pressures in the source chamber of 10<sup>-4</sup> Torr, and ionization chamber pressures of 10<sup>-7</sup> Torr during continuous flow of He or Ar. The reactor assembly is shown in Fig. 8.1, which illustrates a few new design features. The alumina heat shield is now held tightly in place with a home-built, custom fit Swagelok nut. A small stainless steel disc is included that has electrical feedthroughs installed to help stabilize the delicate (0.005") wires leading to the Type-C thermocouple.

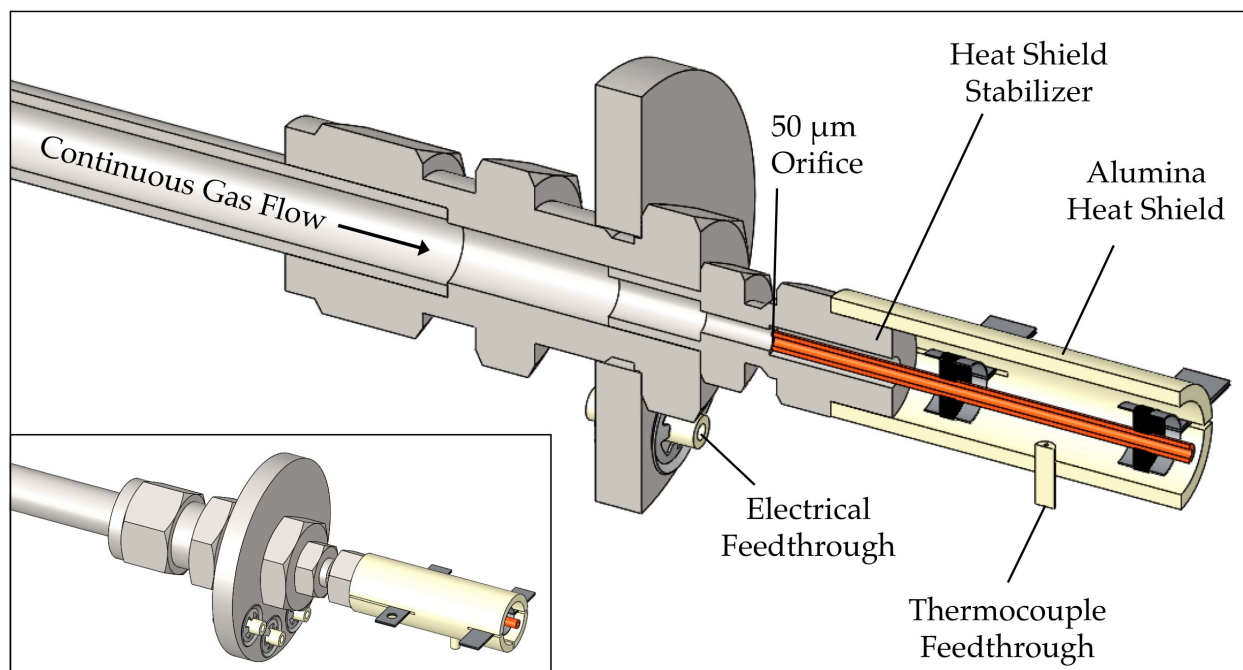


Fig. 8.1. Continuous flow heated micro-reactor assembly (inset) and larger cutaway diagram. The 50  $\mu\text{m}$  orifice limits the gas flow so that a pulsed valve is not needed to maintain appropriate upstream and downstream pressures. New design features are highlighted that help stabilize the assembly to prevent misalignment and increase thermocouple lifetime.

The detection mechanism in this experiment also adds important experimental information. Rather than a standard TOF configuration, the design of the ion optics in the interaction chamber allows us to detect both the cations and electrons formed from a single laser pulse. The count rate is intentionally attenuated so that only 1 in 10 laser pulses leads to a photoionization event, which would be challenging to maintain without the high repetition rate of the laser system (10 kHz). For a given ionization event, it is possible to correlate individual cations and their corresponding photoelectrons. The detectors for both the cations and the electrons are position sensitive so given a sufficiently small ionization volume, the distance traveled in the directions transverse to the flight axis can be used to calculate the kinetic energy of the charged particles. By plotting only the electrons detected in coincidence with a given

cation  $m/z$ , a photoelectron spectrum (PE) can be recorded. Although the instrument resolution is limited to about 0.75 eV, features in these photoelectron spectra can be identified and used as a diagnostic of given isomers. As long as two isomers have IEs that differ by more than roughly 1 eV, this detection scheme can be used to identify which isomers are present at a given  $m/z$ . Additionally, if a molecule in the molecular beam dissociatively ionizes, this detector can be used to identify the fragment mass as a product of dissociative ionization. The photoelectrons detected in coincidence with the dissociative ionization fragment will correspond to the PE spectrum of the parent molecule and not the fragment. As long as the PE spectra (or simply the IE) of the parent and the fragment are both known, peaks resulting from dissociative ionization can be removed from the recorded PIMS spectra during post-processing. These are major advantages over the Nd:YAG based TOF PIMS instruments that have been the workhorse of this experimental technique in the past.

### III. Results and Discussion

#### A. Isomer Identification

An ideal proof of concept system for this new VUV based PIMS experiment is to compare two stable gas-phase isomers by their ionization energy. For this, we compare two  $C_4H_6$  isomers, 1-butyne ( $CH_3CH_2C\equiv CH$ ) and 1,3-butadiene ( $CH_2=CHCH=CH_2$ ). This test case does not require heating the micro-reactor since both hydrocarbons are stable and can be entrained in the gas-phase using their vapor pressure at room temperature. The photoelectron spectrum of 1-butyne is shown in Fig. 8.2, where only the photoelectron counts recorded in coincidence  $m/z$  54 cations are plotted. The ionization energy of 1-butyne was previously established<sup>[6]</sup> to be 10.18 eV, which is roughly reproduced by the PE spectrum. The instrument resolution limits assignments

to roughly 0.75 eV and some further calibration is needed that results from day-to-day fluctuation of laser frequency. However, in cases like  $C_4H_6$  where isomers differ by roughly 1 eV, qualitative assignment is straightforward.

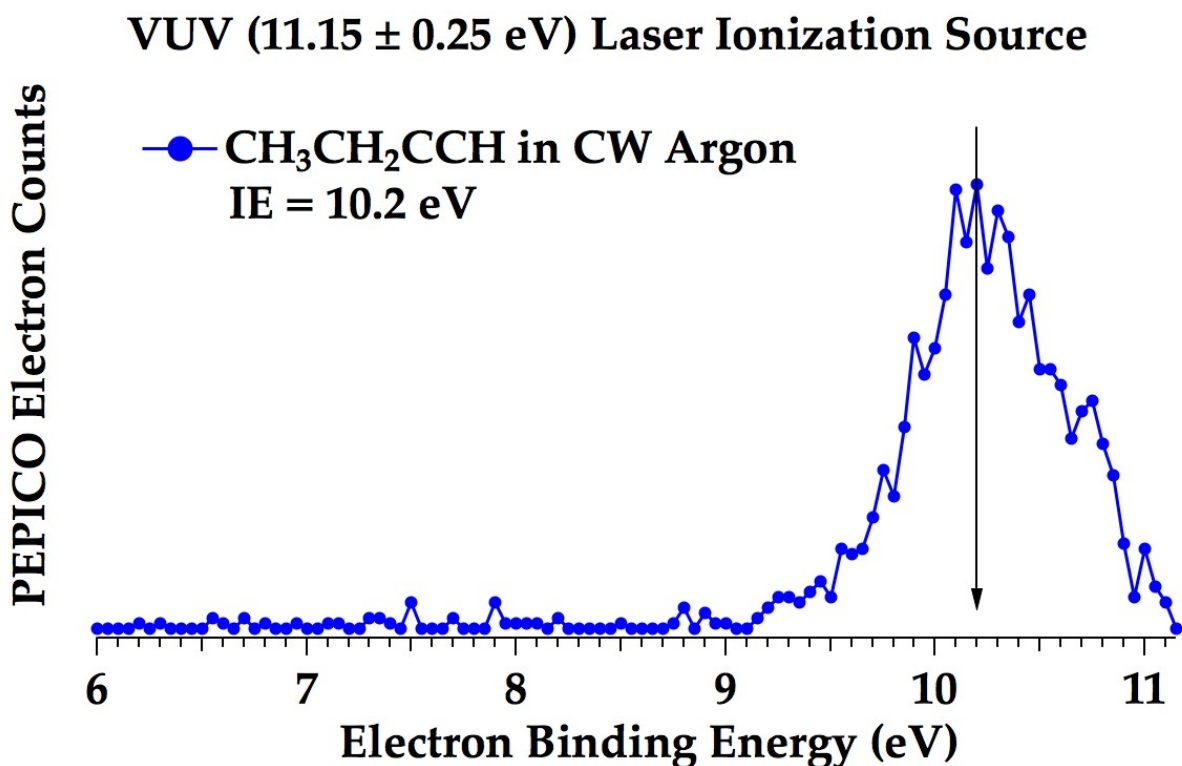


Fig. 8.2. Photoelectron spectrum of 1-butyne flowed through an unheated CW micro-reactor. A premixed gas sample was prepared of 10 % butyne in 5 atm of Ar. The PEPICO detector can be used to identify only photoelectrons detected in the same laser pulse as cations with  $m/z$  54.

The photoelectron spectrum of 1,3-butadiene is shown in the red trace of Fig. 8.3, which clearly differs from the blue trace of 1-butyne reproduced in Fig 8.3. The photoelectron spectrum of a room temperature mixture of the two is included in Fig. 8.3 as well, shown in black. This illustrates that given a mixture of species detected at  $m/z$  54, the presence of either isomer can be identified.



### VUV ( $11.15 \pm 0.25$ eV) Laser Ionization Source, CW Argon

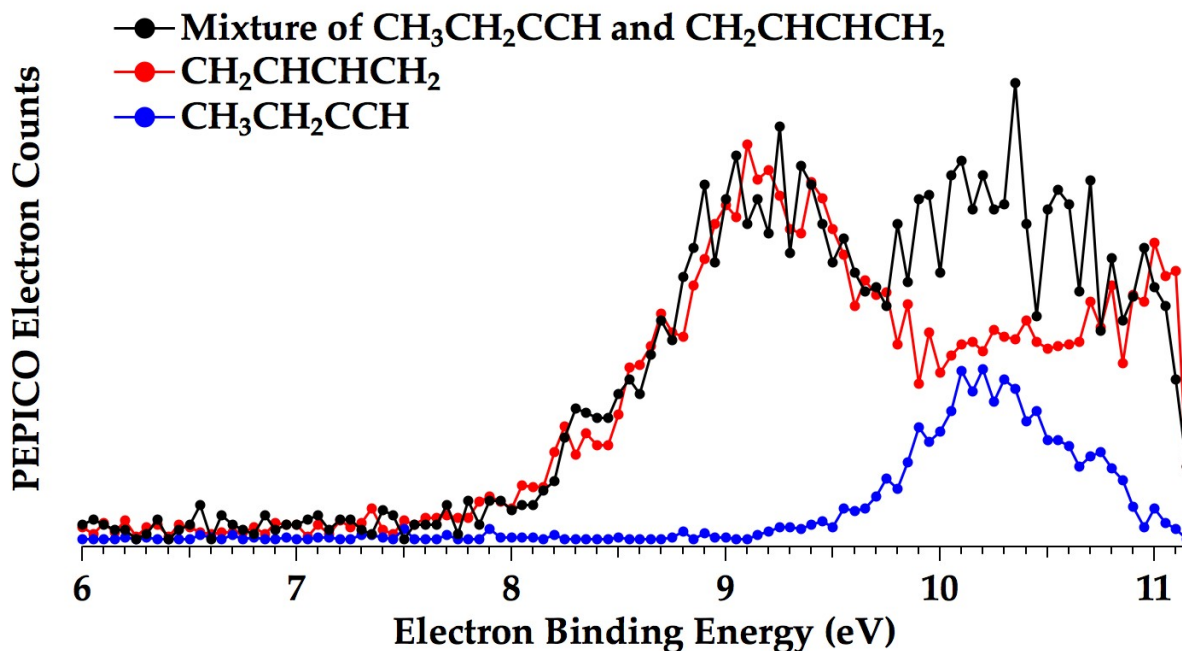


Fig. 8.3. Photoelectron spectrum of 1,3-butadiene (red trace), 1-butyne (blue trace), and a mixture of the two (black trace) flowed through an unheated CW micro-reactor. For each of the three traces, a 5 atm premixed gas sample was prepared of 10 % butadiene, 10 % butyne, or 10 % of both in Ar. In each case, only photoelectrons detected in coincidence with cations of  $m/z$  54 are plotted. The intensities of each are arbitrarily scaled to aid in feature identification. The black trace shows good agreement with butadiene for the peak near 9 eV but above 10 eV the red trace does not reproduce the mixture's spectrum. The peak at roughly 10.2 in butyne is required to match the mixture spectrum.

### B. Disentangling Dissociative Ionization in Mass Spectra

The pyrolysis of alcohols is often complicated by the presence of dissociative ionization peaks that are indistinguishable from true pyrolysis products in 118.2 nm PIMS experiments. The nature of the PEPICO detector allows for simplification of this issue. As an example, the pyrolysis of 2-butanol ( $\text{CH}_3\text{CH}_2\text{CH}(\text{OH})\text{CH}_3$ ) has been investigated in both 118.2 nm PIMS and VUV PEPICO PIMS experiments. Shown in

Fig. 8.4 is the PIMS spectrum of dilute 2-butanol flowed through a pulsed He reactor at room temperature recorded using the 9<sup>th</sup> harmonic of an Nd:YAG laser at 118.2 nm (10.487 eV). The parent peak is observed at  $m/z$  74 as well as multiple peaks at lower masses. Since this spectrum was recorded with a room temperature nozzle, none of the daughter peaks can be attributed to pyrolysis and are instead assigned as dissociative ionization of the parent. As is often the case with alcohols, significant fragmentation occurs after ionization. At elevated temperatures these peaks cannot be distinguished from pyrolysis products, causing potential misinterpretation of the PIMS spectra.

0.07%  $\text{CH}_3\text{CH}_2\text{CH}(\text{OH})\text{CH}_3$  ( $m/z$  74) in Pulsed He

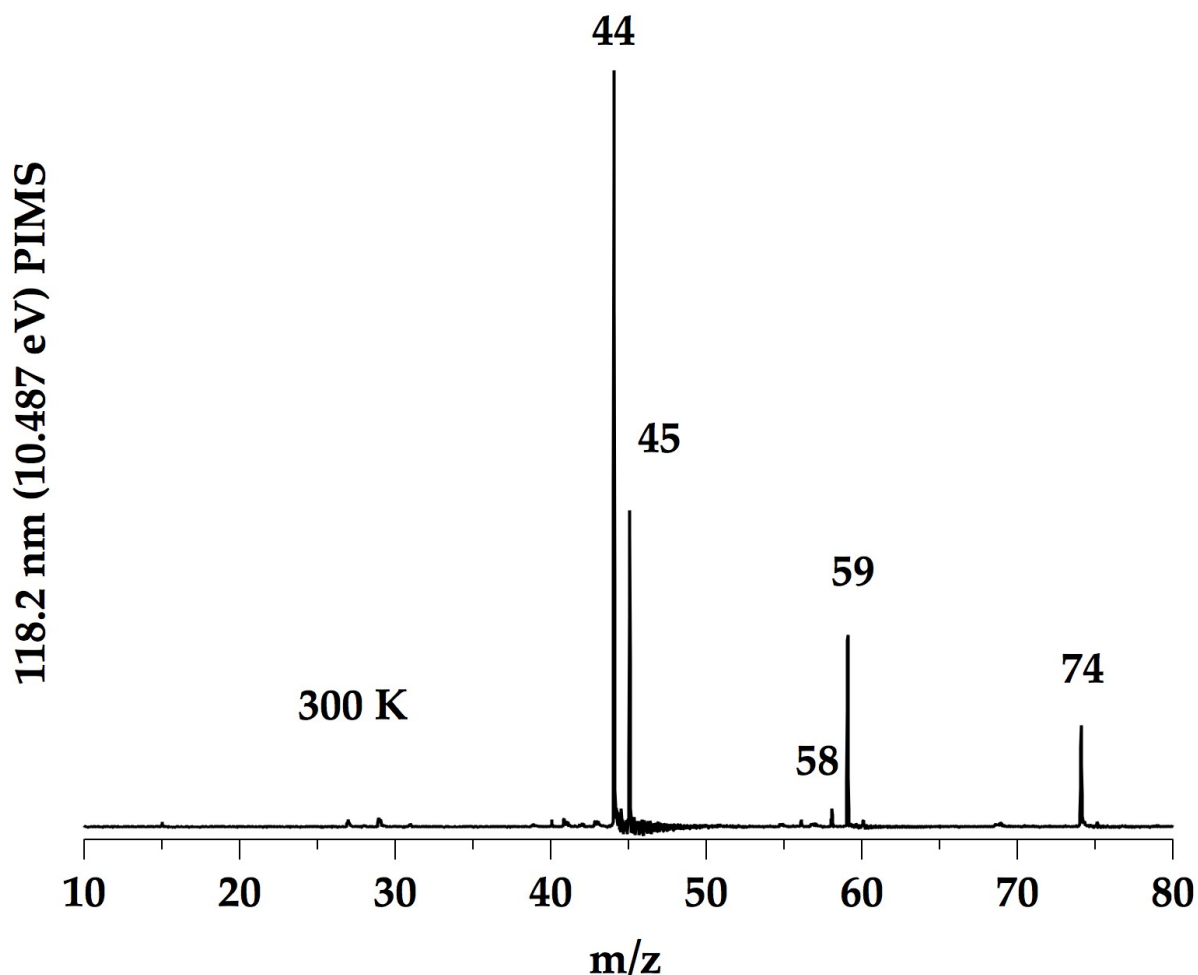


Fig. 8.4. Room temperature PIMS spectra of dilute (0.07 %) 2-butanol in a pulsed He micro-reactor. The ionization source is a 118.2 nm (10.487 eV) laser and PIMS is recorded in a Wiley-McLaren reflectron time-of-flight mass spectrometer. The parent is observed at  $m/z$  74 but is accompanied by multiple other fragments that are assumed to originate from dissociative ionization of 2-butanol.

In contrast, 2-butanol was flowed through the CW He reactor coupled to the VUV PEPICO detector and the dissociative ionization features are immediately identifiable. Fragmentation imparts kinetic energy into the daughter molecules and in the smaller, static electric field of the PEPICO detector, the energy spread in dissociative

ionization fragments results in a broadening of the PIMS features. Wiley-McLaren reflectron TOF instruments use varying electric fields to compensate for this energy spread and are able to refocus the cation signals into sharp features. As seen in Fig. 8.5, the dissociative ionization peaks are much broader than the parent peak at  $m/z$  74, and can be ruled out when considering what species are present in the molecular beam.

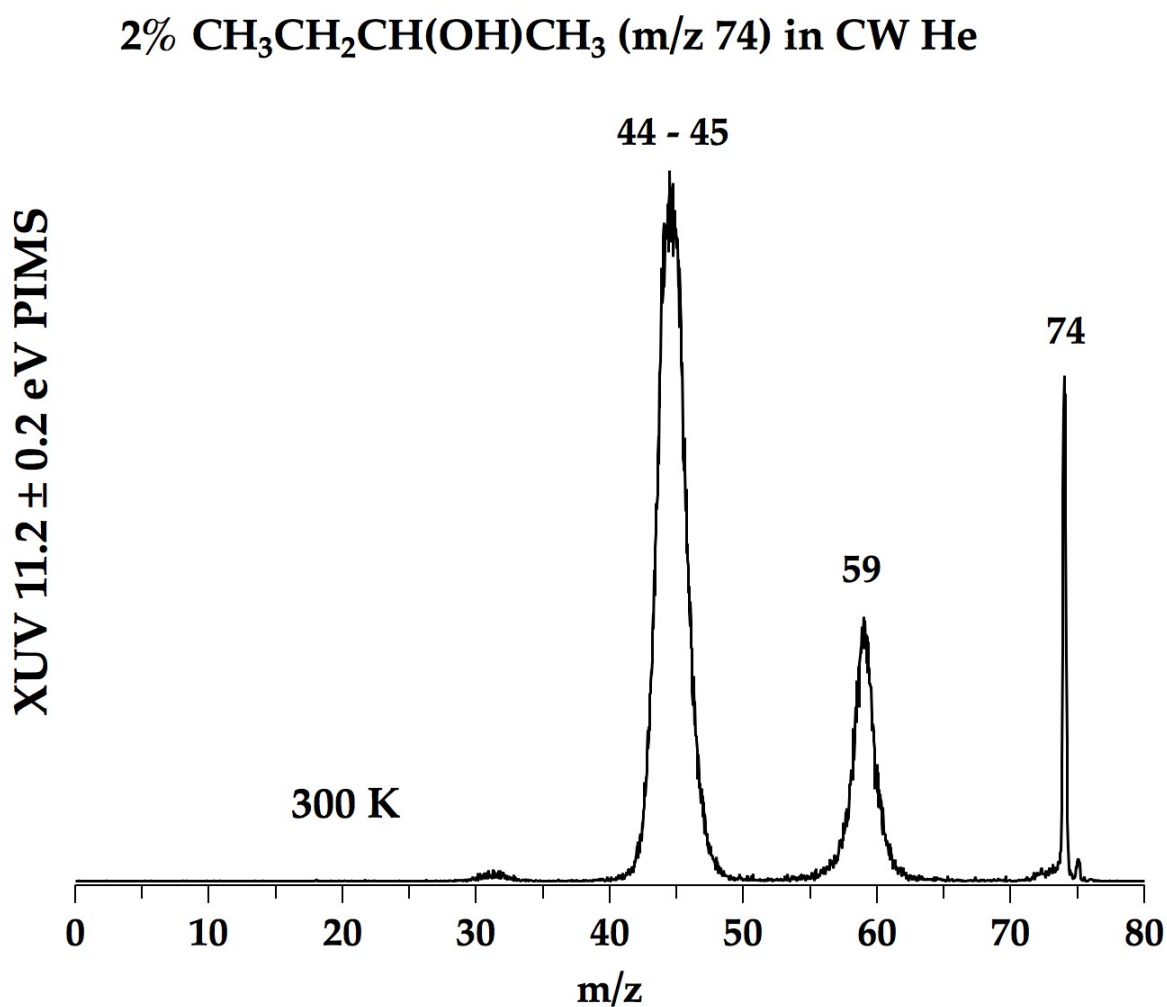


Fig. 8.5. Room temperature PIMS spectra of 2 % 2-butanol in a CW He micro-reactor. The ionization source is an upconverted Ti:sapphire laser yielding  $11.2 \pm 0.2$  eV light. The PEPICO detection source allows identification of dissociative ionization fragments. The parent peak at  $m/z$  74 is narrow but all other peaks have been broadened by their spread in kinetic energy.

Upon heating 2-butanol, dissociative ionization becomes a larger problem. If products are formed at the same mass as dissociative ionization peaks, it is difficult to assign them as thermal products. As new features appear in the PIMS spectra, they may either be the result of thermal decomposition of the parent or dissociative ionization of either the vibrationally excited parent molecules or of the thermal decomposition products. Although the supersonic expansion at the reactor's exit should cool all fragments, vibrational excitation often persists due to inefficient cooling.<sup>[9]</sup> Fig 8.6 shows the 118.2 nm PIMS spectra resulting from pyrolysis of 2-butanol at 1200 K in a pulsed He micro-reactor. Multiple new features are observed upon heating, the largest of which are  $m/z$  15, 28, 40, 41, 42, 44, 45, 54, 56, and 59. Depletion of the parent at  $m/z$  74 indicates that thermal decomposition is occurring but unfortunately, due to the presence of the dissociative ionization signals at room temperature, features at  $m/z$  44, 45 and 59 cannot be confidently identified as pyrolysis products.

0.07%  $\text{CH}_3\text{CH}_2\text{CH}(\text{OH})\text{CH}_3$  (m/z 74) in Pulsed He

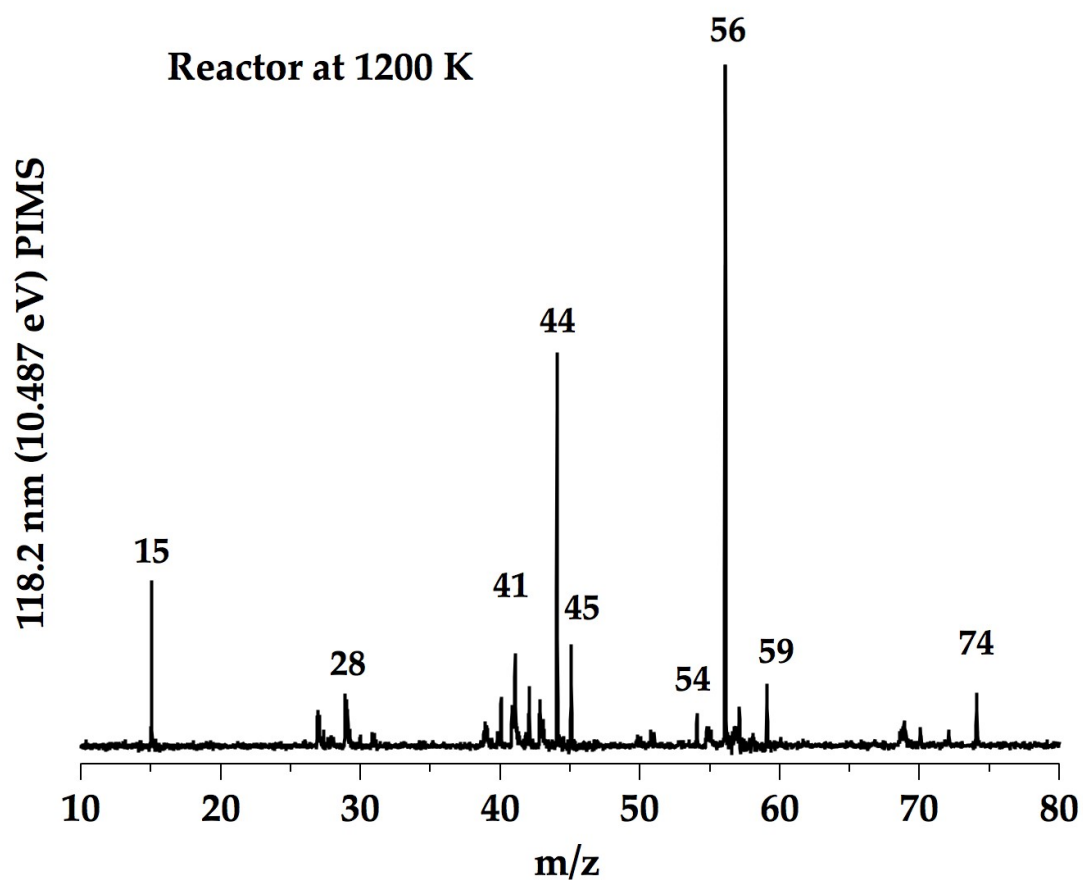


Fig. 8.6. PIMS of 0.07 % 2-butanol in a pulsed He micro-reactor at 1200 K, recorded with a 118.2 nm ionization source. The features at 44, 45, and 59 are also observed in room temperature PIMS spectra and are thus challenging to assign.

2% CH<sub>3</sub>CH<sub>2</sub>CH(OH)CH<sub>3</sub> (m/z 74) in CW He

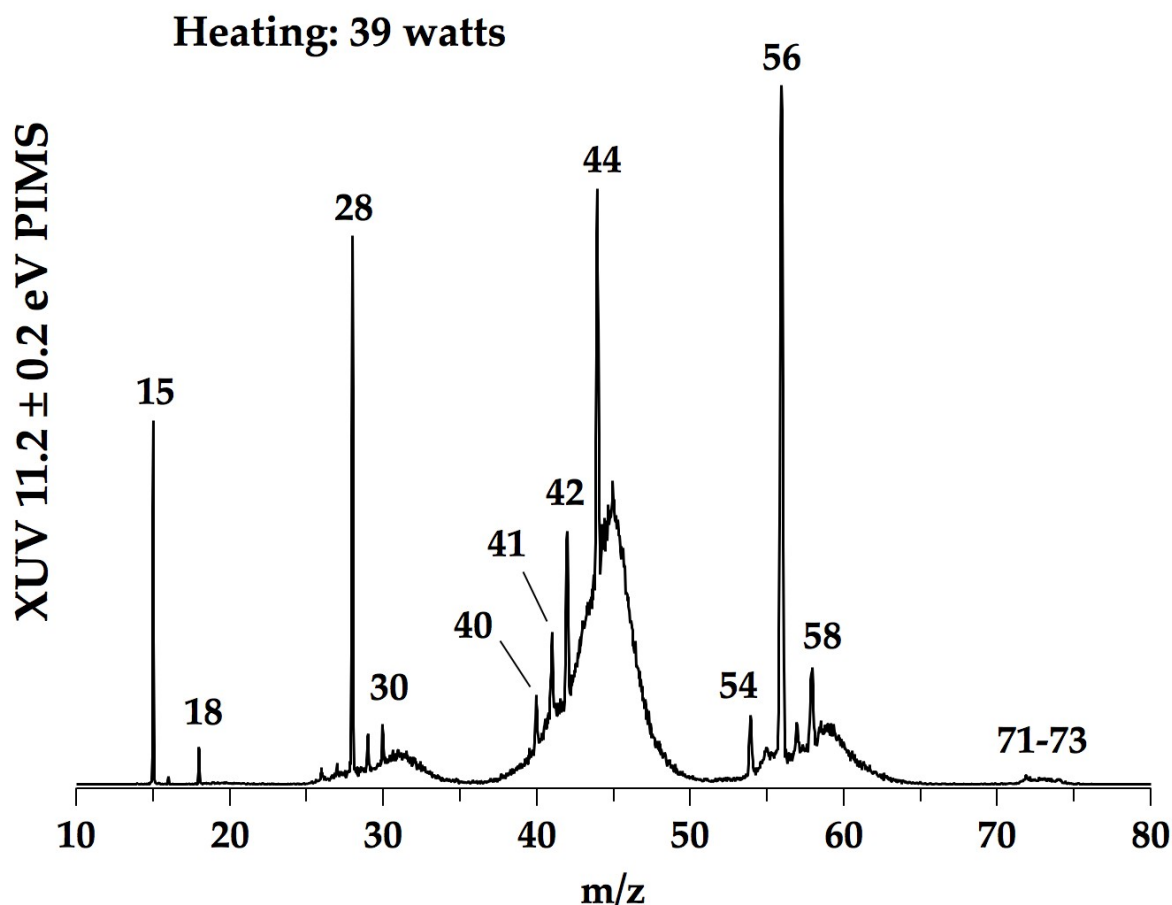


Fig. 8.7. PIMS of 2 % 2-butanol pyrolyzed in CW helium flowed through a micro-reactor heated with 3 Amps operating at 13 Volts. This is observationally approximated to be a reactor wall temperature of 1200 K. The narrow peaks are attributed to pyrolysis products and the broad peaks (roughly m/z 30, 45, 59 and 72) are now assigned to dissociative ionization.

Under similar conditions the experiment was repeated using the VUV PEPICO experiment and the PIMS spectrum is shown in Fig. 8.7. By comparing Fig. 8.6 and Fig. 8.7 we now can directly identify which species are pyrolysis products and which result from dissociative ionization. In Fig 8.6, the features at m/z 45 and 59 result from dissociative ionization but the remaining features all appear to be thermal products of 2-butanol pyrolysis and must be accounted for when examining detailed decomposition

pathways. An experimental detail worth noting here is that the current PEPICO experimental setup does not allow for direct wall temperature measurements. Instead, the current run through the resistively heated reactor can be directly controlled but the wall temperature must be roughly approximated by comparing product appearance and precursor depletion. Fig. 8.7 was recorded with current = 3 A and voltage = 13 V, corresponding to 39 watts of power. Future versions of the experiment can make use of Type-C thermocouples attached directly to the reactor to monitor temperature more accurately.

In addition to the PIMS spectra available with this detection scheme, photoelectron (PE) spectra can also be recorded. By keeping the ion count rate low (roughly one count per 10 laser pulses) it is possible to correlate electrons and cations from a single ionization event and experimentally resolve the energy of the electron. For a given cation  $m/z$ , the electrons can be plotted against electron kinetic energy to yield low-resolution PE spectra. The instrument resolution combined with the laser linewidth limit the PE spectra such that the full width at half maximum (FWHM) of the narrowest features is roughly 0.8 eV but this is sufficient to provide information regarding the species present at a given  $m/z$ .

Shown in Fig. 8.8 is the PE spectrum coincident with cations of  $m/z$  15 that are produced during the pyrolysis of 2-butanol. Given the composition of the precursor, the only reasonable assignment for this species is methyl radical ( $\text{CH}_3$ ). The frequency axis electron binding energy (eBE) shown in Fig. 8.8 (and all following PE figures) was made by assigning the laser energy so that the PE spectrum in Fig 8.8 matches the known ionization energy<sup>[10]</sup> of methyl radical ( $\text{IE}(\text{CH}_3) = 9.8380 \pm 0.0004$  eV). The laser



energy is taken to be 11.0 eV, which is within the accepted  $\pm 0.2$  eV uncertainty of the laser.

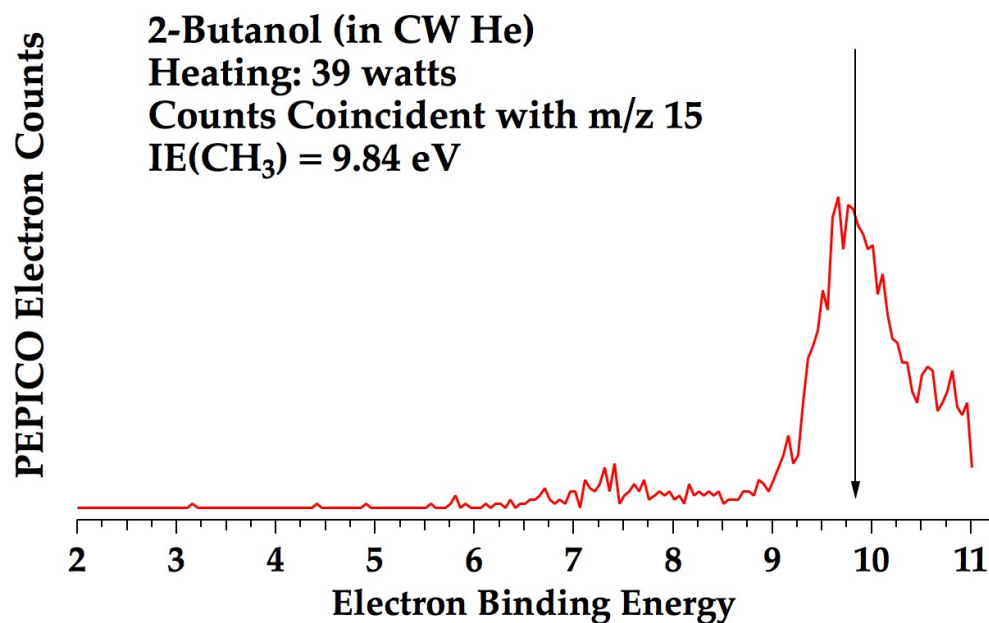


Fig. 8.8. PE spectrum of the species with  $m/z$  15, assigned to be methyl radical. Given  $\text{IE}(\text{CH}_3) = 9.84$  eV, the electron binding energy is determined from the experimentally recorded eKE of the coincident photoelectrons. The spectrum was recorded during pyrolysis of 2-butanol in CW He in a heated micro-reactor.

To corroborate this method of determining the frequency axis, the PE spectrum coincident with the cation with  $m/z$  28 is shown in Fig. 8.9. This is very likely signal from ethylene ( $\text{CH}_2=\text{CH}_2$ ) given the small number of molecules with a mass of 28 amu that can be made with C, H and O atoms. The assumed 11.0 eV photon energy agrees very well with the PE spectrum, as indicated by the black arrow that marks the ionization energy of ethylene<sup>[11]</sup> ( $\text{IE}(\text{CH}_2=\text{CH}_2) = 10.51268 \pm 0.00003\text{eV}$ ).

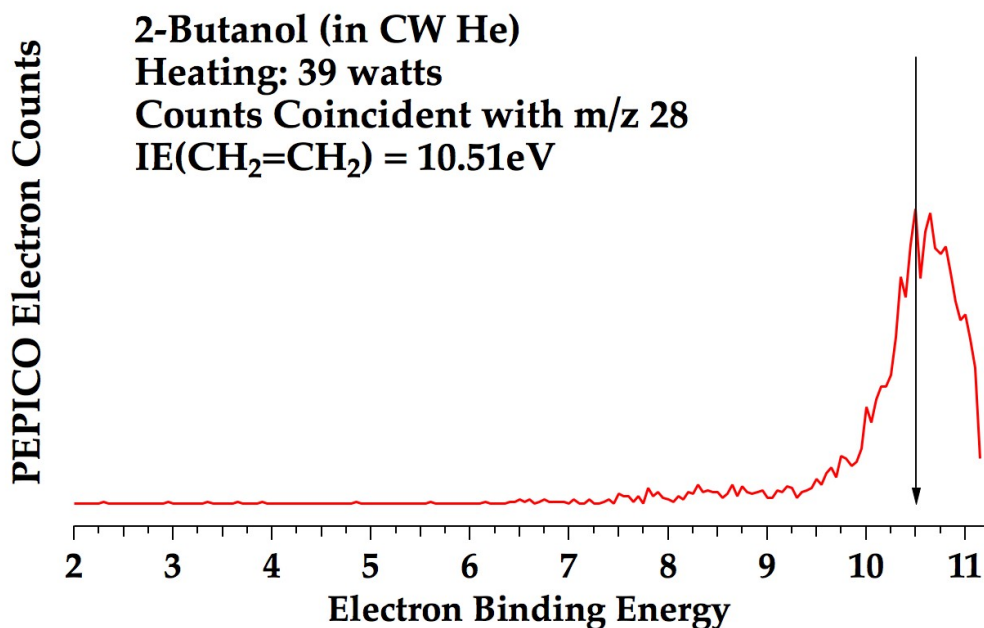


Fig. 8.9. PE spectrum of the species with m/z 28, assigned to be ethylene. The electron binding energy is determined from the experimentally recorded eKE from m/z 15 but shows good agreement with ethylene. The spectrum was recorded during pyrolysis of 2-butanol in CW He in a heated micro-reactor.

These PE spectra are especially useful when cation signal can be assigned to more than one species. In the pyrolysis of 2-butanol, two cases have been examined. Given the potential set of pyrolysis pathways present, the feature at m/z 56 could either be 1-butene<sup>[12]</sup> (IE(CH<sub>2</sub>=CHCH<sub>2</sub>CH<sub>3</sub>) = 9.55 ± 0.06 eV) or 2-butene<sup>[6]</sup> (IE(CH<sub>3</sub>CH=CHCH<sub>3</sub>) = 9.12 ± 0.02 eV). Fig. 8.10 shows the PE spectrum of the unidentified feature at m/z 56. Although more detailed calibration of this method is still required, the PE spectrum shows provocative agreement with the ionization energies of the two butene isomers. The wider feature (FWHM = 1.1 eV) appears to be consistent with a mixture of the two isomers.

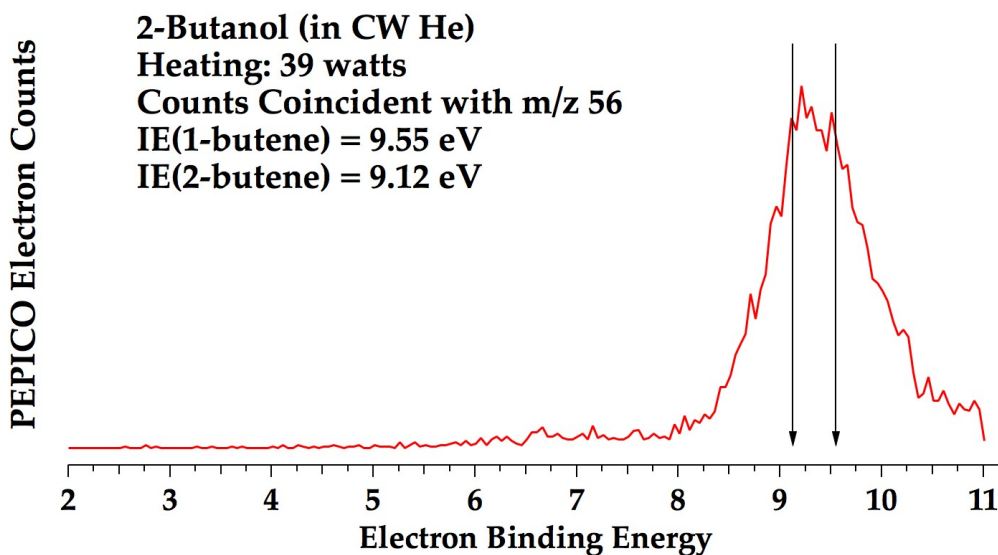


Fig. 8.10. PE spectrum of the species with  $m/z$  56, cautiously assigned to a mixture of 1-butene and 2-butene. The black arrows mark the ionization energy of the two isomers. The spectrum was recorded during pyrolysis of 2-butanol in CW He in a heated micro-reactor.

The PE spectrum of  $m/z$  44 is also of interest because two isomers are possible during pyrolysis of 2-butanol, vinyl alcohol ( $\text{CH}_2=\text{CHOH}$ ) and acetaldehyde ( $\text{CH}_3\text{CHO}$ ). The isomers are likely distinguishable using PE spectra due to their 1.1 eV difference in ionization energy:<sup>[13-14]</sup>  $\text{IE}(\text{CH}_3\text{CHO}) = 10.2295 \pm 0.0007$  eV and  $\text{IE}(\text{CH}_2=\text{CHOH}) \leq 9.33 \pm 0.05$  eV. Shown in Fig. 8.11 is the PE spectrum coincident with  $m/z$  44 (red trace) along with the IE of both isomers indicated with black arrows. To help identify which isomer(s) is present, the room temperature PE spectrum of acetaldehyde is shown (black trace) over the same spectral region. The enhancement of the pyrolysis spectrum towards the red end of Fig. 8.11 also indicates the presence of vinyl alcohol, which has the lower ionization energy.

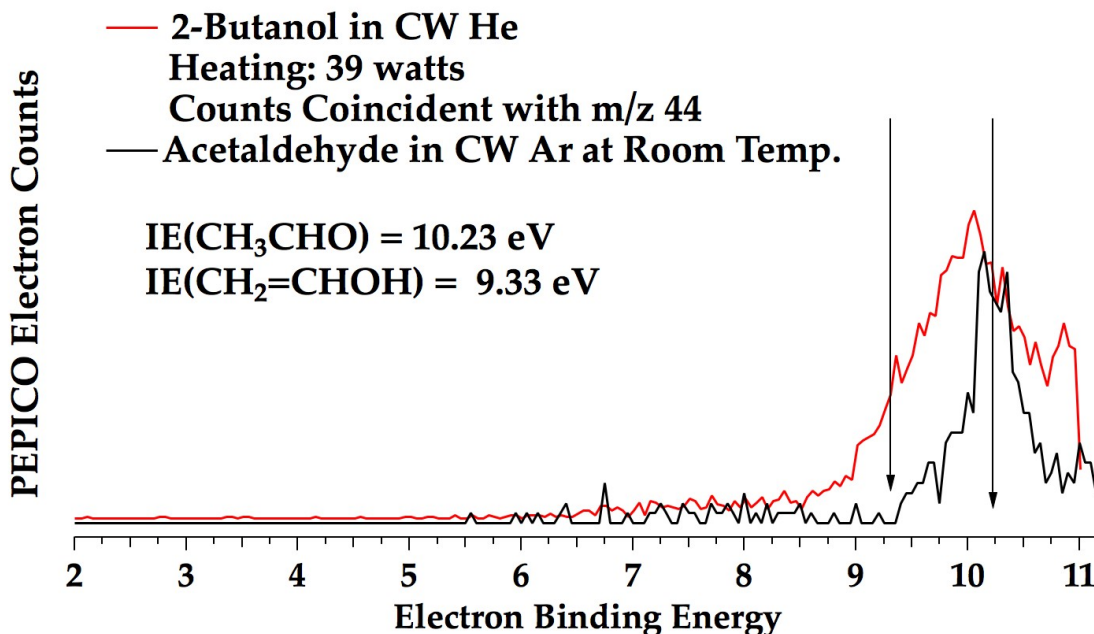


Fig. 8.11. PE spectrum of the species coincident with  $m/z$  44, potentially assigned to a mixture of acetaldehyde and vinyl alcohol. The black arrows mark the ionization energies of the two isomers. The spectrum was recorded during pyrolysis of 2-butanol in CW He in a heated micro-reactor.

#### IV. Conclusions

A new combination of VUV laser, PEPICO detector, and heated micro-reactor has been assembled that allows more informative PIMS spectra to be taken. In contrast to tunable synchrotron-based ionization sources, this system offers tabletop operation yet still provides isomer specific information and can be used to disentangle dissociative ionization features from pyrolysis products. The PEPICO detector permits measuring photoelectron spectra that allow assignment of fragments based on their ionization energy and/or photoelectron spectra. In the pyrolysis of 2-butanol, dissociative ionization can be identified in PIMS spectra and individual thermal decomposition fragments have been identified directly.

## References for Chapter 8

- [1] S. E. Van Bramer and M. V. Johnston. 10.5-eV photoionization mass spectrometry of aliphatic compounds. *Journal of the American Society for Mass Spectrometry* **1990**, *1*, 419-426.
- [2] X. Xing, B. Reed, K.-C. Lau, C. Y. Ng, X. Zhang and G. Barney Ellison. Vacuum ultraviolet laser pulsed field ionization-photoelectron study of allyl radical  $\text{CH}_2\text{CHCH}_2$ . *The Journal of Chemical Physics* **2007**, *126*, 171101.
- [3] W. C. Wiley and I. H. McLaren. Time - of - Flight Mass Spectrometer with Improved Resolution. *Review of Scientific Instruments* **1955**, *26*, 1150-1157.
- [4] T. K. Ormond, P. Hemberger, T. P. Troy, M. Ahmed, J. F. Stanton and G. B. Ellison. The ionisation energy of cyclopentadienone: a photoelectron-photoion coincidence study. *Molecular Physics* **2015**, *113*, 2350-2358.
- [5] W. G. Mallard, J. H. Miller and K. C. Smyth. The ns Rydberg series of 1,3-trans-butadiene observed using multiphoton ionization. *Journal of Chemical Physics* **1983**, *79*, 5900-5905.
- [6] G. Bieri, F. Burger, E. Heilbronner and J. P. Maier. Valence Ionization Energies of Hydrocarbons. *Helvetica Chimica Acta* **1977**, *60*, 2213-2233.
- [7] D. Shiner, J. M. Gilligan, B. M. Cook and W. Lichten.  $\text{H}_2$ ,  $\text{D}_2$ , and HD ionization-potentials by accurate calibration of several iodine lines. *Physical Review A* **1993**, *47*, 4042-4045.
- [8] E. Gagnon, A. S. Sandhu, A. Paul, K. Hagen, A. Czasch, T. Jahnke, P. Ranitovic, C. Lewis Cocke, B. Walker, M. M. Murnane and H. C. Kapteyn. Time-resolved momentum imaging system for molecular dynamics studies using a tabletop ultrafast extreme-ultraviolet light source. *Review of Scientific Instruments* **2008**, *79*, 063102.
- [9] C.-H. Chang and D. J. Nesbitt. Spectroscopy and Dynamics of Jet-Cooled Polyynes in a Slit Supersonic Discharge: Sub-Doppler Infrared Studies of Diacetylene  $\text{HCCCCH}$ . *The Journal of Physical Chemistry A* **2015**, *119*, 7940-7950.

- [10] J. A. Blush, P. Chen, R. T. Wiedmann and M. G. White. Rotationally resolved threshold photoelectron-spectrum of the methyl radical. *Journal of Chemical Physics* **1993**, *98*, 3557-3559.
- [11] X. Xing, B. Reed, M. K. Bahng and C. Y. Ng. Infrared-vacuum ultraviolet pulsed field ionization-photoelectron study of  $C_2H_4^+$  using a high-resolution infrared laser. *Journal of Physical Chemistry A* **2008**, *112*, 2572-2578.
- [12] C. E. van Der Meij, J. Van Eck and A. Niehaus. The decomposition of  $C_4H_8^+$  complexes at controlled internal energies. *Chemical Physics* **1989**, *130*, 325-334.
- [13] D. J. Knowles and A. J. C. Nicholson. Ionization energies of formic and acetic-acid monomers. *Journal of Chemical Physics* **1974**, *60*, 1180-1181.
- [14] C. A. Taatjes, N. Hansen, A. McIlroy, J. A. Miller, J. P. Senosiain, S. J. Klippenstein, F. Qi, L. S. Sheng, Y. W. Zhang, T. A. Cool, J. Wang, P. R. Westmoreland, M. E. Law, T. Kasper and K. Kohse-Hoinghaus. Enols are common intermediates in hydrocarbon oxidation. *Science* **2005**, *308*, 1887-1889.



## Bibliography

- Agafonov, G. L., Naydenova, I., Vlasov, P. A. and Warnatz, J. Detailed kinetic modeling of soot formation in shock tube pyrolysis and oxidation of toluene and n-heptane. *Proceedings of the Combustion Institute* **2007**, 31, 575-583.
- Alexiou, A. and Williams, A. Soot Formation in Shock-Tube Pyrolysis of Toluene, Toluene-Methanol, Toluene-Ethanol, and Toluene-Oxygen Mixtures. *Combustion and Flame* **1996**, 104, 51-65.
- Angell, C. L. Vapor-phase infrared spectrum and structure of fulvenallene. *Journal of Molecular Structure* **1971**, 10, 265-273.
- Applegate, B. E., Bezant, A. J. and Miller, T. A. The Jahn-Teller and related effects in the cyclopentadienyl radical. II. Vibrational analysis of the  $A^2A_2'' - X^2E_1''$  electronic transition. *Journal of Chemical Physics* **2001**, 114, 4869-4882.
- Astholz, D. C., Brouwer, L. and Troe, J. High-temperature ultraviolet-absorption spectra of polyatomic-molecules in shock-waves. *Berichte Der Bunsen-Gesellschaft-Physical Chemistry Chemical Physics* **1981**, 85, 559-564.
- Astholz, D. C. and Troe, J. Thermal-decomposition of benzyl radicals in shock-waves. *Journal of the Chemical Society-Faraday Transactions II* **1982**, 78, 1413-1421.
- Baer, T., Morrow, J. C., Shao, J. D. and Olesik, S. Gas-phase heats of formation of  $C_7H_7^+$  isomers - *meta*-tolyl, *para*-tolyl, and benzyl ions. *Journal of the American Chemical Society* **1988**, 110, 5633-5638.
- Bandy, R. E., Lakshminarayan, C., Frost, R. K. and Zwier, T. S. The Ultraviolet Photochemistry of Diacetylene - Direct Detection of Primary Products of the Metastable  $C_4H_2^* + C_4H_2$  Reaction. *Journal of Chemical Physics* **1993**, 98, 5362-5374.
- Baraban, J. H., David, D. E., Ellison, G. B. and Daily, J. W. An optically accessible pyrolysis microreactor. *Review of Scientific Instruments* **2016**, 87, 014101.
- Baskir, E. G., Maltsev, A. K., Korolev, V. A., Khabashesku, V. N. and Nefedov, O. M. Generation and ir spectroscopic study of benzyl radical. *Russian Chemical Bulletin* **1993**, 42, 1438-1440.



- Bennett, J. E., Mile, B. and Thomas, A. Electron spin resonance spectrum of phenyl radical prepared by chemical reaction at 77 K. *Chemical Communications* **1965**, 265-267.
- Bethardy, G. A., Wang, X. L. and Perry, D. S. The role of molecular flexibility in accelerating intramolecular vibrational-relaxation. *Canadian Journal of Chemistry* **1994**, 72, 652-659.
- Bieri, G., Burger, F., Heilbronner, E. and Maier, J. P. Valence Ionization Energies of Hydrocarbons. *Helvetica Chimica Acta* **1977**, 60, 2213-2233.
- Blanksby, S. J. and Ellison, G. B. Bond dissociation energies of organic molecules. *Accounts of Chemical Research* **2003**, 36, 255-263.
- Blitz, M., Pilling, M. J., Robertson, S. H. and Seakins, P. W. Direct studies on the decomposition of the tert-butoxy radical and its reaction with NO. *Physical Chemistry Chemical Physics* **1999**, 1, 73-80.
- Blush, J. A., Chen, P., Wiedmann, R. T. and White, M. G. Rotationally Resolved Threshold Photoelectron-Spectrum of the Methyl Radical. *Journal of Chemical Physics* **1993**, 98, 3557-3559.
- Blush, J. A., Chen, P., Wiedmann, R. T. and White, M. G. Rotationally resolved threshold photoelectron-spectrum of the methyl radical. *Journal of Chemical Physics* **1993**, 98, 3557-3559.
- Blush, J. A., Clauberg, H., Kohn, D. W., Minsek, D. W., Zhang, X. and Chen, P. Photoionization Mass and Photoelectron-Spectroscopy of Radicals, Carbenes, and Biradicals. *Accounts Chem. Res.* **1992**, 25, 385-392.
- Bodi, A., Johnson, M., Gerber, T., Gengeliczki, Z., Sztaray, B. and Baer, T. Imaging photoelectron photoion coincidence spectroscopy with velocity focusing electron optics. *Review of Scientific Instruments* **2009**, 80, 034101.
- Bohm, H. and Jander, H. PAH formation in acetylene-benzene pyrolysis. *Physical Chemistry Chemical Physics* **1999**, 1, 3775-3781.
- Boyle, J. and Pfefferle, L. Study of higher hydrocarbon production during ethylacetylene pyrolysis using laser-generated vacuum-ultraviolet photoionization detection. *Journal of Physical Chemistry* **1990**, 94, 3336-3340.

- Braun-Unkhoff, M., Frank, P. and Just, T. High-temperature reactions of benzyl radicals. *Berichte Der Bunsen-Gesellschaft-Physical Chemistry Chemical Physics* **1990**, *94*, 1417-1425.
- Brezinsky, K. The high-temperature oxidation of aromatic hydrocarbons. *Progress in Energy and Combustion Science* **1986**, *12*, 1-24.
- Bridgwater, A. V. Review of fast pyrolysis of biomass and product upgrading. *Biomass & Bioenergy* **2012**, *38*, 68-94.
- Bridgwater, A. V., Meier, D. and Radlein, D. An overview of fast pyrolysis of biomass. *Organic Geochemistry* **1999**, *30*, 1479-1493.
- Brouwer, L., Müller-Markgraf, W. and Troe, J. Thermal-decomposition of ethylbenzene in shock-waves. *Berichte Der Bunsen-Gesellschaft-Physical Chemistry Chemical Physics* **1983**, *87*, 1031-1036.
- Brouwer, L. D., Müller-Markgraf, W. and Troe, J. Thermal-decomposition of toluene - a comparison of thermal and laser-photochemical activation experiments. *Journal of Physical Chemistry* **1988**, *92*, 4905-4914.
- Brown, A. L., Dayton, D. C., Nimlos, M. R. and Daily, J. W. Design and characterization of an entrained flow reactor for the study of biomass pyrolysis chemistry at high heating rates. *Energy and Fuels* **2001**, *15*, 1276-1285.
- Buckingham, G. T., Chang, C.-H. and Nesbitt, D. J. High-Resolution Rovibrational Spectroscopy of Jet-Cooled Phenyl Radical: The  $\nu_{19}$  Out-of-Phase Symmetric CH Stretch. *The Journal of Physical Chemistry A* **2013**, *117*, 10047-10057.
- Buckingham, G. T., Ormond, T. K., Porterfield, J. P., Hemberger, P., Kostko, O., Ahmed, M., Robichaud, D. J., Nimlos, M. R., Daily, J. W. and Ellison, G. B. The Thermal Decomposition of the Benzyl Radical in a Heated Micro-Reactor: I. Experimental Findings. *Journal of Chemical Physics* **2015**, *142*, 044307-044320.
- Buckingham, G. T., Ormond, T. K., Porterfield, J. P., Hemberger, P., Kostko, O., Ahmed, M., Robichaud, D. J., Nimlos, M. R., Daily, J. W. and Ellison, G. B. The thermal decomposition of the benzyl radical in a heated micro-reactor. I. Experimental findings. *The Journal of Chemical Physics* **2015**, *142*, 044307.

- Bunker, P. R., Jensen, P., Canada, N. R. C. and Program, N. R. C. C. M. P., *Molecular Symmetry and Spectroscopy*, NRC Research Press, **2006**, p. 90-92.
- Burger, J. L., Lovestead, T. M. and Bruno, T. J. Composition of the C-6+ Fraction of Natural Gas by Multiple Porous Layer Open Tubular Capillaries Maintained at Low Temperatures. *Energy & Fuels* **2016**, *30*, 2119-2126.
- Butcher, V., Costa, M. L., Dyke, J. M., Ellis, A. R. and Morris, A. A study of the phenyl radical by vacuum ultraviolet photoelectron-spectroscopy. *Chemical Physics* **1987**, *115*, 261-267.
- Callegari, A., Merker, U., Engels, P., Srivastava, H. K., Lehmann, K. K. and Scoles, G. Intramolecular vibrational redistribution in aromatic molecules. I. Eigenstate resolved CH stretch first overtone spectra of benzene. *Journal of Chemical Physics* **2000**, *113*, 10583-10596.
- Cavallotti, C., Derudi, M. and Rota, R. On the mechanism of decomposition of the benzyl radical. *Proceedings of the Combustion Institute* **2009**, *32*, 115-121.
- Cavallotti, C., Mancarella, S., Rota, R. and Carra, S. Conversion of C<sub>5</sub> Into C<sub>6</sub> Cyclic Species Through the Formation of C<sub>7</sub> Intermediates. *Journal of Physical Chemistry A* **2007**, *111*, 3959-3969.
- Cernicharo, J., Heras, A. M., Tielens, A., Pardo, J. R., Herpin, F., Guelin, M. and Waters, L. Infrared Space Observatory's discovery of C<sub>4</sub>H<sub>2</sub>, C<sub>6</sub>H<sub>2</sub>, and benzene in CRL 618. *Astrophysical Journal* **2001**, *546*, L123-L126.
- Chang, C.-H. and Nesbitt, D. J. Spectroscopy and Dynamics of Jet-Cooled Polyynes in a Slit Supersonic Discharge: Sub-Doppler Infrared Studies of Diacetylene HCCCCH. *The Journal of Physical Chemistry A* **2015**, *119*, 7940-7950.
- Chen, P. *Supersonic Jets of Organic Radicals*, Eds.: C. Y. Ng, T. Baer and I. Powis, John Wiley, Cambridge, UK, **1994**, pp. 371-397.
- Chen, P., Colson, S. D., Chupka, W. A. and Berson, J. A. Flash Pyrolytic Production of Rotationally Cold Free-Radicals in a Supersonic Jet - Resonant Multiphoton Spectrum of the 3P <sup>2</sup>A<sub>2</sub>" Origin Band of CH<sub>3</sub>. *Journal of Physical Chemistry* **1986**, *90*, 2319-2321.

- Chen, P., Pallix, J. B., Chupka, W. A. and Colson, S. D. Resonant multiphoton ionization spectrum and electronic-structure of CH radical - new states and assignments above 50,000 cm<sup>-1</sup>. *Journal of Chemical Physics* **1987**, 86, 516-521.
- Cherchneff, I., Barker, J. R. and Tielens, A. Polycyclic aromatic hydrocarbon formation in carbon-rich stellar envelopes. *Astrophysical Journal* **1992**, 401, 269-287.
- Clary, D. C., Lovejoy, C. M., Oneil, S. V. and Nesbitt, D. J. Infrared-spectrum of NeHF. *Physical Review Letters* **1988**, 61, 1576-1579.
- Cohen, M. J., Handy, N. C., Hernandez, R. and Miller, W. H. Cumulative reaction probabilities for H + H<sub>2</sub> → H<sub>2</sub> + H from a knowledge of the anharmonic-force field. *Chemical Physics Letters* **1992**, 192, 407-416.
- Condirston, D. A. and Laposa, J. D. Vibrational-spectra of styrene-H8, styrene-D3, styrene-D5, and styrene-D8. *Journal of Molecular Spectroscopy* **1976**, 63, 466-477.
- Cook, B. R., Wilkinson, B. B., Culross, C. C., Holmes, S. M. and Martinez, L. E. Hydrogen transfer induced cleavage of biaryl bonds. *Energy & Fuels* **1997**, 11, 61-75.
- Coveleskie, R. A., Dolson, D. A. and Parmenter, C. S. A direct view of intramolecular vibrational redistribution in s1 para-difluorobenzene. *Journal of Chemical Physics* **1980**, 72, 5774-5775.
- da Silva, G. Oxidation of Carboxylic Acids Regenerates Hydroxyl Radicals in the Unpolluted and Nighttime Troposphere. *Journal of Physical Chemistry A* **2010**, 114, 6861-6869.
- da Silva, G. and Bozzelli, J. W. Benzoyl Radical Decomposition Kinetics: Formation of Benzaldehyde plus H, Phenyl + CH<sub>2</sub>O, and Benzene plus HCO. *Journal of Physical Chemistry A* **2009**, 113, 6979-6986.
- da Silva, G. and Trevitt, A. J. Chemically activated reactions on the C<sub>7</sub>H<sub>5</sub> energy surface: propargyl plus diacetylene, i-C<sub>5</sub>H<sub>3</sub> + acetylene, and n-C<sub>5</sub>H<sub>3</sub> + acetylene. *Physical Chemistry Chemical Physics* **2011**, 13, 8940-8952.
- da Silva, G., Trevitt, A. J., Steinbauer, M. and Hemberger, P. Pyrolysis of fulvenallene (C<sub>7</sub>H<sub>6</sub>) and fulvenallenyl (C<sub>7</sub>H<sub>5</sub>): Theoretical kinetics and experimental product detection. *Chemical Physics Letters* **2011**, 517, 144-148.

- Dagaut, P., Pengloan, G. and Ristori, A. Oxidation, Ignition and Combustion of Toluene: Experimental and Detailed Chemical Kinetic Modeling. *Physical Chemistry Chemical Physics* **2002**, *4*, 1846-1854.
- Dagaut, P., Ristori, A., El Bakali, A. and Cathonnet, M. Experimental and Kinetic Modeling Study of the Oxidation of n-Propylbenzene. *Fuel* **2002**, *81*, 173-184.
- Davis, S., Farnik, M., Uy, D. and Nesbitt, D. J. Concentration modulation spectroscopy with a pulsed slit supersonic discharge expansion source. *Chemical Physics Letters* **2001**, *344*, 23-30.
- Derudi, M., Polino, D. and Cavallotti, C. Toluene and Benzyl Decomposition Mechanisms: Elementary Reactions and Kinetic Simulations. *Physical Chemistry Chemical Physics* **2011**, *13*, 21308-21318.
- Dong, F., Davis, S. and Nesbitt, D. J. Slit discharge IR spectroscopy of a jet-cooled cyclopropyl radical: Structure and intramolecular tunneling dynamics. *Journal of Physical Chemistry A* **2006**, *110*, 3059-3070.
- Dooley, S., Won, S. H., Chaos, M., Heyne, J., Ju, Y., Dryer, F. L., Kumar, K., Sung, C.-J., Wang, H., Oehlschlaeger, M. A., Santoro, R. J. and Litzinger, T. A. A Jet Fuel Surrogate Formulated by Real Fuel Properties. *Combustion and Flame* **2010**, *157*, 2333-2339.
- Dyke, J. M., Ozeki, H., Takahashi, M., Cockett, M. C. R. and Kimura, K. A study of phenylacetylene and styrene, and their argon complexes PA-Ar and ST-Ar with laser threshold photoelectron spectroscopy. *The Journal of Chemical Physics* **1992**, *97*, 8926-8933.
- Ehrenfreund, P. Astrophysical chemistry: Molecules on a space odyssey. *Science* **1999**, *283*, 1123-1124.
- Eiden, G. C., Weinhold, F. and Weisshaar, J. C. Photoelectron-spectroscopy of free-radicals with  $\text{cm}^{-1}$  resolution - the benzyl cation. *Journal of Chemical Physics* **1991**, *95*, 8665-8668.
- Elder, F. A. and Parr, A. C. Photoionization of the Cycloheptatrienyl Radical. *Journal of Chemical Physics* **1969**, *50*, 1027-1028.

- Ellison, G. B., Davico, G. E., Bierbaum, V. M. and DePuy, C. H. Thermochemistry of the benzyl and allyl radicals and ions. *International Journal of Mass Spectrometry and Ion Processes* **1996**, 156, 109-131.
- Ervin, K. M., Ho, J. and Lineberger, W. C. A STUDY OF THE SINGLET AND TRIPLET-STATES OF VINYLIDENE BY PHOTOELECTRON-SPECTROSCOPY OF  $\text{H}_2\text{C}=\text{C}^-$ ,  $\text{D}_2\text{C}=\text{C}^-$ , AND  $\text{HDC}=\text{C}^-$  — VINYLIDENE ACETYLENE ISOMERIZATION. *Journal of Chemical Physics* **1989**, 91, 5974-5992.
- Fischer, K. H., Hemberger, P., Bodi, A. and Fischer, I. Photoionisation of the tropylium radical. *Beilstein Journal of Organic Chemistry* **2013**, 9, 681-688.
- Freel, K., Lin, M. C. and Heaven, M. C. Cavity ring-down spectroscopy of the phenyl radical in a pulsed discharge supersonic jet expansion *Chemical Physics Letters* **2011**, 507, 216-220.
- Frenklach, M., Clary, D. W., Gardiner, W. C. and Stein, S. E. Twentieth Symposium (International) on Combustion Detailed kinetic modeling of soot formation in shock-tube pyrolysis of acetylene. *Symposium (International) on Combustion* **1984**, 20, 887-901.
- Frenklach, M. and Feigelson, E. D. Formation of polycyclic aromatic-hydrocarbons in circumstellar envelopes. *Astrophysical Journal* **1989**, 341, 372-384.
- Friderichsen, A. V., Radziszewski, J. G., Nimlos, M. R., Winter, P. R., Dayton, D. C., David, D. E. and Ellison, G. B. The infrared spectrum of the matrix-isolated phenyl radical. *Journal of the American Chemical Society* **2001**, 123, 1977-1988.
- Friderichsen, A. V., Shin, E.-J., Evans, R. J., Nimlos, M. R., Dayton, D. C. and Ellison, G. B. The Pyrolysis of Anisole ( $\text{C}_6\text{H}_5\text{OCH}_3$ ) Using a Hyperthermal Nozzle. *Fuel* **2001**, 80, 1747-1755.
- Frisch, M., Trucks, G., Schlegel, H., Scuseria, G., Robb, M., Cheeseman, J., Zakrzewski, V., Montgomery Jr, J., Stratmann, R. and Burant, J. *Gaussian 98, revision A. 7; Gaussian, Inc, Pittsburgh, Pa, 1998.*
- Frisch, M., Trucks, G., Schlegel, H., Scuseria, G., Robb, M., Cheeseman, J., Zakrzewski, V., Montgomery Jr, J., Stratmann, R. E. and Burant, J. *Gaussian 98, revision a. 7; gaussian, Inc., Pittsburgh, PA, 1998.*

- Fröchtenicht, R., Hippler, H., Troe, J. and Toennies, J. P. Photon-induced unimolecular decay of the benzyl radical - 1<sup>st</sup> direct identification of the reaction pathway to C<sub>7</sub>H<sub>6</sub>. *Journal of Photochemistry and Photobiology a-Chemistry* **1994**, *80*, 33-37.
- Furimsky, E. Catalytic hydrodeoxygenation. *Applied Catalysis a-General* **2000**, *199*, 147-190.
- Fuson, N., Garrigou-Lagrange, C. and Josien, M. L. Spectre infrarouge et attribution des vibrations des toluènes C<sub>6</sub>H<sub>5</sub>CH<sub>3</sub>, C<sub>6</sub>H<sub>5</sub>CD<sub>3</sub> et C<sub>6</sub>D<sub>5</sub>CD<sub>3</sub>. *Spectrochimica Acta* **1960**, *16*, 106-127.
- Fuson, N., Garrigoulagrange, C. and Josien, M. L. Spectre Infrarouge et Attribution des Vibrations des Toluènes C<sub>6</sub>H<sub>5</sub>CH<sub>3</sub>, C<sub>6</sub>H<sub>5</sub>CD<sub>3</sub> et C<sub>6</sub>D<sub>5</sub>CD<sub>3</sub>. *Spectrochimica Acta* **1960**, *16*, 106-127.
- Gagnon, E., Sandhu, A. S., Paul, A., Hagen, K., Czasch, A., Jahnke, T., Ranitovic, P., Lewis Cocke, C., Walker, B., Murnane, M. M. and Kapteyn, H. C. Time-resolved momentum imaging system for molecular dynamics studies using a tabletop ultrafast extreme-ultraviolet light source. *Review of Scientific Instruments* **2008**, *79*, 063102.
- Gao, H., Xu, Y. T., Yang, L., Lam, C. S., Wang, H. L., Zhou, J. A. and Ng, C. Y. High-resolution threshold photoelectron study of the propargyl radical by the vacuum ultraviolet laser velocity-map imaging method. *Journal of Chemical Physics* **2011**, *135*, 224304
- Giegerich, J. and Fischer, I. Photodissociation dynamics of fulvenallene, C<sub>7</sub>H<sub>6</sub>. *Physical Chemistry Chemical Physics* **2013**, *15*, 13162-13168.
- Glassman, I. and Yetter, R. A., *Combustion, 4th Edition*, **2008**, p.
- Goddard, W. A., Dunning, T. H., Hunt, W. J. and Hay, P. J. Generalized valence bond description of bonding in low-lying states of molecules. *Accounts of Chemical Research* **1973**, *6*, 368-376.
- Golden, D. M. Yet another look at the reaction CH<sub>3</sub> + H + M = CH<sub>4</sub> + M. *International Journal of Chemical Kinetics* **2008**, *40*, 310-319.

- Guan, Q., Urness, K. N., Ormond, T. K., David, D. E., Ellison, G. B. and Daily, J. W. The Properties of a Micro-Reactor for the Study of the Unimolecular Decomposition of Large Molecules. *International Reviews in Physical Chemistry* **2014**, 33, 447-487.
- Gunion, R. F., Gilles, M. K., Polak, M. L. and Lineberger, W. C. Ultraviolet photoelectron-spectroscopy of the phenide, benzyl and phenoxide anions, with *ab initio* calculations. *International Journal of Mass Spectrometry and Ion Processes* **1992**, 117, 601-620.
- H.-J. Werner, P. J. K., G. Knizia, F. R. Manby, M. Schütz, P. Celani, W. Györffy, D. Kats, T. Korona, R. Lindh, A. Mitrushenkov, G. Rauhut, K. R. Shamasundar, T. B. Adler, R. D. Amos, A. Bernhardsson, A. Berning, D. L. Cooper, M. J. O. Deegan, A. J. Dobbyn, F. Eckert, E. Goll, C. Hampel, A. Hesselmann, G. Hetzer, T. Hrenar, G. Jansen, C. Köppl, Y. Liu, A. W. Lloyd, R. A. Mata, A. J. May, S. J. McNicholas, W. Meyer, M. E. Mura, A. Nicklaß, D. P. O'Neill, P. Palmieri, D. Peng, K. Pflüger, R. Pitzer, M. Reiher, T. Shiozaki, H. Stoll, A. J. Stone, R. Tarroni, T. Thorsteinsson, M. Wang *Molpro, Version 2002.6*, University of Birmingham: Birmingham, UK, **2003**.
- Haber, K. S., Zwanziger, J. W., Campos, F. X., Wiedmann, R. T. and Grant, E. R. Direct determination of the adiabatic ionization potential of NO<sub>2</sub> by multiresonant optical absorption. *Chemical Physics Letters* **1988**, 144, 58-64.
- Harwit, M. *The Herschel Mission*, Eds.: P. R. Wesselius and H. Olthof, **2004**, pp. 568-572.
- Heimann, P. A., Koike, M., Hsu, C. W., Blank, D., Yang, X. M., Suits, A. G., Lee, Y. T., Evans, M., Ng, C. Y., Flaim, C. and Padmore, H. A. Performance of the vacuum ultraviolet high-resolution and high-flux beamline for chemical dynamics studies at the Advanced Light Source. *Review of Scientific Instruments* **1997**, 68, 1945-1951.
- Heitner, C., Dimmel, D. and Schmidt, J., *Lignin and lignans: advances in chemistry*, CRC press, **2010**, p.
- Herbst, E. Chemistry in the interstellar-medium. *Annual Review of Physical Chemistry* **1995**, 46, 27-53.
- Herndon, W. C. and Lowry, L. L. Mechanism of Pyrolysis of Bicyclo [2.2.1] Heptadiene. Kinetics of Bicyclo [2.2.1] Heptadiene to Toluene Isomerization. *Journal of the American Chemical Society* **1964**, 86, 1922-1926.



- Hopkins, J. B., Powers, D. E. and Smalley, R. E. Predissociation probes of vibrational-energy localization. *Journal of Chemical Physics* **1981**, *74*, 745-747.
- Hopkins, J. B., Powers, D. E. and Smalley, R. E. Vibrational-relaxation in jet-cooled alkylbenzenes .1. Absorption-spectra. *Journal of Chemical Physics* **1980**, *72*, 5039-5048.
- Houle, F. A. and Beauchamp, J. L. Detection and investigation of allyl and benzyl radicals by photoelectron-spectroscopy. *Journal of the American Chemical Society* **1978**, *100*, 3290-3294.
- Hu, T. Q., James, B. R., Rettig, S. J. and Lee, C. L. Stereoselective hydrogenation of lignin degradation model compounds. *Canadian Journal of Chemistry-Revue Canadienne De Chimie* **1997**, *75*, 1234-1239.
- Ichino, T., Wren, S. W., Vogelhuber, K. M., Gianola, A. J., Lineberger, W. C. and Stanton, J. F. The vibronic level structure of the cyclopentadienyl radical. *Journal of Chemical Physics* **2008**, *129*, 084310.
- Ikeda, N., Nakashima, N. and Yoshihara, K. Observation of the ultraviolet-absorption spectrum of phenyl radical in the gas-phase. *Journal of the American Chemical Society* **1985**, *107*, 3381-3382.
- Jacox, M. E. The vibrational-energy levels of small transient molecules isolated in neon and argon matrices. *Chemical Physics* **1994**, *189*, 149-170.
- Jacox, M. E. and Thompson, W. E. The infrared spectroscopy and photochemistry of NO<sub>3</sub> trapped in solid neon. *Journal of Chemical Physics* **2008**, *129*, 2043061-2043015.
- Jagod, M. F. and Oka, T. Inertial defects of planar symmetric top molecules. *Journal of Molecular Spectroscopy* **1990**, *139*, 313-327.
- Jochowitz, E. B., Zhang, X., Nimlos, M. R., Varner, M. E., Stanton, J. F. and Ellison, G. B. Propargyl Radical: *ab initio* Anharmonic Modes and the Polarized Infrared Absorption Spectra of Matrix-Isolated HCCCH<sub>2</sub>. *Journal of Physical Chemistry A* **2005**, *109*, 3812-3821.
- Johnson, M., Bodi, A., Schulz, L. and Gerber, T. Vacuum ultraviolet beamline at the Swiss Light Source for chemical dynamics studies. *Nuclear Instruments & Methods*

*in Physics Research Section a-Accelerators Spectrometers Detectors and Associated Equipment* **2009**, 610, 597-603.

Johnson, R. D. Excited electronic states of the tropylium (*cyclo-C<sub>7</sub>H<sub>7</sub>*) radical. *Journal of Chemical Physics* **1991**, 95, 7108-7113.

Jones, J., Bacskay, G. B. and Mackie, J. C. Decomposition of the benzyl radical: Quantum chemical and experimental (shock tube) investigations of reaction pathways. *Journal of Physical Chemistry A* **1997**, 101, 7105-7113.

Kaiser, R. I., Asvany, O., Lee, Y. T., Bettinger, H. F., Schleyer, P. V. and Schaefer, H. F. Crossed beam reaction of phenyl radicals with unsaturated hydrocarbon molecules. I. Chemical dynamics of phenylmethylacetylene (C<sub>6</sub>H<sub>5</sub>CCCH<sub>3</sub>; X<sup>1</sup>A') formation from reaction of C<sub>6</sub>H<sub>5</sub> (X<sup>2</sup>A<sub>1</sub>) with methylacetylene, CH<sub>3</sub>CCH (X<sup>1</sup>A<sub>1</sub>) *Journal of Chemical Physics* **2000**, 112, 4994-5001.

Kasai, P. H., Hedaya, E. and Whipple, E. B. Electron spin resonance study of phenyl radicals isolated in an argon matrix at 4 K. *Journal of the American Chemical Society* **1969**, 91, 4364-4368.

Kaufmann, M., Broderick, B. M. and Douberly, G. E., *70th International Symposium on Molecular Spectroscopy* **2015**.

Kazakov, A. and Frenklach, M. Dynamic modeling of soot particle coagulation and aggregation: Implementation with the method of moments and application to high-pressure laminar premixed flames. *Combustion and Flame* **1998**, 114, 484-501.

Kemper, M. J. H., Vandijk, J. M. F. and Buck, H. M. Backtracking algorithm for exact counting of internal molecular energy-levels. *Chemical Physics Letters* **1978**, 53, 121-124.

Knothe, G. Analyzing biodiesel: Standards and other methods. *Journal of the American Oil Chemists Society* **2006**, 83, 823-833.

Knowles, D. J. and Nicholson, A. J. C. Ionization energies of formic and acetic-acid monomers. *Journal of Chemical Physics* **1974**, 60, 1180-1181.

Knyazev, V. D. and Slagle, I. R. Kinetics of the reaction between propargyl radical and acetylene. *Journal of Physical Chemistry A* **2002**, 106, 5613-5617.

- Kohn, D. W., Clauberg, H. and Chen, P. Flash Pyrolysis Nozzle for Generation of Radicals in a Supersonic Jet Expansion. *Review of Scientific Instruments* **1992**, *63*, 4003-4005.
- Langseth, A. and Stoicheff, B. P. High resolution raman spectroscopy of gases .6. Rotational spectrum of symmetric benzene-d-3. *Canadian Journal of Physics* **1956**, *34*, 350-353.
- Laufer, A. H. An excited-state of acetylene - photochemical and spectroscopic evidence. *Journal of Chemical Physics* **1980**, *73*, 49-52.
- Laufer, A. H. and Fahr, A. Reactions and kinetics of unsaturated C<sub>2</sub> hydrocarbon radicals. *Chemical Reviews* **2004**, *104*, 2813-2832.
- Lehmann, K. K., Scoles, G. and Pate, B. H. Intramolecular dynamics from eigenstate-resolved infrared-spectra. *Annual Review of Physical Chemistry* **1994**, *45*, 241-274.
- Lima, A. L. C., Farrington, J. W. and Reddy, C. M. Combustion-Derived Polycyclic Aromatic Hydrocarbons in the Environment—A Review. *Environmental Forensics* **2005**, *6*, 109-131.
- Lockyer, N. P. and Vickerman, J. C. Single photon ionisation mass spectrometry using laser-generated vacuum ultraviolet photons. *Laser Chemistry* **1997**, *17*, 139-159.
- Logan, C. F. and Chen, P. Ab initio calculation of hydrogen abstraction reactions of phenyl radical and *p*-benzyne. *Journal of the American Chemical Society* **1996**, *118*, 2113-2114.
- Lovejoy, C. M. and Nesbitt, D. J. Mode specific internal and direct rotational predissociation in HeHF, HeDF, and HeHCl - vanderwaals complexes in the weak binding limit. *Journal of Chemical Physics* **1990**, *93*, 5387-5407.
- Lovejoy, C. M. and Nesbitt, D. J. Rotational predissociation, vibrational mixing, and vanderwaals intermolecular potentials of NeDF. *Journal of Chemical Physics* **1991**, *94*, 208-223.
- Lu, K. T., Eiden, G. C. and Weisshaar, J. C. Toluene Cation - Nearly Free Rotation of the Methyl-Group. *Journal of Physical Chemistry* **1992**, *96*, 9742-9748.

- Luu, S. H., Glanzer, K. and Troe, J. Thermal Isomerization in Shock-Waves and Flash-Photolysis of Cycloheptatriene .3. *Berichte der Bunsen-Gesellschaft-Physical Chemistry Chemical Physics* **1975**, 79, 855-858.
- Luu, S. H., Glänzer, K. and Troe, J. Thermal isomerization in shock waves and flash photolysis of cycloheptatriene, III. *Berichte der Bunsengesellschaft für physikalische Chemie* **1975**, 79, 855-858.
- Magnelli, B., Lutz, D., Santini, P., Saintonge, A., Berta, S., Albrecht, M., Altieri, B., Andreani, P., Aussel, H., Bertoldi, F., Bethermin, M., Bongiovanni, A., Capak, P., Chapman, S., Cepa, J., Cimatti, A., Cooray, A., Daddi, E., Danielson, A. L. R., Dannerbauer, H., Dunlop, J. S., Elbaz, D., Farrah, D., Schreiber, N. M. F., Genzel, R., Hwang, H. S., Ibar, E., Ivison, R. J., Le Floc'h, E., Magdis, G., Maiolino, R., Nordon, R., Oliver, S. J., Perez Garcia, A., Poglitsch, A., Popesso, P., Pozzi, F., Riguccini, L., Rodighiero, G., Rosario, D., Roseboom, I., Salvato, M., Sanchez-Portal, M., Scott, D., Smail, I., Sturm, E., Swinbank, A. M., Tacconi, L. J., Valtchanov, I., Wang, L. and Wuyts, S. A Herschel view of the far-infrared properties of submillimetre galaxies. *Astronomy & Astrophysics* **2012**, 539.
- Mallard, W. G., Miller, J. H. and Smyth, K. C. The ns Rydberg series of 1,3-*trans*-butadiene observed using multiphoton ionization. *Journal of Chemical Physics* **1983**, 79, 5900-5905.
- Marinov, N. M., Pitz, W. J., Westbrook, C. K., Castaldi, M. J. and Senkan, S. M. Modeling of aromatic and polycyclic aromatic hydrocarbon formation in premixed methane and ethane flames. *Combustion Science and Technology* **1996**, 116, 211-287.
- Marker, T. L., Felix, L. G., Linck, M. B. and Roberts, M. J. Integrated Hydropyrolysis and Hydroconversion (IH2) for the Direct Production of Gasoline and Diesel Fuels or Blending Components from Biomass, Part 1: Proof of Principle Testing. *Environmental Progress & Sustainable Energy* **2012**, 31, 191-199.
- McIlroy, A., Lascola, R., Lovejoy, C. M. and Nesbitt, D. J. Structural dependence of hydrogen fluoride vibrational red shifts in argon-hydrogen fluoride ( $\text{Ar}_n\text{HF}$ ,  $n=1-4$ ), via high-resolution slit jet infrared spectroscopy. *The Journal of Physical Chemistry* **1991**, 95, 2636-2644.
- McIlroy, A. and Nesbitt, D. J. High - resolution, slit jet infrared spectroscopy of hydrocarbons: Quantum state specific mode mixing in CH stretch - excited propyne. *The Journal of Chemical Physics* **1989**, 91, 104-113.

- McIlroy, A. and Nesbitt, D. J. Large-amplitude skeletal isomerization as a promoter of intramolecular vibrational-relaxation in ch stretch excited hydrocarbons. *Journal of Chemical Physics* **1994**, *101*, 3421-3435.
- McIlroy, A., Nesbitt, D. J., Kerstel, E. R. T., Pate, B. H., Lehmann, K. K. and Scoles, G. Sub-doppler, infrared-laser spectroscopy of the propyne 2- $\nu$ (1) band - evidence of z-axis coriolis dominated intramolecular state mixing in the acetylenic ch stretch overtone. *Journal of Chemical Physics* **1994**, *100*, 2596-2611.
- McMahon, R. J., McCarthy, M. C., Gottlieb, C. A., Dudek, J. B., Stanton, J. F. and Thaddeus, P. The radio spectrum of the phenyl radical. *Astrophysical Journal* **2003**, *590*, L61-L64.
- Mebel, A. M., Lin, M. C., Yu, T. and Morokuma, K. Theoretical study of potential energy surface and thermal rate constants for the  $C_6H_5 + H_2$  and  $C_6H_6 + H$  reactions. *Journal of Physical Chemistry A* **1997**, *101*, 3189-3196.
- Miller, J. A. and Melius, C. F. Kinetic and thermodynamic issues in the formation of aromatic-compounds in flames of aliphatic fuels. *Combustion and Flame* **1992**, *91*, 21-39.
- Miller, J. A., Pilling, M. J. and Troe, J. Unravelling combustion mechanisms through a quantitative understanding of elementary reactions. *Proceedings of the Combustion Institute* **2005**, *30*, 43-88.
- Morgan, W. A., Feigelson, E. D., Wang, H. and Frenklach, M. A new mechanism for the formation of meteoritic kerogen-like material. *Science* **1991**, *252*, 109-112.
- Moskaleva, L. V. and Lin, M. C. Unimolecular isomerization/decomposition of cyclopentadienyl and related bimolecular reverse process: *Ab initio* MO/statistical theory study. *Journal of Computational Chemistry* **2000**, *21*, 415-425.
- Moss, D. B. and Parmenter, C. S. Acceleration of intramolecular vibrational redistribution of methyl internal-rotation - a chemical timing study of *p*-fluorotoluene and *p*-fluorotoluene- $D_3$ . *Journal of Chemical Physics* **1993**, *98*, 6897-6905.
- Mueller, C. J., Cannella, W. J., Bruno, T. J., Bunting, B., Dettman, H. D., Franz, J. A., Huber, M. L., Natarajan, M., Pitz, W. J., Ratcliff, M. A. and Wright, K. Methodology for Formulating Diesel Surrogate Fuels with Accurate

- Compositional, Ignition-Quality, and Volatility Characteristics. *Energy & Fuels* **2012**, 26, 3284-3303.
- Müller-Markgraf, W. and Troe, J. Thermal decomposition of benzyl iodide and of benzyl radicals in shock waves. *The Journal of Physical Chemistry* **1988**, 92, 4899-4905.
- Nandi, S., Arnold, P. A., Carpenter, B. K., Nimlos, M. R., Dayton, D. C. and Ellison, G. B. Polarized infrared absorption spectra of matrix-isolated allyl radicals. *Journal of Physical Chemistry A* **2001**, 105, 7514-7524.
- Nandi, S., Blanksby, S. J., Zhang, X., Nimlos, M. R., Dayton, D. C. and Ellison, G. B. Polarized infrared absorption spectrum of matrix-isolated methylperoxyl radicals,  $\text{CH}_3\text{OO} \cdot$ . *Journal of Physical Chemistry A* **2002**, 106, 7547-7556.
- Nesbitt, D. J. and Field, R. W. Vibrational energy flow in highly excited molecules: Role of intramolecular vibrational redistribution. *Journal of Physical Chemistry* **1996**, 100, 12735-12756.
- Nicolaides, A., Smith, D. M., Jensen, F. and Radom, L. Phenyl radical, cation, and anion. The triplet-singlet gap and higher excited states of the phenyl cation. *Journal of the American Chemical Society* **1997**, 119, 8083-8088.
- Oehlschlaeger, M. A., Davidson, D. F. and Hanson, R. K. High-temperature thermal decomposition of benzyl radicals. *Journal of Physical Chemistry A* **2006**, 110, 6649-6653.
- Ohyama, S., Popp, K. E., Kung, M. C. and Kung, H. H. Effect of vanadia on the performance of NiO in vapor-phase oxidative decarboxylation of benzoic acid to phenol. *Catalysis Communications* **2002**, 3, 357-362.
- Oka, T. On negative inertial defect. *Journal of Molecular Structure* **1995**, 352, 225-233.
- Oka, T. and Morino, Y. Calculation of inertia defect .1. General formulation. *Journal of Molecular Spectroscopy* **1961**, 6, 472-482.
- Ormond, T. K., Hemberger, P., Troy, T. P., Ahmed, M., Stanton, J. F. and Ellison, G. B. The ionisation energy of cyclopentadienone: a photoelectron-photoion coincidence study. *Molecular Physics* **2015**, 113, 2350-2358.

- Ormond, T. K., Scheer, A. M., Nimlos, M. R., Robichaud, D. J., Daily, J. W., Stanton, J. F. and Ellison, G. B. Polarized Matrix Infrared Spectra of Cyclopentadienone: Observations, Calculations, and Assignment for an Important Intermediate in Combustion and Biomass Pyrolysis. *J. Phys. Chem. A* **2014**, *118*, 708-718.
- Ormond, T. K., Scheer, A. M., Nimlos, M. R., Robichaud, D. J., Daily, J. W., Stanton, J. F. and Ellison, G. B. Polarized Matrix Infrared Spectra of Cyclopentadienone: Observations, Calculations, and Assignment for an Important Intermediate in Combustion and Biomass Pyrolysis. *Journal of Physical Chemistry A* **2014**, *118*, 708-718.
- Ormond, T. K., Scheer, A. M., Nimlos, M. R., Robichaud, D. J., Troy, T. P., Ahmed, M., Daily, J. W., Nguyen, T. L., Stanton, J. F. and Ellison, G. B. Pyrolysis of Cyclopentadienone: Mechanistic Insights from a Direct Measurement of Product Branching Ratios. *The Journal of Physical Chemistry A* **2015**, *119*, 7222-7234.
- Pacansky, J. and Bargon, J. Low-temperature photochemical studies on acetyl benzoyl peroxide - observation of methyl and phenyl radicals by matrix-isolation infrared spectroscopy. *Journal of the American Chemical Society* **1975**, *97*, 6896-6897.
- Pamidimukkala, K. M., Kern, R. D., Patel, M. R., Wei, H. C. and Kiefer, J. H. High-Temperature Pyrolysis of Toluene. *Journal of Physical Chemistry* **1987**, *91*, 2148-2154.
- Park, J., Dyakov, I. V. and Lin, M. C. FTIR and mass-spectrometric measurements of the rate constant for the  $C_6H_5 + H_2$  reaction. *Journal of Physical Chemistry A* **1997**, *101*, 8839-8843.
- Parker, D. S. N., Zhang, F., Kim, Y. S., Kaiser, R. I., Landera, A., Kislov, V. V., Mebel, A. M. and Tielens, A. G. G. M. Low temperature formation of naphthalene and its role in the synthesis of PAHs (Polycyclic Aromatic Hydrocarbons) in the interstellar medium. *Proceedings of the National Academy of Sciences of the United States of America* **2012**, *109*, 53-58.
- Parmenter, C. S. and Stone, B. M. The methyl rotor as an accelerating functional-group for ivr. *Journal of Chemical Physics* **1986**, *84*, 4710-4711.
- Pate, B. H., Lehmann, K. K. and Scoles, G. The onset of intramolecular vibrational-energy redistribution and its intermediate case - the nu-1 and 2-nu-1 molecular-beam, optothermal spectra of trifluoropropyne. *Journal of Chemical Physics* **1991**, *95*, 3891-3916.

- Pedley, J. B., Naylor, R. D. and Kirby, S. P., *Thermochemistry of Organic Compounds*, Chapman and Hall, New York, **1986**, p. 87-222.
- Pilbratt, G. L., Riedinger, J. R., Passvogel, T., Crone, G., Doyle, D., Gageur, U., Heras, A. M., Jewell, C., Metcalfe, L., Ott, S. and Schmidt, M. Herschel Space Observatory An ESA facility for far-infrared and submillimetre astronomy. *Astronomy & Astrophysics* **2010**, *518*, 1-6.
- Pine, A. S. High-resolution methane nu-3-band spectra using a stabilized tunable difference-frequency laser system. *Journal of the Optical Society of America* **1976**, *66*, 97-108.
- Pino, T., Guthe, F., Ding, H. and Maier, J. P. Gas-phase electronic spectrum of the tropyli C<sub>7</sub>H<sub>7</sub> radical. *Journal of Physical Chemistry A* **2002**, *106*, 10022-10026.
- Pliva, J. and Pine, A. S. Analysis of the 3-mu-m bands of benzene. *Journal of Molecular Spectroscopy* **1987**, *126*, 82-98.
- Pliva, J. and Pine, A. S. The spectrum of benzene in the 3-mu-m region - the nu-12 fundamental-band. *Journal of Molecular Spectroscopy* **1982**, *93*, 209-236.
- Polino, D. and Cavallotti, C. Fulvenallene Decomposition Kinetics. *Journal of Physical Chemistry A* **2011**, *115*, 10281-10289.
- Polino, D., Famulari, A. and Cavallotti, C. Analysis of the Reactivity on the C<sub>7</sub>H<sub>6</sub> Potential Energy Surface. *Journal of Physical Chemistry A* **2011**, *115*, 7928-7936.
- Polino, D. and Parrinello, M. Combustion Chemistry via Metadynamics: Benzyl Decomposition Revisited. *Journal of Physical Chemistry A* **2015**, *119*, 978-989.
- Porter, G. and Savadatt, Mi. Electronic Spectra of Benzyl - A New Transition. *Spectrochimica Acta* **1966**, *22*, 803-806.
- Poutsma, J. C., Nash, J. J., Paulino, J. A. and Squires, R. R. Absolute heats of formation of phenylcarbene and vinylcarbene. *Journal of the American Chemical Society* **1997**, *119*, 4686-4697.
- Pratt, S. T., Dehmer, P. M. and Dehmer, J. L. Zero-kinetic-energy photoelectron-spectroscopy from the A <sup>1</sup>A<sub>g</sub> state of acetylene - renner-teller interactions in the



- trans-bending vibration of  $C_2H_2^+ X^2\Pi_u$ . *Journal of Chemical Physics* **1993**, 99, 6233-6244.
- Pratt, S. T., Dehmer, P. M. and Dehmer, J. L. Zero-Kinetic-Energy Photoelectron-Spectroscopy from the  $\tilde{a}^1A_u$  State of Acetylene - Renner-Teller Interactions in the Trans-Bending Vibration of  $C_2H_2^+ X^2\Pi_u$ . *Journal of Chemical Physics* **1993**, 99, 6233-6244.
- Radziszewski, J. G. Electronic absorption spectrum of phenyl radical. *Chemical Physics Letters* **1999**, 301, 565-570.
- Radziszewski, J. G., Nimlos, M. R., Winter, P. R. and Ellison, G. B. Infrared absorption spectroscopy of the phenyl radical. *Journal of the American Chemical Society* **1996**, 118, 7400-7401.
- Rao, V. S. and Skinner, G. B. Formation of Hydrogen Atoms in Pyrolysis of Ethylbenzene Behind Shock Waves. Rate Constants for the Thermal Dissociation of the Benzyl Radical. *Proceedings of the Combustion Institute* **1986**, 21, 809-814.
- Rao, V. S. and Skinner, G. B. Formation of hydrogen atoms in pyrolysis of ethylbenzene behind shock waves. Rate constants for the thermal dissociation of the benzyl radical. *Proceedings of the Combustion Institute* **1986**, 21, 809-814.
- Richter, H. and Howard, J. B. Formation of polycyclic aromatic hydrocarbons and their growth to soot - a review of chemical reaction pathways. *Progress in Energy and Combustion Science* **2000**, 26, 565-608.
- Robichaud, D., Nimlos, M. and Ellison, G. B. *Pyrolysis Mechanisms of Lignin Model Compounds Using a Heated Micro-Reactor*, Eds.: M. Schlaf and Z. C. Zhang, Springer Singapore, **2016**, pp. 145-171.
- Rohrs, H. W., Wickham-Jones, C. T., Berry, D., Ellison, G. B. and Argrow, B. M. FTIR Absorption Spectroscopy of Jet-Cooled Radicals. *Review of Scientific Instruments* **1995**, 66, 2430.
- Ruscic, B. and Berkowitz, J. Photoionization mass-spectrometric studies of the isomeric transient species  $CD_2OH$  and  $CD_3O$ . *Journal of Chemical Physics* **1991**, 95, 4033-4039.

- Satink, R. G., Meijer, G. and von Helden, G. Infrared spectroscopy of neutral C<sub>7</sub>H<sub>7</sub> isomers: Benzyl and tropyli. *Journal of the American Chemical Society* **2003**, *125*, 15714-15715.
- Sato, S., Kojima, T., Byodo, K., Shinohara, H., Yanagihara, S. and Kimura, K. ZEKE electron spectroscopy of alkylbenzene-argon van der Waals complexes. *Journal of Electron Spectroscopy and Related Phenomena* **2000**, *112*, 247-255.
- Savee, J. D., Private communication, 2014
- Savee, J. D., Privately communicated., 2014
- Savee, J. D., Selby, T. M., Welz, O., Taatjes, C. A. and Osborn, D. L. Time- and Isomer-Resolved Measurements of Sequential Addition of Acetylene to the Propargyl Radical. *The Journal of Physical Chemistry Letters* **2015**, 4153-4158.
- Savee, J. D., Soorkia, S., Welz, O., Selby, T. M., Taatjes, C. A. and Osborn, D. L. Absolute photoionization cross-section of the propargyl radical. *Journal of Chemical Physics* **2012**, *136*, 134307-134317.
- Savee, J. D., Zador, J., Hemberger, P., Sztaray, B., Bodi, A. and Osborn, D. L. Threshold Photoelectron Spectrum of the Benzyl Radical. *Molecular Physics* **2015**, *113*, 2217-2227.
- Scheer, A. M., Ph.D. Thesis, *Thermal Decomposition Mechanisms of Lignin Model Compounds: From Phenol to Vanillin*, University of Colorado, Department of Chemistry and Biochemistry, **2011**
- Scheer, A. M., Mukarakate, C., Robichaud, D. J., Ellison, G. B. and Nimlos, M. R. Radical Chemistry in the Thermal Decomposition of Anisole and Deuterated Anisoles: An Investigation of Aromatic Growth. *Journal of Physical Chemistry A* **2010**, *114*, 9043-9056.
- Scheer, A. M., Mukarakate, C., Robichaud, D. J., Nimlos, M. R., Carstensen, H.-H. and Ellison, G. B. Unimolecular Thermal Decomposition of Phenol and d<sub>5</sub>-Phenol: Direct Observation of Cyclopentadiene Formation via Cyclohexadienone,. *Journal of Chemical Physics* **2012**, *136*, 044309-044320

- Schulenburg, A. M., Meisinger, M., Radi, P. P. and Merkt, F. The formaldehyde cation: Rovibrational energy level structure and Coriolis interaction near the adiabatic ionization threshold. *Journal of Molecular Spectroscopy* **2008**, *250*, 44-50.
- Seburg, R. A., Hill, B. T. and Squires, R. R. Synthesis, properties and reactivity of the phenylcarbene anion in the gas phase. *Journal of the Chemical Society-Perkin Transactions 2* **1999**, 2249-2256.
- Shapero, M., Cole-Filipiak, N. C., Haibach-Morris, C. and Neumark, D. M. Benzyl Radical Photodissociation Dynamics at 248 nm. *Journal of Physical Chemistry A* **2015**, *119*, 12349-12356.
- Sharp, E. N., Roberts, M. A. and Nesbitt, D. J. Rotationally resolved infrared spectroscopy of a jet-cooled phenyl radical in the gas phase. *Physical Chemistry Chemical Physics* **2008**, *10*, 6592-6596.
- Shimanouchi, T., *Tables of Vibrational Frequencies, Consolidated Vol. I*, NSRDS-NBS 39, **1972**, p.
- Shimanouchi, T. *Tables of Vibrational Frequencies, Consolidated Volume I*, NSRDS-NBS 39, **1972**.
- Shiner, D., Gilligan, J. M., Cook, B. M. and Lichten, W. H<sub>2</sub>, D<sub>2</sub>, and HD ionization-potentials by accurate calibration of several iodine lines. *Physical Review A* **1993**, *47*, 4042-4045.
- Shukla, B., Susa, A., Miyoshi, A. and Koshi, M. *In Situ* Direct Sampling Mass Spectrometric Study on Formation of Polycyclic Aromatic Hydrocarbons in Toluene Pyrolysis. *Journal of Physical Chemistry A* **2007**, *111*, 8308-8324.
- Sioutis, I., Stakhursky, V. L., Tarczay, G. and Miller, T. A. Experimental Investigation of the Jahn-Teller Effect in the Ground and Excited Electronic States of the Tropylium Radical. Part II. Vibrational Analysis of the A <sup>2</sup>E<sub>3</sub>"-X <sup>2</sup>E<sub>2</sub>" Electronic Transition. *Journal of Chemical Physics* **2008**, *128*, 084311 - 084329.
- Sivaramakrishnan, R., Su, M. C. and Michael, J. V. H- and D-atom formation from the pyrolysis of C<sub>6</sub>H<sub>5</sub>CH<sub>2</sub>Br and C<sub>6</sub>H<sub>5</sub>CD<sub>2</sub>Br: Implications for high-temperature benzyl decomposition. *Proceedings of the Combustion Institute* **2011**, *33*, 243-250.

- Sivaramakrishnan, R., Su, M. C. and Michael, J. V. H- and D-Atom Formation from the Pyrolysis of C<sub>6</sub>H<sub>5</sub>CH<sub>2</sub>Br and C<sub>6</sub>H<sub>5</sub>CD<sub>2</sub>Br: Implications for High-Temperature Benzyl Decomposition. *Proceedings of the Combustion Institute* **2011**, *33*, 243-250.
- Sivaramakrishnan, R., Tranter, R. S. and Brezinsky, K. High Pressure Pyrolysis of Toluene. 1. Experiments and Modeling of Toluene Decomposition. *Journal of Physical Chemistry A* **2006**, *110*, 9388-9399.
- Skeen, S. A., Michelsen, H. A., Wilson, K. R., Popolan, D. M., Violi, A. and Hansen, N. Near-threshold photoionization mass spectra of combustion-generated high-molecular-weight soot precursors. *Journal of Aerosol Science* **2013**, *58*, 86-102.
- Smith, R. D. Direct mass-spectrometric study of the mechanism of toluene pyrolysis at high-temperatures. *Journal of Physical Chemistry* **1979**, *83*, 1553-1556.
- Stakhursky, V. L., Sioutis, I., Tarczay, G. and Miller, T. A. Computational Investigation of the Jahn-Teller Effect in the Ground and Excited Electronic States of the Tropyli Radical. Part I. Theoretical Calculation of Spectroscopically Observable Parameters. *Journal of Chemical Physics* **2008**, *128*, 084310-084323.
- Steinbauer, M., Hemberger, P., Fischer, I. and Bodi, A. Photoionization of C<sub>7</sub>H<sub>6</sub> and C<sub>7</sub>H<sub>5</sub>: Observation of the Fulvenallenyl Radical. *Chem phys chem* **2011**, *12*, 1795-1797.
- Strausz, O. P., Mojelsky, T. W., Payzant, J. D., Olah, G. A. and Prakash, G. K. S. Upgrading of Alberta's heavy oils by superacid-catalyzed hydrocracking. *Energy & Fuels* **1999**, *13*, 558-569.
- Sustmann, R., Brandes, D., Lange, F. and Nuchter, U. Rearrangements of Free-Radicals.11. Sigmatropic And Electrocyclic Reactions of Bicyclo [3.2.0] Heptadienyl Radicals, 3-Quadricyclanyl Radicals, and 7-Norbornadienyl Radical. *Chemische Berichte* **1985**, *118*, 3500-3512.
- Szwarc, M. The C-H bond energy in toluene and xylenes. *Journal of Chemical Physics* **1948**, *16*, 128-136.
- Taatjes, C. A., Hansen, N., McIlroy, A., Miller, J. A., Senosiain, J. P., Klippenstein, S. J., Qi, F., Sheng, L. S., Zhang, Y. W., Cool, T. A., Wang, J., Westmoreland, P. R., Law, M. E., Kasper, T. and Kohse-Hoinghaus, K. Enols are common intermediates in hydrocarbon oxidation. *Science* **2005**, *308*, 1887-1889.

- Tardy, D. C., Rabinovitch, B. S. and Whitten, G. Z. Vibration-Rotation Energy-Level Density Calculations. *Journal of Chemical Physics* **1968**, *48*, 1427-1429.
- Traeger, J. C. and McLoughlin, R. G. Photo-ionization study of energetics of  $C_7H_7^+$  ion formed from  $C_7H_8$  precursors. *International Journal of Mass Spectrometry and Ion Processes* **1978**, *27*, 319-333.
- Traeger, J. C. and McLoughlin, R. G. Threshold photoionization and dissociation of toluene and cycloheptatriene. *Journal of the American Chemical Society* **1977**, *99*, 7351-7352.
- Urness, K. N., Guan, Q., Golan, A., Daily, J. W., Nimlos, M. R., Stanton, J. F., Ahmed, M. and Ellison, G. B. Pyrolysis of Furan in a Microreactor *Journal of Chemical Physics* **2013**, *139*, 124305-124314
- Van Bramer, S. E. and Johnston, M. V. 10.5-eV photoionization mass spectrometry of aliphatic compounds. *Journal of the American Society for Mass Spectrometry* **1990**, *1*, 419-426.
- van Der Meij, C. E., Van Eck, J. and Niehaus, A. The decomposition of  $C_4H_8^+$  complexes at controlled internal energies. *Chemical Physics* **1989**, *130*, 325-334.
- Vasiliou, A., Nimlos, M. R., Daily, J. W. and Ellison, G. B. Thermal Decomposition of Furan Generates Propargyl Radicals. *Journal of Physical Chemistry A* **2009**, *113*, 8540-8547.
- Vasiliou, A., Piech, K. M., Zhang, X., Nimlos, M. R., Ahmed, M., Golan, A., Kostko, O., Osborn, D. L., Daily, J. W., Stanton, J. F. and Ellison, G. B. The products of the thermal decomposition of  $CH_3CHO$ . *Journal of Chemical Physics* **2011**, *135*, 14306-14311.
- Vasiliou, A., Piech, K. M., Zhang, X., Nimlos, M. R., Ahmed, M., Kostko, O., Golan, A., Osborn, D. L., Daily, J. W., Stanton, J. F. and Ellison, G. B. The products of the thermal decomposition of  $CH_3CHO$ . *Journal of Chemical Physics* **2011**, *135*, 14306-14311.
- Vasiliou, A. K., Kim, J. H., Ormond, T. K., Piech, K. M., Urness, K. N., Scheer, A. M., Robichaud, D. J., Mukarakate, C., Nimlos, M. R., Daily, J. W., Guan, Q., Carstensen, H.-H. and Ellison, G. B. Biomass Pyrolysis: Thermal Decomposition Mechanisms of Furfural and Benzaldehyde *Journal of Chemical Physics* **2013**, *139*, 104310.

- Vasiliou, A. K., Piech, K. M., Reed, B., Zhang, X., Nimlos, M. R., Ahmed, M., Golan, A., Kostko, O., Osborn, D. L., Urness, K. N., David, D. E., Daily, J. W., Stanton, J. F. and Ellison, G. B. Thermal Decomposition of CH<sub>3</sub>CHO Studied by Matrix Infrared Spectroscopy and Photoionization Mass Spectroscopy *Journal of Chemical Physics* **2012**, *137*, 164308.
- Whitten, G. Z. and Rabinovitch, B. S. Accurate and Facile Approximations for Vibrational Energy-Level Sums. *Journal of Chemical Physics* **1963**, *38*, 2466-2473.
- Widicus Weaver, S. L., Remijan, A. J., McMahan, R. J. and McCall, B. J. A search for *ortho*-benzynes (*o*-C<sub>6</sub>H<sub>4</sub>) in CRL 618. *Astrophysical Journal Letters* **2007**, *671*, L153-L156.
- Wiley, W. C. and McLaren, I. H. Time-of-Flight Mass Spectrometer with Improved Resolution. *Review of Scientific Instruments* **1955**, *26*, 1150-1157.
- Winkler, M. and Sander, W. Isolation of the phenyl cation in a solid argon matrix. *Angewandte Chemie-International Edition* **2000**, *39*, 2014-2016.
- Woods, P. M., Millar, T. J. and Zijlstra, A. A. The synthesis of benzene in the proto-planetary nebula CRL 618. *Astrophysical Journal* **2002**, *574*, L167-L170.
- Wörner, H. J. and Merkt, F. Diradicals, antiaromaticity, and the pseudo-Jahn-Teller effect: Electronic and rovibronic structures of the cyclopentadienyl cation. *Journal of Chemical Physics* **2007**, *127*, 034303.
- Xing, X., Reed, B., Bahng, M. K. and Ng, C. Y. Infrared-vacuum ultraviolet pulsed field ionization-photoelectron study of C<sub>2</sub>H<sub>4</sub><sup>+</sup> using a high-resolution infrared laser. *Journal of Physical Chemistry A* **2008**, *112*, 2572-2578.
- Xing, X., Reed, B., Lau, K.-C., Ng, C. Y., Zhang, X. and Barney Ellison, G. Vacuum ultraviolet laser pulsed field ionization-photoelectron study of allyl radical CH<sub>2</sub>CHCH<sub>2</sub>. *The Journal of Chemical Physics* **2007**, *126*, 171101.
- Xing, X., Reed, B., Lau, K. C., Ng, C. Y., Zhang, X. and Ellison, G. B. Vacuum Ultraviolet Laser Pulsed Field Ionization-Photoelectron Study of Allyl Radical CH<sub>2</sub>CHCH<sub>2</sub>. *Journal of Chemical Physics* **2007**, *126*, 171170-171174.
- Yu, T. and Lin, M. C. Kinetics of phenyl radical reactions studied by the cavity-ring-down method. *Journal of the American Chemical Society* **1993**, *115*, 4371-4372.

- Yu, T. and Lin, M. C. Kinetics of the  $C_6H_5 + NO$  Association Reaction. *Journal of Physical Chemistry* **1994**, *98*, 2105-2109.
- Yu, T. and Lin, M. C. Kinetics of the  $C_6H_5 + O_2$  Reaction at Low-Temperatures. *Journal of the American Chemical Society* **1994**, *116*, 9571-9576.
- Zhang, T., Zhang, L., Hong, X., Zhang, K., Qi, F., Law, C. K., Ye, T., Zhao, P. and Chen, Y. An Experimental and Theoretical Study of Toluene Pyrolysis With Tunable Synchrotron VUV Photoionization and Molecular-Beam Mass Spectrometry. *Combustion and Flame* **2009**, *156*, 2071-2083.
- Zhang, T. C., Zhang, L. D., Hong, X., Zhang, K. W., Qi, F., Law, C. K., Ye, T. H., Zhao, P. H. and Chen, Y. L. An experimental and theoretical study of toluene pyrolysis with tunable synchrotron VUV photoionization and molecular-beam mass spectrometry. *Combustion and Flame* **2009**, *156*, 2071-2083.
- Zhang, X. and Chen, P. Photoelectron-spectrum of *o*-benzyne - ionization-potentials as a measure of singlet triplet gaps. *Journal of the American Chemical Society* **1992**, *114*, 3147-3148.
- Zhang, X., Friderichsen, A. V., Nandi, S., Ellison, G. B., David, D. E., McKinnon, J. T., Lindeman, T. G., Dayton, D. C. and Nimlos, M. R. Intense, hyperthermal source of organic radicals for matrix-isolation spectroscopy. *Review of Scientific Instruments* **2003**, *74*, 3077-3086.
- Zhang, X., Maccarone, A. T., Nimlos, M. R., Kato, S., Bierbaum, V. M., Ellison, G. B., Ruscic, B., Simmonett, A. C., Allen, W. D. and Schaefer, H. F. Unimolecular Thermal Fragmentation of *ortho*-Benzyne. *Journal of Chemical Physics* **2007**, *126*, 044312 - 044322.
- Zhang, X., Maccarone, A. T., Nimlos, M. R., Kato, S., Bierbaum, V. M., Ellison, G. B., Ruscic, B., Simmonett, A. C., Allen, W. D. and Schaefer, H. F. Unimolecular thermal fragmentation of *ortho*-benzyne. *Journal of Chemical Physics* **2007**, *126*, -.
- Zhu, R. S., Raghunath, P. and Lin, M. C. Effect of Roaming Transition States upon Product Branching in the Thermal Decomposition of  $CH_3NO_2$ . *The Journal of Physical Chemistry A* **2013**, *117*, 7308-7313.

## Appendix A

### Hydropyrolysis of Other Substituted Aromatic Species

I. n-propylbenzene ( $C_6H_5CH_2CH_2CH_3$ )

II. Isopropylbenzene ( $C_6H_5CH(CH_3)_2$ )

III. Styrene ( $C_6H_5CH=CH_2$ )

IV. Phenol ( $C_6H_5OH$ )

V. Anisole ( $C_6H_5OCH_3$ )

VI. Benzyl phenyl ether ( $C_6H_5CH_2OC_6H_5$ )



# I. n-propylbenzene ( $C_6H_5CH_2CH_2CH_3$ )

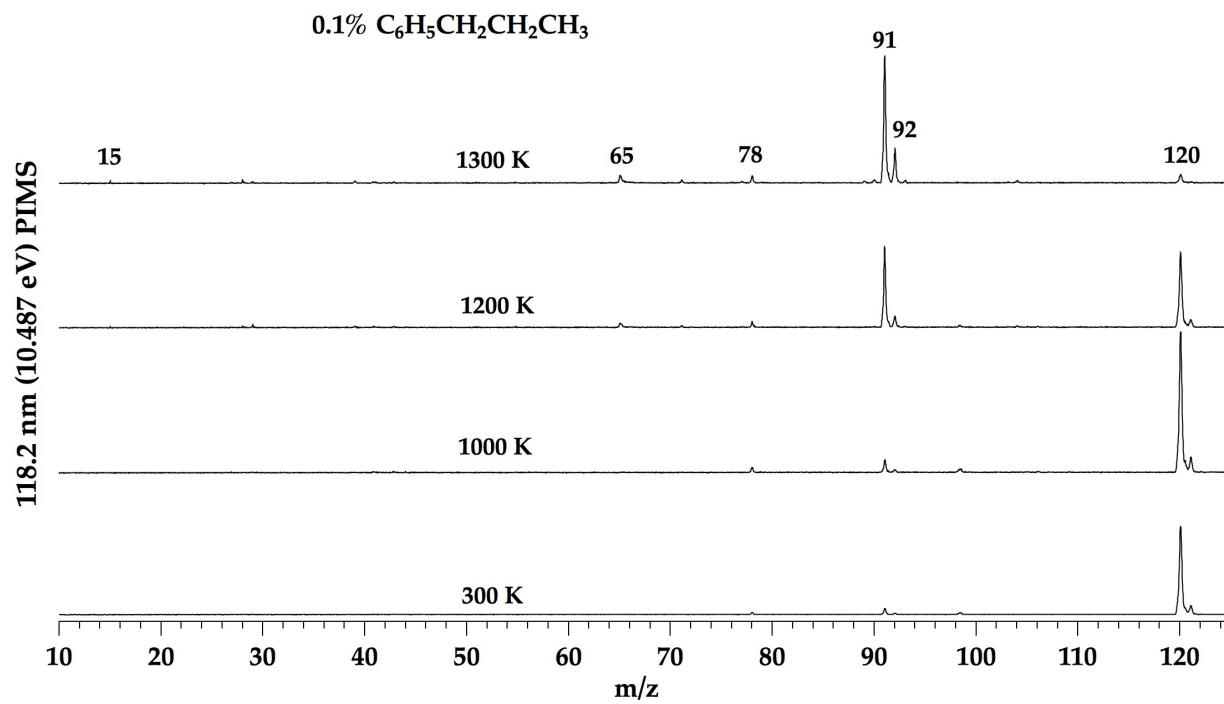


Fig. A.1. PIMS spectra recorded with 118.2 nm radiation of the pyrolysis of n-propylbenzene ( $m/z$  120) at reactor temperatures up to 1300 K. Pulsed helium carrier gas was prepared with 0.1% precursor. The main products are assigned as methyl radical ( $m/z$  15), cyclopentadienyl radical ( $m/z$  65), a weak signal of benzene ( $m/z$  78), benzyl radical ( $m/z$  91), and toluene ( $m/z$  92).

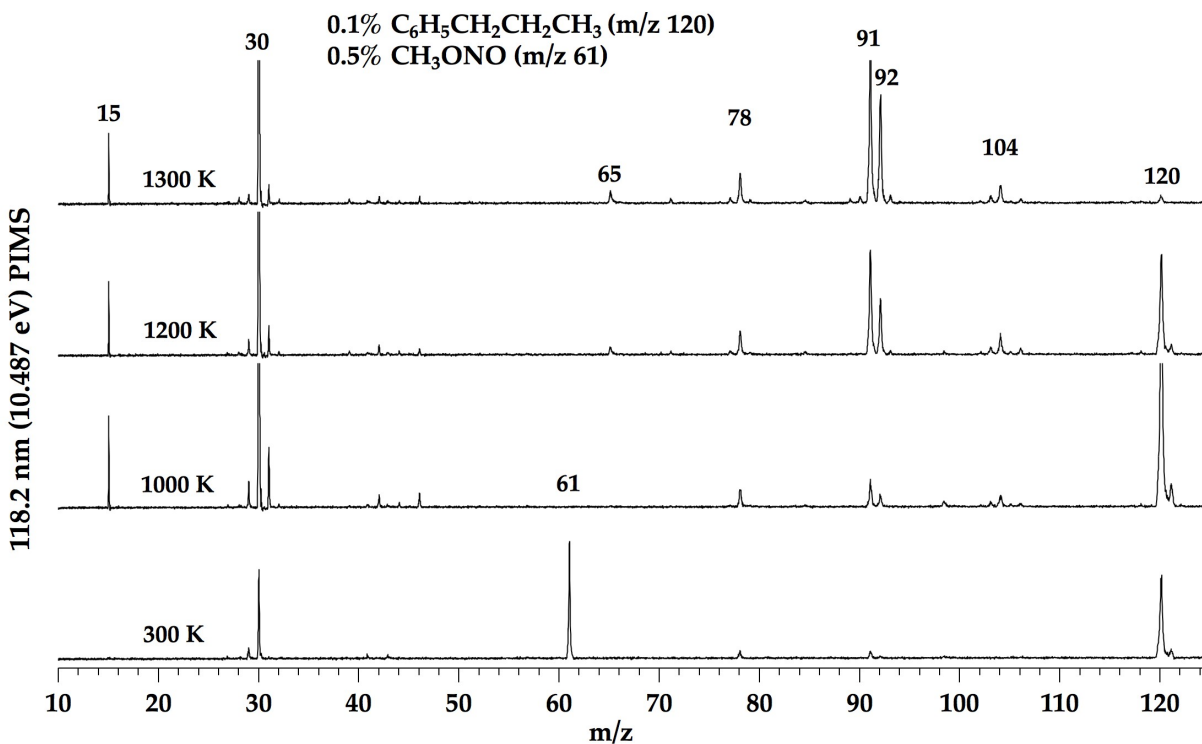


Fig. A.2. PIMS spectra recorded with 118.2 nm radiation of the pyrolysis of 0.1% n-propylbenzene (m/z 120) mixed with 0.5% methyl nitrite (m/z 61) at reactor temperatures up to 1300 K in a pulsed helium carrier gas. The hydrolysis products are assigned to be an enhancement of methyl radical (m/z 15), an enhancement of benzene (m/z 78), an enhancement of toluene (m/z 92), and the appearance of styrene (m/z 104).

## II. Isopropylbenzene ( $C_6H_5CH(CH_3)_2$ )

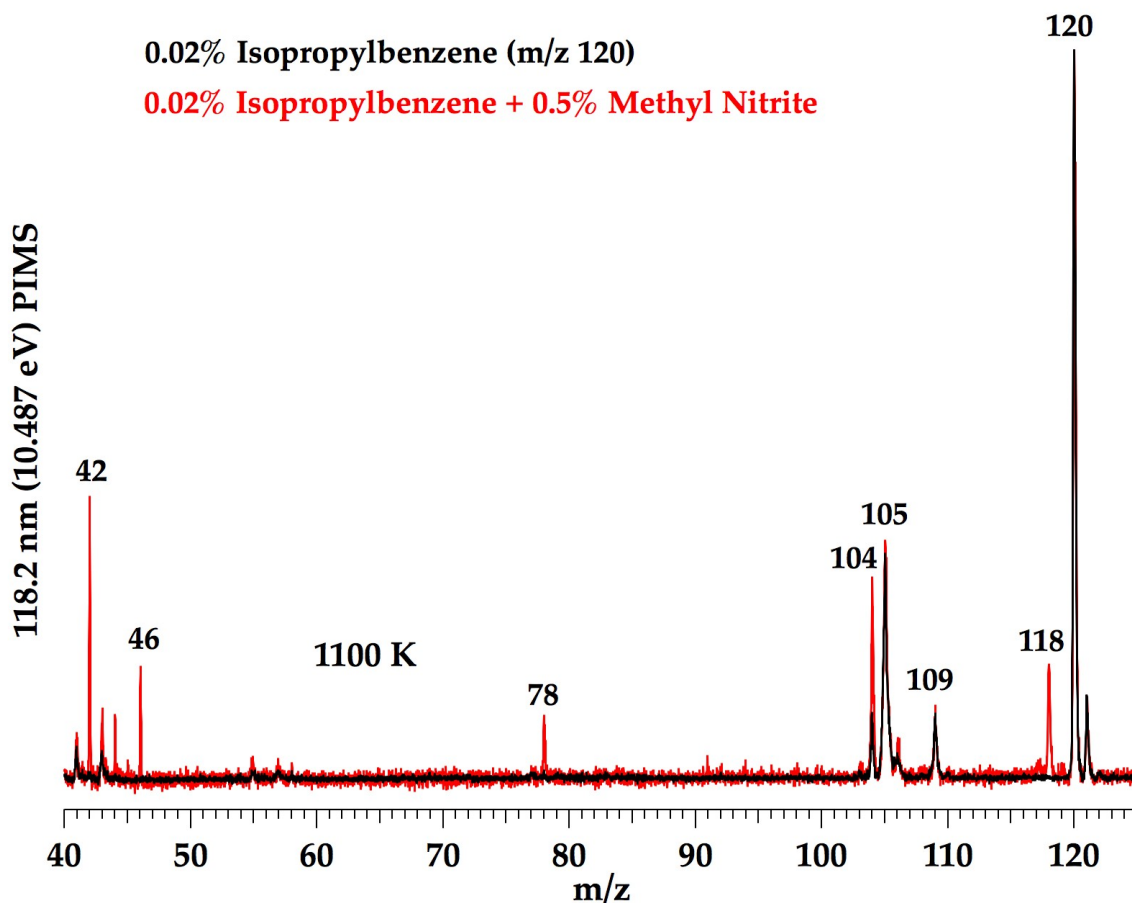


Fig. A.3. PIMS spectra recorded with 118.2 nm radiation of the pyrolysis of 0.02% isopropylbenzene ( $m/z$  120) shown in black the pyrolysis of a mixture of 0.02% isopropylbenzene with 0.5% methyl nitrite ( $m/z$  61) at reactor temperature of 1100 K in a pulsed helium carrier gas. In the pyrolysis of isopropylbenzene, the largest decomposition feature is found at  $m/z$  105, which could result from loss of methyl radical. This process would yield a resonance stabilized benzyl-like radical ( $C_6H_5CHCH_3$ ). Interestingly, there is no evidence of hydrogen loss that would result in another resonance stabilized radical,  $C_6H_5C(CH_3)_2$ . The hydrolysis products are assigned to be the appearance of benzene ( $m/z$  78), the enhancement of styrene ( $m/z$  104) and the appearance of a feature at 118, likely  $\alpha$ -methylstyrene ( $C_6H_5C(CH_3)=CH_2$ ). The peak at 109 is believed to be either a contaminant or the dissociative ionization of the parent. The group of peaks between  $m/z$  40 and 46 are unassigned.

### III. Styrene ( $C_6H_5CH=CH_2$ )

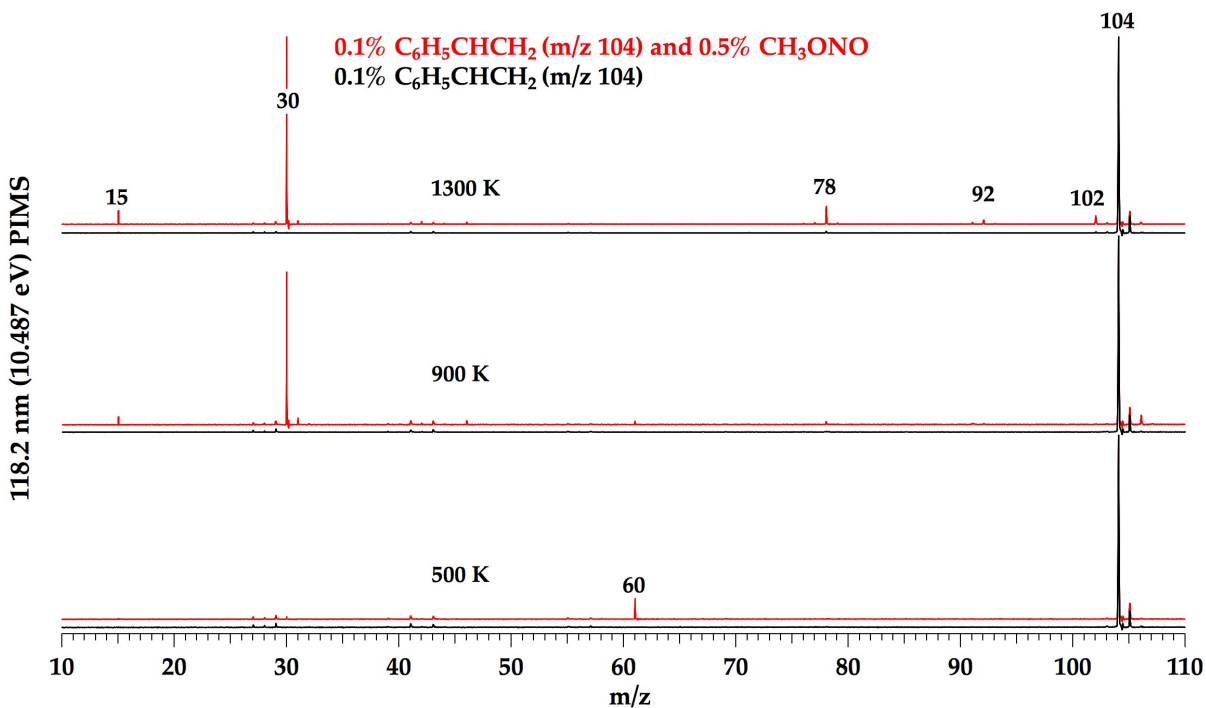


Fig. A.4. Overview of the PIMS spectra recorded with 118.2 nm radiation of the pyrolysis of 0.1% styrene ( $m/z$  104) shown in black the pyrolysis of a mixture of 0.1% isopropylbenzene with 0.5% methyl nitrite ( $m/z$  61) at reactor temperatures up to 1300 K in a pulsed helium carrier gas. The pyrolysis of styrene shows no decomposition at these temperatures. The hydrolysis products are assigned to be the appearance of benzene ( $m/z$  78), the appearance of  $m/z$  92 that is likely toluene, and the appearance of a feature at 102, likely phenylacetylene  $C_6H_5C\equiv CH$ ).

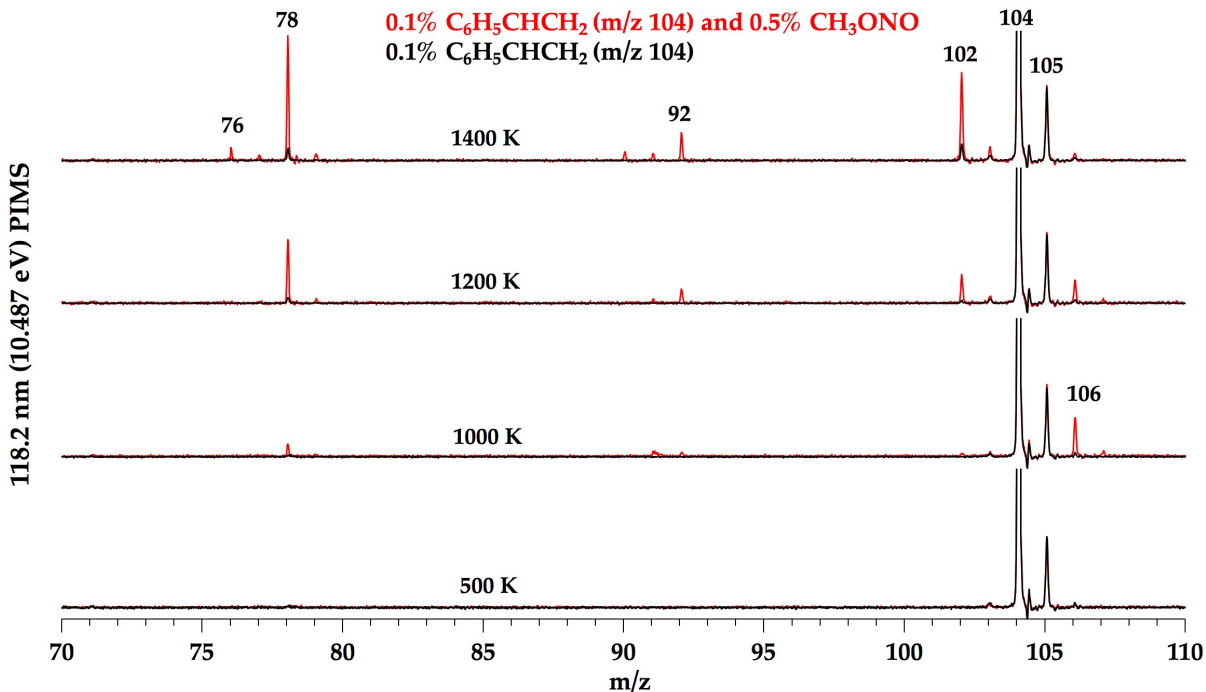


Fig. A.5. PIMS spectra recorded with 118.2 nm radiation of the pyrolysis of 0.1% styrene ( $m/z$  104) shown in black the pyrolysis of a mixture of 0.1% isopropylbenzene with 0.5% methyl nitrite ( $m/z$  61) at reactor temperatures up to 1300 K in a pulsed helium carrier gas. The vertical axis range is decreased help identify the weak features within the mass-to-charge range of  $m/z$  70 to  $m/z$  110. Here we see very weak features in the 1300 K pyrolysis of styrene at  $m/z$  102 (likely phenylacetylene,  $C_6H_5C\equiv CH$ ) and  $m/z$  78, likely benzene. A few new weak features are observed in the hydrolysis spectra, namely  $m/z$  76 (likely *ortho*-benzyne),  $m/z$  90 and 91, potentially fulvenallene ( $C_5H_4C=CH_2$ ) and benzyl radical ( $C_6H_5CH_2$ ). We also observe a small peak at  $m/z$  106 at reactor temperatures 1000 K and 1200 K. This is consistent with two subsequent additions of hydrogen atom, which has not been observed before in a micro-reactor pyrolysis experiment. Hydrogen addition to the terminal carbon of the side-chain double bond will be facilitated by the formation of a benzyl-like radical that would be resonant with the aromatic ring. This stable adduct could survive and react with a second hydrogen atom to form ethylbenzene ( $C_6H_5CH_2CH_3$ ).

#### IV. Phenol ( $C_6H_6OH$ )

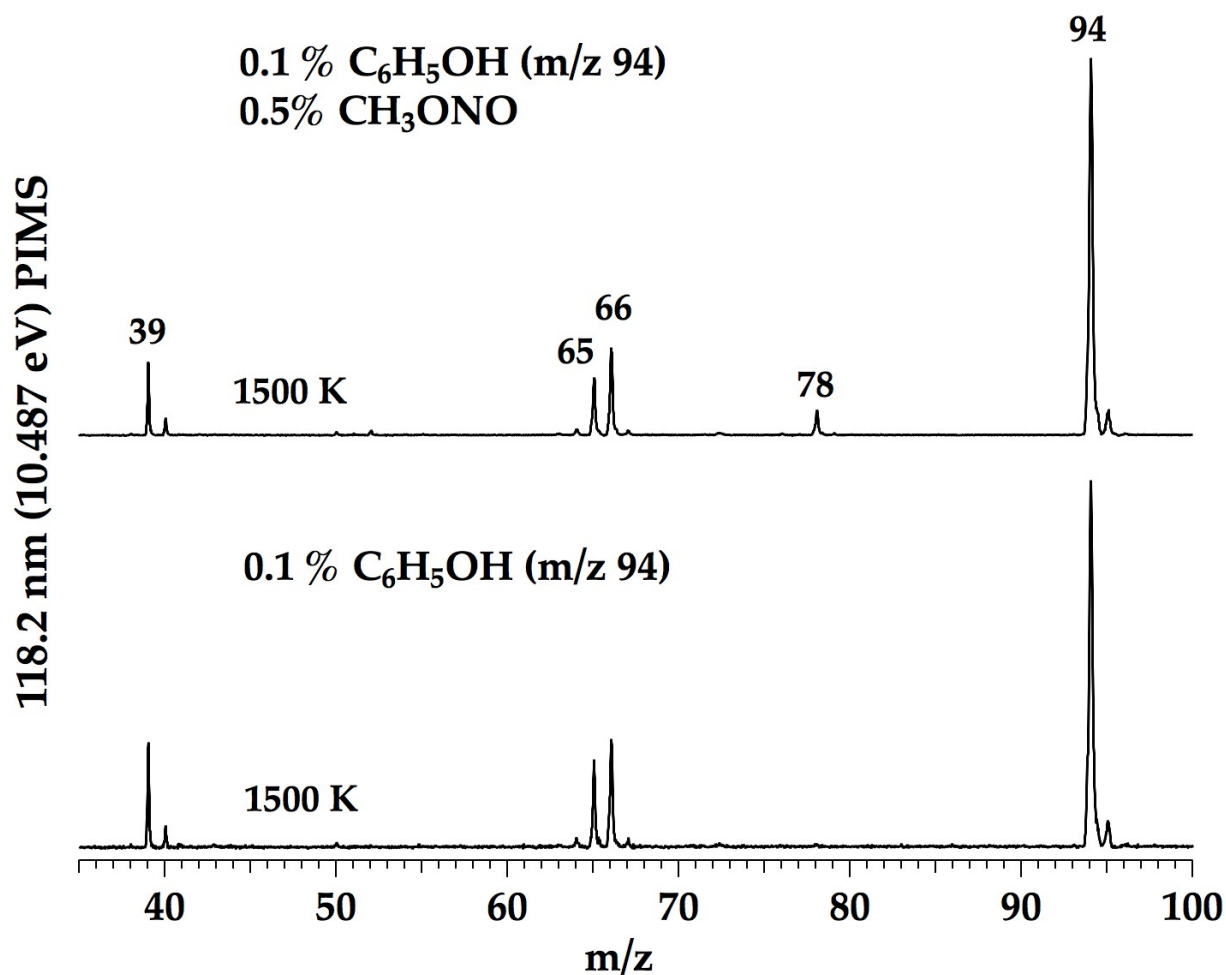


Fig. A.6. PIMS spectra recorded with 118.2 nm radiation of the pyrolysis of 0.1% phenol ( $m/z$  94) shown in bottom trace and the pyrolysis of a mixture of 0.1% phenol with 0.5% methyl nitrite ( $m/z$  61) at reactor temperature of 1500 K in a pulsed helium carrier gas. In the pyrolysis of phenol, the decomposition features are  $m/z$  39 (propargyl radical),  $m/z$  65 (cyclopentadienyl radical), and  $m/z$  66 (cyclopentadiene). The only hydroxyrolysis product is observed with the appearance of benzene ( $m/z$  78).

## V. Anisole ( $C_6H_5OCH_3$ )

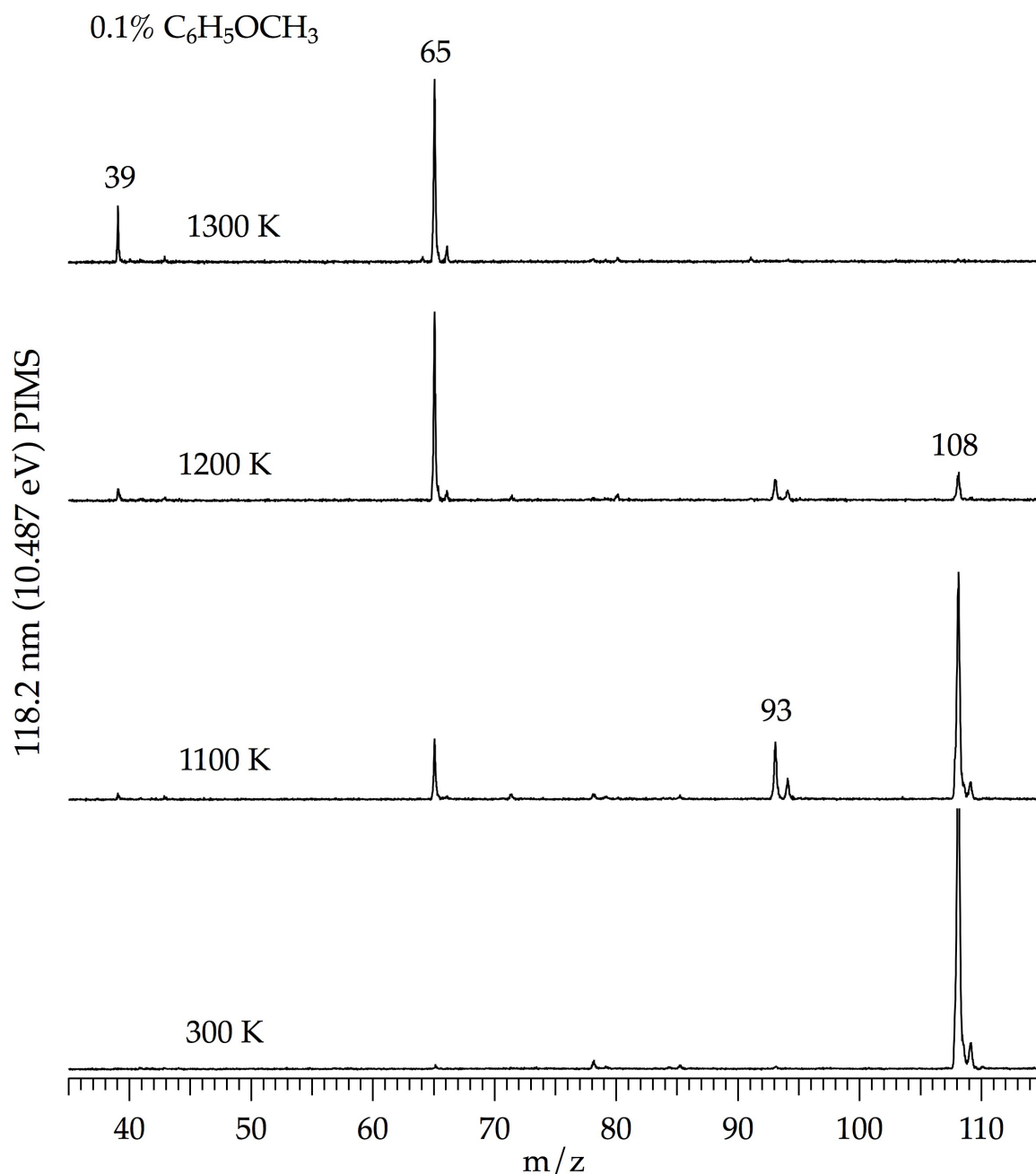


Fig. A.7. PIMS spectra recorded with 118.2 nm radiation of the pyrolysis of 0.1% anisole ( $m/z$  108) at reactor temperatures up to 1300 K in a pulsed helium carrier gas. In the pyrolysis of phenol, the decomposition features are  $m/z$  39 (propargyl radical),  $m/z$  65 (cyclopentadienyl radical),  $m/z$  93 (phenoxy radical,  $C_6H_5O$ ) and a weak feature at  $m/z$  94, likely phenol.

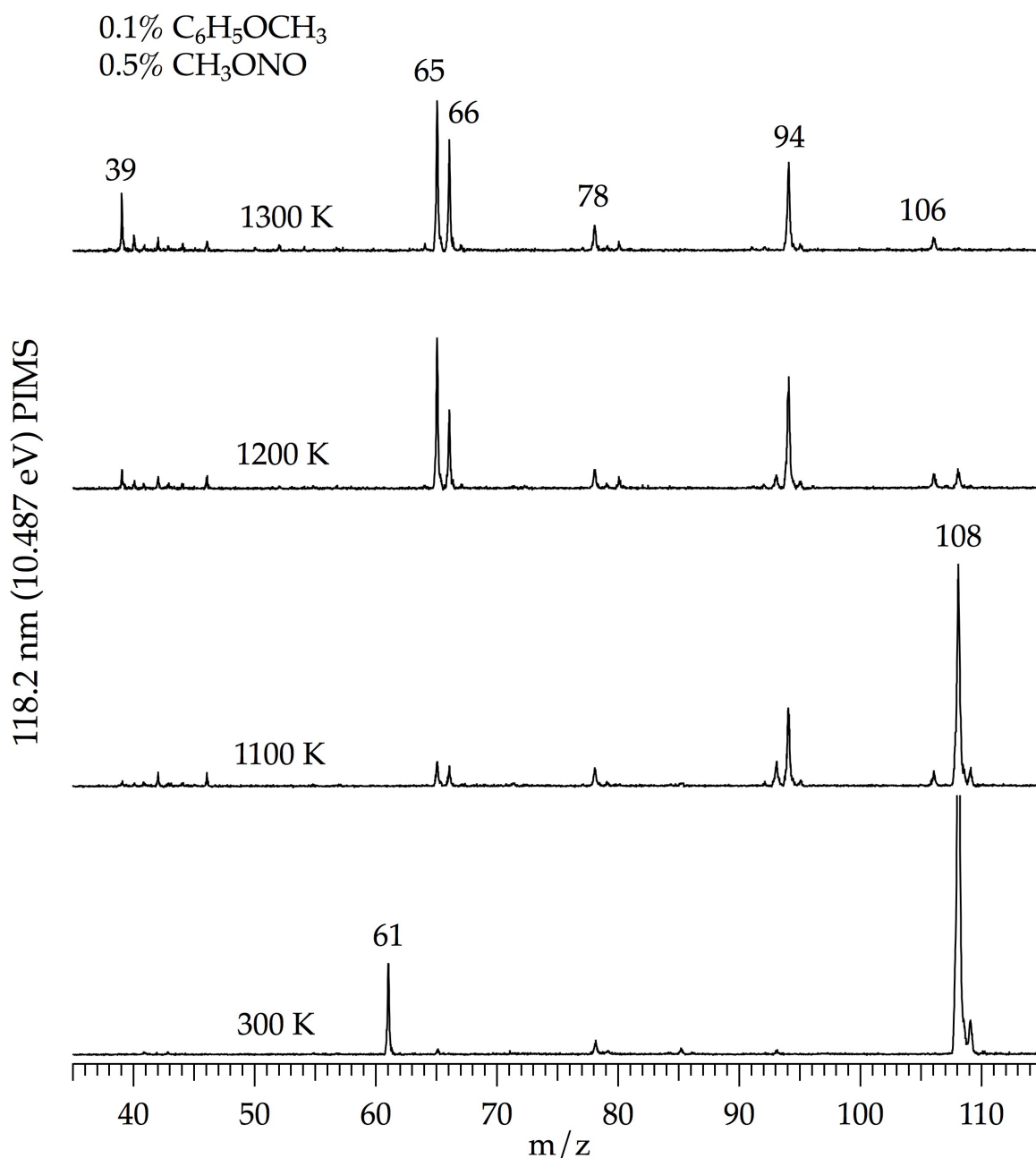


Fig. A.8. PIMS spectra recorded with 118.2 nm radiation of the pyrolysis of 0.1% anisole ( $m/z$  108) mixed with 0.5% methyl nitrite ( $m/z$  61) at reactor temperatures up to 1300 K in a pulsed helium carrier gas. By comparing with Fig. A.7 we can conclude that the hydrolysis products are  $m/z$  66 (cyclopentadiene),  $m/z$  78 (benzene), an depletion of  $m/z$  93 and enhancement of  $m/z$  94, which we conclude results from hydrogen addition to phenoxy radical to form phenol, and a small peak at  $m/z$  106, which remains unassigned at this time.



## VI. Benzyl phenyl ether ( $C_6H_5CH_2OC_6H_5$ )

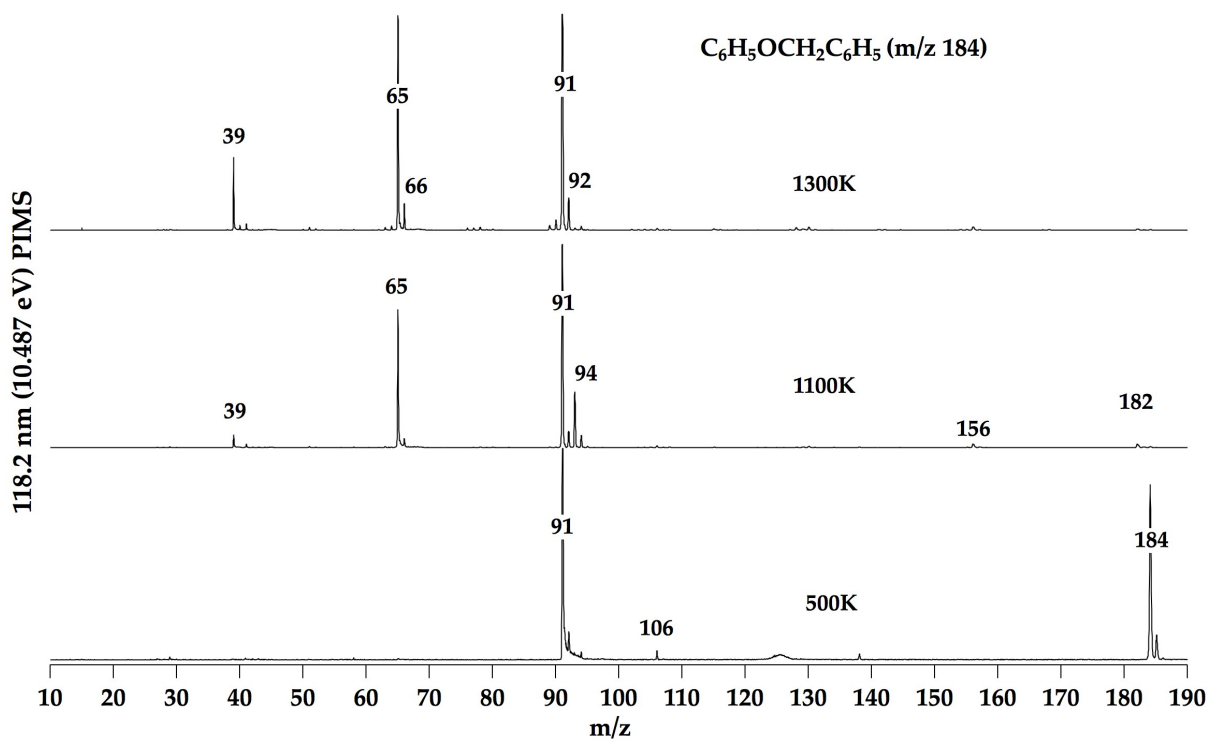


Fig. A.9. PIMS spectra recorded with 118.2 nm radiation of the pyrolysis of a dilute but unknown concentration of benzyl phenyl ether ( $m/z$  184) at reactor temperatures up to 1300 K in a pulsed helium carrier gas. The pyrolysis of benzyl phenyl ether appears to be the sum of benzyl radical decomposition and phenol decomposition, implying that the main pathway is initial cleavage of the C-O bond that bridges the two rings. The main products are  $m/z$  39 (propargyl radical),  $m/z$  65 (cyclopentadienyl radical),  $m/z$  66 (cyclopentadiene),  $m/z$  89 (fulvenallenyl radical,  $C_5H_4C\equiv CH$ ),  $m/z$  90 (fulvenallene,  $C_5H_4C=CH_2$ ),  $m/z$  91 (benzyl radical),  $m/z$  92 (toluene),  $m/z$  93 (phenoxy radical,  $C_6H_5O$ ), and  $m/z$  94 ( $C_6H_5OH$ ). The weak feature at 106 is likely a contaminant of ethylbenzene ( $C_6H_5CH_2CH_3$ ) and the weak feature at  $m/z$  156 remains unassigned but may be the result of dissociative ionization.

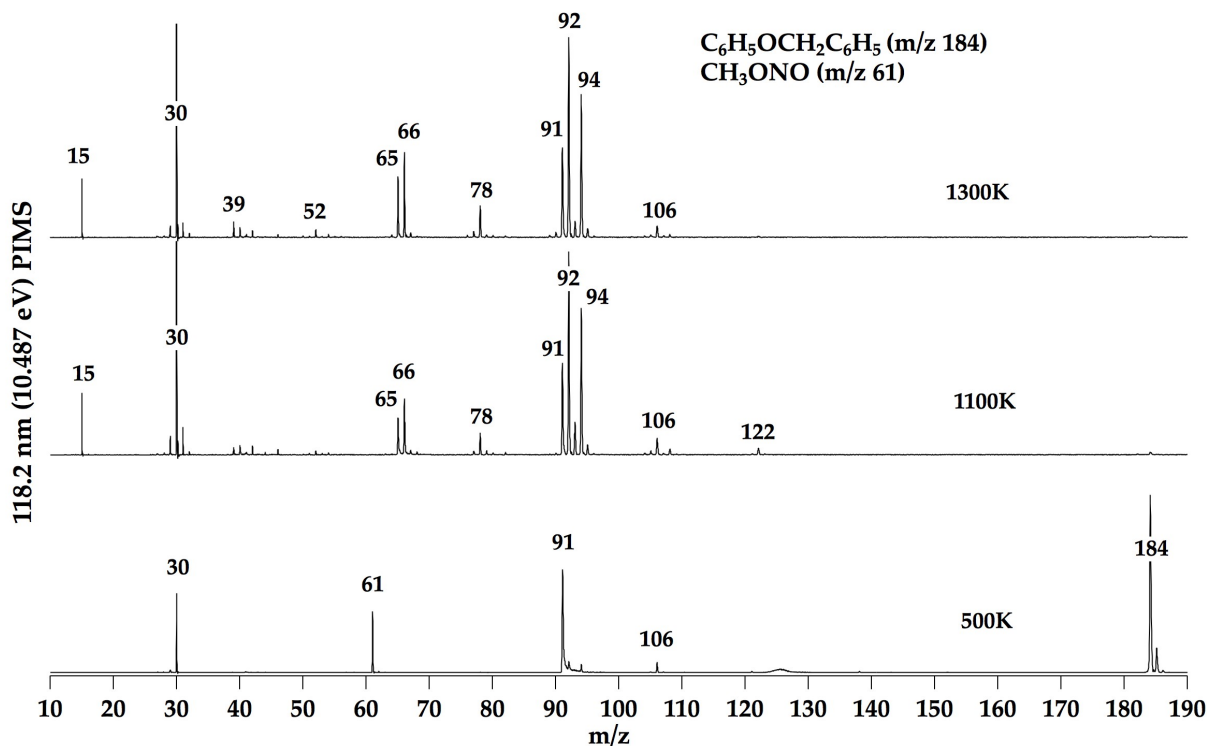


Fig. A.10. PIMS spectra recorded with 118.2 nm radiation of the pyrolysis of a dilute but unknown concentration of benzyl phenyl ether ( $m/z$  184) mixed with 0.5% methyl nitrite ( $m/z$  61) at reactor temperatures up to 1300 K in a pulsed helium carrier gas. By comparing with Fig. A.9 we can conclude that the hydrolysis products are  $m/z$  52 (unassigned), an enhancement of  $m/z$  66 (cyclopentadiene), and the appearance of  $m/z$  78 (benzene). There is also a weak feature at  $m/z$  122, which is also unassigned. There is a strong enhancement of  $m/z$  94 at 1300 K compared to that observed in Fig. A.9. This could be the result of hydrogen atom addition to phenoxy radical to form phenol, which is then more resistant to thermal decomposition. At 1300 K will decompose to CO and cyclopentadiene but phenol is stable until heating to 1500 K. A similar effect is observed with  $m/z$  92, which is likely hydrogen addition to benzyl radical to form toluene, which is also more resistant to decomposition.



## Appendix B

### Supplementary Material for Chapter 6

#### Possible Thermal Pathways for Benzyl-d<sub>2</sub> Radical Decomposition

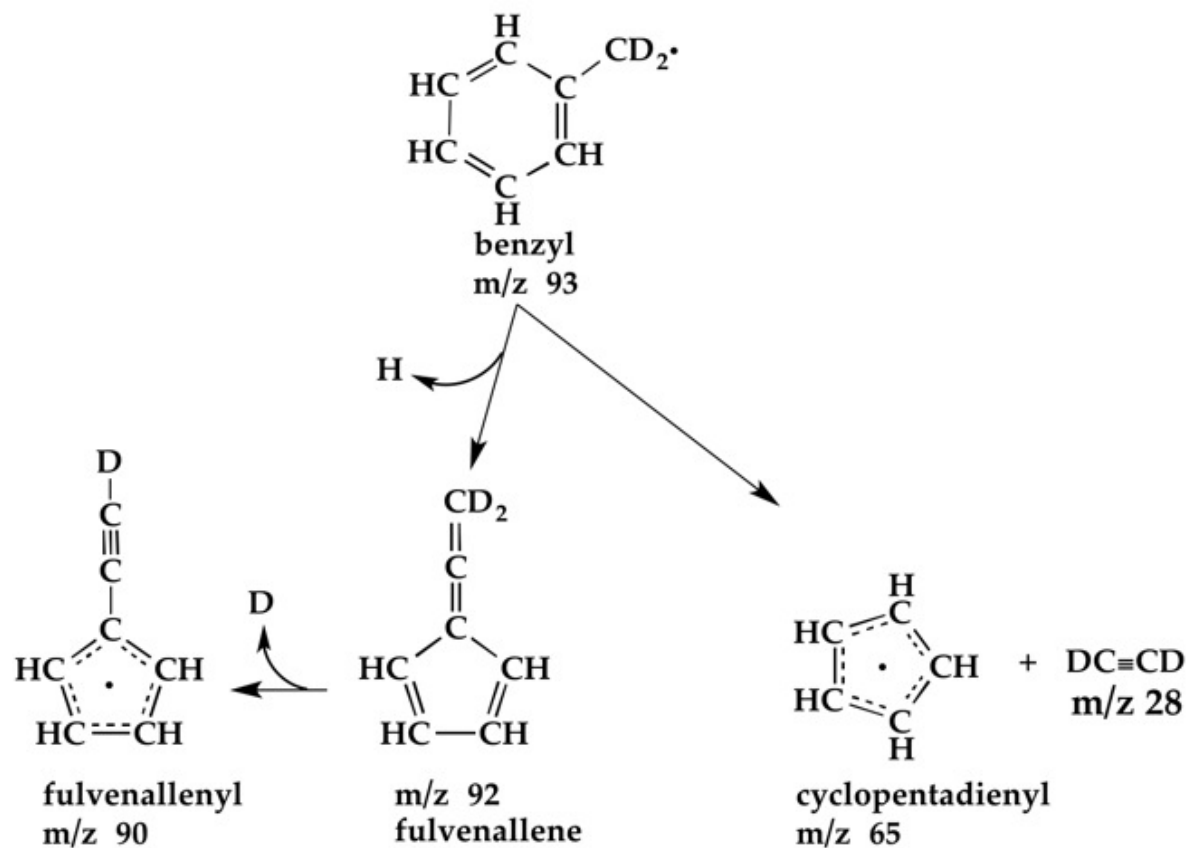


Fig. B.1. Benzyl radical-d<sub>2</sub> is proposed to decompose not through direct bond breakage but through isomerization(s) reaction. Loss of one H atom can lead to fulvenallene (C<sub>5</sub>H<sub>4</sub>=C=CD<sub>2</sub>, m/z 92), and loss of a D atom would produce the fulvenallenyl radical (C<sub>5</sub>H<sub>4</sub>—C≡CD, m/z 90).

## Possible Thermal Pathways for Benzyl-d<sub>5</sub> Radical Decomposition

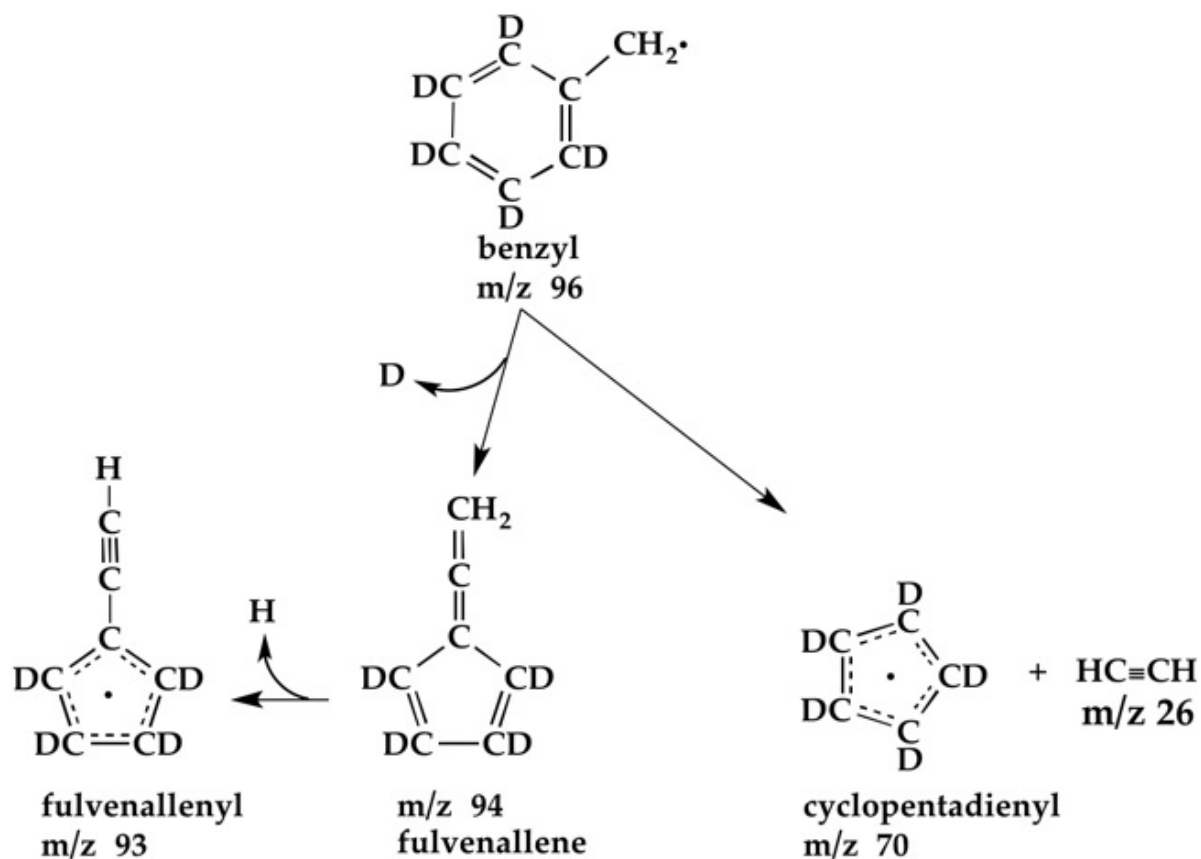


Fig. B.2. Benzyl radical-d<sub>5</sub> is proposed to decompose not through direct bond breakage but through isomerization(s) reaction. Loss of one D atom can lead to fulvenallene (C<sub>5</sub>D<sub>4</sub>=C=CH<sub>2</sub>, m/z 94) and loss of a H atom would produce the fulvenallenyl radical (C<sub>5</sub>D<sub>4</sub>-C≡CH, m/z 93).

## Possible Thermal Pathways for $^{13}\text{C}$ -Benzyl Radical Decomposition

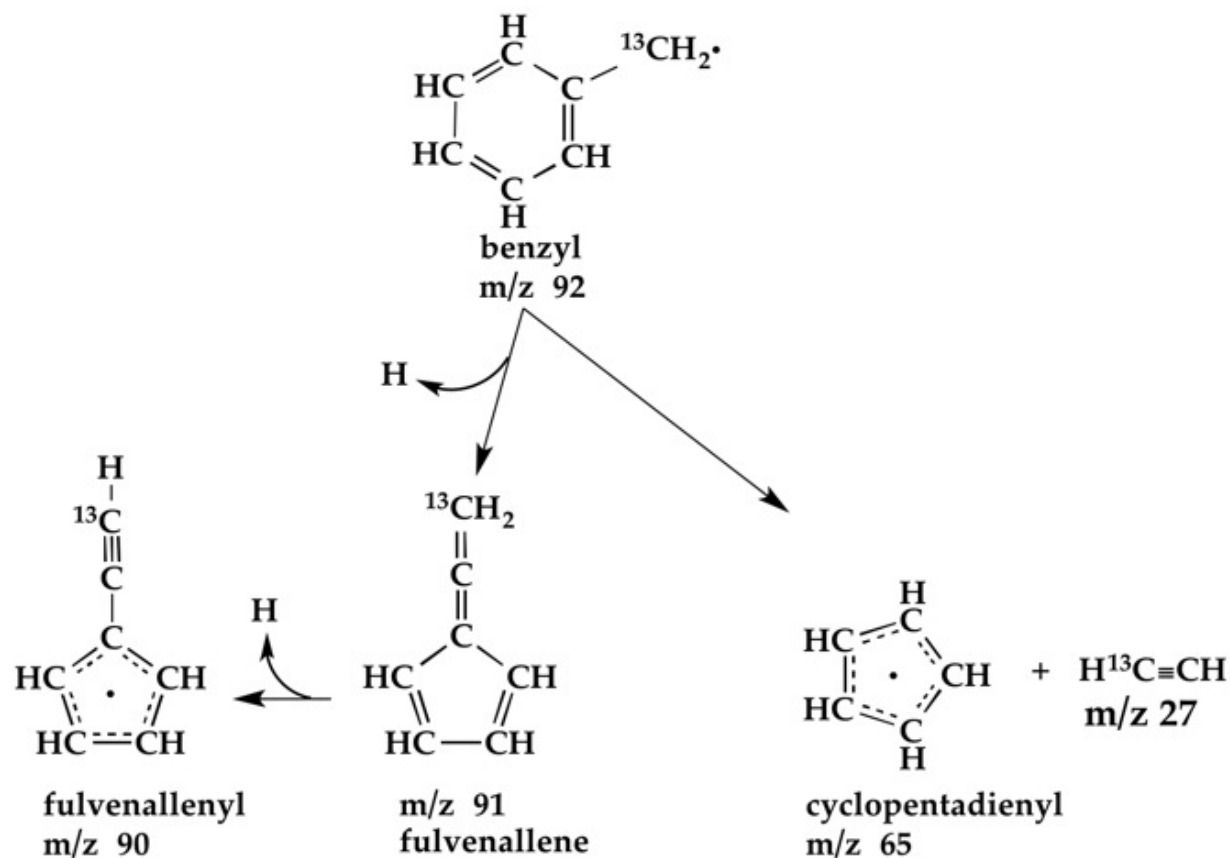


Fig. B.3.  $^{13}\text{C}$  labeled benzyl radical is proposed to decompose not through direct bond breakage but through isomerization(s) reaction. Loss of one H atom can lead to fulvenallene ( $\text{C}_5\text{H}_4=\text{C}=\text{C}^{13}\text{H}_2$ , m/z 91) and a second H atom loss would produce the fulvenallenyl radical ( $\text{C}_5\text{H}_4-\text{C}\equiv\text{C}^{13}\text{H}$ , m/z 90).

	Mode	Description	Decomposition of Ethylbenzene at 1500 K in a Neon Matrix (this work)		Various Experimental Findings	
			$\nu(\text{cm}^{-1})$	$\nu(\text{cm}^{-1})$	Intensity or Absorbance Ratio	
Propargyl Radical (CH <sub>2</sub> CCH)		Propargyl Radical (CH <sub>2</sub> CCH)		Argon Matrix <sup>1</sup>		
	a1	1 CH <sub>2</sub> CC-H stretch	3321	3308.5 ± 0.05	100	
		2 sym H <sub>2</sub> C-CCH stretch		3028.3 ± 0.06	2	
		3 CH <sub>2</sub> C=CH - CH <sub>2</sub> -CCH stretch		1935.4 ± 0.4	4	
		4 H <sub>2</sub> -CCH scissors		1440.4 ± 0.5	2 ± 1	
		5 CH <sub>2</sub> C=CH + CH <sub>2</sub> -CCH stretch		1061.6 ± 0.8	7 ± 1	
	b1	6 H <sub>2</sub> C-CCH umbrella	687.3	686.6 ± 0.4	44 ± 4	
		7 CH <sub>2</sub> CC-H out-of-plane bend		483.6 ± 0.5	63 ± 7	
		8 CH <sub>2</sub> -C=CH out-of-plane bend				
	b2	9 asym H <sub>2</sub> C-CCH stretch				
		10 H <sub>2</sub> C-CCH + CH <sub>2</sub> -C=CH in-plane bend		1016.7 ± 0.4	2	
		11 CH <sub>2</sub> CC-H in-plane bend		620 ± 2	33 ± 4	
		12 CH <sub>2</sub> -C=CH in-plane bend				
	2 <sup>7</sup> CH <sub>2</sub> CC-H out-of-plane bend		972.6	~8		
Acetylene (HCCH)		Acetylene (HCCH)		Neon Matrix <sup>2</sup>		
		$\sigma_u^+$ CH stretch	3297.0	3297.1	1.2778	
		$\sigma_u^+$ CH stretch	3296.3	3296.4	1.088	
		$\sigma_u^+$ CH stretch	3284.0	3284	1.78	
		$\sigma_u^+$ CH stretch	3281.8	3281.8	1.05	
	$\pi_u$ CH Bend	732.1	731.99	>6		
Methyl Acetylene (CH <sub>3</sub> CCH)		Methyl Acetylene (CH <sub>3</sub> CCH)		Argon Matrix <sup>1</sup>		
	a1(z)	1 C-H stretch		3322.9		
		2 CH <sub>3</sub> sym stretch				
		3 C=C stretch				
		4 CH <sub>3</sub> sym def				
		5 C-C stretch		926.6		
	e(x,y)	6 CH <sub>3</sub> deg stretch				
		7 CH <sub>3</sub> def def				
		8 CH <sub>3</sub> rock				
		9 C-H bend	630.4 and 628	630.6 and 628.9		
	10 CCC bend					
Methyl Radical (CH <sub>2</sub> )		Methyl Radical (CH <sub>3</sub> )		Neon Matrix <sup>3</sup>		
	a1'	1 CH stretch				
	a2''	2 umbrella mode	618.8	617	VS	
	e'	3 CH stretch	3170	3162	WM	
e''	4 deformation		1396	W		

	Mode	Description	Decomposition of Ethylbenzene at 1500 K in a Neon Matrix (this work)	Various Experimental Findings		
			$\nu(\text{cm}^{-1})$	$\nu(\text{cm}^{-1})$	Intensity or Absorbance Ratio	
o - Benzyne (cyc-C <sub>6</sub> H <sub>4</sub> )		o - Benzyne (cyc-C <sub>6</sub> H <sub>4</sub> )		Neon Matrix <sup>4</sup>		
	a1	1 CH stretch		3094	WM	
		2 CH stretch		3071	W	
		3 C=C stretch		1846	W	
		4 mixed		1415	VW	
		5 mixed		1271	W	
		6 CH deformation		1055	WM	
		7 ring stretch		1039	M	
		8 ring stretch		982	WM	
		9 ring deformation		589	VW	
	b1	14 CH wag		838	VW	
		15 CH wag	737.8	737	S	
		16 ring torsion		388	WM	
		17 CH stretch		3086	M	
		18 CH stretch		3049	VW	
		19 ring stretch		1451	M	
		20 mixed		1394	WM	
		21 mixed		1307	VW	
		22 mixed		1094	W	
		23 ring deformation		849	MS	
		24 ring deformation	473.0	472	VS	
	Cyclopentadienyl Radical (C <sub>5</sub> H <sub>5</sub> )		Cyclopentadienyl Radical (C <sub>5</sub> H <sub>5</sub> )		Gas Phase <sup>5</sup> & Argon Matrix <sup>6</sup>	
		a1'	2	1072.6	1071 <sup>5</sup>	
		a2'	3	1242	1244 <sup>5</sup>	
a2'		4	overlap	661 <sup>6</sup>	S	
e1'		5		3079 <sup>6</sup>	WM	
		6	1385.3	1383 <sup>6</sup>	M	
		7		1001 <sup>5</sup>		
e1		8	overlap	766 <sup>5</sup>		
e2'		10		1320 <sup>5</sup>		
		11		1041 <sup>5</sup>		
		12		872 <sup>5</sup>		
e2		13		861 <sup>5</sup>		
		14	576.4	576 <sup>5</sup>		
Benzyl Radical (C <sub>6</sub> H <sub>5</sub> CH <sub>2</sub> )			Benzyl Radical (C <sub>6</sub> H <sub>5</sub> CH <sub>2</sub> )		Argon Matrix <sup>7</sup>	
	A1	1 CH stretch	3071.5	3069	W	
	A1	2 C-CH <sub>2</sub> stretch		1469	M	
	A1	3 CH <sub>2</sub> deformation	1408	1409	M	
	A1	4 CH <sub>2</sub> deformation		1264	M	
	A1	5 CH deformation		1015	W	
	B1	6 ring deformation		882	W	
	B1	7 ring deformation	762	762	VS	
	B1	8 CH <sub>2</sub> wag		710.9	W	
	B1	9 CH <sub>2</sub> wag	668.5	667	S	
	B2	10 CH <sub>2</sub> wag		465	S	
	B2	11 CH <sub>2</sub> a-stretch	3118	3111	W	
	B2	12 ring stretch	1448	1446	M	
	B2	13 ring stretch		1305	W	
B2	14 CH deformation		948.1	W		



	Mode	Description	Decomposition of Ethylbenzene at 1500 K in a Neon Matrix (this work)	Various Experimental Findings	
			$\nu(\text{cm}^{-1})$	$\nu(\text{cm}^{-1})$	Intensity or Absorbance Ratio
Fulvenallene ( $\text{C}_5\text{H}_4=\text{C}=\text{CH}_2$ )		Fulvenallene ( $\text{C}_5\text{H}_4=\text{C}=\text{CH}_2$ )		Gas Phase <sup>a</sup>	
	A1	1 CH stretch		3135	M
	A1	2 CH stretch		3092	M
	A1	3 $\text{CH}_2$ sym. stretch		2966	W
	A1	4 C-C sym. stretch	1488	1486	MS
	A1	5 CH bend		1362	W
	A1	6 CH bend		1320	W
	A1	7 $\text{CH}_2$ sym scissors		1432	W
	A1	8 $\text{C}=\text{C}$ sym stretch		1078	W
	A1	9 $\text{C}=\text{C}$ asymmetric stretch	1929	1935	S
	A1	10 C-C stretch		985	VW
	A1	11 C-C stretch	885.9	886	MS
	A1	12 ring breathing			
	A2	13 $\text{CH}_2$ twist			
	A2	14 CH bend			
	A2	15 CH bend			
	A2	16 ring bend			
	B1	17 CH stretch		3122	W
	B1	18 CH stretch		3071	W
	B1	19 C-C asym stretch		1655	VW
	B1	20 CH bend			
	B1	21 CH bend		1170	VW
	B1	22 $\text{CH}_2$ wag	840	844	MS
	B1	23 $\text{C}=\text{C}=\text{C}$ bend			
	B1	24 $\text{C}=\text{C}=\text{C}$ wag			
	B1	25 C-C-C stretch		810	VW
	B1	26 ring bend		530	VW
	B2	27 $\text{CH}_2$ asym stretch		3010	VW
	B2	28 CH bend	755	754	S
	B2	29 CH bend		733	W
	B2	30 $\text{CH}_2$ rock		604	M
	B2	31 $\text{C}=\text{C}=\text{C}$ bend			
	B2	32 $\text{C}=\text{C}=\text{C}$ rock			
B2	33 ring bend				

Mode	Description	Decomposition of Ethylbenzene at 1500 K in a Neon Matrix (this work)		Various Experimental Findings	
		$\nu(\text{cm}^{-1})$	$\nu(\text{cm}^{-1})$	Intensity or Absorbance Ratio	
Ethylbenzene (C <sub>6</sub> H <sub>5</sub> -CH <sub>2</sub> -CH <sub>3</sub> )	Ethylbenzene (C <sub>6</sub> H <sub>5</sub> CH <sub>2</sub> CH <sub>3</sub> )			Gas Phase <sup>9</sup> & Liquid Phase <sup>9</sup>	
	a' fundamental				
	a'' fundamental			295	
	$\delta(\text{CCC})$ , a' fundamental			365	
	a' fundamental			404	
	295 + 158 = 453 (A'')			455	
	a' fundamental			486	
	a' fundamental			556	
	a' fundamental			624	
	a' fundamental		699	697 (gas)	S
	399 + 314 = 713			722	
	2 x 365 = 730 (A')			735	
	a' fundamental		752.5	752 (gas)	S
	a' fundamental		773.3	773 (gas)	M
	a'' fundamental; CH <sub>2</sub> rock			787	
	a' fundamental			840	
	404 + 486 = 890 (A'')			887	
	a' fundamental			904 (gas)	W
	C-C stretch a' fundamental			967 (gas)	W
	a' fundamental			1003	
	CH <sub>3</sub> rock, a' fundamental		1025.6	1026 (gas)	M
	a' fundamental		1032	1033 (gas)	M
	a'' fundamental		1066	1064	
	CH <sub>3</sub> rock, a'' fundamental			1091	
	404 + 696 = 1100 (A'')			1111	
	a' fundamental			1156	
	a' fundamental			1179	
	a' fundamental				
	CH <sub>2</sub> wag and twist, a' + a' fundamentals			1245	
	904 + 404 = 1308 (A'')			1310	
	2a'' fundamentals			1326 (gas)	M
	CH <sub>3</sub> sym. Deformation a' fundamentals			1379 (gas)	M
	314 + 1091 = 1405 (A')			1422 (gas)	W
	CH <sub>2</sub> antisym def. + CH <sub>2</sub> bend		1450	1460 (gas)	S
	2a' + a'' fundamentals		1457		
	a'' fundamental		1469.9	1464	
	a' fundamental		1500	(gas)	S
	a'' fundamental			1587	
	a' fundamental		1614	1613	
	745 + 904 = 1649 (A')		1630	1653	
	840 + 904 = 1744 (A'')			1745	
	985 + 787 = 1772 (A''); 1003 + 771 = 1774 (A'); 1-31 + 745 = 1776 (A')		1788	1776	
	840 + 964 = 1804 (A')		1801	1800 (gas)	M
	904 + 964 = 1868 (A'')		1866	1866	
	1037 + 840 = 1877 (A''); 1179 + 696 = 1875 (A')		1883	1880 (gas)	M
904 + 985 = 1889 (A')			1890		
964 + 985 = 1949 (A'')			1960 (gas)	M	
CH <sub>3</sub> and CH <sub>2</sub> sym stretch (2a')			2886 (gas)	S	
2 x 1456 = 2912 (A')					

	Mode	Description	Decomposition of Ethylbenzene at 1500 K in a Neon Matrix (this work)		Various Experimental Findings	
			$\nu(\text{cm}^{-1})$	$\nu(\text{cm}^{-1})$	Intensity or Absorbance Ratio	
		Ethylbenzene ( $\text{C}_6\text{H}_5\text{CH}_2\text{CH}_3$ ) Continued				
Ethylbenzene continued		$\text{CH}_3$ antisym stretch ( $a'$ )		2943 (gas)	S	
		$\text{CH}_3$ and $\text{CH}_2$ antisym st. ( $a' + a''$ )		2974 (gas)	S	
		$a'$ fundamental		3039 (gas)	S	
		$a''$ fundamental		3053 (gas)	S	
		$a'$ and $a''$ fundamentals	3075	3075 (gas)	S	
Diacetylene (HCCCCH)		Diacetylene (HCCCCH)		Gas Phase <sup>10</sup>		
	1	CH stretch				
	2	$\text{C}=\text{C}$ stretch				
	3	$\text{C}-\text{C}$ stretch				
	4	CH stretch	(overlap)	3329	VS	
	5	$\text{C}=\text{C}$ stretch		2020	M	
	6	CH bend				
	7	CCC bend				
	8	CH bend	(overlap)	630	VS	
9	CCC bend					

VS = Very strong  
 S = Strong  
 MS = Medium strong  
 M = Medium  
 WM = Medium Weak  
 W = Weak  
 VW = Very Weak  
 (overlap) = Peak is too close to neighboring peak to be uniquely assigned

#### References

- E. B. Jochowitz, X. Zhang, M. R. Nimlos, M. E. Varner, J. F. Stanton, G. B. Ellison, *J. Phys. Chem. A* **109**, 3812 (2005)
- Direct study of acetylene performed in a neon matrix in our group. Assignments compared to Shimanouchi, T., *Tables of Molecular Vibrational Frequencies Consolidated Volume I*, National Bureau of Standards, 1972, 1-160.
- A. Snelson, *J. Phys. Chem.* **74**, 537 (1970)
- J. G. Radziszewski, B. A. Hess Jr., R. Zahradnik, *J. Am. Chem. Soc.* **114**, 52 (1992)
- B. E. Applegate, A. J. Bezant, T. A. Miller, *J. Chem. Phys.* **114**, 4869 (2001)
- V. A. Korolev, O. M. Nefedov, *Russ. Chem. Bull.* **42**, 1436 (1993)
- E. G. Baskir, A. K. Maltsev, V. A. Korolev, V. N. Khabashesku, O. M. Nefedov, *Russ. Chem. Bull.* **42**, 1438 (1993)
- C. L. Angell, *J. Mol. Struct.* **10**, 265 (1971)
- J. H. S. Green, *Spectrochim. Acta* **18**, 39 (1962)
- Shimanouchi, T., *Tables of Molecular Vibrational Frequencies Consolidated Volume I*, National Bureau of Standards, 1972, 1-160.

Table B.1. Summary of all known vibrational modes for molecules anticipated to be found in the decomposition of benzyl radical from an ethylbenzene precursor. The features assigned in the decomposition spectra that are consistent with known vibrational mode are indicated in the fourth column, "Decomposition of Ethylbenzene at 1500 K in a Neon Matrix (this work)".

## Appendix C

### Decomposition mechanisms for C<sub>5</sub> Ring Radicals

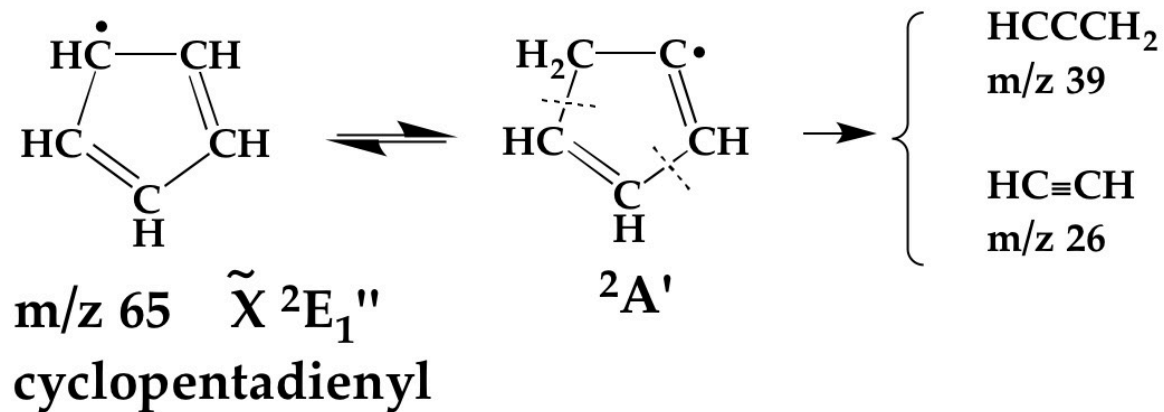


Fig. C.1. Proposed decomposition mechanism for cyclopentadienyl radical to form propargyl radical and acetylene.

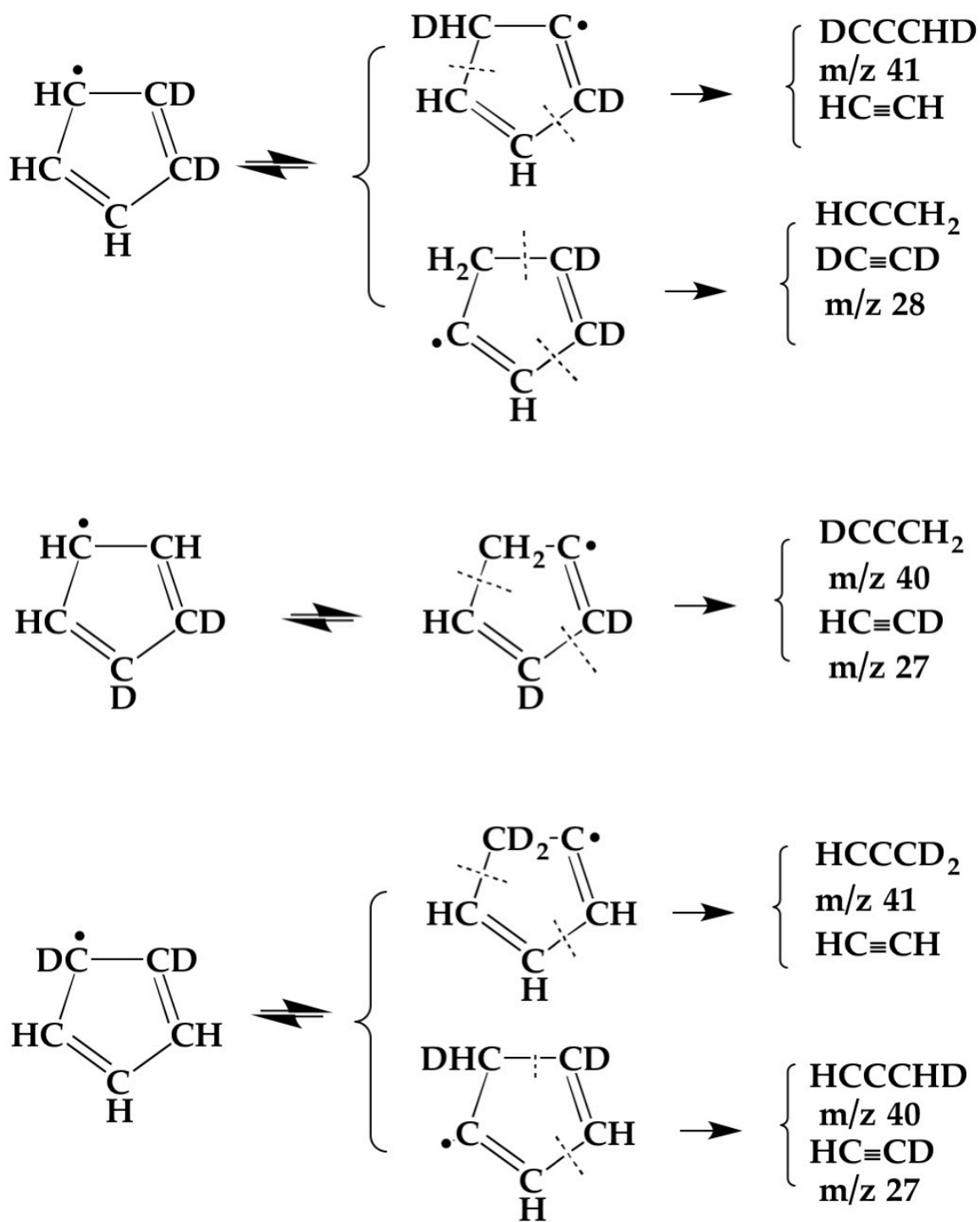


Fig. C.2. Proposed decomposition mechanism for  $\alpha,\beta$ -d<sub>2</sub> cyclopentadienyl radical to form propargyl radical and acetylene with all H/D combinations that can be produced.

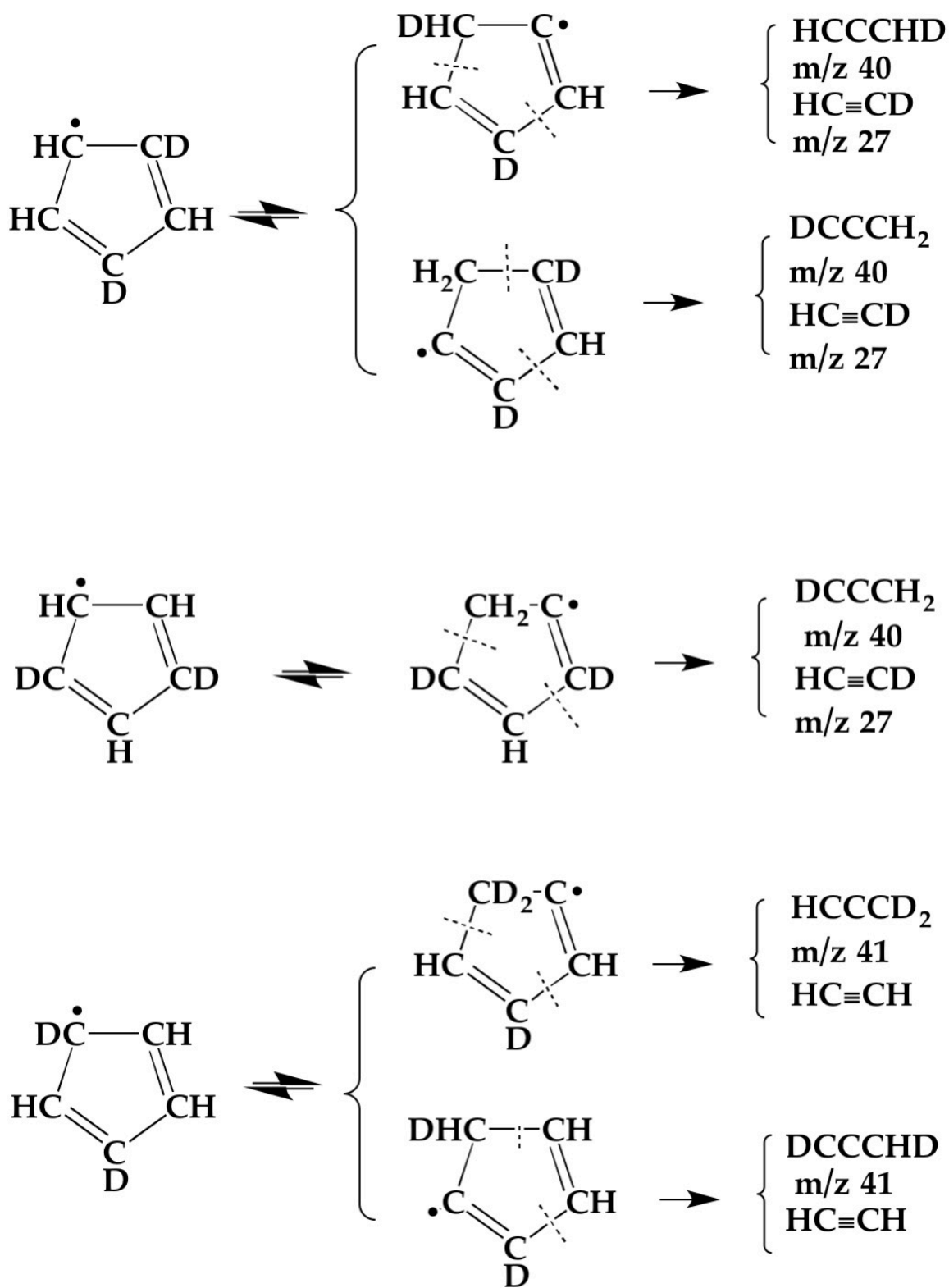


Fig. C.3. Proposed decomposition mechanism for  $\alpha,\gamma$ -d<sub>2</sub> cyclopentadienyl radical to form propargyl radical and acetylene with all H/D combinations that can be produced.

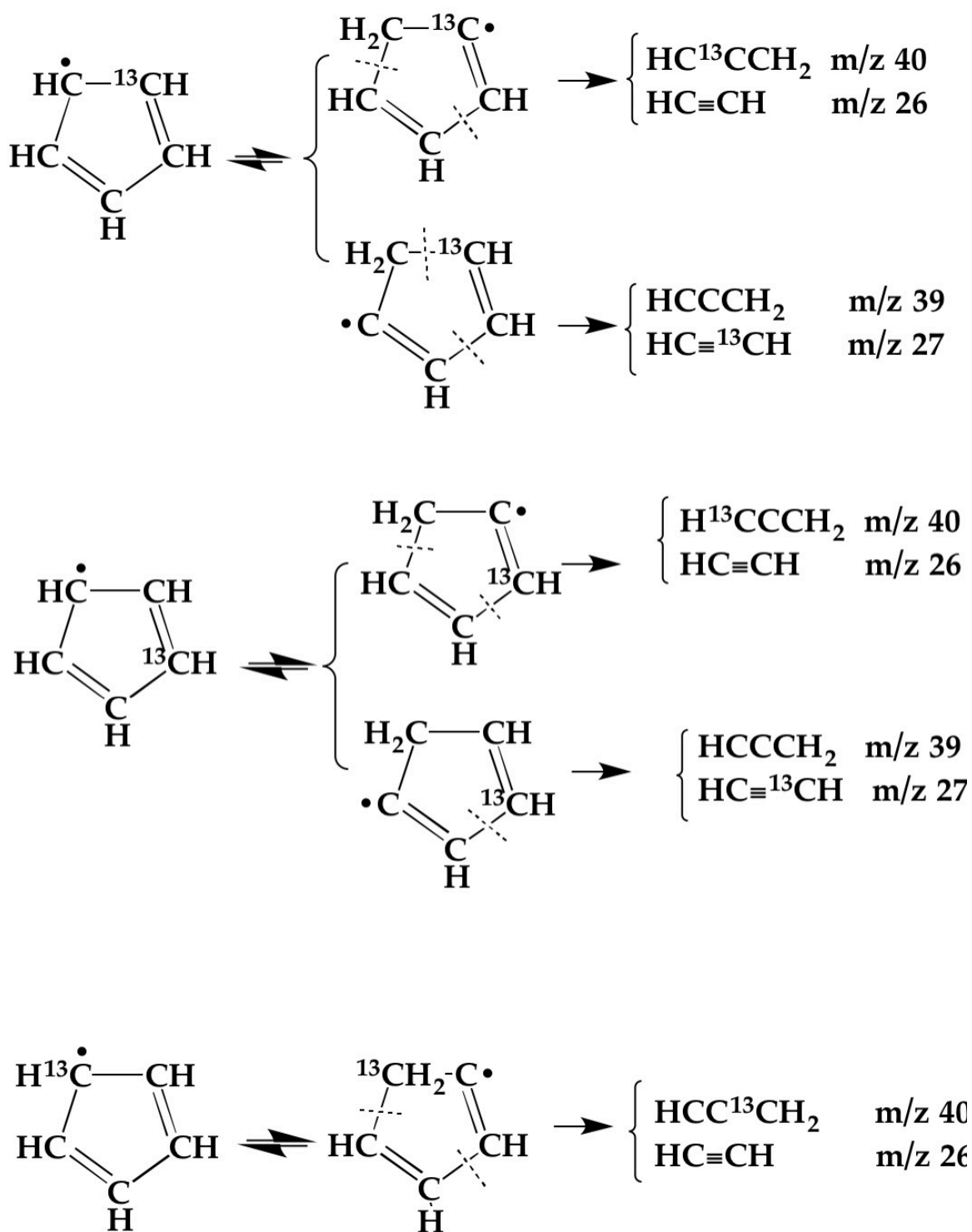


Fig. C.4. Proposed decomposition mechanism for  $^{13}\text{C}$  labeled cyclopentadienyl radical to form propargyl radical and acetylene with all  $^{13}\text{C}/^{12}\text{C}$  combinations that can be produced.

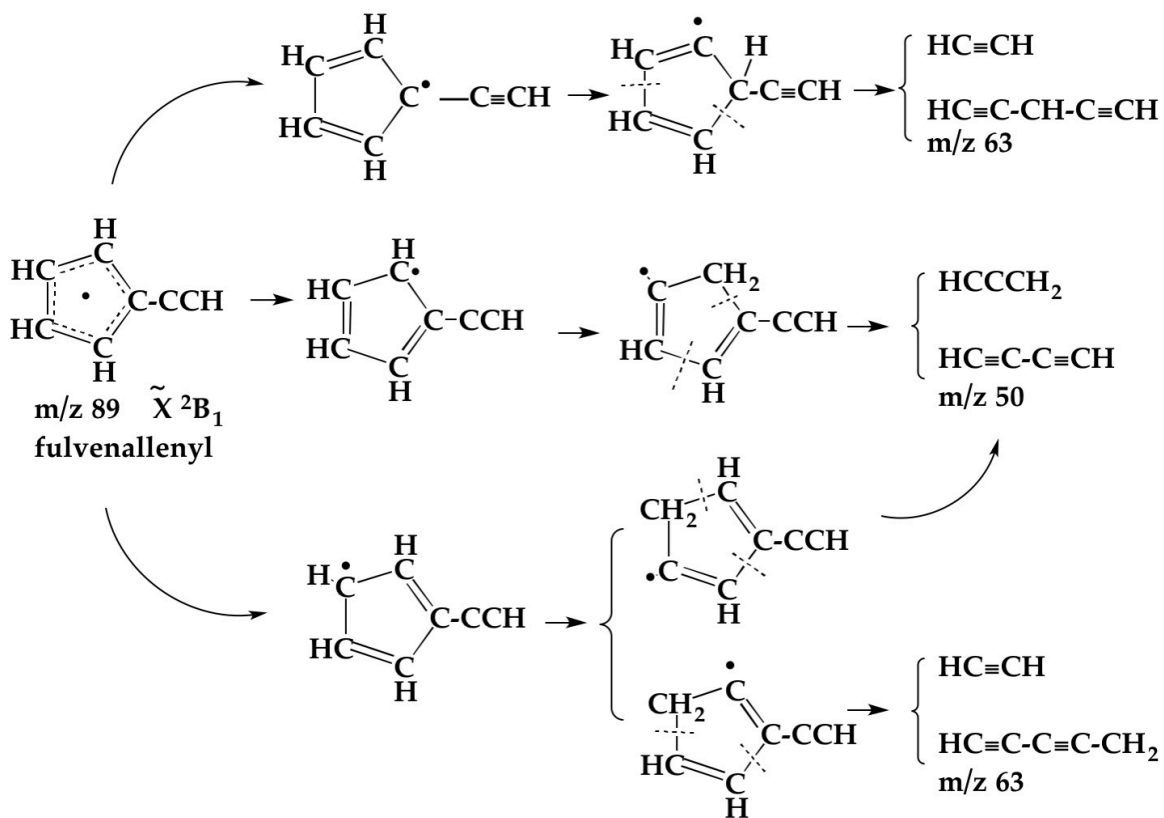


Fig. C.5. Proposed decomposition mechanism for fulvenallenyl radical to form acetylene, propargyl radical, diacetylene,  $\text{HC}\equiv\text{C}-\text{CH}-\text{C}\equiv\text{CH}$  radical and  $\text{HC}\equiv\text{C}-\text{CC}\equiv\text{CH}_2$  radical using similar decomposition patterns as those found for cyclopentadienyl radical decomposition.



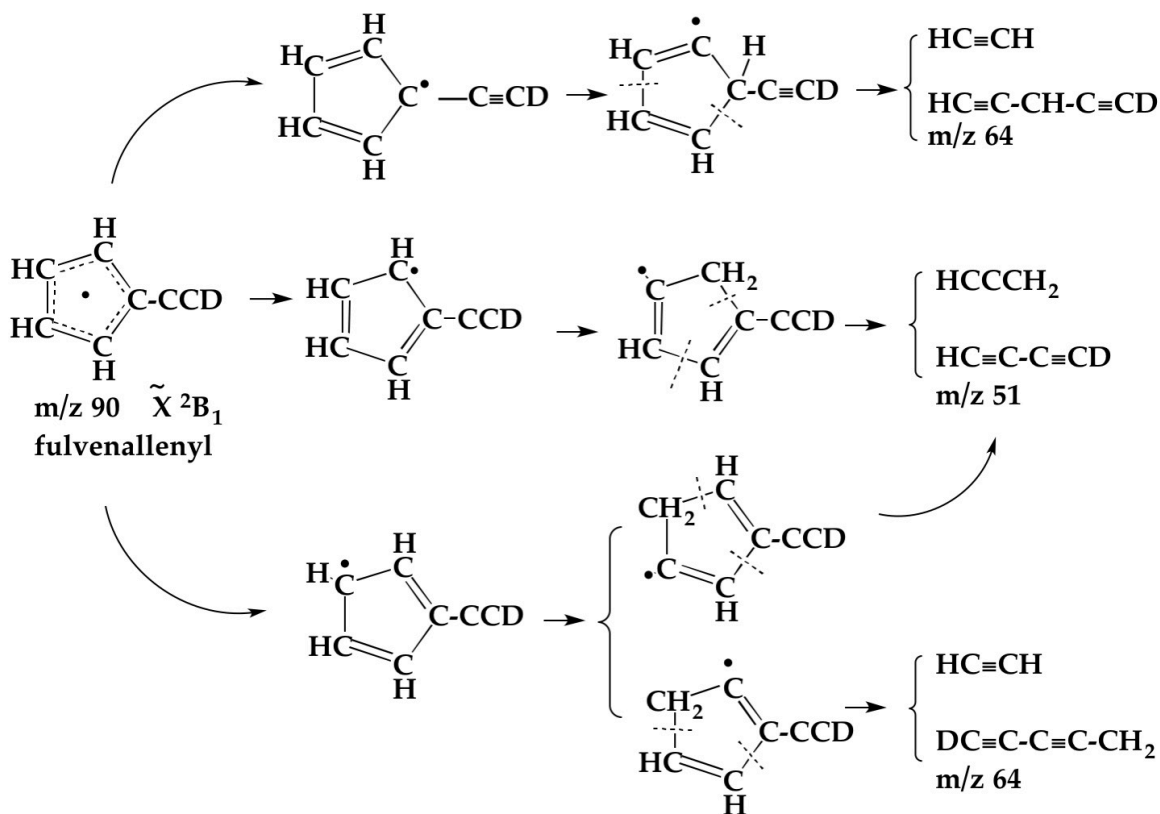


Fig. C.6. Proposed decomposition mechanism for fulvenallenyl radical- $d_1$  to form acetylene, propargyl radical, diacetylene,  $\text{HC}\equiv\text{C}-\text{CH}-\text{C}\equiv\text{CH}$  radical and  $\text{HC}\equiv\text{C}-\text{CC}\equiv\text{CH}_2$  radical with all H/D combinations that can be produced. Mechanisms are outlined using similar decomposition patterns to those found in cyclopentadienyl radical decomposition.

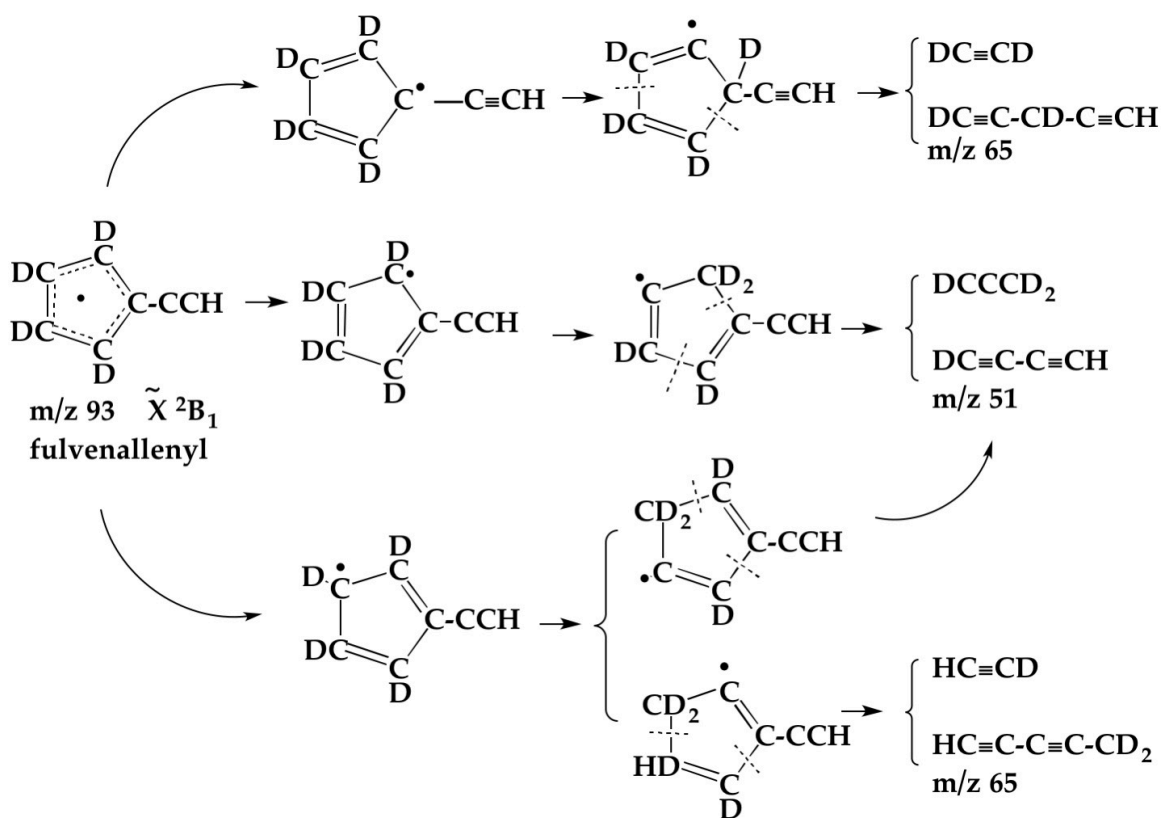


Fig. C.7. Proposed decomposition mechanism for fulvenallenyl radical- $d_4$  to form acetylene, propargyl radical, diacetylene,  $\text{HC} \equiv \text{C} \text{---} \text{CH} \text{---} \text{C} \equiv \text{CH}$  radical and  $\text{HC} \equiv \text{C} \text{---} \text{CC} \equiv \text{CH}_2$  radical with all H/D combinations that can be produced. Mechanisms are outlined using similar decomposition patterns to those found in cyclopentadienyl radical decomposition.



## Appendix D

### Additional Data for Benzyl Radical Pyrolysis

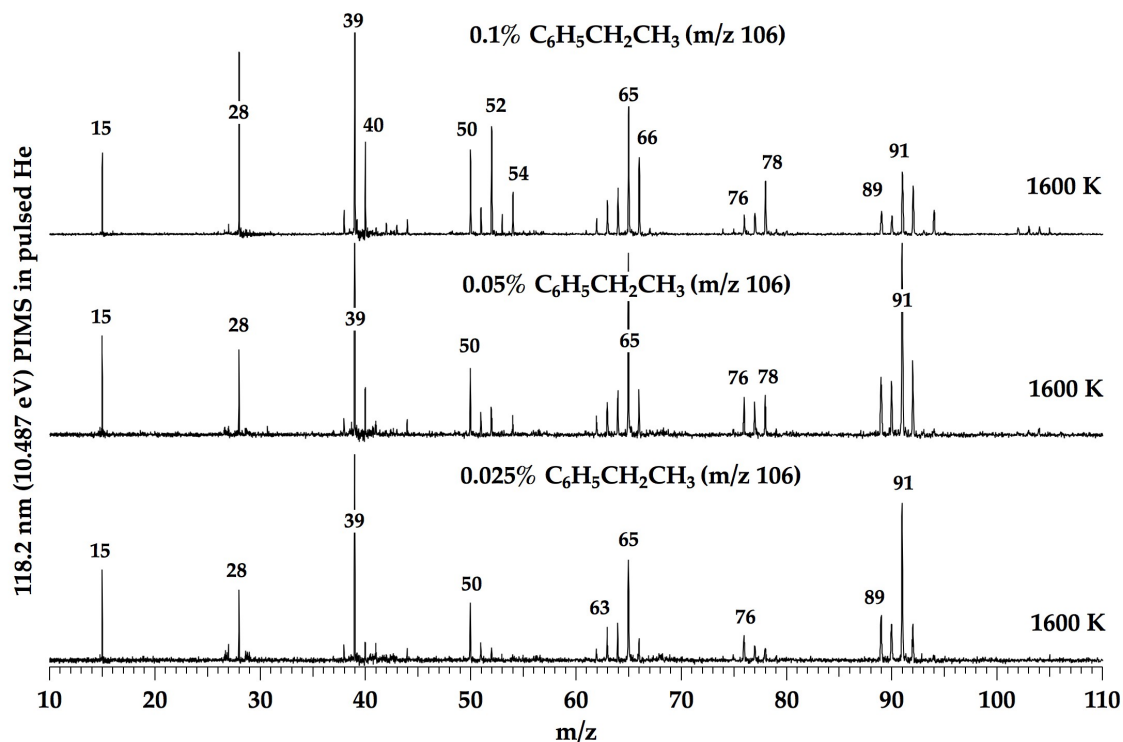


Fig. D.1. PIMS spectra comparing the effect of concentration on the product ratios in ethylbenzene pyrolysis with a pulse micro-reactor. The lower trace was recorded at 0.025 % ethylbenzene in helium, the middle at 0.05%, and the top trace at 0.1%. The peaks that gain intensity as concentration increases are concluded to be the result of bimolecular chemistry.

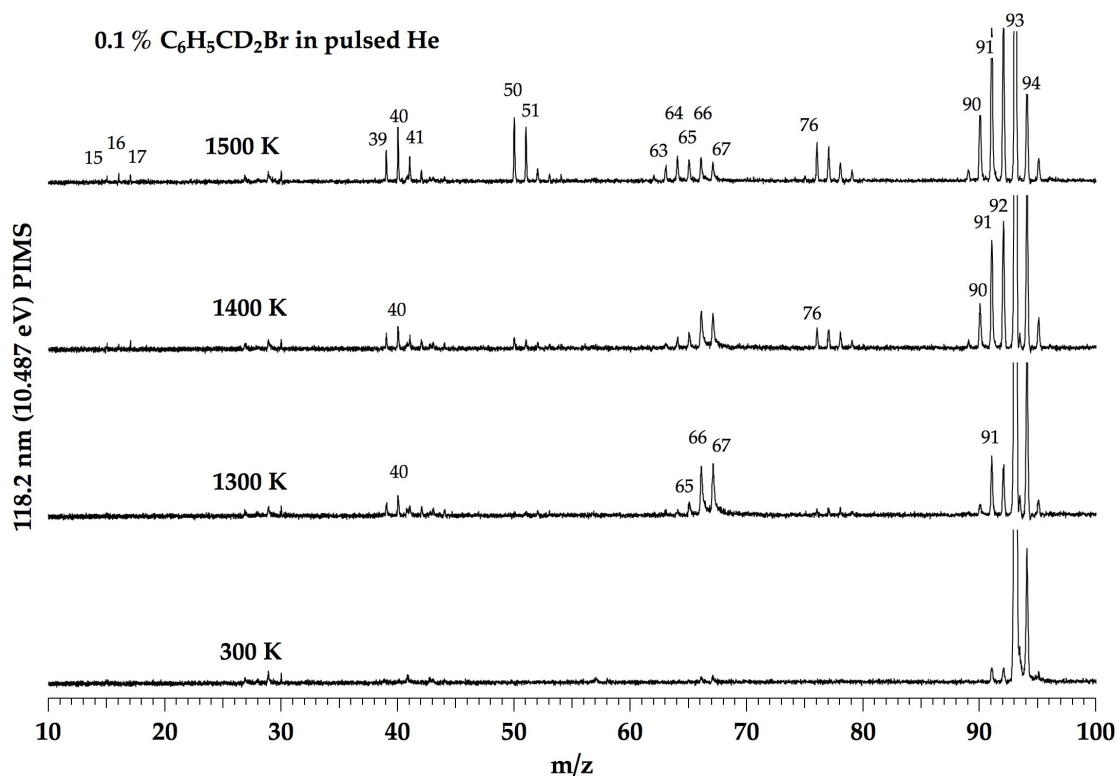


Fig. D.2. PIMS spectra of 0.1 % benzyl bromide-d<sub>2</sub> pyrolysis recorded with a 118.2 nm ionization source and a pulse He flow. At 1500 K we observe three different isotopomers of methyl radical: m/z 15 (CH<sub>3</sub>), m/z 16 (CH<sub>2</sub>D), and m/z 17 (CHD<sub>2</sub>). This may indicate either i) that α methyl-phenyl radical equilibrates with benzyl radical and can exchange H and D atoms multiple times or ii) that methyl radical-d<sub>2</sub> reacts with hydrogen atoms and can exchange H and D atoms to effectively scramble the H/D ratio.

## Appendix E

### Supplemental Figures for Chapter 7

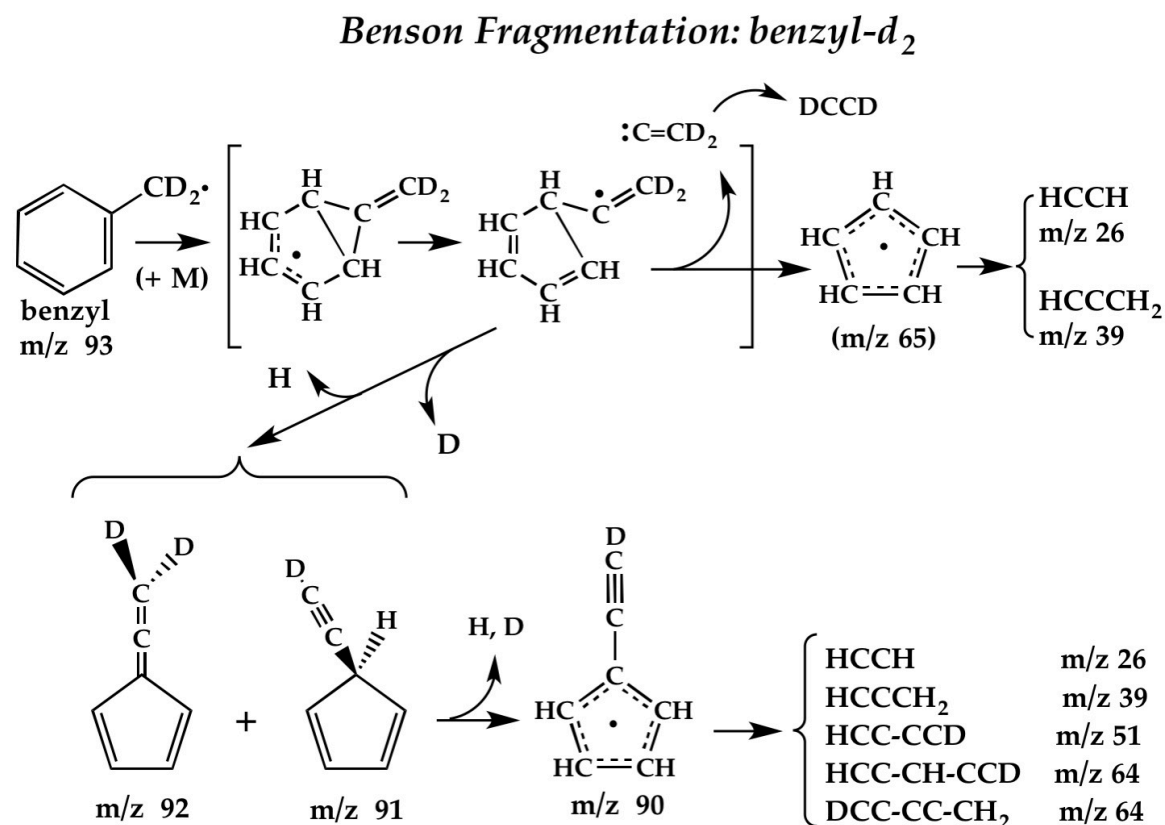


Fig. E.1. The “extended” Benson Fragmentation of benzyl radical-d<sub>2</sub>. The original pathway suggested H atom loss and formation of the fulvenallenyl radical (C<sub>5</sub>H<sub>4</sub>C≡CD). This suggestion also implies formation of the cyclopentadienyl radical and acetylene. The bicyclic radicals and vinylidene (:C=CD<sub>2</sub>) will not be stable in the hot micro-reactor and are enclosed in brackets. The tropyli radical (C<sub>7</sub>H<sub>7</sub>) does not participate.

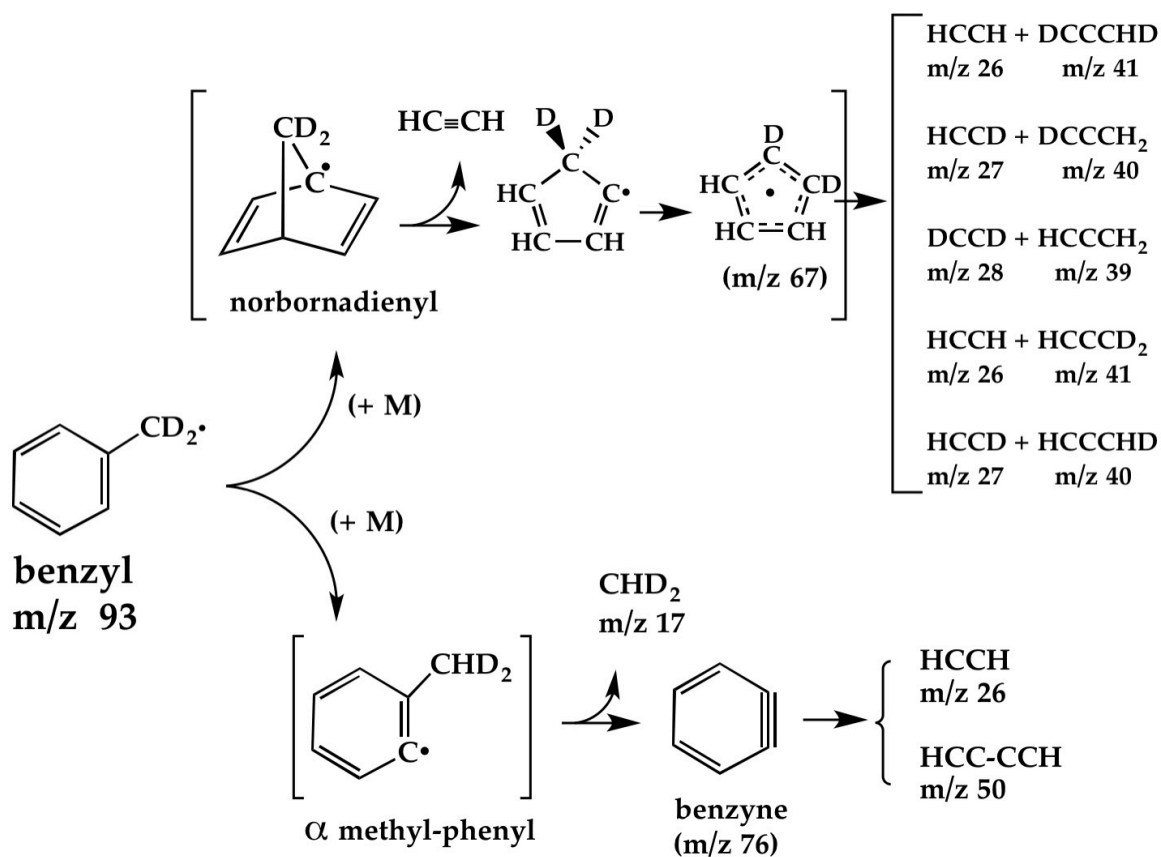


Fig. E.2. Fragmentation pathways of the benzyl radical- $d_2$  are shown. The internal H-atom abstraction from the ring that leads to the formation of the  $\alpha$  methyl-phenyl radical will be endothermic by roughly 1 eV. It also requires a curve-crossing from the  $^2B_1$  benzyl radical to the  $^2A'$  methyl-phenyl ( $\sigma$  radical). Decomposition of the  $\alpha$  methyl-phenyl radical produces  $\text{CHD}_2$  and  $o\text{-C}_6\text{H}_4$ . A second pathway is the isomerization of benzyl to the bridgehead norbornadienyl radical. The  $\alpha$  methyl-phenyl radicals, bridgehead norbornadienyl radicals, and cyclopentadienyl radicals will not be stable in the hot micro-reactor and are enclosed in brackets.

### Benson Fragmentation: benzyl- $d_5$

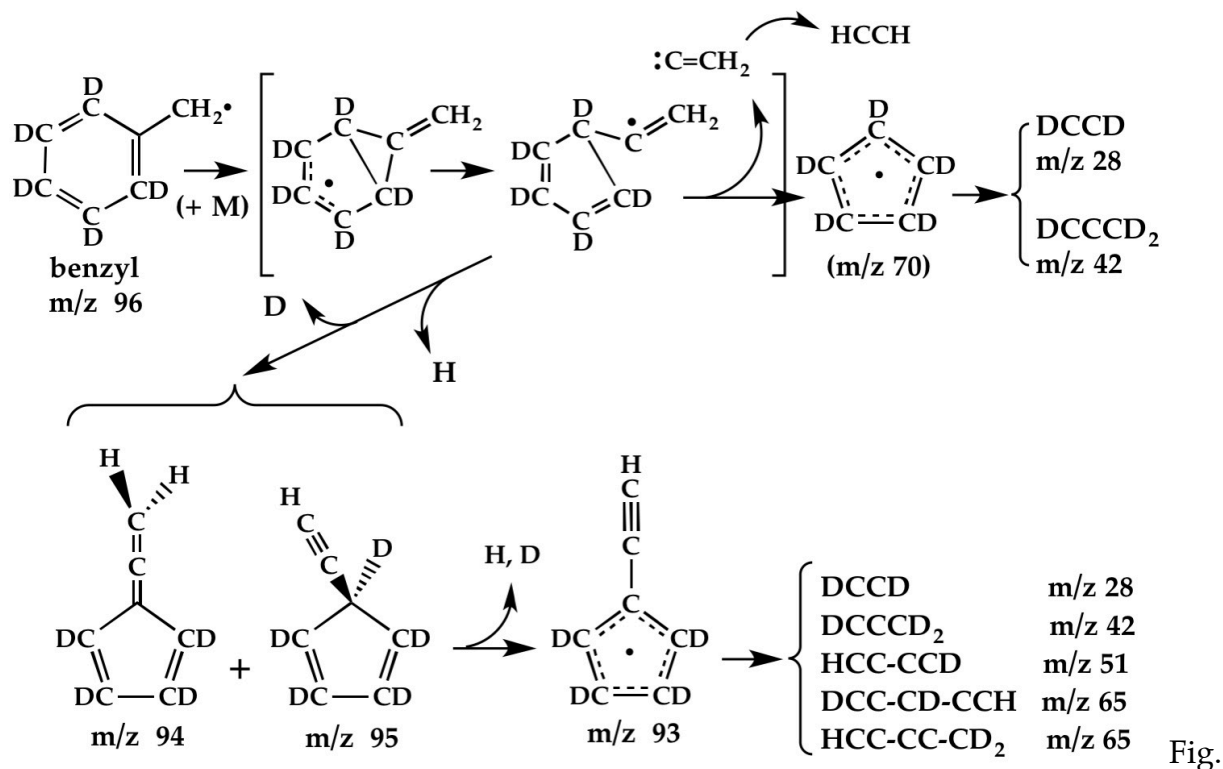


Fig. E.3. The “extended” Benson Fragmentation of benzyl radical- $d_5$ . The original pathway suggested D atom loss and formation of the fulvenallenyl radical ( $C_5D_4C\equiv CH$ ). This suggestion also implies formation of the cyclopentadienyl radical and acetylene. The bicyclic radicals and vinylidene ( $:C=CH_2$ ) will not be stable in the hot micro-reactor and are enclosed in brackets. The tropyl radical ( $C_7H_7$ ) does not participate.



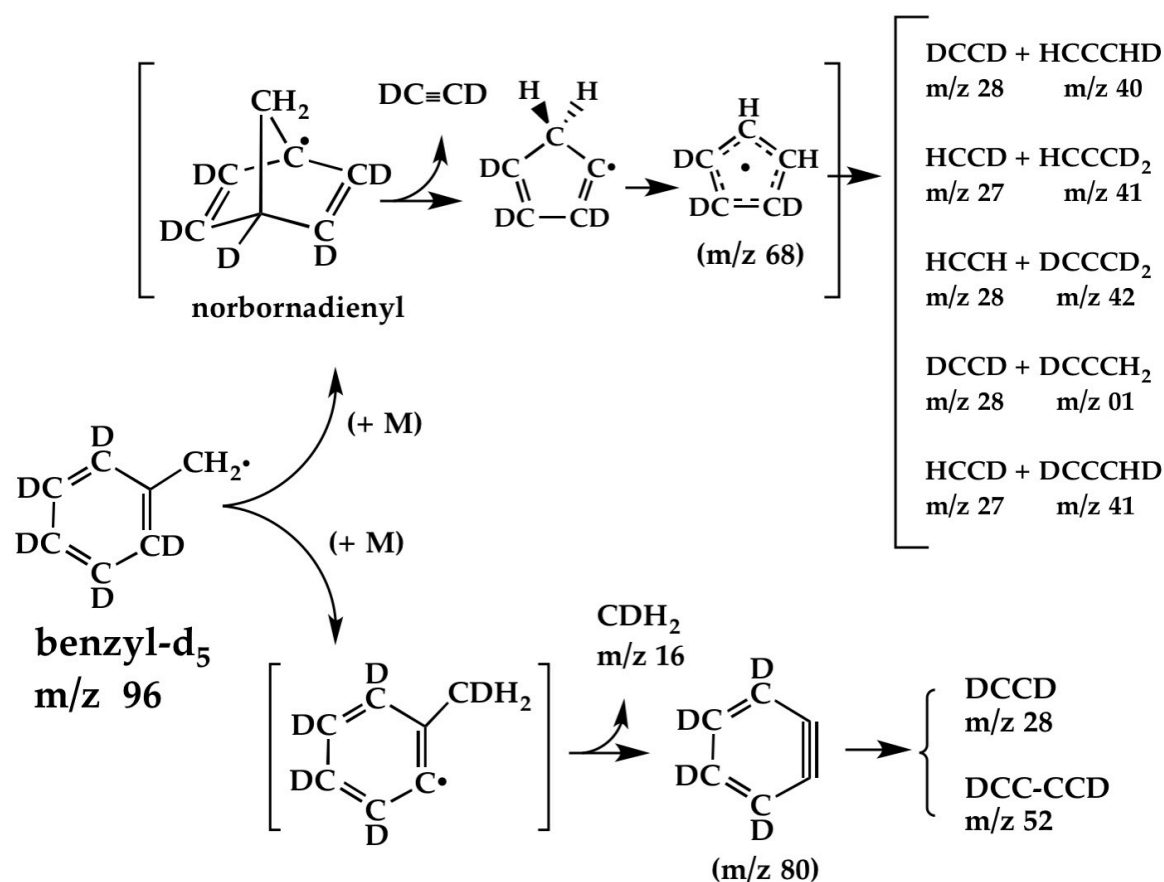


Fig. E.4. Fragmentation pathways of the benzyl radical- $d_5$  are shown. The internal D-atom abstraction from the ring that leads to the formation of the  $\alpha$  methyl-phenyl radical will be endothermic by roughly 1 eV. It also requires a curve-crossing from the  $^2B_1$  benzyl radical to the  $^2A'$  methyl-phenyl ( $\sigma$  radical). Decomposition of the  $\alpha$  methyl-phenyl radical produces CDH<sub>2</sub> and  $o$ -C<sub>6</sub>D<sub>4</sub>. A second pathway is the isomerization of benzyl to the bridgehead norbornadienyl radical. The  $\alpha$  methyl-phenyl radicals, bridgehead norbornadienyl radicals, and cyclopentadienyl radicals will not be stable in the hot micro-reactor and are enclosed in brackets.

### Benson Fragmentation: benzyl-<sup>13</sup>C

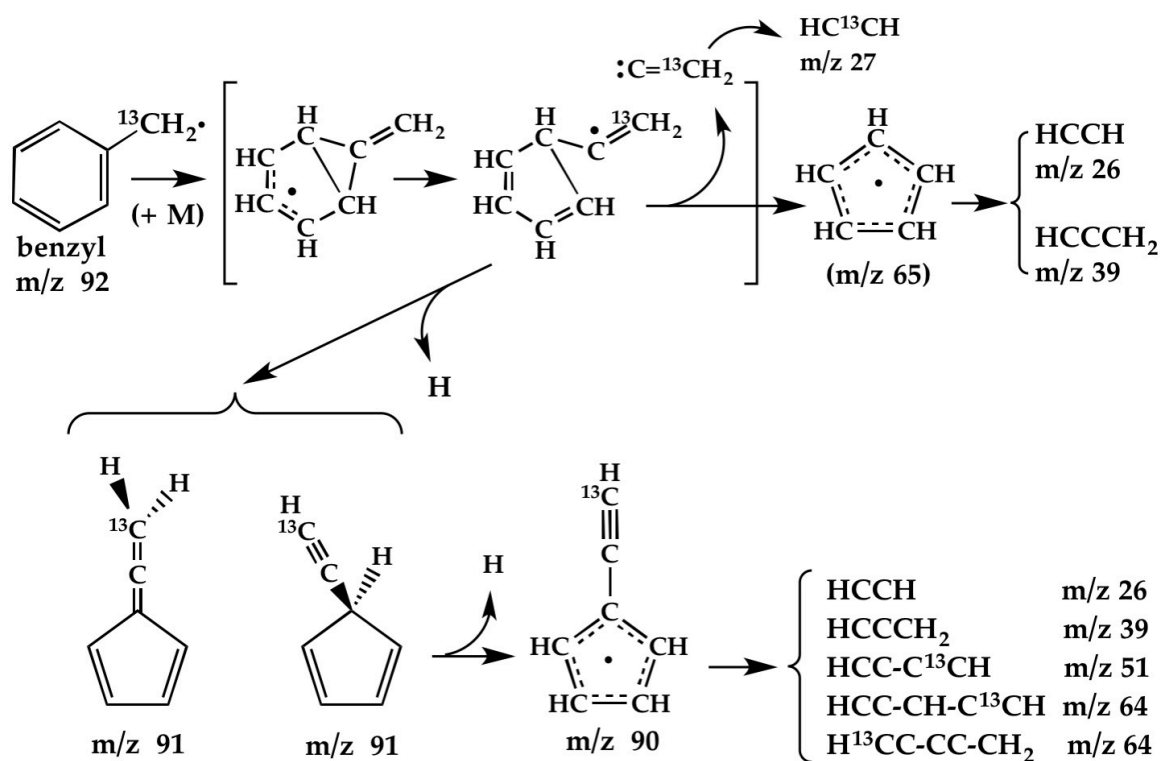


Fig. E.5. The “extended” Benson Fragmentation of <sup>13</sup>C labeled benzyl radical. The original pathway suggested H atom loss and formation of the fulvenallenyl radical ( $\text{C}_5\text{H}_4\text{C}\equiv\text{}^{13}\text{CH}$ ). This suggestion also implies formation of the cyclopentadienyl radical and acetylene. The bicyclic radicals and vinylidene ( $\text{:C}=\text{}^{13}\text{CH}_2$ ) will not be stable in the hot micro-reactor and are enclosed in brackets. The tropyli radical ( $\text{C}_7\text{H}_7$ ) does not participate.

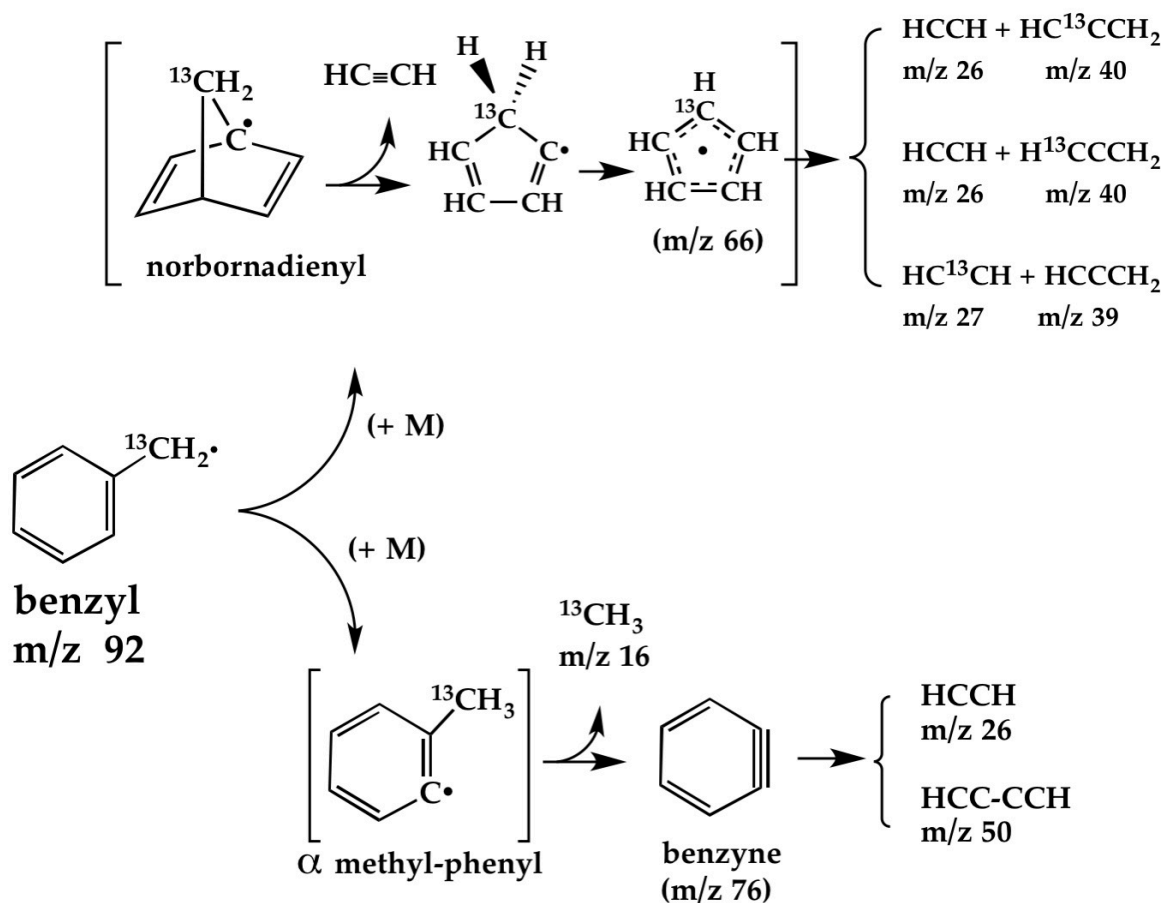


Fig. E.6. Fragmentation pathways of the  $^{13}\text{C}$  labeled benzyl radical are shown. The internal H-atom abstraction from the ring that leads to the formation of the  $\alpha$  methyl-phenyl radical will be endothermic by roughly 1 eV. It also requires a curve-crossing from the  $^2\text{B}_1$  benzyl radical to the  $^2\text{A}'$  methyl-phenyl ( $\sigma$  radical). Decomposition of the  $\alpha$  methyl-phenyl radical produces  $^{13}\text{CH}_3$  and  $o\text{-C}_6\text{H}_4$ . A second pathway is the isomerization of benzyl to the bridgehead norbornadienyl radical. The  $\alpha$  methyl-phenyl radicals, bridgehead norbornadienyl radicals, and cyclopentadienyl radicals will not be stable in the hot micro-reactor and are enclosed in brackets.

## Appendix F

### Resonance Stabilization Energy

To attempt to quantify the relative electron delocalization stabilization of resonance stabilized hydrocarbon radicals, we compiled a table that uses relative bond strengths as an indicator of radical stability. Resonance stabilization is important in combustion because in order for the unpaired electron to react with another molecule, the localization of the electron to form a new bond requires losing the delocalization benefit. In an attempt to quantify this effect, we assembled previously reported experimental measurements<sup>[1-21]</sup> that allow the comparison of different bond dissociation enthalpies. By comparing resonance stabilized radical products and radicals with localized electrons, we approximate the energetic benefit of electron delocalization. Table F.1 summarizes these findings. The bond dissociation enthalpy at 298 K ( $D_{298}$ ) is calculated as the difference of the heat of formation ( $\Delta_f H_{298}$ ) of the radical products and the parent species, see equation (1).

$$\Delta_f H_{298}(\text{R}) + \Delta_f H_{298}(\text{H}) - \Delta_f H_{298}(\text{RH}) = D_{298}(\text{R-H}) \quad (1)$$

The bond dissociation enthalpy at 0 K ( $D_0$ ) is calculated by relating the appearance potential (AP) of a cation from the parent and the ionization of the radical (IE) as summarized in equation (2).

$$\text{AP}(\text{R}^+ \leftarrow \text{RH}) - \text{IE}(\text{R}) = D_0(\text{R-H}) \quad (2)$$

The radicals of interest were compared to two or three similar radicals where the unpaired electron is localized on a specific carbon atom.

Table F.1 indicates that even though benzyl is energetically more stable than troyl radical, the calculated resonance energy of troyl is more than twice that of benzyl radical (24.8 kcal mol<sup>-1</sup> for troyl versus 11.4 kcal mol<sup>-1</sup> for benzyl). All the radicals investigated in Table F.1 have significant resonance stabilization of at least 11.5 kcal mol<sup>-1</sup> (roughly 0.5 eV). This implies that these hydrocarbon radicals will be relatively resistant to oxidative addition of O<sub>2</sub> because such reactions will be roughly 0.5 eV less exothermic than those with equivalent radicals that lack electron delocalization.

		298 K		0 K		Refer-ences	
		DH <sub>298</sub> (kcal/mol)	Resonance Energy	D <sub>0</sub> (kcal/mol)	Resonance Energy	298 K	0 K
Benzyl Radical	C <sub>6</sub> H <sub>5</sub> CH <sub>2</sub> -CH <sub>2</sub> C <sub>6</sub> H <sub>5</sub>	65.2 ± 0.7		77 ± 2		1,2	7,8
	CH <sub>3</sub> CH <sub>2</sub> -CH <sub>2</sub> CH <sub>3</sub>	88.0 ± 0.6		102 ± 1.2		1,2	9,10
			11.4 ± 0.9		12.5 ± 2.3		
	C <sub>6</sub> H <sub>5</sub> CH <sub>2</sub> -H	89.8 ± 0.6				1,2,3	
	CH <sub>3</sub> CH <sub>2</sub> -H	101.1 ± 0.4				1,2,3	
			11.4 ± 0.7				
Tropyl Radical	C <sub>7</sub> H <sub>7</sub> -H	73.9 ± 0.9				1,3,4	
	(CH <sub>3</sub> ) <sub>2</sub> CH-H	98.6 ± 0.4				1,2,3	
			24.8 ± 1.0				
	C <sub>7</sub> H <sub>7</sub> -C <sub>7</sub> H <sub>7</sub>			42.8 ± 1.2			12,13
	(CH <sub>3</sub> ) <sub>2</sub> CH-CH(CH <sub>3</sub> ) <sub>2</sub>			93.2 ± 1.7		1,2	14,15
				25.2 ± 2			
Cyclopentadienyl Radical	C <sub>5</sub> H <sub>5</sub> -H	83.3 ± 1.4				1,3,5	
	(CH <sub>3</sub> ) <sub>2</sub> CH-H	98.6 ± 0.4				1,2,3	
			15.4 ± 1.5				
	C <sub>5</sub> H <sub>5</sub> -H			80 ± 12			16,17
	(CH <sub>3</sub> ) <sub>2</sub> CD-D			97 ± 1			15,18
					17 ± 12		
Allyl Radical	H <sub>2</sub> C=CH-CH <sub>2</sub> -H	88.2 ± 0.7		86 ± 2		1,3,6	20,21
	CH <sub>3</sub> CH <sub>2</sub> -H	101.1 ± 0.4		104.5 ± 1.9		1,2,3	10,22
			12.9 ± 0.8		18.1 ± 3		
	H <sub>2</sub> C=CH-CH <sub>2</sub> -CH=CH <sub>2</sub>	61.6 ± 1.0				1,6	
	CH <sub>3</sub> CH <sub>2</sub> -CH <sub>2</sub> CH <sub>3</sub>	88.0 ± 0.6				1,2,3	
			13.2 ± 1.2				
Propargyl Radical	HC≡C-CH <sub>2</sub> -H	88.9 ± 0.2				1,3,6	
	CH <sub>3</sub> CH <sub>2</sub> -H	101.1 ± 0.4				1,2,3	
			12.2 ± 0.5				
	H <sub>2</sub> C=C=CH-H	87.6 ± 0.3				1,3,6	
	CH <sub>3</sub> CH <sub>2</sub> -H	101.1 ± 0.4				1,2,3	
			13.5 ± 0.5				

Table F.1. Resonance energies of hydrocarbon radicals calculated from experimental values at 298 K and 0 K.

## References for Appendix F

- [1] J. B. Pedley, R. D. Naylor and S. P. Kirby, *Thermochemistry of Organic Compounds*, Chapman and Hall, New York, **1986**, p. 87-222.
- [2] S. J. Blanksby and G. B. Ellison. Bond dissociation energies of organic molecules. *Accounts of Chemical Research* **2003**, *36*, 255-263.
- [3] L. V. Gurvich, I. V. Veyts, C. B. Alcock and V. S. Iorish, *Thermodynamic Properties of Individual Substances*, Hemisphere, New York City, **1991**, p. 42-43.
- [4] J. C. Traeger and R. G. McLoughlin. Photo-ionization study of energetics of  $C_7H_7^+$  ion formed from  $C_7H_8$  precursors. *International Journal of Mass Spectrometry and Ion Processes* **1978**, *27*, 319-333.
- [5] T. Ichino, S. W. Wren, K. M. Vogelhuber, A. J. Gianola, W. C. Lineberger and J. F. Stanton. The vibronic level structure of the cyclopentadienyl radical. *Journal of Chemical Physics* **2008**, *129*, 084310.
- [6] M. S. Robinson, M. L. Polak, V. M. Bierbaum, C. H. DePuy and W. C. Lineberger. Experimental Studies of Allene, Methylacetylene, and the Propargyl Radical - Bond-Dissociation Energies, Gas-Phase Acidities, and Ion-Molecule Chemistry. *Journal of the American Chemical Society* **1995**, *117*, 6766-6778.
- [7] F. W. McLafferty, T. Wachs, C. Lifshitz, G. Innorta and P. Irving. Substituent effects in unimolecular ion decompositions. XV. Mechanistic interpretations and the quasi-equilibrium theory. *Journal of the American Chemical Society* **1970**, *92*, 6867-6880.
- [8] G. C. Eiden, F. Weinhold and J. C. Weishaar. Photoelectron-spectroscopy of free-radicals with  $cm^{-1}$  resolution - the benzyl cation. *Journal of Chemical Physics* **1991**, *95*, 8665-8668.
- [9] I. Omura. Mass Spectra at Low Ionizing Voltage and Bond Dissociation Energies of Molecular Ions from Hydrocarbons. *Bulletin of the Chemical Society of Japan* **1961**, *34*, 1227-1233.
- [10] B. Ruscic, J. Berkowitz, L. A. Curtiss and J. A. Pople. The ethyl radical: Photoionization and theoretical studies. *The Journal of Chemical Physics* **1989**, *91*, 114-121.

- [11] F. A. Elder and A. C. Parr. Photoionization of cycloheptatrienyl radical. *Journal of Chemical Physics* **1969**, *50*, 1027-1028.
- [12] K. H. Fischer, P. Hemberger, A. Bodi and I. Fischer. Photoionisation of the tropyli radical. *Beilstein Journal of Organic Chemistry* **2013**, *9*, 681-688.
- [13] B. Steiner, C. F. Giese and M. G. Inghram. Photoionization of Alkanes. Dissociation of Excited Molecular Ions. *The Journal of Chemical Physics* **1961**, *34*, 189-220.
- [14] F. A. Houle and J. L. Beauchamp. Photoelectron spectroscopy of methyl, ethyl, isopropyl, and tert-butyl radicals. Implications for the thermochemistry and structures of the radicals and their corresponding carbonium ions. *Journal of the American Chemical Society* **1979**, *101*, 4067-4074.
- [15] A. G. Harrison, P. Haynes, S. McLean and F. Meyer. The Mass Spectra of Methyl-Substituted Cyclopentadienes. *Journal of the American Chemical Society* **1965**, *87*, 5099-5105.
- [16] H. J. Wörner and F. Merkt. Diradicals, antiaromaticity, and the pseudo-Jahn-Teller effect: Electronic and rovibronic structures of the cyclopentadienyl cation. *Journal of Chemical Physics* **2007**, *127*, 034303.
- [17] J. M. Williams and W. H. Hamill. Ionization Potentials of Molecules and Free Radicals and Appearance Potentials by Electron Impact in the Mass Spectrometer. *The Journal of Chemical Physics* **1968**, *49*, 4467-4477.
- [18] C. Lifshitz and M. Shapiro. Isotope Effects on Metastable Transitions. II.  $\text{CH}_3\text{CD}_2\text{CH}_3$  and  $\text{CD}_3\text{CH}_2\text{CD}_3$ . *The Journal of Chemical Physics* **1967**, *46*, 4912-4920.
- [19] F. P. Lossing. Free Radicals by Mass Spectrometry. XLIII. Ionization Potentials and Ionic Heats of Formation for Vinyl, Allyl, and Benzyl Radicals. *Canadian Journal of Chemistry* **1971**, *49*, 357-362.
- [20] F. A. Houle and J. L. Beauchamp. Detection and investigation of allyl and benzyl radicals by photoelectron-spectroscopy. *Journal of the American Chemical Society* **1978**, *100*, 3290-3294.
- [21] W. A. Chupka and J. Berkowitz. Photoionization of ethane, propane, and n-butane with mass analysis. *The Journal of Chemical Physics* **1967**, *47*, 2921-2933.





## Appendix G

### Energy Levels and Symmetries of the Cyclic $C_nH_n$ Molecules ( $n = 3$ to $7$ )

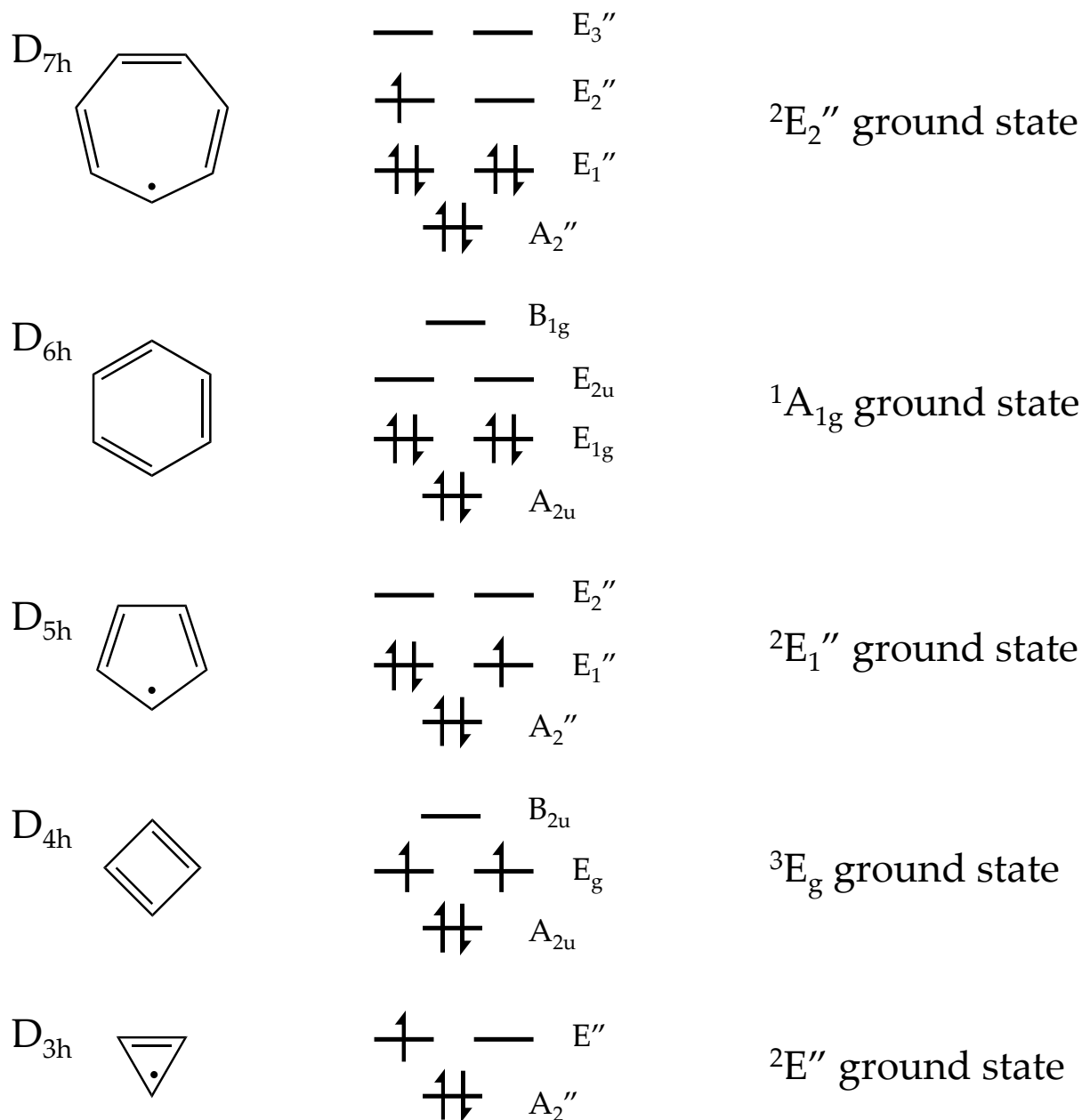


Fig. G.1. Chemical drawings, energy levels, electron occupation, and symmetries of the ground state for the five smallest cyclic  $C_nH_n$  molecules: cyclopropenyl radical ( $C_3H_3$ ), cyclobutadiene ( $C_4H_4$ ), cyclopentadienyl radical ( $C_5H_5$ ), benzene ( $C_6H_6$ ), and cycloheptatrienyl (tropylium) radical ( $C_7H_7$ )

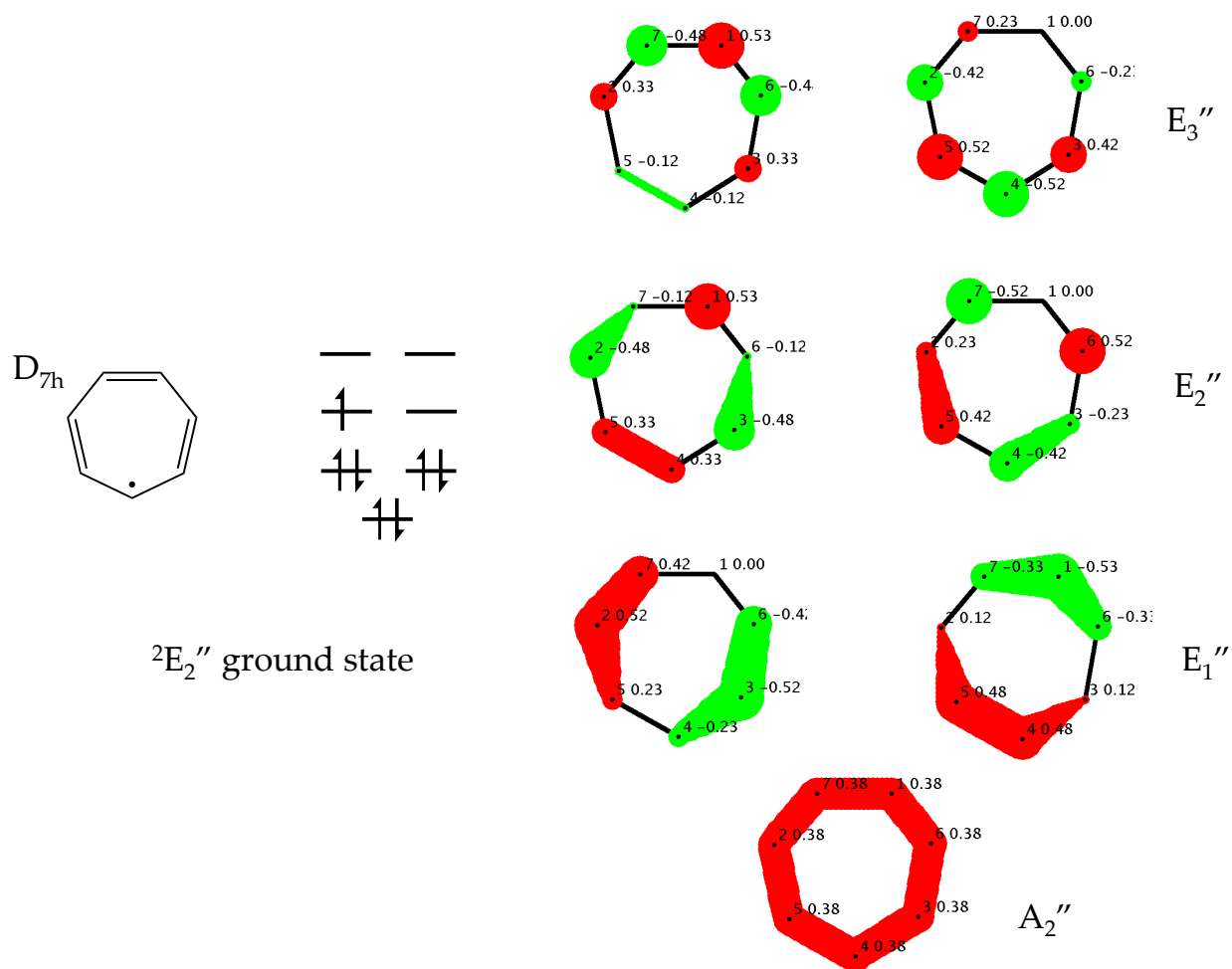


Fig. G. 2. Cartoon drawings of the 7  $\pi$ -electron molecular orbitals of tropylium radical. Black text on the cartoons indicates carbon atom number (1 through 7) followed by sign and intensity of the wave function at that location.

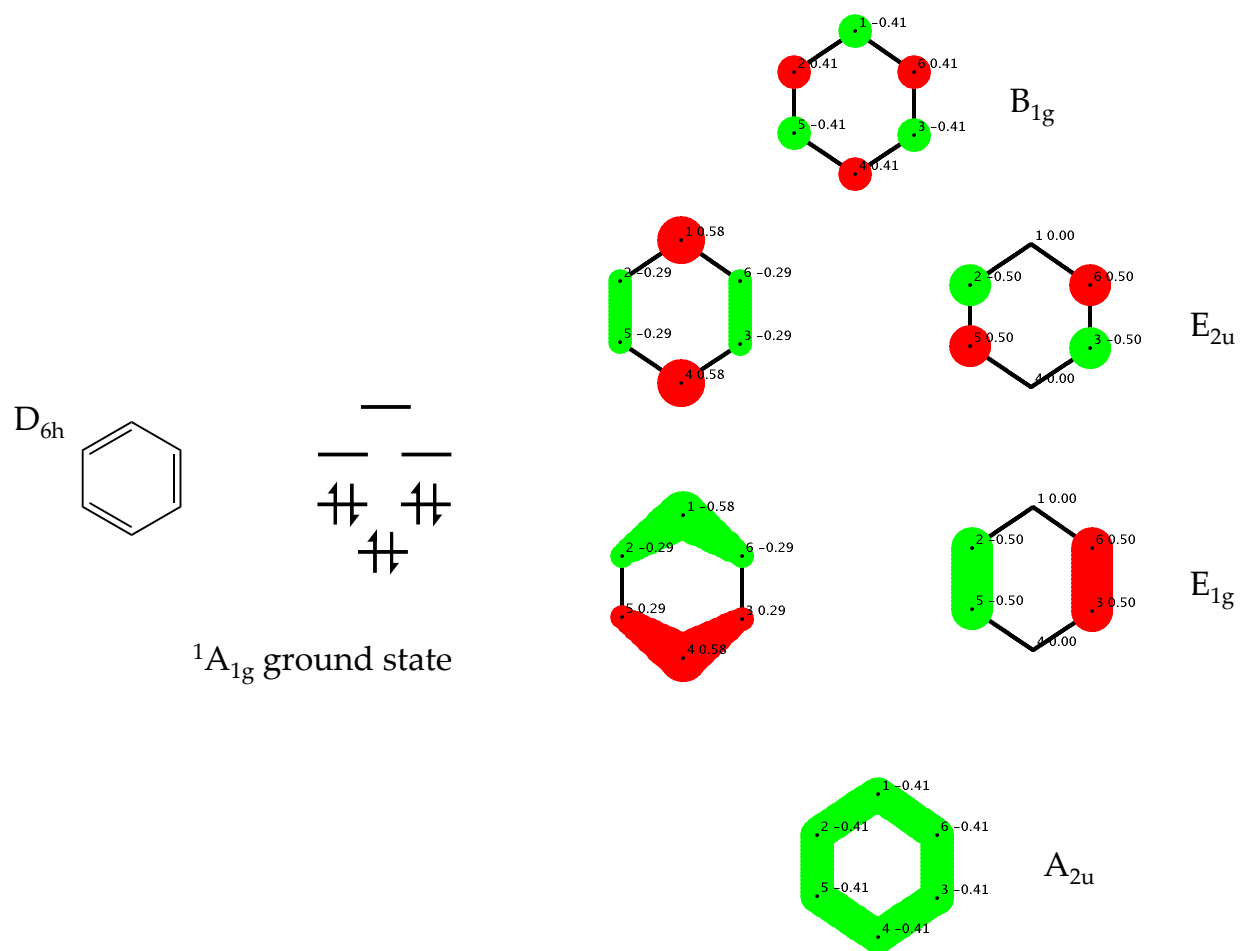


Fig. G. 3. Cartoon drawings of the 6  $\pi$ -electron molecular orbitals of benzene. Black text on the cartoons indicates carbon atom number (1 through 6) followed by the sign and intensity of the wavefunction at that location.

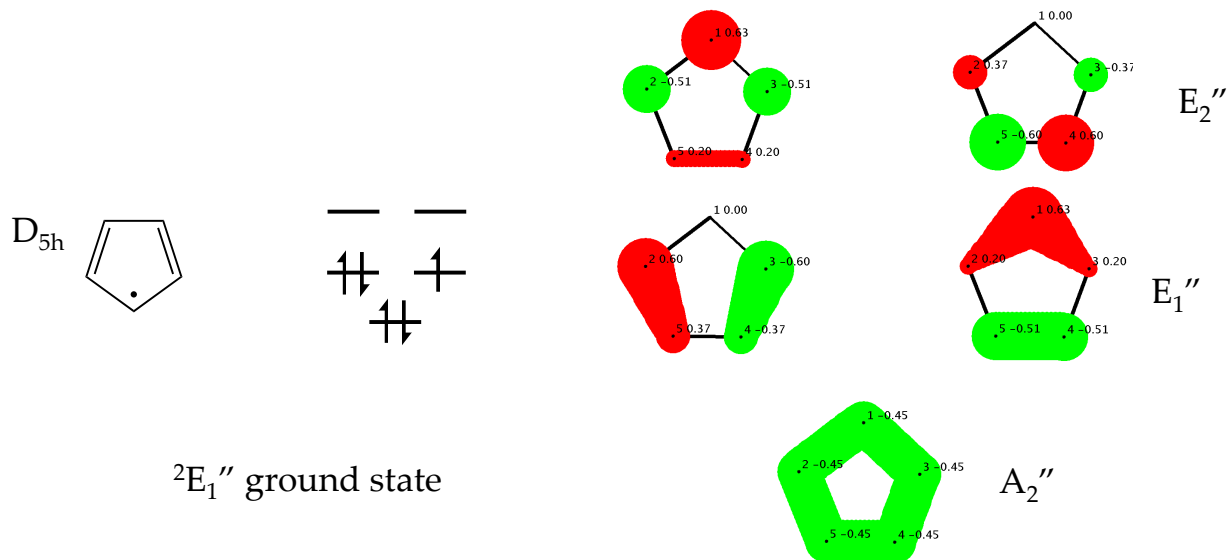


Fig. G. 4. Cartoon drawings of the 5  $\pi$ -electron molecular orbitals of cyclopentadienyl radical. Black text on the cartoons indicates carbon atom number (1 through 5) followed by the sign and intensity of the wave function at that location.

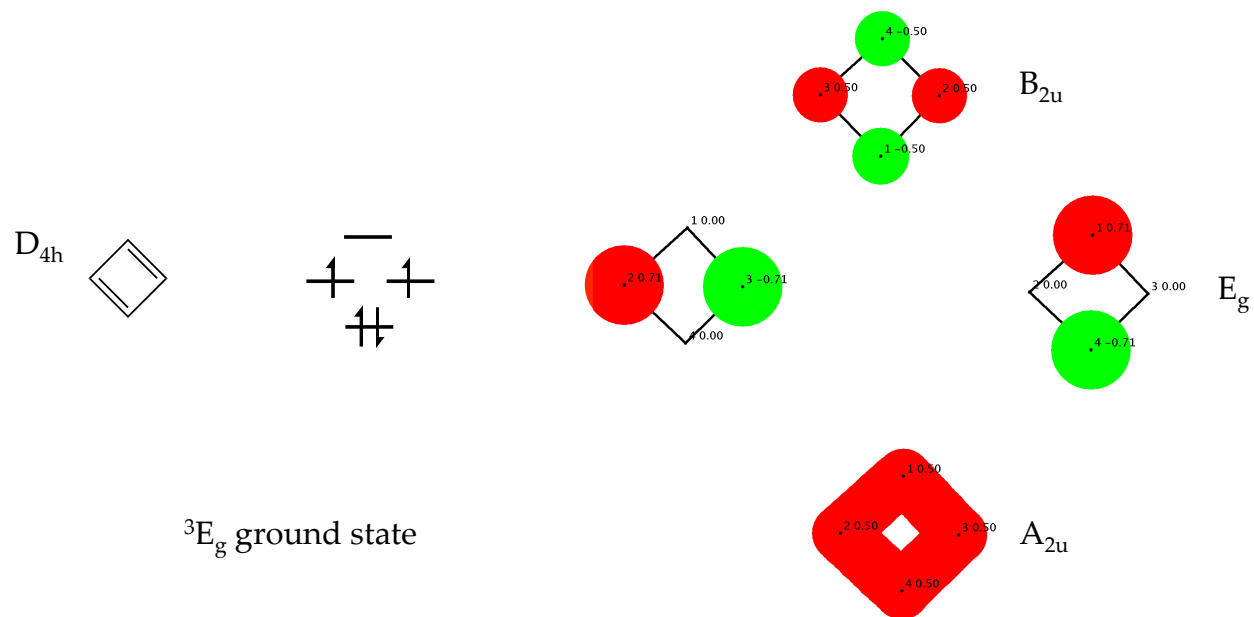


Fig. G. 5. Cartoon drawings of the 4  $\pi$ -electron molecular orbitals of cyclobutadiene. Black text on the cartoons indicates carbon atom number (1 through 4) followed by the sign and intensity of the wave function at that location.

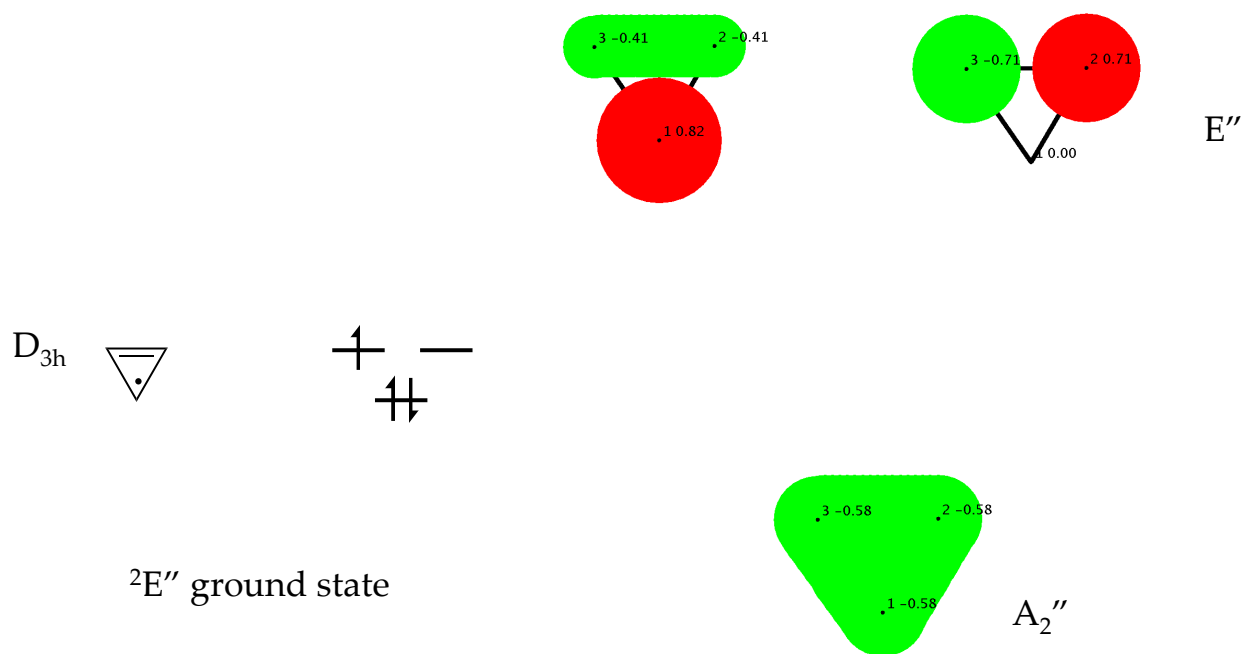


Fig. G. 6. Cartoon drawings of the 3  $\pi$ -electron molecular orbitals of cyclopropenyl radical. Black text on the cartoons indicates carbon atom number (1 through 3) followed by the sign and intensity of the wave function at that location.

Orbital symmetries were determined using guidance from the book Chemical Applications of Group Theory, 3<sup>rd</sup> Edition.<sup>[1]</sup>

Figures G.2, G.3, G.4, G.5, and G.6 were generated using the Simple Hückel Molecular Orbital Theory Calculator (SHMO).<sup>[2]</sup>

## References for Appendix G

- [1] F. A. Cotton, *Chemical applications of group theory*, 3<sup>rd</sup> Edition, John Wiley & Sons, 1990, p. 150-155.
- [2] A. Rauk, *Simple Huckel Molecular Orbital Program*, Java, Applet, 2010  
<http://www.ucalgary.ca/rauk/shmo>